

Photophysics and dynamics of complex chemical systems

Thesis Submitted for the degree of

Doctor of Philosophy (Science)

Of

Jadavpur University

By

Ejaj Tarif



Department of Chemical, Biological and Macromolecular Sciences

S. N. Bose National Centre for Basic Sciences

Block – JD, Sector – III, Salt Lake City

Kolkata - 700106, India

July 2019

सत्येन्द्र नाथ बसु राष्ट्रीय मौलिक विज्ञान केन्द्र
SATYENDRA NATH BOSE NATIONAL
CENTRE FOR BASIC SCIENCES
सत्येन्द्र नाथ बसु जातीय मौलिक विज्ञान केन्द्र

CERTIFICATE FROM THE SUPERVISOR

This is to certify that the thesis entitled “**Photophysics and dynamics of complex chemical systems**” submitted by **Sri Ejaj Tarif** (Index No:217/15/chem./24), who got his name registered on 28/10/2015 for the award of Ph.D. (Science) degree of Jadavpur University, is absolutely based upon his own work under the supervision of Professor Ranjit Biswas and that neither this thesis nor any part of it has been submitted for either any degree/diploma or any other academic award anywhere before.

Ranjit Biswas
25 July 2019

Dr. Ranjit Biswas

Senior Professor,

Department of Chemical, Biological and Macromolecular Sciences

S. N. Bose National Centre for Basic Sciences

Block-JD, Sector-III, Salt Lake,

Kolkata-700106, West Bengal, India

DR. RANJIT BISWAS

Senior Professor

Dept. of Chemical, Biological & Macromolecular Sciences
S. N. Bose National Centre for Basic Sciences
Block - JD, Sector-III, Salt Lake, Kolkata - 700 106, India

ब्लॉक-जे.डी. सेक्टर-III, सॉल्ट लेक, कोलकाता-700 098, Block-JD, Sector-III, Salt Lake, Kolkata - 700 098

दूरभाष / Phones : (00) 91-(0)33-2335 5706-8, 2335 3057/61, 2335 0312 / 1313

टेलीफैक्स / TELEFAX : +91-33-2335 3477 / 2335 1364 / 2335 9176

वेबसाइट / Website: <http://www.bose.res.in>

FUNDED BY DEPARTMENT OF SCIENCE & TECHNOLOGY, GOVERNMENT OF INDIA

निधिवद्ध विज्ञान और प्रौद्योगिकी विभाग भारत सरकार द्वारा

**Dedicated to
My Mother Mahmuda Islam
&
My Father Saidul Islam**

Acknowledgement

I have lived and worked in S. N. Bose National Centre for Basic Sciences for about five years as a research scholar in the department of Chemical, Biological and Macromolecular Sciences (CBMS). Now it is a high time to acknowledge the support of all the people whom I have come across during this academic journey.

First of all, it is my contentment to express cordial thanks and humble gratitude to my supervisor Prof. Ranjit Biswas for his continuous motivation and fostering. I feel myself very much fortunate to have him as my guide in my work. It is a lesson of life to get trained under his guidance. He gave me the opportunity to think and work independently. He also taught me how to think a problem from every possible perspective. His extensive knowledge, extreme dedication to work and immense enthusiasm to study new things will remain as an inspiration of my life. His kind and affectionate attitude to me is worth cherishing for entire life.

I am thankful to Prof. Priyadarsi De, IISER, Kolkata, Prof. Pratik Sen, IIT, Kanpur, and Prof. Anjan Barman, SNBNCBS, for collaborations. My sincere thanks are for Prof. Mark Maroncelli, Pennsylvania State University, USA for kindly allowing me to access his spectra analysis software. I would also like to thank faculty members of the Centre especially those who have helped me to upgrade myself through their valuable questions and suggestions.

I would like to thank all of the members of my thesis committee, for giving their precious times to me from their extremely busy schedule.

I am also thankful to every person associated with the procuring and maintaining the instrumental facility of S. N. Bose National Centre for Basic Sciences (SNBNCBS). I would like to thank Dean (Academic Programme)'s Office for their help over the years.

I express my earnest thanks to all of my labmates Juriti, Atanu, Kajal, Dhruvajyoti, Jayanta, Narayan, Arnab, Soumita, Indrajit, Dr. Sirshendu Dinda from PCCP lab. They were like extended family here providing a healthy and homely atmosphere around me. They were always with me irrespective of the situation. I want to thank Dr. Kallol Mukherjee and Dr. Anuradha Das for helping me in learning instrument handling and the protocol of research at the initial

stage of my PhD tenure. I would also like to thank Dr. Tamisra Pal, Dr. Sandipa Indra, Dr. Suman Das for helping me in many ways.

I am very much thankful to all the academic and non-academic staffs of SNBNCBS for their continuous supports. I heartily acknowledge the help and assistance received from the Dean (Academic Program) office of the Centre.

I convey my sincere regards to Dr. Parijat Das for her tender and caring act during visits to her home. The moments spent with the adorable duo of Rwitoban and Arshaman will be a memory of life.

I want to thank all the staffs of SNB mess and BHAGIRATHI canteen for their untiring efforts to provide healthy delicious foods.

I am grateful to all my teachers of my life. Each of them has significant impact on my life.

I will be always grateful to my maternal grandfather late Kalu Ali Mondal, my maternal grandmother late Rokiya Bibi, parental grandfather late Ahmmad Mondal, my parental grandmother late. Jamela Bibi, my loving sister Shaqia Mehebuba, Brother-in-Law Noor Selim, my niece Natasha Mehebuba.

I would like to thank all of my friends.

Finally, I want to express my gratitude from the bottom of my heart to two best persons of my life my parents, Mahmuda Islam and Saidul Islam for their loves, blessings and lessons.

Abstract

This Thesis deals with the study of interaction and dynamics of several complex chemical systems that include naturally abundant deep eutectic solvents (NADESs), binary mixtures, and bio-mimetic systems (micelle), employing time (picoseconds)-resolved fluorescence (TRF) and MHz-GHz dielectric relaxation (DR) spectroscopic techniques. Time-resolved measurement of dissolved dipolar solute in prepared NADESs depict fractional viscosity dependence of reorientation motion of the solute at well above (~70-130 K) the glass transition temperature of the medium. This sort of viscosity decoupling of transport properties is usually observed for deeply supercooled liquids near glass transition. DR spectroscopy coupled with TRF measurements reveal that water-polyhydroxy alcohol mixtures considered here are mildly spatio-temporally heterogeneous. Dynamics of those mixtures are different from bulk water and depend on concentrations of polyhydroxy alcohol. In addition, DR timescales appear to suggest the origin being the reorientation and H-bond relaxation dynamics, excluding the possibility of full molecular rotations. Amphiphilic diblock copolymer form micelles in aqueous medium and the interfacial dynamics of these micelles are qualitatively similar to other micelle-forming systems. DR measurements at the highest of the polymer concentrations considered suggest the presence of aqueous dynamics slower than that for neat bulk water, although evidence for such “slow” dynamics at lower concentrations has not been detected in the present DR measurements. Impact of the connector atom between the head and the tail part of the surfactant in the structure and interfacial dynamics of their micelles explored via dynamic light scattering (DLS), TRF and DR spectroscopy measurements. Interestingly, a significant impact of linkage atom on size of the micelles and associated interfacial dynamics has been observed.

Chapter 1 of this Thesis presents a brief introduction to the work and the related literature. In Chapter 2, a concise description of the used experimental techniques and data analysis protocols are provided. Chapters 3 and 4 report preparation of naturally abundant deep eutectic solvents (NADESs), and investigation of interaction and dynamics in them employing steady state and time-resolved fluorescence spectroscopic measurements. Medium heterogeneity of water-xylitol mixtures are discussed in Chapter 5 with the help of DR and TRF measurements. In Chapter 6 structure and dynamics of the micellar solution prepared from amphiphilic diblock copolymers

are elaborated. Chapter 7 contains the impact of connector atom of head and tail part of the surfactant in the dynamics of their aqueous micellar solutions. Concluding remarks and some important future problems are provided in Chapter 8.

List of Publications

1. “Dynamics of a PEG based non-ionic deep eutectic solvent: Temperature dependence” by Kallol Mukherjee, **Ejaj Tarif**, Anjan Barman and Ranjit Biswas *Fluid Phase Equilib.* **448**, 22 (2017).
2. “Dielectric relaxation in acetamide + urea deep eutectics and neat molten urea: Origin of time scales via temperature dependent measurements and computer simulations” by Kallol Mukherjee, Suman Das, **Ejaj Tarif**, Anjan Barman and Ranjit Biswas *J. Chem. Phys.* **149**, 124501 (2018).
3. “Exploring Aqueous Solution Dynamics of Amphiphilic Diblock Copolymer: Dielectric Relaxation and Time-resolved Fluorescence Measurements” by **Ejaj Tarif**, Biswajit Saha, Kallol Mukherjee, Priyadarsi De and Ranjit Biswas *J. Phys. Chem. B* **123**, 5892 (2019)
3. “Are Water-Xylitol Mixtures Heterogeneous? An Investigation Employing Composition and Temperature Dependent Dielectric Relaxation and Time-Resolved Fluorescence Measurements” by **Ejaj Tarif**, Kallol Mukherjee, Anjan Barman and Ranjit Biswas *J. Chem. Sci.* **131**:43 (2019).
5. “Solvent dependent relaxation dynamics in lithium ion battery electrolytes: Coupling to medium friction” by Kajal Kumbhakar, **Ejaj Tarif**, Kallol Mukherjee, and Ranjit Biswas *J. Mol. Liq.* **290**, 111225 (2019).
6. “Interaction and Dynamics in a Fully Biodegradable Glucose-Containing Naturally Abundant Deep Eutectic Solvent (NADES): Temperature Dependent Time-Resolved Fluorescence Measurements” by **Ejaj Tarif**, Jayanta Mondal and Ranjit Biswas (**JPC B, 2019, Under Revision**)
7. “Dynamics at the non-ionic micelle/water interface: Impact of linkage substitution” by **Ejaj Tarif**, Kallol Mukherjee, Kajal Kumbhakar, Anjan Barman and Ranjit Biswas (**JCP, 2019, Submitted**)
8. “Interaction and dynamics in betaine based deep eutectic solvent: Temperature dependent time-resolved fluorescence spectroscopic measurements” by **Ejaj Tarif**, Jayanta Mondal and Ranjit Biswas (**To be submitted**)

9. *“Diffusion in Ionic Acetamide Deep Eutectic Solvents: Fluorescence Up-conversion and Fluorescence Correlation Spectroscopic Measurements”* by Navin Subba, **Ejaj Tarif**, Pratik Sen, and Ranjit Biswas (**To be submitted**)
10. *“Temperature dependent dielectric relaxation dynamics of (acetamide+electrolyte) deep eutectic solvents in the frequency window $0.2 \leq \nu / \text{GHz} \leq 50$ ”* by Kallol Mukherjee, Suman Das, **Ejaj Tarif**, Anjan Barman and Ranjit Biswas (**To be submitted**)
11. *“Effects of functional group of the hydrogen bond donor in choline chloride based DESs-A fluorescence spectroscopic outlook”* by Anuradha Das, Ejaj Tarif and Ranjit Biswas (**To be submitted**)
12. *“Anomalous dynamics in aqueous hyaluronic acid gel: A probe dependent fluorescence study”* by **Ejaj Tarif**, Kajal Kumbhakar, Kallol Mukherjee, and Ranjit Biswas (**Manuscript in Preparation**)
13. *“Interaction and dynamics in cryoprotectant systems based on polyhydroxy alcohols and sugars: Temperature dependent fluorescence measurements”* by Kajal Kumbhakar, **Ejaj Tarif**, and Ranjit Biswas (**Manuscript in Preparation**).
14. *“Fluorescence spectroscopic study of proline based DES: Temperature dependent fluorescence spectroscopic study”* by Jayanta Mondal, **Ejaj Tarif** and Ranjit Biswas (**Manuscript in Preparation**)

Contents

Chapter 1: Introduction.....	1
Chapter 2: Experimental Techniques and Data Analysis Methods.....	15
2.1 Steady State Absorption Data Collection.....	15
2.2 Steady State Fluorescence Data Collection.....	16
2.3 TCSPC Technique.....	17
2.4 Data Analysis.....	18
2.4.1 Solvation Dynamics.....	18
2.4.2 Rotational Dynamics.....	20
2.5 Dielectric Relaxation Spectroscopy.....	22
2.5.1 Introduction.....	22
2.5.2 Measurements.....	23
2.5.3 Different Mathematical Models and Data Analysis.....	24
2.5.3.1 Debye Model.....	24
2.5.3.2 Non-Debye Model.....	24
2.5.3.3 Data Processing.....	25
2.5.3.4 Conductivity Corrections.....	26

Chapter 3: Interaction and Dynamics in a Fully Biodegradable Glucose-Containing Naturally Abundant Deep Eutectic Solvent (NADES): Temperature Dependent Time-Resolved Fluorescence Measurements.....28

3.1 Introduction.....28

3.2 Experimental Details.....30

3.2.1 Materials and Sample Preparation.....30

3.2.2 Steady State Measurements.....32

3.2.3 Time-Resolved Fluorescence Measurements.....32

3.3 Results and Discussion.....32

3.3.1 Steady State Spectroscopic Results.....32

3.3.2 Solute Rotation and Viscosity Coupling.....34

3.3.3 Solvation Dynamics.....40

3.4. Conclusion.....44

Chapter 4: Interaction and Dynamics in Betaine Based Deep Eutectic Solvent: Temperature Dependent Time-Resolved Fluorescence Spectroscopic Measurements.....51

4.1 Introduction.....51

4.2 Experimental Details.....53

4.2.1 Sample Preparation.....53

4.2.2 Steady State Measurements.....54

4.2.3 Time-Resolved Fluorescence Measurements.....	54
4.3 Results and Discussion.....	55
4.3.1 Steady State Absorption and Emission of Two Different Probes: Hydrophobic C153 and Hydrophilic C343.....	55
4.3.2 Solute Rotation: Coupling with Medium Viscosity.....	57
4.3.3 Solvation Dynamics.....	62
4.4 Conclusion.....	64
Chapter 5: Are Water-Xylitol Mixtures Heterogeneous? An Investigation Employing Composition and Temperature Dependent Dielectric Relaxation and Time-Resolved Fluorescence Measurements.....	72
5.1 Introduction.....	72
5.2 Experimental Details.....	75
5.2.1 Sample Preparation.....	75
5.2.2 Viscosity and Refractive Index Measurements.....	76
5.2.3 Steady State and Time-Resolved Fluorescence Measurements.....	76
5.2.4 Dielectric Relaxation Spectroscopy.....	76
5.3 Results and Discussion.....	77
5.3.1 Dielectric Relaxation Measurements: Concentration and Temperature Dependence.....	77
5.3.2 Steady State Measurements.....	81
5.3.3 Time-Resolved Fluoresce Measurements.....	85

5.4. Conclusion.....	89
----------------------	----

Chapter 6: Exploring Aqueous Solution Dynamics of an Amphiphilic Diblock Copolymer: Dielectric Relaxation and Time-Resolved Fluorescence Measurements.....94

6.1 Introduction.....	94
-----------------------	----

6.2 Experimental Section.....	96
-------------------------------	----

6.2.1 Materials and Sample Preparation.....	96
---	----

6.2.2 Dynamic Light Scattering (DLS).....	97
---	----

6.2.3 Density, Viscosity and Refractive Index Measurements.....	97
---	----

6.2.4 Steady State Measurements.....	97
--------------------------------------	----

6.2.5 Time-Resolved Fluorescence Measurements.....	97
--	----

6.2.6 Dielectric Relaxation Spectroscopy.....	98
---	----

6.3 Results and Discussion.....	98
---------------------------------	----

6.3.1 Self-Assembly Behaviour of the Diblock Copolymers.....	98
--	----

6.3.2 Steady State Absorption and Emission.....	99
---	----

6.3.3 Solute Rotation and Probe Location.....	101
---	-----

6.3.4 Dielectric Relaxation.....	105
----------------------------------	-----

6.4 Conclusion.....	107
---------------------	-----

Chapter 7: Dynamics at the Non-Ionic Micelle/Water Interface: Impact of Linkage Substitution.....112

7.1 Introduction.....112

7.2 Experimental Section.....114

7.2.1 Sample Details.....114

7.2.2 Density and Viscosity Measurements.....115

7.2.3 Dynamic Light Scattering (DLS) Measurements.....115

7.2.4 Differential Scanning Calorimetric (DSC) Measurements.....115

7.2.5 Steady State Measurements.....115

7.2.6 Time-Resolved fluorescence measurements.....115

7.2.7 Dielectric Relaxation Spectroscopy116

7.3. Results and Discussion.....116

7.3.1 Steady State Measurements.....116

7.3.2 Time-Resolved Fluorescence Measurements.....118

7.3.2.1 Rotational Anisotropy Decay, $r(t)$, Analysis: Slower
Probe Rotation in OTG.....118

7.3.2.2 Solvation Dynamics Study: Slower Solvation in OTG.....121

7.3.3 DRS Data Analysis.....124

7.4. Conclusion.....125

Chapter 8: Concluding Remarks and Future Problems.....	132
8.1 Temperature Dependent Dielectric Relaxation (DR) Study of Naturally Abundant Deep Eutectic Solvents (NADESs)	132
8.2 Heterogeneity Aspects in Non-Ionic DESs: Temperature Dependent Time-Resolved Fluorescence and Dielectric Relaxation Measurements.....	133
8.3 Interaction and Dynamics of Amino Acid Based Deep Eutectic Solvents: Temperature Dependent TRF and DRS Measurements.....	133
8.4 Impact of the Spacer (-CH ₂ -) on the Dynamics and Physical Properties of Amino Acid Based DESs.....	134
8.5 High Viscous NADES Based on Glucose, Tartaric Acid and Water.....	134
8.6 Acid-Induced Fluorescence of Polyethylenimine (PEI) Aggregates: A Spectroscopic Study.....	134
 Appendix A.a.....	136
Appendix A.b.....	148
Appendix A.c.....	155
Appendix A.d.....	158
Appendix A.e.....	170

Chapter 1

Introduction

Solvents are essential and critical part of industrial processes covering synthesis, purification, drying, filtration, cleaning, and a gamut of other applications. As chemical reactions, yield, extraction, dissolution, biological functions etc. strongly depend on a variety of solvent properties that include dissolution power, polarity, viscosity, volatility, inflammability, electrochemical window, thermal resistance and, most importantly, ecological footprint. Large-scale commercial application demands cost-effective handling, transportation and usage protocol. Low procurement cost, easy recovery and recyclability construct a symbiotic loop between the production end and the users' space, and provides a window for generating new classes of solvents through liquid solvent engineering in order to serve the desired purpose.¹⁻¹³ Unfortunately, a large portion of industrial solvents are conventional organic solvents and many of these are tagged with environmental and health issues.¹⁴⁻¹⁸ Hence, a search for eco-friendly, cost effective alternative to the conventional organic solvent with desirable properties has led to the invention of new classes of solvents: gas expanded liquids (GXLs),¹⁹⁻²¹ room temperature super critical fluids (RTSFs),²²⁻²⁴ room temperature ionic liquids (RTILs),²⁵⁻²⁸ deep eutectic solvents (DESs)²⁹⁻³⁴ etc. Among these non-conventional alternatives some are eco-friendly or with low ecological footprint, DESs are considered to be a few steps ahead because of their low cost, easy transportation and preparation route, and moreover, a huge number of probable combinations of constituents for preparation of DESs. These properties open up several possibilities to get eco-friendly solvents with desirable properties.^{31,35-46} DESs are multi-component molten mixtures with a much lower melting temperature (T_m) than that of the individual constituents. Deep depression of freezing point of DESs is the outcome of extensive H-bonding among the ingredients and gain in entropy due to the transformation from solid to liquid state. For the universal necessity of low toxic, biocompatible and biodegradable solvents or reaction media, attempts have been made to find out solutions from the Nature itself. This has led to the findings of naturally abundant deep eutectic solvents (NADES), prepared from primary metabolites, such as amino acids, organic acids, urea, sugars. This satisfies the primary aspect of non-hazardous solvent systems because of their inherent greenness and eco-sustainability.^{36,43,47-}

⁵⁰ Interestingly, these NADESs have been used extensively in solubilization of organic

compounds, therapeutic system, biotransformation, biodiesel production, extraction of bioactive substances, CO₂ and SO₂ absorption, Li-ion batteries, as drug carrier and reaction media.^{35,43,51-60} Therefore, DESs, as designer solvents, demand comprehensive understanding for smart and vast applications in industry. Here basic science research can contribute to a large extent, and assist significantly to the appropriate choice and smarter applications for solvent systems through supplying the critical knowledge needed to tailor reactions for desired products.

Structure and functionality of biologically important molecules like proteins depend on the interaction of their building blocks (amino acids) with cell fluid such as water.⁶¹⁻⁶⁵ Thus, understanding the interaction of biomolecules with water is important. Interestingly, in many cases these interactions are tuned with the introduction of osmolytes (sugar, polyhydroxy alcohol) during the protection of the protein at a very low temperature. This is cryopreservation of bio-moieties. Aqueous solutions of sugar or polyhydroxy alcohol are known to stabilize proteins and other biological substances.⁶⁵⁻⁶⁹ This has been done by tuning the interspecies interaction in the system. There seems to be a relationship between cryoprotection and solution-phase spatio-temporal heterogeneity,⁷⁰ although a well-documented investigative study on this inter-connection is yet to be conducted. Therefore, a thorough understanding of microscopic interaction and dynamics in aqueous phase of amino acid, sugar, polyhydroxy alcohol and their mixtures is essential for broad-spectrum applications and specific use, such as, cryo-preservation.

Miscellaneous biomimetic self-assembled structures like micelles, reverse micelles, vesicles, macromolecules and polymer aggregates with multifarious morphology are in extensive use in several fields: Their usage include as nanocarriers for drug and gene delivery, diagnostic imaging agents, and as model systems for confined reaction media.⁷¹⁻⁷⁵ Research on these complex systems has been continued for the last several decades and still continuing. Interfacial heterogeneity of the confined systems has an impact on reactions occurring at interfaces.^{76,77} A thorough knowledge of microenvironment structure, dynamics and interaction of biomimetic systems is therefore essential for applications.

Photo-physics deals with study of physical properties of targeted materials or molecules through radiation-matter interaction. In the present context this connects to measurements of quantum yields, excited state fluorescence lifetimes, radiative and non-radiative rates of a fluorescent molecule. These are inherent properties of a probe solute, and a given medium can have non-

trivial impact on these properties. Consequently, these probe solutes are often used as reporters for probing polarity and relaxation dynamics in host media. Photo excitation changes the dipole moment of such dipolar probe molecules (dissolved at a very low concentration in a medium) through charge redistribution. In time-resolved studies, this change in solute dipole moment is initiated by shining it with a laser pulse, and then the fluorescence energy is followed as a function of time. When this fluorescent solute is dissolved in a solvent, the time-dependent fluorescence carries the information regarding the dynamic readjustment of the host solvent molecules in a response to the sudden change in the solute dipole moment. With time the fluorescence energy changes to lower energy and this can be tracked via the dynamic (or time-resolved) fluorescence Stokes shift measurements.^{78,79} Interestingly, time-resolved Stokes shift measurements are frequently utilized to understand interaction and dynamics in a given medium.⁸⁰⁻⁹²

Study of photophysics and dynamics of complex chemical systems is extremely important for a variety of reasons. For example, selection of a correct reaction medium for a particular chemical reaction is predominantly guided by the knowledge of reaction timescale and the timescale of solvent reorganization. While understanding reaction timescale falls in the domain of photophysics, exploring solvent effects brings in the dynamical studies in the scenario. The interrelationship between solvent effects and reaction kinetics then creates the necessary symbiosis between theory and experiments, and provides the crucial tool for optimization. This optimization has greater importance for biological systems because numerous chemical reactions occur inside living cells in complex environments at mild thermodynamic conditions following catalytic pathways. Note in dynamic Stokes shift measurements it is assumed that the excited solute does not influence natural dynamics of the medium. Initially, at ground state (S_0) dissolved solute remains in equilibrium with its surrounding (solvents). Photo excitation with proper light (energy) leads solute to the first excited state (S_1) followed by charge redistribution. In this scenario solvent dipoles arrange themselves in a way that the energy of the solute-solvent composite system gets minimized. The time evolution of this energy minimization process reflected in time-resolved emission spectra (TRES) of the solute. Note the relaxation dynamics is associated with the rearrangement of solvent molecules and have an impact over reaction rate occurring within the medium.^{79,93-96} Apart from the time dependent solvent relaxation and other associated phenomena, solvation dynamics measurements also reveal information regarding

intermolecular interactions.⁹⁷⁻⁹⁹ Another important method, dynamic fluorescence anisotropy measurements, provide information about frictions exerted by the medium to a rotating solute dissolved in it. Time-resolved fluorescence anisotropy measurement uncover solute-medium interaction and is complementary to dynamic Stokes shift measurements.^{87-90,100-103} Stokes shift and dynamic anisotropy measurements together serve as an efficient tool to map the dynamic friction exerted by a given medium, and is the only way to visualize a microscopic quantity like dynamic friction.

Steady state fluorescence spectroscopy has also contributions to reveal the medium structure and its interaction with the dipolar solute probe. Photoexcited solutes emit from lowest vibrational level of completely equilibrated first singlet excited state (S_1) irrespective of the excitation wavelength ($\lambda_{exc.}$) (Kasha's rule).^{104,105} However, red shift is observed for fluorescence emission with longer excited wavelengths of a dissolved solute in several complex media.^{70, 89,97,106-108} This red shift with longer excitation wavelength emerges due to the different microscopic environment with solvent density fluctuation timescale comparable or less than the lifetime of solute probe. Observation of such excitation energy dependence suggest heterogeneous solvation environment around the probe molecule.

Dynamics of dipolar molecules can be measured using dielectric relaxation spectroscopy (DRS). This is different from dynamic Stokes shift measurements in the sense that DRS does not need any foreign molecule as a reporter, and thus the inherent dynamics of a pristine medium is directly probed. In DRS measurements frequency dependent electromagnetic field is employed to perturb the dipolar system under investigation, and subsequent polarization response of the medium particles are monitored as a function of frequency.¹⁰⁹⁻¹¹⁵ This technique is useful to report reorientational dynamics (of dipoles) occurring within the timescale ranging from a few picoseconds to nanoseconds in a MHz-GHz frequency window, and has been successfully employed for various complex systems.¹¹⁶⁻¹²⁰ However, this method has not been extensively used in the present Thesis work; rather has been used as a complementary experimental method in some cases to augment discussion of results obtained via fluorescence spectroscopy.

In this Thesis we have explored temperature dependent interaction and dynamics of DESs, temperature and compositions dependent medium heterogeneity of water-polyhydroxy alcohols

mixtures, interfacial solution phase dynamics of amphiphilic diblock copolymer and alkyl polyglucosides (APGs) surfactants. All these have been performed by employing steady state, time-resolved fluorescence spectroscopy and dielectric relaxation spectroscopy.^{121,122}

In chapter 2 details of experimental techniques, data recording process and method of data analysis are discussed.

In chapter 3 we have discussed preparation of a new room temperature DES composed of glucose, urea, water (6:4:1; weight ratio) and also explored its relaxation dynamics via temperature dependent time-resolved fluorescence measurements employing hydrophilic and hydrophobic solute probes. Differential scanning calorimetry (DSC) measurements indicate a glass transition temperature (T_g) of ~ 236 K. Measured viscosity coefficients (η) vary from ~ 600 cP to ~ 100 cP in the temperature range, $318 \leq T/K \leq 343$, and exhibit Arrhenius-type temperature dependence with an activation energy ~ 65 kJmol⁻¹. Interestingly, this DES forms a stable liquid at ~ 300 K but is too viscous to be accurately measured by us below 318 K. Temperature dependent dynamic fluorescence anisotropy measurements using hydrophobic and hydrophilic solutes of similar sizes reveal bi-exponential kinetics, and Arrhenius-type temperature dependence for solute rotation times ($\langle \tau_r \rangle$) but with significantly decreased activation energies, ~ 31 kJmol⁻¹ (hydrophobic) and ~ 21 kJmol⁻¹ (hydrophilic). Deviation from hydrodynamics is further reflected in the strong fractional viscosity dependence of $\langle \tau_r \rangle$: $\langle \tau_r \rangle \propto (\eta/T)^p$ with $p \sim 0.3-0.5$, indicating pronounced temporal heterogeneity in the relaxation dynamics. Dynamic fluorescence Stokes shift measurements (temporal resolution ~ 85 ps) produce dynamic shifts of $\sim 500-700$ cm⁻¹, bi-exponential solvation energy relaxation with time constants in the range ~ 0.2 ns and ~ 4 ns, and estimated missing amplitudes of $\sim 65-75\%$. Impact of density difference between non-polar solvent and this DES on the estimated missing amplitudes is explored via measuring the temperature dependent densities and refractive indices of this DES. Lifetime measurements suggest considerable temperature dependence for the hydrophobic solute but no such dependence for the hydrophilic one. Excitation energy dependence of fluorescence emission of various solutes with widely different lifetimes indicates mild spatial heterogeneity for this DES.

Chapter 4 contain details about the preparation of deep eutectic solvent composed of betaine, urea and water (11.7:12:1; weight ratio), and study of its interaction and dynamics using temperature dependent time-resolved fluorescence measurements. We have employed two different solute probes, hydrophilic and hydrophobic. Temperature dependent measurements of solution density, refractive index and viscosity coefficient of DES have been performed for characterization and understanding the time-resolved fluorescence response of different solutes dissolved in this DES. This DES is highly viscous with viscosity coefficient $\sim 45\text{-}430$ cP in the temperature range measured. All measurements have been done in a temperature range $\sim 90 - 130$ K above the thermodynamic glass transition temperature ($T_g \sim 218$ K from DSC measurements) for this tri-component DES. Steady state fluorescence measurements employing different probes with disparate lifetimes suggest near-homogeneity in the solution structure. However, time-resolved fluorescence anisotropy measurements employing a couple of these fluorescent probes that differ in chemical nature (hydrophobic or hydrophilic) suggest a strongly heterogeneous relaxation dynamics through a fractional viscosity dependence of the measured solute rotation times, $\langle \tau_r \rangle \propto (\eta/T)^p$, with $p \sim 0.5$. Dynamic Stokes shift measurements reflect observed dynamic shifts in the $500\text{-}700$ cm^{-1} range with missing amplitude of $\sim 65\text{-}75\%$. Temperature dependent bi-exponential solvation response functions with time constants of ~ 0.2 ns and ~ 4 ns have been detected, and these timescales have been argued to originate from orientational relaxations coupled to collective structural H-bond fluctuations.

Aqueous xylitol solutions at six different concentrations were studied in chapter 5 employing dielectric relaxation (DR) and time-resolved fluorescence (TRF) measurements in the temperature range $295 - 323$ K. The focus was to explore the solution heterogeneity aspect via monitoring the viscosity coupling of the average relaxation rates at various temperatures. TRF measurements were done using both hydrophobic and hydrophilic probes to explore the preferences, if any, for solute locations in these binary mixtures. Energy selective population excitations and the corresponding fluorescence emissions did not suggest any significant spatial heterogeneity in solution structure within the lifetimes of these probes. DR measurements and TRF experiments indicated mild deviations from the hydrodynamic viscosity dependence of the measured relaxation rates. All these suggest mild spatio-temporal heterogeneity for these water-xylitol mixtures in the temperature range considered. In addition, DR timescales appear to

originate from reorientational and H-bond relaxation dynamics, excluding the possibility of full molecular rotations.

In chapter 6 we explored interactions of amphiphilic diblock copolymers (these polymer were synthesized and characterized by Prof. Priyadarsi De's group, IISER, Kolkata)¹²¹ with water molecules and the subsequent aqueous solution dynamics by employing time-resolved fluorescence measurements (TRF) and megahertz-gigahertz dielectric relaxation (DR) experiments. The synthesized amphiphilic diblock copolymer is poly(2-(((*tert*-butoxycarbonyl)alanyl)oxy)ethyl methacrylate)-*b*-poly(polyethylene glycol monomethyl ether methacrylate) (P(Boc-L-Ala-HEMA)-*b*-PPEGMA)).¹²¹ Dynamic light scattering (DLS) measurements of aqueous solutions indicate the formation of 14-20 nm particles, from the balance between the chain lengths of the hydrophobic (P(Boc-L-Ala-HEMA)) and hydrophilic (PPEGMA) segments. The critical micelle concentration (CMC) of the P(Boc-L-Ala-HEMA)-*b*-PPEGMA block copolymer at different block lengths in aqueous media, determined *via* steady state fluorescence measurements, is very low (~4-8 mg/L), and the resultant micellar size has been found to be insensitive to the polymer concentration. Interfacial and bulk aqueous dynamics have been investigated by tracking the solution frictional resistance on rotational motion of dissolved hydrophobic and hydrophilic dipolar solute probes of comparable sizes. Time-resolved fluorescence anisotropy measurements reflect biphasic temporal profile for the frictional resistance. Interestingly, the hydrophobic probe, due to its preferential location at the micellar interface, experiences greater frictional resistance than the hydrophilic counter-part, although the latter reports stronger polymer concentration dependence of the frictional retardation than the former. DR measurements at the highest of the polymer concentrations considered, suggest the presence of aqueous dynamics slower than that for neat bulk water, although evidence for such “slow” dynamics at lower concentrations has not been detected in the present DR measurements.

In chapter 7 we have made an attempt to explore the impact of substituting the glycoside linkage, the connector atom in between the head and the tail part of the surfactant, by the thioglycoside linkage on the dynamics at the non-ionic surfactant/water interface of the micelles employing time-resolved fluorescence (TRF) and dielectric relaxation (DR) spectroscopic techniques. We have utilized *n*-octyl- β -D-glucopyranoside (OG) and *n*-octyl- β -D-thioglucoopyranoside (OTG) as non-ionic surfactants and coumarin 153 (C153) as a primary local reporter for optical

measurements. There is no significant difference in the steady state spectral features of C153 for these two surfactant solutions, however comparison of the same with pure water gives us an idea about the probe location in both the mediums and later it has been confirmed by the TRF measurements. Dynamic light scattering (DLS) measurements in these solutions suggests that the OTG micelles are ~ 4 times larger than the OG micelles. Interestingly, significant differences in the rotational and solvation dynamics of the probe molecule in these two micellar solutions have been revealed by the TRF measurements. Moreover, we have not found any signature of bound water molecules in our dielectric relaxation spectroscopic (DRS) and differential scanning calorimetric (DSC) measurements for studied surfactant concentrations. Nevertheless, like other surfactant molecules, here also we have observed slow solvation dynamics of the fluorescent probe molecule, despite of having no slow water dynamics (other than bulk water dynamics) in DRS measurements. Solute motion has been argued to be the origin for this slow solvation component as DR measurements do not indicate presence of comparable relaxation component from the medium.

Thesis ended with chapter 8, contains conclusion and some relevant future problems.

References:

1. G. R. Fleming and P. G. Wolynes, *Phys. Today* **43**, 36 (1990).
2. J. T. Hynes, *Ann. Rev. Phys. Chem.* **36**, 573 (1985).
3. P. J. Rossky and J. D. Simon, *Nature* **370**, 263 (1994).
4. G. Carrea, G. Ottolina, S. Riva, *Trends in Biotechnology* **13**, 63 (1995).
5. A. C. Kumoro, M. Hasan and H. Singh, *Science Asia* **35**, 306 (2009).
6. S. Visht and S. Chaturvedi, *CPR* **2**, 584 (2012).
7. L. A. Johnson and E. W. Lusas, *JAOCS* **60**, 229 (1983).
8. E. A. Brignole, S. Bottini and R. Gani, *Fluid Phase Equilib.* **29**, 125 (1986).
9. L. C. Garzón and F. Martínez, *J. Solution Chem.* **33**, 1379 (2004).
10. A. Grubenmann, *Dyes and Pigments* **21**, 273 (1993).
11. P. M. Wiggins, *Microbiol Res.* **54**, 432 (1990).
12. L. D. Barron, L. Hecht, G. Wilson, *Biochemistry* **36**, 13143 (1997).
13. E. A. Vogler, *Adv. Colloid Interface Sci.* **74**, 69 (1998).
14. M. Ikeda, *Toxicol. Lett.* **64**, 191 (1992).
15. M. Aksoy, *Environ. Health Perspect.* **82**, 193 (1989).
16. B. W. Lee, K. T. Kelsey, D. M. Hashimoto, B. Yakes and T. Seitz, *J. Occup. Environ. Med.* **39**, 960 (1997).
17. D. Majumdar, C. Dutta and S. Sen, *Transport. Res. D-TR E.* **13**, 524 (2008).
18. D. Prat, J. Hayler and A. Wells, *Green Chem.* **16**, 4546 (2014).
19. A. M. Scurto, K. Hutchenson and B. Subramaniam, *ACS Symposium Series*, **1006**, 3 (2009).
20. J. P. Hallett, C. L. Kitchens, R. Hernandez, C. L. Liotta and C. A. Eckert, *Acc. Chem. Res.* **39**, 531 (2006).
21. C. A. Eckert, C. L. Liotta, D. Bush, J. S. Brown and J. P. Hallett, *J. Phys. Chem. B* **108**, 18108 (2004).
22. C. A. Eckert, B. L. Knutson and P. G. Debenedetti, *Nature* **383**, 313 (1996).
23. J. E. Lewis, R. Biswas, A. G. Robinson, and M. Maroncelli, *J. Phys. Chem. B* **105**, 3306 (2001).
24. S. V. Dzyuba and R. A. Bartsch, *Angew. Chem. Int. Ed.* **42**, 148 (2003).
25. M. J. Earle and K. R. Seddon, *Pure Appl. Chem.* **72**, 1391 (2000).

26. M. Maroncelli, X. X. Zhang, M. Liang, D. Roy and N. P. Ernsting, *Faraday Discuss.* **154**, 409 (2012).
27. B. L. Bhargava and S. Balasubramanian, *J. Phys. Chem. B* **111**, 4477 (2007).
28. H. K. Kashyap and R. Biswas, *J. Phys. Chem. B* **112**, 12431 (2008).
29. E. L. Smith, A. P. Abbott, K. S. Ryder, *Chem. Rev.* **114**, 11060 (2014).
30. Q. H. Zhang, K. D. O. Vigier, S. Royer, F. Jerome, *Chem. Soc. Rev.* **41**, 7108 (2012).
31. M. Francisco, A. Bruinhorst, and M. C. Kroon, *Angew. Chem. Int. Ed.* **52**, 3074 (2013).
32. B. Guchhait, S. Das, S. Daschakraborty and R. Biswas, *J. Chem. Phys.* **140**, 104514 (2014).
33. A. Das, S. Das and R. Biswas, *Chem. Phys. Lett.* **581**, 47 (2013).
34. K. Mukherjee, S. Das, E. Tarif, A. Barman, and R. Biswas, *J. Chem. Phys.* **149**, 124501 (2018).
35. A. Paiva, R. Craveiro, I. Aroso, M. Martins, R. L. Reis and A. R. C. Duarte, *ACS Sustainable Chem. Eng.* **2**, 1063 (2014).
36. A. P. Abbott, D. Boothby, G. Capper, D. L. Davies, and R. K. Rasheed, *J. Am. Chem. Soc.* **126**, 9142 (2004).
37. D. V. Wagle, H. Zhao and G. A. Baker, *Acc. Chem. Res.* **47**, 2299 (2014).
38. P. D. de María and Z. Maugeri, *Curr. Opin. Chem. Biol.* **15**, 220 (2011).
39. J. H. Clark and S. J. Tavener, *Org. Process Res. Dev.* **11**, 149 (2007).
40. W. M. Nelson, *Green solvents for chemistry, Perspectives and Practice*, New York, NY: Oxford University Press New York, 2003.
41. J. M. DeSimone, *Science* **297**, 799 (2002).
42. A. Das, S. Das, R. Biswas *J. Chem. Phys.* **142**, 034505 (2015).
43. M. Espino, M. Á. Fernández, F. J. V. Gomez and M. F. Silva, *TrAC Trends in Analytical Chemistry* **76**, 126 (2016).
44. K. Mukherjee, E. Tarif, A. Barman, R. Biswas, *Fluid Phase Equilib.* **448**, 22 (2017).
45. M. Francisco, A. van den Bruinhorst, and M.C. Kroon, *Green Chem.* **14**, 2153 (2012).
46. S. Rajkhowa, A. Das, S. Mahiuddin, and R. Biswas, *J. Chem. Eng. Data* **57**, 3467 (2012).
47. Y. Dai, J. van Spronsen, G.-J. Witkamp, R. Verpoorte and Y. H. Choi, *Anal. Chim. Acta* **766**, 61 (2013).
48. S. Gore, S. Baskaran, and B. Koenig, *Green Chem.* **13** 1009 (2011).

49. W-C. Huang, D. Zhao, N. Guo, C. Xue and X. Mao, *J. Agric. Food Chem.* **66**, 11897 (2018).
50. Y. H. Choi, J. van Spronsen, Y. Dai, M. Verberne, F. Hollmann, Isabel W.C.E. Arends, G. J. Witkamp, and R. Verpoorte, *Plant Physiol.* **156**, 1701 (2011).
51. E. Durand, J. Lecomte, B. Baréa, G. Piombo, E. Dubreucq and P. Villeneuve, *Process Biochem.* **47**, 2081 (2012).
52. A. Hayyan, M. A. Hashim, M. Hayyan, F. S. Mjalli and I. M. AlNashef, *J. Clean. Prod.* **65**, 246 (2014).
53. Z-F. Wei, X-Q. Wang, X. Peng, W. Wang, C-J. Zhao, Y-G. Zu, Y-J. Fu, *Ind. Crop. Prod.* **63**, 175 (2015).
54. R. J. Sánchez-Leija, J. A. Pojman, G. Luna-Bárcenas, and J. D. Mota-Morales, *J. Mater. Chem. B* **2**, 7495 (2014).
55. M. H. Zainal-Abidin, M. Hayyan, A. Hayyan and N. S. Jayakumar, *Anal. Chim. Acta* **979**, 1 (2017).
56. M. Faggian, S. Sut, B. Perissutti, V. Baldan, I. Grabnar and S. Dall'Acqua, *Molecules* **21**, 1531 (2016).
57. I. M. Aroso, R. Craveiro, Â. Rocha, M. Dionísio, S. Barreiros, R. L. Reis, A. Paiva and A. R. C. Duarte, *Int. J. Pharm.* **492**, 73 (2015).
58. M. B. Haider, D. Jha, B. M. Sivagnanam and R. Kumar, *J. Chem. Eng. Data* **63**, 2671 (2018).
59. S. Sun, Y. Niu, Q. Xu, Z. Sun, and X. Wei, *Ind. Eng. Chem. Res.* **54**, 8019 (2015).
60. L. Millia, V. Dall'Asta, C. Ferrara, V. Berbenni, E. Quartarone, F. M. Perna, V. Capriati, P. Mustarelli, *Solid State Ionics* **323**, 44 (2018).
61. B. Alberts, A. Johnson, J. Lewis, M. Raff, K. Roberts and P. Walter, New York: Garland Science; 2002.
62. L. Degreve, G.H. Brancaleoni, C. A. Fuzo, M.R. Lourenzoni, F.M. Mazze, A.M. Namba, and D.S. Vieira, *Brazilian Journal of Physics*, **34**, 102 (2004).
63. P. Csermely, *Cell. mol. Biol.* **47**, 0145-5680/01 (2001).
64. J. D. Batchelor, A. Olteanu, A. Tripathy and G. J. Pielak, *J. Am. Chem. Soc.* **126**, 1958 (2004).
65. J. K. Kaushik and R. Bhat, *J. Phys. Chem. B* **102**, 7058 (1998).

66. N. Gheibi, A. A. Saboury, K. Haghbeen and A. A. Moosavi-Movahedi, *J. Biosci.* **31** 355 (2006).
67. J. F. Back, D. Oakenfull and M. B. Smith, *Biochemistry* **18** (23), 5191(1979).
68. N. K. Jain and I. Roy *Protein Sci.* **18**, 24 (2009).
69. S. Ohtake, Y. J. Wang, *J Pharm Sci.* **100**, 2020 (2011).
70. S. Indra and R. Biswas, *J. Phys. Chem. B* **120**, 11214.
71. K. Kataoka, A. Harada, Y. Nagasaki, *Adv. Drug Deliv. Rev.* **47**, 113 (2001).
72. X. B. Xiong, A. Falamarzian, S. M. Garg, and A. Lavasanifar, *J. Controlled Release* **155**, 248 (2011).
73. S. Mukherjee, H. Dinda, L. Shashank, I. Chakraborty, R. Bhattacharyya, J. D. Sarma, R. Shunmugam, *Macromolecules* **48**, 6791 (2015).
74. T. Dwars, E. Paetzold, G. *Angew. Chem. Int. Ed.* **44**, 7174 (2005).
75. U. Mandal, S. Ghosh, S. Dey, A. Adhikari, K. Bhattacharyya, *J. Chem. Phys.* **128**, 164505 (2008).
76. B. Samiey, C.-H. Cheng, J. Wu, *J. Chem.* **2014**, 908476 (2014).
77. N. Nandi, K. Bhattacharyya, B. Bagchi, *Chem. Rev.* **100**, 2013 (2000).
78. . B. Bagchi, D. W. Oxtoby and G. R. Fleming, *Chem. Phys.* **86**, 257 (1984).
79. M. Maroncelli, J. MacInnis and G. R. Fleming, *Science* **243**, 1674 (1989).
80. M. L. Horng, J. A. Gardecki, A. Papazyan and M. Maroncelli, *Phys. Chem.* **99**, 17311 (1995).
81. K. Bhattacharyya, *Acc. Chem. Res.* **36**, 95 (2003).
82. R. Jimenez, G. R. Fleming, P. V. Kumar and M. Maroncelli, *Nature* **369**, 471 (1994).
83. W. H. Thompson, *Annu. Rev. Phys. Chem.* **62**, 599 (2011).
84. H. Shirota, A. M. Funston, J. F. Wishart and E. W. Castner, Jr. *J. Chem. Phys.* **122**, 184512 (2005).
85. R. E. Riter, E. P. Undiks and N. E. Levinger, *J. Am. Chem. Soc.* **120**, 6062 (1998).
86. R. Karmakar and A. Samanta, *J. Phys. Chem. A* **106**, 4447 (2002).
87. B. Guchhait, R. Biswas and P. K. Ghorai, *J. Phys. Chem. B* **117**, 3345 (2013).
88. B. Guchhait and R. Biswas, *J. Chem. Phys.* **140**, 104514 (2014).
89. A. Das and R. Biswas, *J. Phys. Chem. B* **119**, 10102 (2015).

90. S. Indra and R. Biswas, *J. Phys. Chem. B* **120**, 11214 (2016).
91. K. Mukherjee, A. Barman and R. Biswas, *J. Mol. Liq.* **222**, 495 (2016).
92. R. S. Moog and M. Maroncelli, *J. Phys. Chem.* **95**, 10359 (1991).
93. M. L. Horng, K. Dahl, G. Jones II and M. Maroncellia, *Chem. Phys. Lett.* **315**, 363 (1999).
94. M. Liu, N. Ito, M. Maroncelli, D. H. Waldeck, A. M. Oliver and M. N. Paddon-Row, *J. Am. Chem. Soc.* **127**, 17867 (2005).
95. G. v. d. Zwan and J. T. Hynes, *Chem. Phys.* **152**, 169 (1991).
96. J. T. Hynes, J. D. Simon, (editor) : *Charge-Transfer Reactions and Solvation Dynamics in Ultrafast Dynamics of Chemical Systems*, Kluwer, Dodrecht, (1994); p345.
97. J. R. Lakowicz, *Principles of Fluorescence Spectroscopy*. New York : Kluwer Academic/Plenum, **1999**.
98. H. Lee, G. Lee, J. Jeon, and M. Cho, *J. Phys. Chem. A* **116**, 347 (2012).
99. H. A. R. Gazi and R. Biswas, *J. Chem. Sci.* **123**, 265 (2011).
100. M.-L. Horng, J. A. Gardecki and M. Maroncelli, *J. Phys. Chem. A* **101**, 1030 (1997).
101. G. B. Dutt, *Chem. Phys. Chem.* **6**, 413 (2005).
102. G. B. Dutt and T. K. Ghanty, *J. Phys. Chem. A* **108**, 6090 (2004).
103. A. Das, R. Biswas and J. Chakrabarti, *Chem. Phys. Lett.* **558**, 36 (2013).
104. M. Kasha, *Discuss. Faraday Soc.* **9**, 14 (1950).
105. J. B. Birks, *Photophysics of Aromatic Molecules*; Wiley-Interscience: London, 1970.
106. A. Samanta, *J. Phys. Chem. B*, 2006, 110, 13704.
107. A. P. Demchenko, *Luminescence* **17**, 19 (2002).
108. K. Itoh and T. Azumi, *J. Chem. Phys.* **62**, 3431 (1975).
109. D. W. Davidson and R. H. Cole, *J. Chem. Phys.* **19**, 1484 (1951).
110. U. Kaatze and K. Giese, *J. Phys. E* **13**, 133 (1980).
111. F. Stickel, E. W. Fischer and R. Richert, *J. Chem. Phys.* **102**, 6251 (1995)
112. J. Barthel, K. Bachhuber, R. Buchner and H. Hetzenauer, *Chem. Phys. Lett.* **165**, 369 (1990).
113. N. Nandi, K. Bhattacharyya and B. Bagchi, *Chem. Rev.* **100**, 2013 (2000).
114. K. Asami, *Prog. Polym. Sci.* **27**, 1617 (2002).
115. F. Kremer and A. Schönhal, *Broadband Dielectric Measurement Techniques (10^6 Hz to 10^{12} Hz)*. (Springer, 2012).

116. Y. Feldman, I. Ermolina and Y. Hayashi, IEEE Trans. Dielectr. Electr. Insul **10**, 728 (2003).
117. R. Bergman and J. Swenson, Nature 403, 283 (2000)
118. J. Barthel, R. Buchner, P.-N. Eberspächer, M. Münsterer, J. Stauber and B. Wurm, J. Mol. Liq. **78**, 83 (1998)
119. K. Mukherjee, A. Das, S. Choudhury, A. Barman and R. Biswas, J. Phys. Chem. B **119**, 8063 (2015).
120. R. Buchner, G. T. Hefter and P. M. May, J. Phys. Chem. A **103**, 1 (1999).
121. E. Tarif, B. Saha, K. Mukherjee, P. De, R. Biswas, J. Phys. Chem. B **123**, 5892 (2019).
122. E. Tarif, K. Mukherjee, A. Barman, R. Biswas, J. Chem. Sci. **131**, 43 (2019).

Chapter 2

Experimental Techniques and Data Analysis Methods

The most used experimental techniques for the investigation of various complex chemical systems discussed in this Thesis are steady state absorption and emission spectroscopy, Time-resolved Fluorescence spectroscopy and Dielectric Relaxation spectroscopy. This chapter mainly contains a brief description of these experimental techniques.

2.1 Steady State Absorption Data Collection

Steady state absorption spectra presented in this thesis have been recorded using UV-2600 (SHIMADZU) spectrophotometer. Fig. 2.1 represents a schematic description of an absorption spectrophotometer. In absorption spectrophotometer, tungsten and deuterium lamp have been used as light sources for the visible and ultraviolet region, respectively. The light from the source lamp directed by a mirror passes through a filter and reaches to the monochromator. Then the diffraction grating present in the monochromator selects a specific wavelength from the incoming light. The light with a specific wavelength (monochromatic light) is split into two beams before it reaches to the sample. One of these two beams used for reference while the other one passes through the sample.

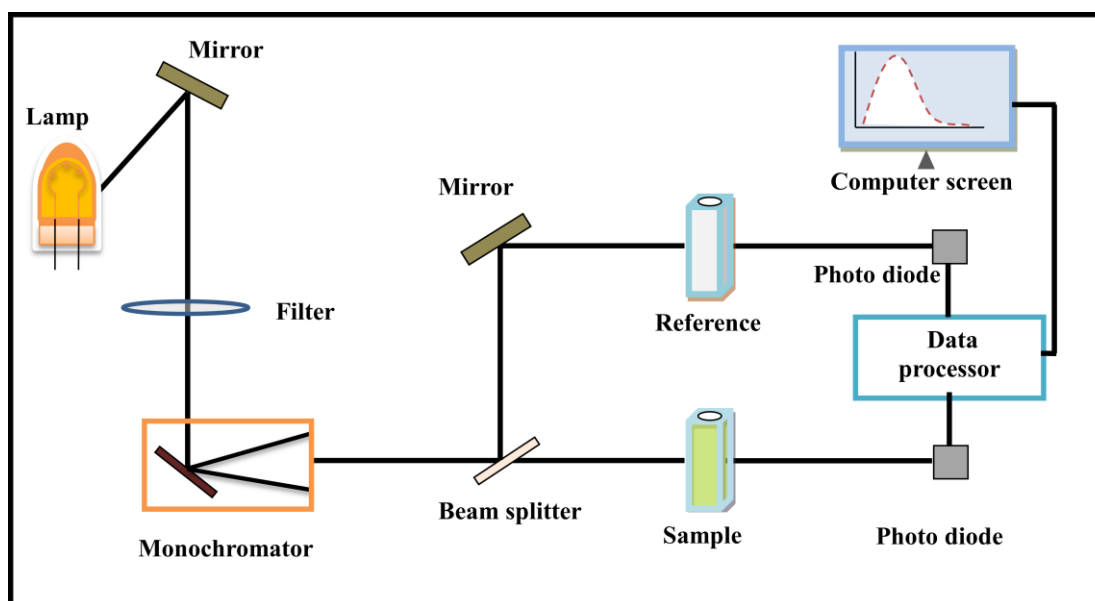


Fig. 2.1 Schematic presentation of an absorption spectrophotometer.

The transmitted light from both reference and sample collected into the photodiode detector. After few sequential steps, signal enhancement, analog to digital conversion, the final absorption data is generated.

Absorbance (A) is proportional to the path length (l), concentration (c) and the molar extinction coefficient (ϵ) of the sample which is the fundamental statement of Beer-Lambert

Law: $A = \log_{10} \frac{I_0}{I} = \epsilon cl$. Where I_0 and I are the intensity of incident light and transmitted light, respectively.

All optical measurements presented in this Thesis are carried out keeping $l = 1\text{cm}$ and $c \leq 10^{-5}\text{M}$.

2.2 Steady State Fluorescence Data Collection

Steady state fluorescence spectroscopy investigates the emission spectra after irradiation by a continuous light (Xe lamp) source. Here, we have used fluorimeter (Fluorolog, Jobin-Yvon, Horiba) for steady state emission measurements. Fig. 2.2 represents a schematic diagram of a fluorescence spectrophotometer. The monochromators help to select specific excitation and emission wavelength and also block the undesired wavelengths (stray light).

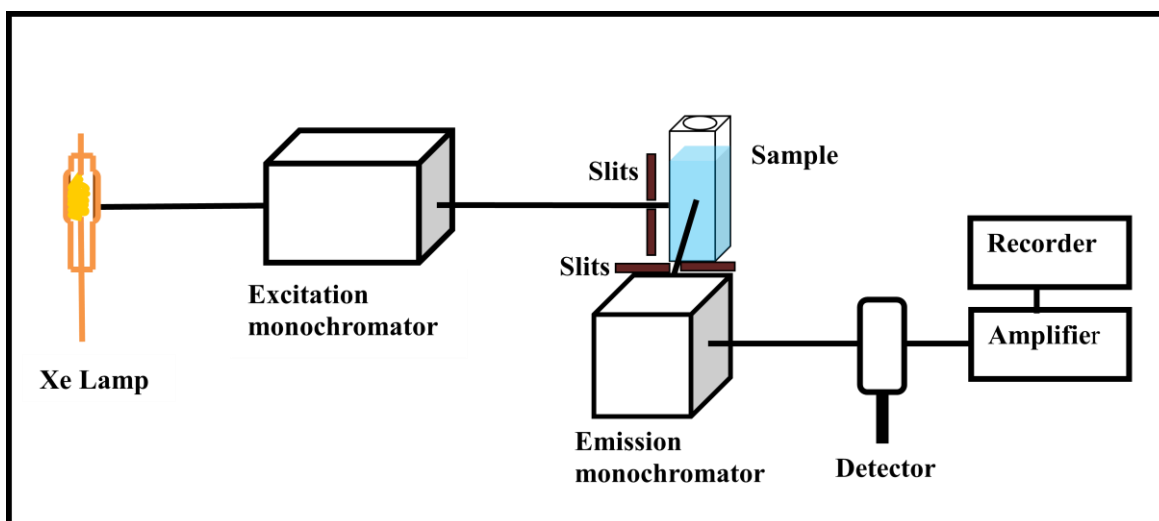


Fig. 2.2 Schematic diagram of a fluorescence spectrophotometer.

The equipped motor in monochromators allows auto scanning of emission and excitation wavelengths. The fluorescence emission detected by photomultiplier tube (PMT) is projected in the computer screen after amplification and appropriate electronic conversion.

2.3 TCSPC Technique

Time-resolved measurements provide more information with much complexity than steady state measurements. Time-resolved data presented in this thesis have been recorded using Time-Correlated Single Photon Counting (TCSPC) system from Edinburg (U.K.). Fig. 2.3 is the schematic representation of a typical TCSPC set-up. TCSPC follow the principle that the probability distribution for emission of a single photon from a single fluorophore molecule after its excitation is identical to the time-dependent fluorescence intensity change of all photons emitted by the fluorophore after excitation.

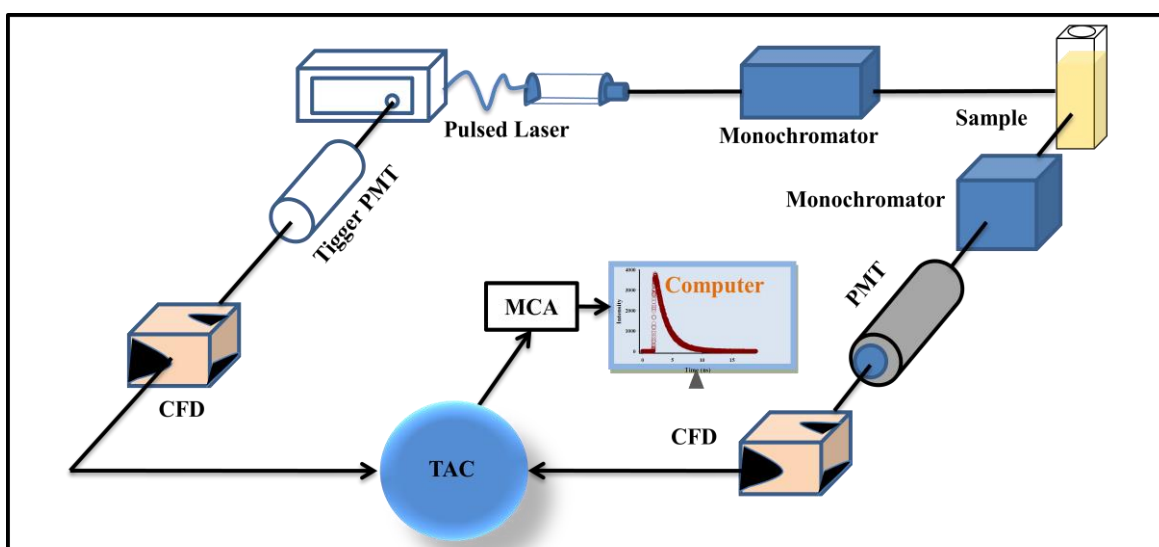


Fig. 2.3 Schematic presentation of a TCSPC set-up.

Excitation pulse from the laser source first excites the fluorophore molecules within the sample cuvette and creates a start signal. For time-resolved measurements, the excitation pulse width should be shorter than the decay lifetime of the sample.¹⁻³ Obtained start signal from the sample successively passes through the constant fraction discriminator (CFD) and time-to-amplitude

converter (TAC). When the signal passes through CFD, it records the laser pulse appearance time while signal through the TAC increases voltage linearly with time i.e. voltage ramp. This voltage ramp gets stopped when the first photon from the fluorophore is detected. Then, the output pulse from the TAC, which is proportional to the delay time (Δt) between the start and stop signal sent to a multichannel analyzer (MCA) for the numerical value generation. From the repetition of the above described process several times and with the help of MCA, a histogram of the decay containing photon count and time channel is created.¹

2.4 Data Analysis

2.4.1 Solvation Dynamics

Steady state absorption and emission spectra of fluorophore molecules within the sample were recorded and solvent blank subtracted for the background correction. Around 14-16 magic angle (54.7°) decay over the steady state emission band were collected to start analysis. We have mostly used external dye molecules coumarin 153 (C153) and coumarin 343 (C343) as fluorophores, the local reporter for our fluorescence measurements. In time-resolved measurements, we have used 409 nm diode laser as an excitation source and the full width at half maxima (FWHM) of the instrument response function (IRF) was ~ 85 ps. General signature of the Stokes shift dynamics was obtained from the only decay in the blue end, and a rise followed by decay in red end emission intensity following laser excitation. The sample response, $I(t)$, was generated from the fluorescence decay, $N(t)$, and instrument response function, $R(t)$, using iterative reconvolution method⁴ in which a nonlinear least square analysis is employed. Intensity decay obtained from TCSPC, fits with a sum of exponentials, $I(t) = \sum_{i=1}^N \alpha_i \exp(-t/\tau_i)$, where α_i is amplitude associated with the characteristic lifetime τ_i . The intensity decays at several wavelengths (λ_j) were fitted with a multi exponential function to get lifetime [$\tau_i(\lambda_j)$] and associated magnitude or pre-exponential factor [$\alpha_i(\lambda_j)$]. The multi exponential fitting function is

$$I(\lambda_j, t) = \sum_{i=1}^N \alpha_i(\lambda_j) \exp(-t/\tau_i(\lambda_j)), \quad (2.1)$$

where $\sum_i \alpha_i(\lambda_j) = 1$.

Thereafter, Time-resolved emission spectra (TRES) were constructed using the well-established method.^{1,4,5} Time-integrated intensity at each wavelength equal to the wavelength dependent steady state emission, $F(\lambda_j)$ was obtained by the formation of a new set of normalized intensity decays. The normalization factor is

$$H(\lambda_j) = \frac{F(\lambda_j)}{\int_0^{\infty} I(\lambda_j, t) dt} = \frac{F(\lambda_j)}{\sum_i \alpha_i(\lambda_j) \tau_i(\lambda_j)}. \quad (2.2)$$

Then the proper normalized decay function obtained by using the following relation,

$$I'(\lambda_j, t) = H(\lambda_j) I(\lambda_j, t) = \alpha'_i(\lambda_j) \exp(-t/\tau_i(\lambda_j)), \quad (2.3)$$

where, $\alpha'_i(\lambda_j) = H(\lambda_j) \alpha_i(\lambda_j)$. By using the values of $I'(\lambda_j, t)$, wavelength and time dependent intensity were calculated. From the wavelength and time dependent intensity, TRES have been constructed and subsequently transferred to the frequency domain for further analysis.⁵ Then, the log-normal line shape function is used to fit individual time-resolved emission spectrum for continuous representation. The peak frequency of the time-resolved emission spectra is used to construct the solvation response function

$$S(t) = \frac{(\nu(t) - \nu(\infty))}{(\nu(0) - \nu(\infty))}, \quad (2.4)$$

where $\nu(0)$, $\nu(t)$ and $\nu(\infty)$ are peak frequency of the reconstructed emission spectra at $t=0$ (instantly after excitation), t (at any time instant) and $t=\infty$ (represents sufficiently long time), respectively. The solvent response function is a normalized function and provides the information about the time dependence of solvent reorganization around the fluorophore molecule when equilibrium charge distributions of fluorophore are altered followed by excitation. It is assumed that the steady state emission takes place from the fully relaxed state and expected to be identical with time-resolved emission spectra at $t=\infty$. In many cases the blue shift in steady state emission is observed as compared to time-resolved emission at $t=\infty$. This

steady state result indicates that the solvent reorganization is not complete within the life time of the fluorophore. Solvation response function, $S(t)$, fits with a multi-exponential function and subsequent integration of that multi-exponential function gives average solvation time as follows:

$$\langle \tau \rangle = \int_0^{\infty} dt S(t) = \int_0^{\infty} dt \left[\sum_i \alpha_i \exp(-t/\tau_i) \right] = \sum_i \alpha_i \tau_i, \quad (2.5)$$

where $\sum_i \alpha_i = 1$, and α_i and τ_i are the amplitude and time constants respectively, related with the i -th component of $S(t)$ decay.

2.4.2 Rotational Dynamics

TCSPC set-up is also used to measure reorientational dynamics of the dissolved fluorophore in the medium and provides valuable information about the time-dependent friction.^{1,4,6} Reorientational dynamics measurements utilized the principle of photoselective excitation of those fluorophore molecules whose absorption transition dipoles are parallel to the electrical vector of polarized excitation light. The emission intensity decays at the parallel and perpendicular emission polarizations depend on the reorientation of the excited fluorophore. For this measurement, the lifetime of dissolved fluorophore molecules has to be comparable or larger than the reorientational time in the medium. Time dependent fluorescence anisotropy, ($r(t)$), is defined as¹

$$r(t) = \frac{I_{para}(t) - I_{perp}(t)}{I_{para}(t) + 2I_{perp}(t)}, \quad (2.6)$$

where I_{para} and I_{perp} represent vertically (parallel) and horizontally (perpendicular) polarized fluorescence emission decay (with respect to the vertically polarized excitation light), respectively. Intensity decays for the time-resolved anisotropy measurements are collected at the peak wavelengths of the steady state emission spectra. Sensitivity of the polarizer for the selection of vertically and horizontally polarized light is crucial for anisotropy measurements. Thus, a correction factor (G) is used to minimize the error originated due to the polarization bias. This correction factor, G, is known as geometric factor and defined as the ratio between the

transmission efficiency for vertically (parallel) light and that of horizontally (perpendicular) polarized light ($G = \frac{I_{para}(t)}{I_{perp}(t)}$). Now the corrected time-resolved fluorescence anisotropy, $r(t)$,

represented as

$$r(t) = \frac{I_{para}(t) - GI_{perp}(t)}{I_{para}(t) + 2GI_{perp}(t)}. \quad (2.7)$$

The geometric factor (G) is obtained by the tail matching of vertically (parallel) and horizontally (perpendicular) polarized fluorescence emission intensity decays.² Now using I_{para} , I_{perp} and G we have constructed $r(t)$ following equation 2.7. Constructed $r(t)$ then fitted with a single or multi-exponential function as follows:

$$r(t) = r(0) \sum_i \alpha_i \exp(-t/\tau_i), \quad (2.8)$$

where τ_i and α_i are the time and associated amplitude of the i -th decay component and $\sum_i \alpha_i = 1$. In this thesis, we have fixed the $r(0)$ at 0.376⁶ for C153 and 0.35⁷ ($r(0)$ value of C343 in glycerol, taken here as initial anisotropy) for C343. As concentration of temperature dependent anisotropy measurements in various medium may give different $r(0)$ values, we have fixed $r(0)$ for each probe molecule because we would like to compare the qualitative difference among the medium frictions resisting the solute rotating in different measured solutions. The average rotational time estimated using the parameters (τ_i, α_i) obtained from the fitting as follows:

$$\langle \tau_r \rangle = \int_0^{\infty} dt [r(t)/r(0)] = \sum_i \alpha_i \tau_i. \quad (2.9)$$

2.5 Dielectric Relaxation Spectroscopy

2.5.1 Introduction

Electric field induced polarization of dielectric normally arises from the distortion of the distribution of the electron cloud or/and the reorientation of molecular dipoles. In liquid phase at room temperature dynamics of microscopic particles such as molecules, atoms, ions are so fast that they are able to respond to the electric field of 10^6 Hz or higher unless field alteration becomes too fast ($\geq 10^{12}$ times per second). Dielectric relaxation (DR) techniques generally measured electronic and nuclear part of polarization in the presence of an external field of frequencies comparable to the microscopic dynamics of the medium.

According to Maxwell's equations⁸, the interaction of the electromagnetic field with matter is expressed as follows

$$\text{rot } \mathbf{E} = -\frac{\partial}{\partial t} \mathbf{B} \quad (2.10)$$

$$\text{rot } \mathbf{H} = \mathbf{j} + \frac{\partial}{\partial t} \mathbf{D} \quad (2.11)$$

$$\text{div } \mathbf{D} = \rho_e \quad (2.12)$$

and

$$\text{div } \mathbf{B} = 0 \quad (2.13)$$

In the above said equations, \mathbf{E} and \mathbf{H} represent the electric and magnetic field, \mathbf{D} the dielectric displacement, \mathbf{B} the magnetic induction, \mathbf{j} the current density and ρ_e the density of charges. For weak electric field the dielectric displacement, \mathbf{D} , can be expressed by

$$\mathbf{D} = \varepsilon^* \varepsilon_0 \mathbf{E} \quad (2.14)$$

where ε_0 ($8.854 \times 10^{-12} \text{ Fm}^{-1}$) is the free space permittivity and ε^* is the complex dielectric function. In Maxwell's equation the complex dielectric function (ε^*) is time dependent, if time dependent phenomena occur within the sample. For a periodic electric field $\mathbf{E}(t) = \mathbf{E}_0 \exp(-i\omega t)$,

where ω is the radial frequency and $i = \sqrt{-1}$, the complex dielectric function, ε^* , is expressed as

$$\varepsilon^*(\omega) = \varepsilon'(\omega) - i\varepsilon''(\omega) \quad (2.15)$$

where ε' and ε'' are the real and imaginary part of the complex dielectric function, respectively.

2.5.2 Measurements

All the dielectric measurements presented in this thesis were measured using PNA-L network analyzer (N5230C) combined with an open-ended coaxial probe (85070E). The measuring frequency range of this instrument is $0.2 \leq \nu / GHz \leq 50$. A schematic representation of the instrument is shown in the Fig. 2.4. Calibration of the instrument has been done prior to each set of measurement using air (for open circuit), shorting block and water.

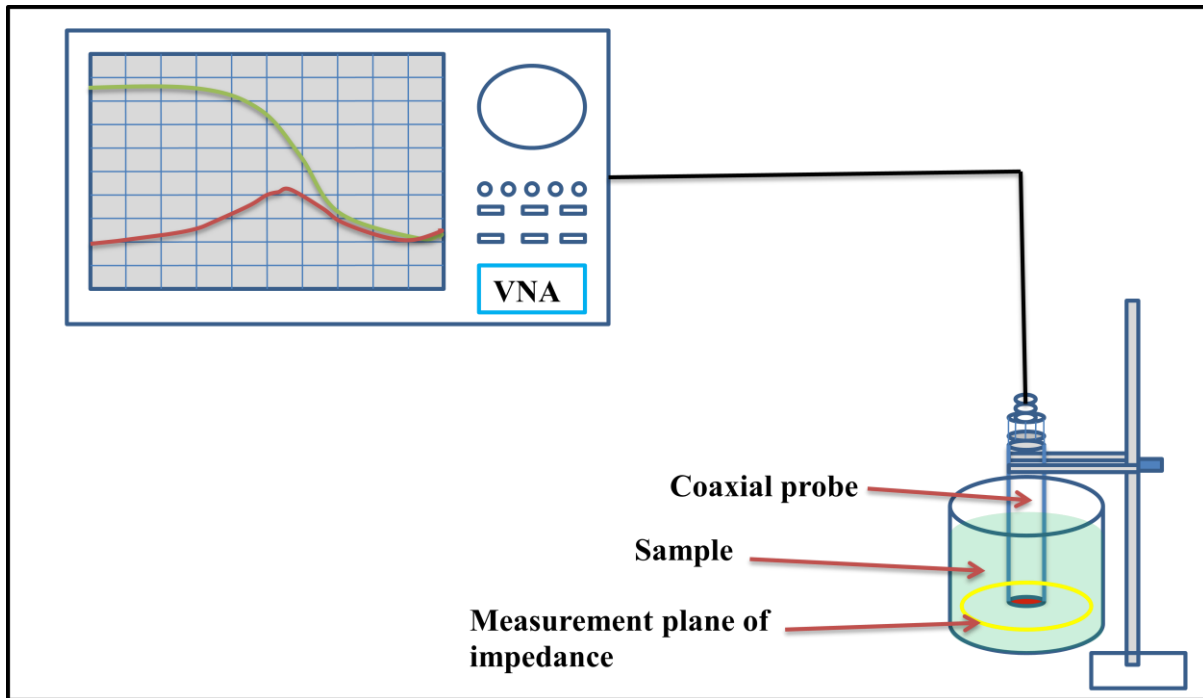


Fig. 2.4 Schematic diagram of DR measurement set-up.

2.5.3 Different Mathematical Models and Data Analysis

Several mathematical models (Debye Model, Non-Debye Model etc.) have been employed to recognize and understand dynamics associated with the orientational polarization.

2.5.3.1 Debye Model

Debye Model is the simplest and standard model to explain the complex dielectric response and also provide characteristic timescale. Debye Model⁹ is expressed as

$$\varepsilon^* = \varepsilon_\infty + \frac{\Delta\varepsilon}{1+i\omega\tau_D} \quad (2.16)$$

where, $\omega (= 2\pi\nu)$ is the angular frequency associated with linear frequency ν . $\Delta\varepsilon (= \varepsilon_s - \varepsilon_\infty)$ is the dielectric strength, ε_s ($\omega \rightarrow 0$) represents static, limiting low frequency dielectric constant and ε_∞ ($\omega \rightarrow \infty$) is the dielectric constant measured at high frequency. τ_D represents characteristic relaxation time.

2.5.3.2 Non-Debye Model

Cole-Cole model¹⁰ is normally used to describe a symmetric broadening of the dielectric function and expressed as

$$\varepsilon^* = \varepsilon_\infty + \frac{\Delta\varepsilon}{1+(i\omega\tau_{cc})^{1-\alpha}} \quad (2.17)$$

where α parameter represents a symmetric broadening of the dielectric function, having value range, $0 \leq \alpha < 1$, and τ_{cc} is the relaxation time.

On the other hand, asymmetric broadening of the dielectric function is well explained by Cole-Davidson model.¹¹⁻¹² Cole-Davidson model is mathematically expressed as

$$\varepsilon^* = \varepsilon_\infty + \frac{\Delta\varepsilon}{(1+i\omega\tau_{CD})^\beta} \quad (2.18)$$

where τ_{CD} is the associated relaxation time, β is the asymmetric parameter and exist within the range $0 < \beta \leq 1$.

Havriliak-Negami (HN) model¹³ is the standard and common model used to characterize complex dielectric function. Havriliak-Negami (HN) model is presented as follow

$$\varepsilon^* = \varepsilon_\infty + \frac{\Delta\varepsilon}{(1 + (i\omega\tau_{HN})^{1-\alpha})^\beta} \quad (2.19)$$

where τ_{HN} is the relaxation time.

In general, dielectric responses obtained from the complex chemical systems are possibly the outcome of a superposition of various relaxation modes. Practically for those systems a sum of Havriliak-Negami (HN) function is used and represented as

$$\varepsilon^* = \varepsilon_\infty + \sum_j \frac{\Delta\varepsilon_j}{(1 + (i\omega\tau_j)^{1-\alpha})^\beta} \quad (2.20)$$

2.5.3.3 Data Processing

Appropriate mathematical models have to select to extract physically significant information from the complex permittivity spectra. These mathematical models are used to fit the obtained complex permittivity data, then quality of the fits are determined by examining both the ‘goodness-of-fit’ parameter (χ^2) and residual. χ^2 is defined as¹⁴

$$\chi^2 = \frac{1}{2m - \ell} \sum_{i=1}^m \left[\left(\frac{\partial\varepsilon_i'}{\sigma(\varepsilon_i')} \right)^2 + \left(\frac{\partial\varepsilon_i''}{\sigma(\varepsilon_i'')} \right)^2 \right] \quad (2.21)$$

where m is the number of data triples ($\nu, \varepsilon', \varepsilon''$), ℓ is the number of adjustable parameters, $\partial\varepsilon_i$ and $\sigma(\varepsilon_i)$ are the residuals and standard deviation of the individual data points, respectively.

2.5.3.4 Conductivity Corrections

Conductivity correction is important for dielectric study of a conducting sample as dc conductivity contributes to the imaginary part of the complex dielectric response. The complex dielectric response for a conducting sample is present as¹⁵⁻¹⁶

$$\varepsilon^* = \varepsilon'(v) - \left[i\varepsilon''(v) + \frac{i\kappa}{2\pi\varepsilon_p v} \right] \quad (2.22)$$

where $v(= \omega/2\pi)$ is the linear frequency, κ is the dc conductivity of the sample and ε_p is the permittivity of the free space.

This correction has been employed in all the dielectric study presented here.

References:

1. J. R. Lakowicz, *Principles of Fluorescence Spectroscopy*. New York :Kluwer Academic/Plenum, 1999.
2. D. V. O'Connor, D. Phillips, *Time-correlated Single Photon Counting*. London :Academic Press, 1984.
3. M. C. Chang, S. H. Courtney, A. J. Cross, R. J. Gulotty, J. W. Pertrich and G. R. Fleming, *Analytical Instrumentation* 14, 433 (1985).
4. D. J. S. Birch and R. E. Imhof, Time-domain fluorescence spectroscopy using time-correlated single-photon counting, in: *Topics in Fluorescence Spectroscopy*, J. R. Lakowicz, Ed., Plenum Press, New York 1, 1 (1991).
5. M. L. Horng, J. A. Gardecki, A. Papazyan and M. Maroncelli, *J. Phys. Chem.* 99, 17311 (1995).
6. M. L. Horng, J. A. Gardecki and M. Maroncelli, *J. Phys. Chem. A* 101, 1030 (1997).
7. S. Koley, H. Kaur and S. Ghosh, *Phys. Chem. Chem. Phys.* 16, 22352 (2014).
8. J. C. Maxwell, *A Treatise on Electricity and Magnetism*. (Clarendon press, 1881)
9. P. J. W. Debye, *Polar Molecules*. (Chemical Catalog Company, Incorporated, 1929).
10. K. S. Cole and R. H. Cole, *J. Chem. Phys.* 9, 341 (1941).
11. D. W. Davidson and R. H. Cole, *J. Chem. Phys.* 18, 1417 (1950).
12. D. W. Davidson and R. H. Cole, *J. Chem. Phys.* 19, 1484 (1951)
13. S. Havriliak and S. Negami, *Polymer* 8, 161 (1967).
14. P. R. Bevington and D. K. Robinson, *Data Reduction and Error Analysis*. (McGraw–Hill, New York, New York, 2003).
15. C. J. F. Böttcher and P. Bordewijk, *Theory of Electric Polarization*. (Elsevier: Amsterdam, The Netherlands, 1978).
16. R. Buchner and J. Barthel, *Annu. Rep. Prog. Chem. Sect. C: Phys. Chem.* 91, 71 (1994).

Chapter 3

Interaction and Dynamics in a Fully Biodegradable Glucose-Containing Naturally Abundant Deep Eutectic Solvent (NADES): Temperature Dependent Time-Resolved Fluorescence Measurements

3.1 Introduction

Solvents, being an essential ingredient in a variety of applications, ranging from cleaning and dissolution to synthesis, extraction, transport and temperature regulation, play a key role in regulating and augmenting various processes that are associated with our existence and sustenance. The necessity of liquid media, either in a living and functional cell or outside of it in a huge chemical factory, is undeniable. A large contingent of these solvents is conventional molecular organic solvents, and therefore, many of them are tagged with serious environmental and health issues.¹⁻⁴ Naturally, a search for environmentally benign and less virulent solvent has led to the advent of new classes of solvents that may cause relatively milder ecological impact. These new solvents include room temperature super critical fluids (RTSFs),^{5,6} gas expanded liquids (GXLs),⁷⁻⁹ room temperature ionic liquids (RTILs)¹⁰⁻¹³ and their aqueous binary mixtures, and deep eutectic solvents (DESs)¹⁴⁻¹⁹. Several from these new classes of solvents may play a role of effective alternatives to hazardous conventional organic solvents, and a careful choice of ingredients can even generate bio-degradable solvent systems. It has been found in several cases that deep eutectic solvents are efficient alternative among these non-conventional eco-friendly media on the grounds of low cost, less toxicity, bio-degradability, non-volatility, non-inflammability, easy preparation route, favorable transportation and other useful solvent properties.^{16,20-28} DESs are multi-component molten mixtures with a significantly lower liquidous temperature than the melting temperature of each of the individual components. Deep depression of freezing point of DESs is a combined result of extensive inter-constituent H-bonding and gain in entropy for being in the liquid phase. Mixture components and composition define physicochemical properties, such as, density, viscosity, polarity, thermal stability, toxicity,

biodegradability etc.²⁷⁻³¹ DESs therefore warrant comprehensive understanding of interaction and dynamics for better and smarter applications as designer solvents.

Recently, naturally abundant deep eutectic solvents (NADES) based on natural compounds, specially primary metabolites, such as, amino acids, organic acids, urea and sugars have received attention because of their inherent greenness and eco-sustainability.^{21,28,32-35} NADESs have been employed as media for dissolution of complex chemical species, drug carrier, therapeutic system, reaction media, biotransformation host, biodiesel production, extraction of bioactive substances, CO₂ and SO₂ absorption, Li-ion batteries and so forth.^{20,28,36-45} Furthermore, it is believed that NADESs can support in organisms biological processes through dissolution of metabolites which are sparingly soluble in water and lipids.^{32,35} Micro-heterogeneity in deep eutectic media has been a recurrent theme while describing interaction and dynamics of these systems.^{46,47} A strong micro-heterogeneous character for ionic DESs was reflected in viscoelastic, magnetic resonance, dielectric relaxation (DR) and time-resolved fluorescence (TRF) measurements, and in simulations.^{17,18,46,48-50} For non-ionic [acetamide+urea] DES, on the other hand, TRF measurements and simulations revealed no such strong solution inhomogeneity,²⁷ although DR measurements indicated that this DES is mildly heterogeneous. Interestingly, a non-ionic DES made of acetamide, urea and polyethylene glycol (PEG) showed moderate heterogeneity features in both TRF and DR measurements.²⁹ However, no attempts have so far been made to explore dynamics and interaction in NADESs that are simultaneously non-ionic and fully biodegradable. In this work we are reporting such a representative study where the system is prepared by mixing glucose (C₆H₁₂O₆), urea (NH₂CONH₂) and water at 6:4:1 weight ratio. Note that ~60 percent of biomass is carbohydrate and an important renewable energy resource.^{51,52} Therefore, for biodegradable NADESs, carbohydrates are a promising component.^{53,54} Urea is the most commonly used nitrogenous fertilizers and known to strongly influence protein stability and functionality.⁵⁵⁻⁶⁰ Moreover, glucose as well as urea (metabolites) helps animals to survive in environments with extreme temperature condition.⁶¹ In fact, carbohydrate based several DESs have already been prepared, their physical properties examined and also applied in various sectors^{20,32,41,53,62-67} but without exploring the interaction and relaxation dynamics. We have used two non reactive fluorescent dyes, coumarin 153 (C153) and coumarin 343(C343), in our time-resolved fluorescence measurements which are well-known dipolar solute probes for investigating interaction and dynamics in a variety of complex chemical systems including bulk

and confining ones.⁶⁸⁻⁷⁵ C343 is chosen because it is a hydrophilic dye and expected to locate itself in the water-rich region in case a microscopic phase segregation exists in this DES, while the hydrophobic dye C153 is likely to probe the water-depleted domains.

3.2 Experimental Details

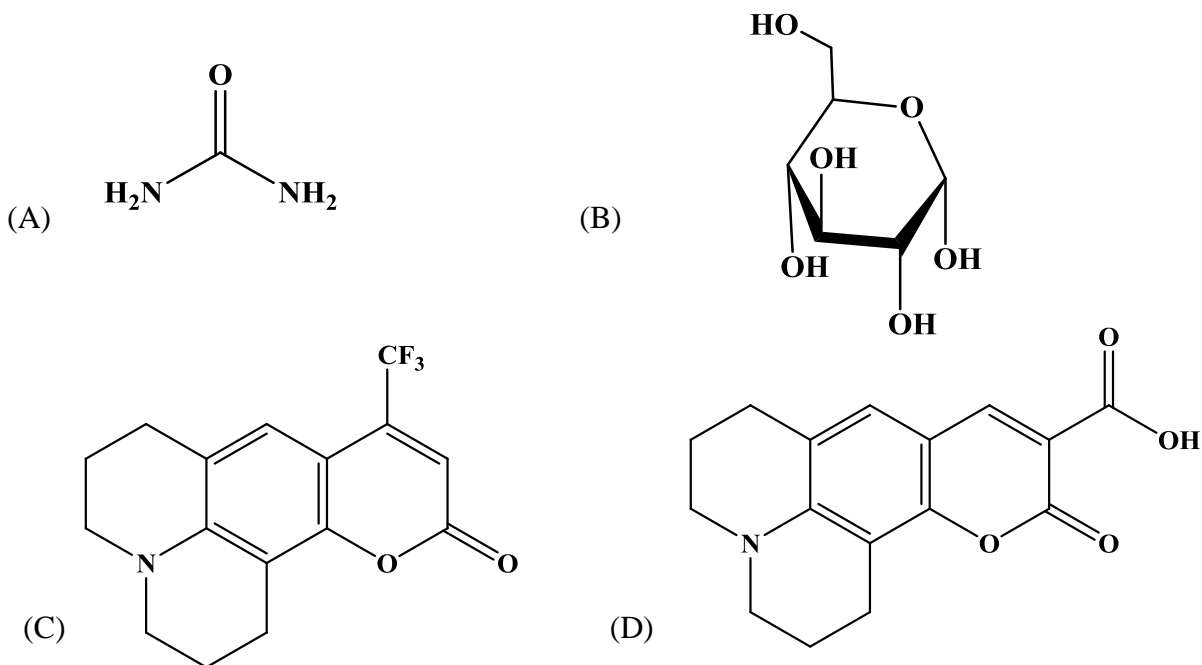
3.2.1 Materials and Sample Preparation

D-Glucose ($\geq 99.5\%$, Sigma-Aldrich, $T_m \approx 423-425$ K), laser grade coumarin 153 (C153) (Sigma-Aldrich) and coumarin 343 (C343) (Sigma-Aldrich) were used as received. Urea ($\geq 98\%$, Sigma-Aldrich, $T_m \approx 405-408$ K) was vacuum-dried (~ 300 K) overnight before use and millipore water was used for sample preparation. Required amount of glucose, urea and water [Glu:Ure:Wat (6:4:1; weight ratio)] were taken in a closed glass container and heated gently at ~ 345 K with continuous stirring at ~ 700 rpm in a hot oil bath under the nitrogen atmosphere (absent of nitrogen may cause caramelization of glucose that complicate the optical measurements because of unwanted absorption in the UV-Vis range) for ~ 3 h. After obtaining a colourless transparent liquid, the temperature was set to 303 K and allowed the obtained liquid to cool to room temperature (~ 303 K) gradually. If all the components in required amounts are mixed and stirred continuously at ~ 303 K, a transparent solution as shown in Fig. A.a.1 (Appendix) was never obtained, although the obtained new DES is liquid at ~ 303 K ($T_f = 299 \pm 2$ K). The above fact supports that the obtained liquid is DES, not a conventional multi-component mixture of glucose, urea and water in solution phase. For optical measurements, we used two dye molecules: C153 (hydrophobic) and C343 (hydrophilic). Stock solutions of C153 and C343 were prepared in carrier solvents. Then few μ L of the stock solution was taken into the preparation glass container prior to the DES component (glucose, urea, water). The carrier solvent was evaporated off. Care was taken to completely dissolve the C153/C343 in the resultant DES solution. The intrinsic absorption of this DES is far away from the solute absorption spectrum in the medium Fig. A.a.2 (Appendix). Thus, it is expected that probe absorption would not be affected by the intrinsic absorption of the DES. Note that the composition of the present DES and the preparation procedure are completely different from a glucose containing DES reported already,⁷⁶ and thus this DES (under study) may be termed as a new one. All samples for measurements were prepared in a tightly humidity controlled environment employing dry

nitrogen atmosphere. For optical measurements, DES was transferred to the preheated quartz cuvette (path length 1 cm) and inserted into preheated sample chamber for thermal equilibration and sufficient time was allowed before measurement at each desired temperature (with uncertainty ± 1 K). Note the concentration of the external probe (C153 or C343, chemical structures are depicted in Scheme 3.1) in DES was maintained at $\leq 10^{-5}$ M in all optical measurements. The appearance of the sample, and the spectral features with and without probe solutes are provided in Fig. A.a.1 and Fig. A.a.2 (Appendix).

Temperature dependent refractive indices, densities and viscosity coefficients of this DES were measured using a temperature controlled refractometer (RUDOLPH, J357), automated density-cum-sound analyzer (Anton Paar, DSA5000) and micro viscometer (AMVn, Anton Paar), respectively.^{17,50,77} These data are summarized in Table A.a.3 (Appendix). Glass transition temperature (T_g) shown in Fig. A.a.4 for this system was measured by a differential scanning calorimeter (DSC TA Instrument Q2000). Note that all measurements were performed well above (≥ 70 K) the T_g of this [Glu+Ure+Wat] DES as the T_g for this system was found to be ~ 236 K.

Scheme 3.1: Chemical structures of (A) Urea, (B) D-Glucose, (C) Coumarin 153 (C153) and (D) Coumarin 343 (C343)



3.2.2 Steady State Measurements

Temperature dependent steady state absorption and emission spectra were collected using a UV–Visible spectrophotometer (UV-2600, Shimadzu), and a fluorimeter (Fluorolog, Jobin-Yvon, Horiba), respectively. Prior to analysis, solvent blanks were subtracted from the probe spectra and transformed properly to the frequency domain for further analyses and frequency determination.^{78,79}

3.2.3 Time-Resolved Fluorescence Measurements

Time-resolved fluorescence measurements were carried out via time-correlated single photon counting (LifeSpec-ps, Edinburgh Instruments, U. K.) technique. Excitation wavelength (LED) was 409 nm. Other details of this setup is described elsewhere.^{80,81} The full width at half-maximum (FWHM) of the instrument response function (IRF) collected with this excitation source and scattering solution was found to be ~85 ps. Based on the standard protocol we have performed dynamic Stokes shift and anisotropy measurements.^{68,81-86} Time-resolved fluorescence intensity decays at magic angle (54.7°) were collected for C153 and C343 in DES at different temperatures to estimate the temperature impact on average excited state lifetimes as were done previously for C153 in aqueous binary mixtures of tetrahydrofuran (THF) and dioxane (Diox).⁸⁷

Details regarding time-resolved fluorescence spectroscopic measurements have been described in chapter 2.

3.3 Results and Discussion

3.3.1 Steady State Spectroscopic Results

Fig. 3.1 represents steady state absorption and emission spectra of C153 (upper panel) and C343 (lower panel) in this non-ionic [Glu+Ure+Wat] DES. For comparison, absorption and emission spectra of these two probes in glycerol (static dielectric constant, $\epsilon_0 \sim 43$ ⁸⁸ at 298 K) are also shown in the same figure. The close similarity of spectra between the DES and glycerol suggests that the solute-solvent interactions in this DES and glycerol are similar. Temperature ($308 \leq T/K \leq 343$) dependent absorption and emission spectra of C153 and C343 in this DES are shown in Fig. A.a.5. Interestingly, spectral features are insensitive to temperature in this range which was also

observed earlier for other non-ionic DESs.^{27,29} Excitation wavelength ($\lambda_{\text{exc.}}$) dependence of the peak frequencies ($\nu_{\text{em.}}$) of fluorescence emission spectra of C153 and C343 in this DES, shown in Fig. A.a.6, reveals the total $\lambda_{\text{exc.}}$ -induced $\nu_{\text{em.}}$ shift is only about 200 cm^{-1} . This suggests that this DES is weakly spatially heterogeneous with respect to $\langle \tau_{\text{lifc}} \rangle$ of these two probes (see Table A.a.7). This spatial inhomogeneity feature was further examined by studying the $\lambda_{\text{exc.}}$ dependence of $\nu_{\text{em.}}$ of a relatively shorter lifetime probe, Trans-2-[4-(dimethylamino)styryl]benzothiazole (DMASBT, $\langle \tau_{\text{lifc}} \rangle \sim 0.7 \text{ ns}$ in this DES at 308 K). Interestingly, data presented in Fig. A.a.6 for DMASBT also shows similar amount of $\lambda_{\text{exc.}}$ -induced $\nu_{\text{em.}}$ shift. Investigation with another probe with longer lifetime, 8-Amino-1-naphthalenesulfonic acid (ANS, $\langle \tau_{\text{lifc}} \rangle \sim 6 \text{ ns}$ ¹⁷), also reveals a shift in $\nu_{\text{em.}}$ of $\sim 200 \text{ cm}^{-1}$ (see Fig. A.a.6), supporting further the view that this DES is only mildly heterogeneous within the $\langle \tau_{\text{lifc}} \rangle$ of $\sim 1\text{-}6 \text{ ns}$.

Next the temperature dependence of $\langle \tau_{\text{lifc}} \rangle$ for C153 and C343 in this DES has been studied and compared with those in a few common polar solvents at ambient condition. These solvents include representatives from non-hydroxylic, and hydroxylic solvents. Measured lifetime data summarized in Table A.a.8 and Table A.a.7 (Appendix) indicate that $\langle \tau_{\text{lifc}} \rangle$ for C153 reduces substantially in this DES compared to those in common ambient solvents, whereas such a change is not registered for C343. A closer look into these lifetime data also suggests that this reduction in $\langle \tau_{\text{lifc}} \rangle$ for C153 is probably linked to the multiple hydroxyl group present in this DES. In addition, C153 shows a stronger temperature dependence ($\sim 30\%$ for the temperature range, $308 \leq T/\text{K} \leq 343$) than C343 in this DES for the same temperature variation.

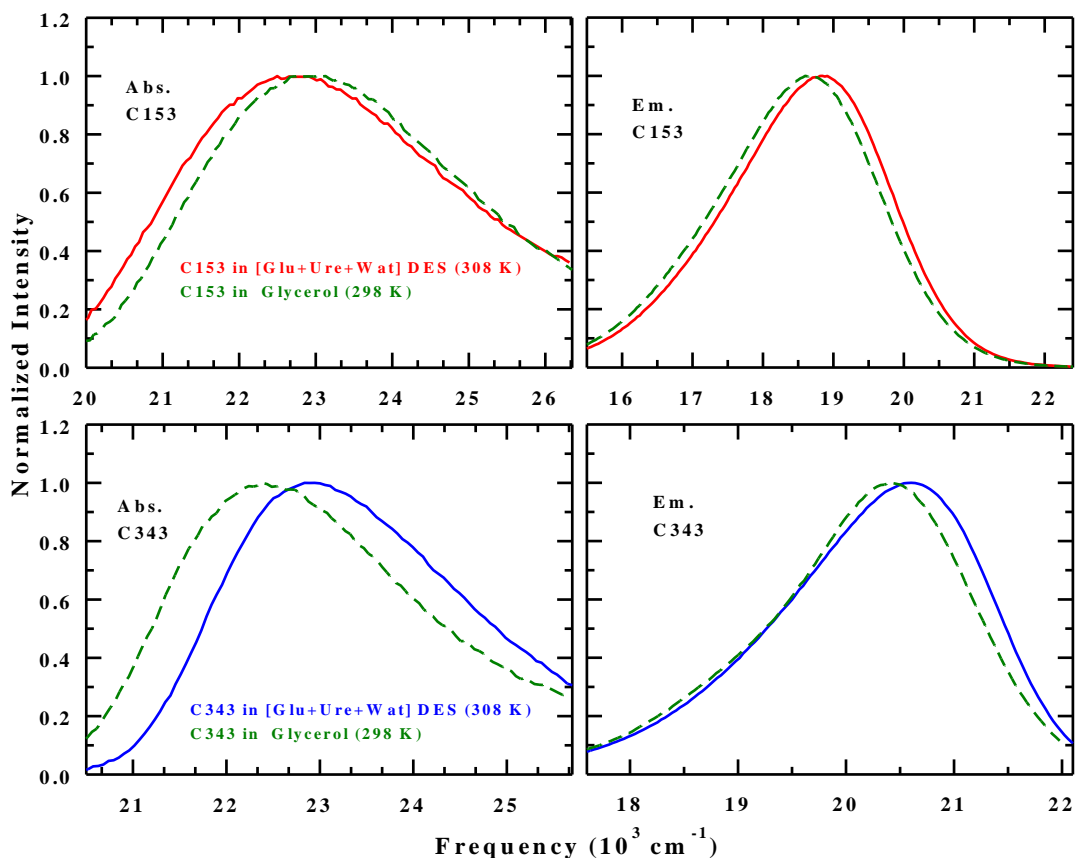


Fig. 3.1: Absorption (left panels) and emission (right panels) spectra of C153 and C343 in [Glu+Ure+Wat] DES at 308 K. Green dashed lines represent the absorption (left) and emission (right) spectra of C153 and C343 in glycerol at 298 K, respectively.

3.3.2 Solute Rotation and Viscosity Coupling

Representative parallel ($I_{\text{para}}(t)$) and perpendicular ($I_{\text{perp}}(t)$) emission intensity decays for C153 and C343 in this DES are shown in Fig. A.a.9 (Appendix). Fig. 3.2 presents the $r(t)$ decays of C153 (upper) and C343 (lower) in this DES at 328 K. Note the bimodal nature of the anisotropy decay for both the solutes. Temperature ($308 \leq T/\text{K} \leq 343$) dependent bi-exponential fit parameters for the $r(t)$ decays are summarized in Table 3.1. These bimodal anisotropy decays are characterized by a fast relaxation of ~ 100 ps timescale, followed by a dominant (~ 70 - 90%) slow

component with a few to several nanosecond relaxation timescale. Average rotational time ($\langle\tau_r\rangle$) becomes faster with temperature as viscosity of the DES decreases.

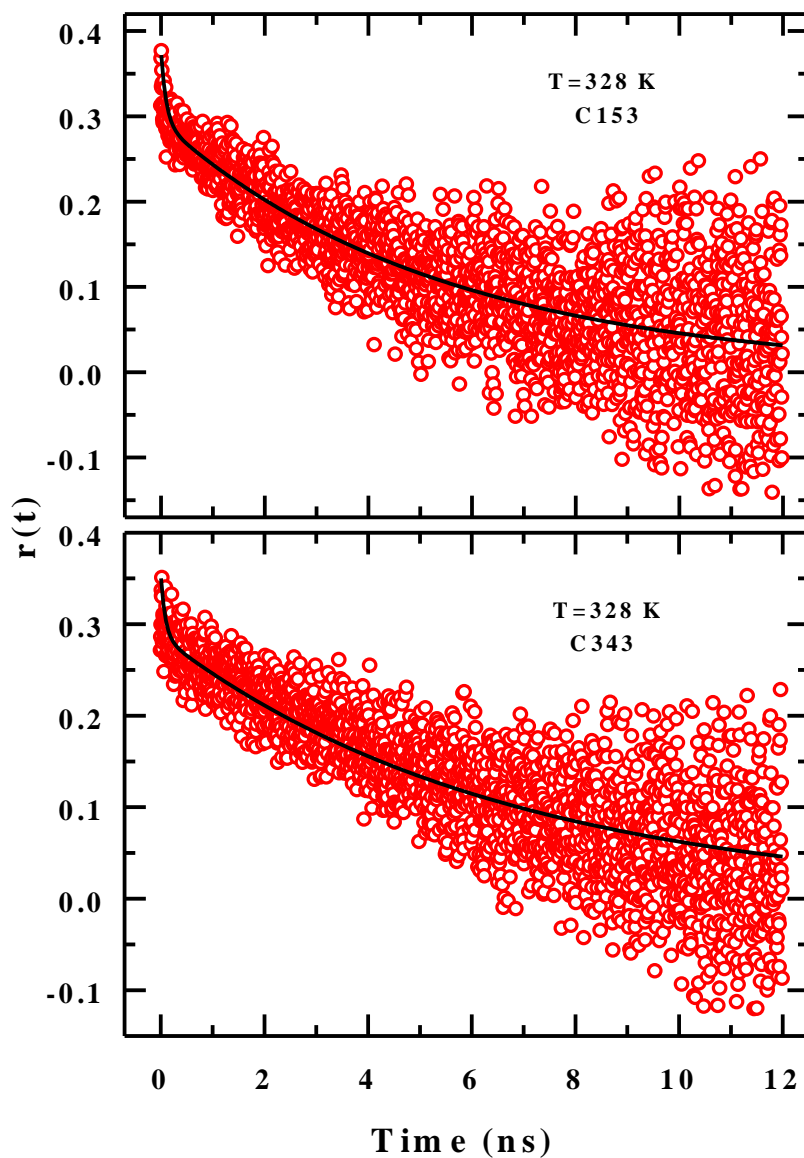


Fig. 3.2: Representative time-resolved fluorescence anisotropy ($r(t)$) decays of C153 (upper panel) and C343 (lower panel) in [Glu+Ure+Wat] DES at 328 K. Lines going through data points denote bi-exponential fits.

Table 3.1: Bi-exponential fit parameters for the temperature dependent $r(t)$ decays of C153 and C343 in [Glu+Ure+Wat] DES.

C153 in [Glu+Ure+Wat] DES					
T(K)	a_1 (%)	τ_1 (ps)	a_2 (%)	τ_2 (ps)	$\langle \tau_r \rangle^a$ (ps)
308					
313					
318	22	85	78	6906	5405
323	22	81	78	6281	4917
328	21	99	79	5379	4270
333	15	111	85	4263	3640
338	13	126	87	3087	2702
343	9	123	91	2632	2406
C343 in [Glu+Ure+Wat] DES					
308					
313					
318	27	69	73	9466	6929
323	27	68	73	7998	5857
328	24	61	76	7267	5538
333	20	63	80	6246	5009
338	17	65	83	5293	4404
343	10	59	90	4098	3694

Fit parameters have been obtained after fixing the r_0 values at 0.376^{82} (C153) and 0.35^{85} (C343). ^aAverage rotational time, $\langle \tau_{rot} \rangle$, can be reproduced within $\pm 10\%$ uncertainty.

Next the coupling between medium viscosity and solute rotation is explored in Fig. 3.3 where $\langle \tau_r \rangle$ is shown as a function of temperature-reduced viscosity, η/T , for both C153 and C343. Clearly, these data depict pronounced fractional viscosity dependence for the rotation time, $\langle \tau_r \rangle \propto (\eta/T)^p$ with $p \sim 0.5$ for C153, and $p \sim 0.3$ for C343. This indicates a strong temporal heterogeneity in the rotational relaxations of these solutes in this DES. This is interesting as no signature of spatial heterogeneity has been detected in the steady state fluorescence measurements for these two solutes and DMASBT in this medium (see Fig. A.a.6). This in turn suggests that the underlying microscopic friction that regulates the solute rotation in this DES is strongly non-Markovian in nature, and such a medium frictional response persists much beyond the inertial timescale. This may arise from non-hydrodynamic moves like jumps punctuated with waiting time distributions for the medium particles as was shown earlier for (acetamide + electrolyte) DES via simulations.⁸⁹

Next we explore the extent of deviation for these measured solute rotation times from the hydrodynamic predictions employing the slip and the stick boundary conditions. The predicted times are obtained from the relation,⁹⁰⁻⁹² $\tau_r = \eta V f C / k_B T$, by using the solute volumes $V^{C153} = 246 \text{ \AA}^3$ and $V^{C343} = 243 \text{ \AA}^3$, shape factor $f^{C153} = 1.71$ and $f^{C343} = 1.99$, $C_{slip}^{C153} = 0.24$ ⁸² and $C_{slip}^{C343} = 0.18$ ⁹³. For stick boundary calculations, $C_{stick}^{solute} = 1$, and other parameters remain the same. The comparison between the measured rotation times and hydrodynamic predictions is also shown in Fig. 3.3. Note the deviation from the hydrodynamic predictions is qualitatively similar for both the solutes: $\langle \tau_r \rangle$ for both the solutes does not conform to the hydrodynamic predictions in the temperature range studied, and exhibit sub-slip behavior at lower temperature (higher viscosity). As already mentioned, this deviation may arise from non-Brownian motional features, such as jumps⁹⁴ and retention of inertia-driven motion that may continue beyond the typical diffusion timescale.^{95,96} Such non-hydrodynamic relaxation mechanisms can significantly diminish the frictional resistance arises from macroscopic solution viscosity, leading to a deviation from the hydrodynamic predictions.

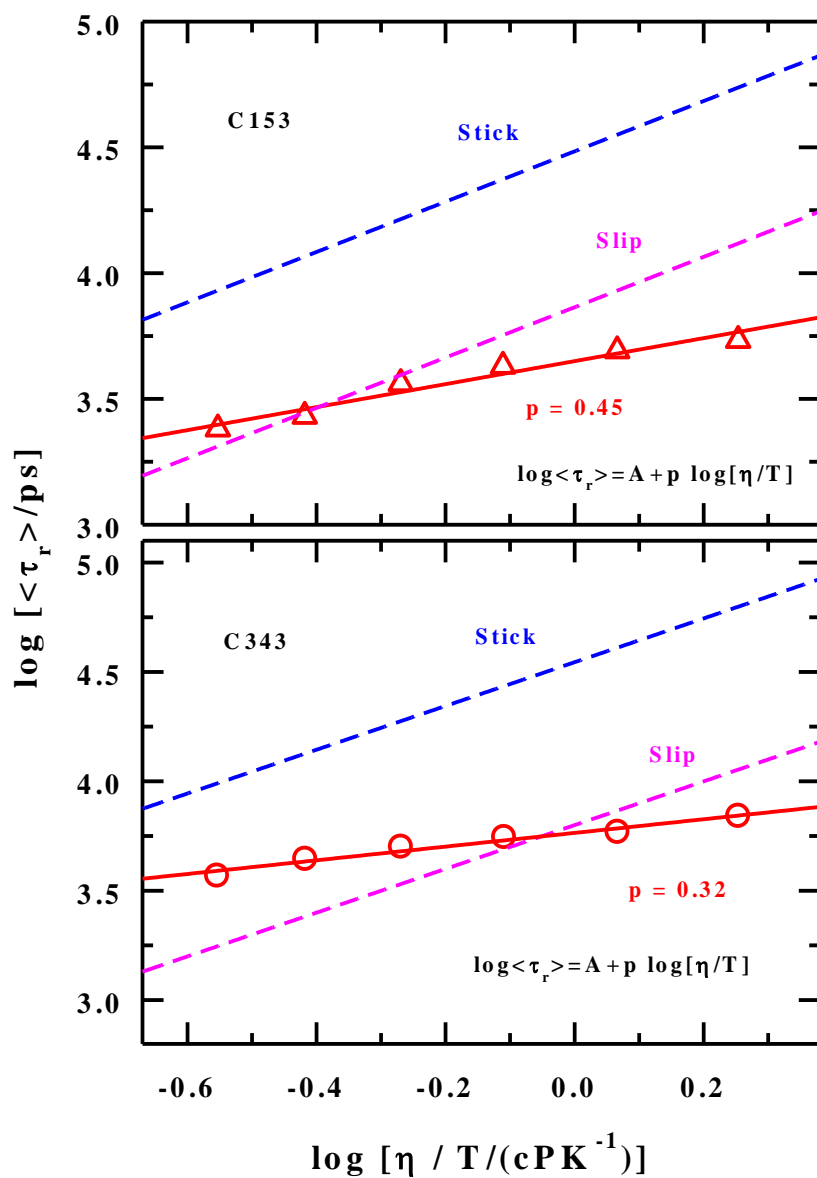


Fig. 3.3: Viscosity coupling of average rotation times ($\langle \tau_r \rangle$) for C153 and C343 in [Glu+Ure+Wat] DES. Temperature-dependent average rotational times are shown as a function of temperature-scaled viscosity (η/T) in a log-log fashion. Lines through the data represent fits to the following expression: $\log \langle \tau_r \rangle = A + p \log [\eta/T]$. Dashed lines represent the hydrodynamic (Stokes-Einstein-Debye) predictions, $\tau^{SED} = (V\eta/k_B T) f C$, where V denotes volume, f shape factor and C solute-solvent coupling parameter, and $k_B T$ Boltzmann constant times the absolute temperature.

Subsequently, activation energies (E_a) associated with solute rotation in this DES and medium viscosity have been estimated from the respective temperature dependent measurements. Arrhenius-type of dependencies have been found for both $\langle\tau_r\rangle$ and η , and are presented in Fig. 3.4. Data in this figure reflect that the activation energy associated with viscosity, $E_a^\eta = 64.7$ kJ mol⁻¹, is ~2-3 times larger than those associated with rotations of C153 ($E_a^{\text{rot,C153}} = 31$ kJ mol⁻¹) and C343 ($E_a^{\text{rot,C153}} = 21.2$ kJ mol⁻¹). This again confirms that solute rotation in this DES is partially decoupled from the frictional resistance arising from the macroscopic medium viscosity, and the extent of decoupling depends upon the nature of solute-medium interaction. This explains the difference in E_a^{rot} values between the hydrophobic solute C153 and the hydrophilic C343, and that between the corresponding exponent (p) values noted in Fig. 3.3.

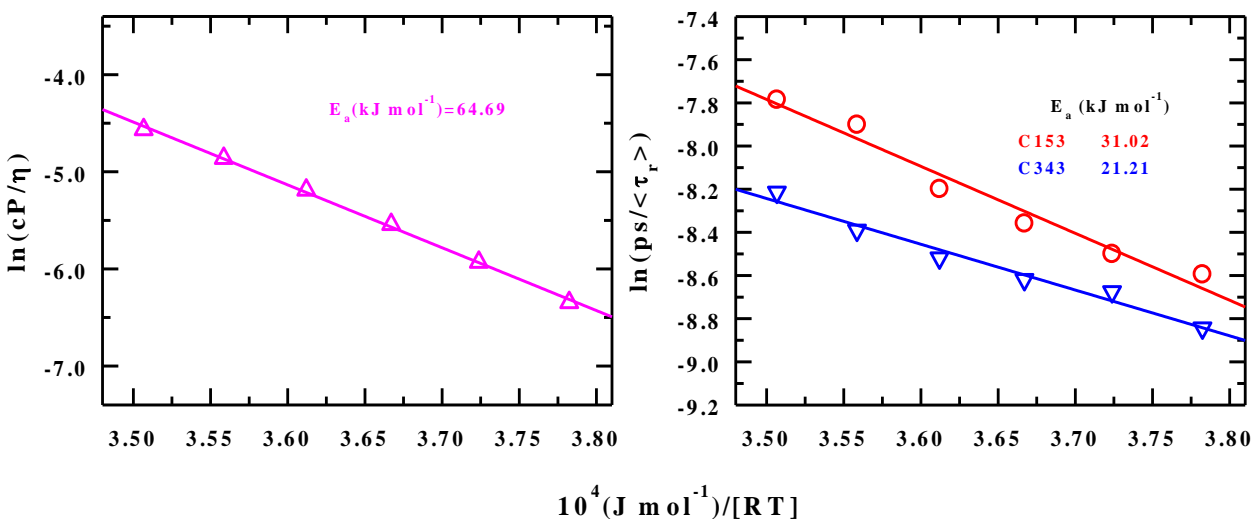


Fig. 3.4: Arrhenius plot for temperature dependent viscosity coefficients (η) for [Glu+Ure+Wat] DES, and average rotation times ($\langle\tau_r\rangle$) of two different solutes dissolved in it. Solid lines represent fits through the respective data sets. Note the activation energies for η and $\langle\tau_r\rangle$. All representations are color coded.

3.3.3 Solvation Dynamics

Next we explore the solvation response in this DES via the dynamic fluorescence Stokes shift measurements employing both C343 and C153 as dipolar solvation probes. First, the existence of the dynamic Stokes shift is checked via collecting the magic angle emission intensity decays at the blue and red wavelengths (with respect to the peak) of the steady state fluorescence emission spectrum of C343 or C153 dissolved in this medium. Decays at the blue wavelength, and rise followed by decay at the red wavelength is a typical signature for the existence of Stokes shift dynamics in a given system.^{46,79} However, in such a multi-component system with extensive inter-species H-bonding, measurements employing a time resolution as broad as ~85 ps may lead to either partial detection or complete missing of the existing Stokes shift dynamics. Fig. A.a.10 presents blue and red wavelength decays at 308 K for C343 and C153 along with fits and fit parameters. Notice in this figure that the signature of Stokes shift dynamics in this DES is evident for C343, while this is completely missing for C153. This is interesting although our earlier measurements with C153 could not detect any Stokes shift dynamics in (acetamide+urea) DES.²⁷ This was attributed mainly to the broad temporal resolution employed and partly to the ultrafast dynamics arising from the low frequency collective modes due to extensive inter- and intra-species H-bonding. In addition, similar non-detection of Stokes shift dynamics was observed earlier for C153 in trehalose/glycerol mixture at higher trehalose loadings and at 298 K.⁹⁷ We speculate that non-detection of Stokes shift dynamics with C153 in the present DES is largely because of the preferential location of C153. That is, C153, because of its hydrophobic character, is probably locating itself in this mixture closer to the glucose unit and surrounded by an environment of extensive H-bonding between carbohydrate hydroxyl (-OH) groups and either amide groups (-NH₂) of urea or -OH groups of water or even both, rendering the dynamics too fast to be detected by the present temporal resolution. C343, on the other hand, may be able to probe a part of the 'slow' dynamics because of its different location steered by its hydrophilic character, and become accessible to the present measurements. We propose that measurements with sharper resolution (for example, fluorescence up-conversion) would allow detection of Stokes shift dynamics with C153, whereas simulations employing realistic interaction potentials might be able to indicate locations of these probes in this DES.

Time-resolved emission spectra (TRES) and steady state emission spectrum of C343 in [Glu+Ure+Wat] DES are shown in the upper panel of Fig.3.5.

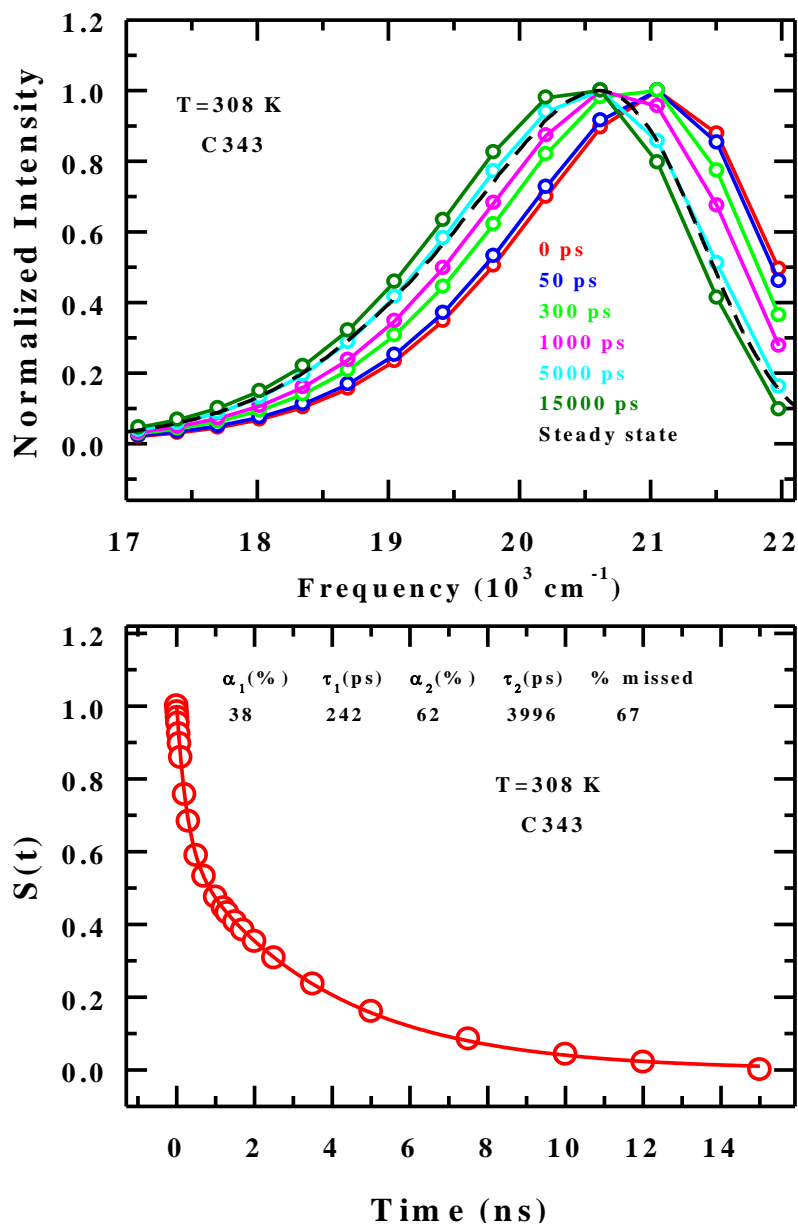


Fig. 3.5: Time-resolved emission spectra (TRES) (upper panel) at different time slices constructed from the measured intensity decays of C343 dissolved in [Glu+Ure+Wat] DES and the corresponding steady state emission spectrum. Solvation response function, $S(t)$, of C343 in [Glu+Ure+Wat] DES at 308 K is shown in the lower panel. Solid line through the data points represents bi-exponential fit to the $S(t)$. Fit parameters are shown in the inset.

These results are obtained for this DES at 308 K. Note that steady state emission spectrum is blue shifted with respect to TRES at $t = \infty$ which suggests that the steady state emission is arising from the incompletely solvent relaxed configuration of the excited solute. The magnitude of the detected dynamic Stokes shift with C343 is $\sim 650 \text{ cm}^{-1}$, with a missing percentage⁹⁸ of $\sim 60\%$. The solvation response function is shown in the lower panel of Fig. 3.5 (lower panel) along with bi-exponential fit and fit parameters. Solvation response for C343 in this DES is characterized by two relaxation components: a relatively faster component ($\sim 40\%$) with a time constant of ~ 250 ps and a slower one ($\sim 60\%$) with a time constant of ~ 4 ns.

In DR and Stokes shift dynamics measurements for (acetamide+urea+PEG) DES at 308 K, a relaxation component with a time constant of ~ 200 ps was observed.²⁹ A combined study of DR and molecular dynamics simulations for (acetamide+urea) DES, on the other hand, reported a relaxation timescale of ~ 100 ps at 335 K, and was attributed to the structural H-bond relaxation.¹⁹ Therefore, the solvation component with ~ 250 ps time constant in the present [Glu+Ure+Wat] DES might have originated from the structural hydrogen bond dynamics coupled to reorientation of the participating dipolar molecules (urea or water, or both). Next question is whether the hydrodynamic rotation of free water, urea or glucose molecules in this DES could generate the ~ 4 ns solvation component. For this, the molecular rotation time for these molecules have been calculated by using the Stokes-Einstein-Debye (SED) relation, $\tau_r = 3\eta V/k_B T$, employing the medium viscosity (η) at 308 K (η at 308 K obtained via extrapolation of the higher temperature data). Molecular rotation times thus calculated are summarized in Table A.a.11 (Appendix; volume of the solute used here are calculated using Ref 103) which suggests that these calculated rotation times are too large to account for the 4 ns solvation timescale. However, if the extent of viscosity decoupling observed for solute (C153 and C343) rotation also dictates the reorientation of these DES component molecules, then non-hydrodynamic angular moves (such as orientation jumps) of water or urea could easily produce a reduced rotation timescale of ~ 2 -5 ns. A systematic incorporation of shape factors⁹⁹ can considerably reduce the rotation times of these component molecules that may also be capable of qualitatively explaining this slow solvation timescale. Another possible origin could be, like in (acetamide+urea+PEG deep eutectics),²⁹ restricted reorientation coupled to cooperative intermolecular H-bond relaxations. This is shown schematically in Fig. A.a.12 (Appendix). We would like to mention here that the present measurements have missed $\sim 60\%$ of the total

solvation response and a complete detection, as found earlier for dynamic Stokes shift studies of ionic liquids,^{100,101,102} may modify and reduce the slow longtime solvation timescale. In such a scenario also, explanations proposed above for the slow solvation component will remain relevant and tenable.

The temperature dependence of solvation response in this DES is shown in Fig. 3.6 along with bi-exponential fits. Fit parameters to the temperature dependent responses, the corresponding observed dynamic shifts ($\Delta\nu_{obs.}$) and the missing percentages of the total response are summarized in Table 3.2. It is clear that the decay of solvation response becomes faster with temperature because of the concomitant decrease in medium viscosity.

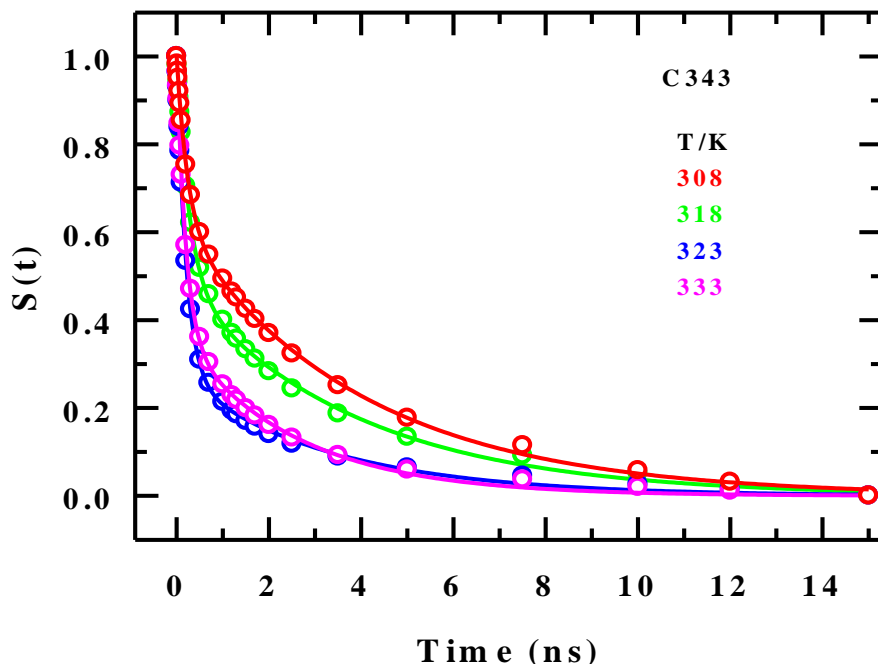


Fig. 3.6: Temperature dependent solvation response functions, $S(t)$, for C343 in [Glu+Ure+Wat] DES. Solid lines going through the data points represent bi-exponential fits. Representations are color-coded.

Note that the magnitude of the missing component is quite large (~65-75%), indicating that these solvation times are associated with large uncertainties. This limits the present dynamic Stokes measurements at further higher temperatures. We would, however, like to point out here that the

estimated missing amplitudes themselves (via Fee-Maroncelli method⁹⁸) may also involve large uncertainties because the density difference between this DES (~1.37 g/cc) and that of a reference non-polar solvent (usually a liquid alkane with density ~0.7 g/cc). Measurements with sharper temporal resolution are therefore warranted for complete measurements of dynamic solvation response in this DES, and also for unraveling the viscosity coupling of solvation times.

Table 3.2: Bi-exponential fit parameters for temperature dependent solvation response functions, $S(t)$, obtained with C343 in [Glu+Ure+Wat] DES along with observed Stokes shift ($\Delta\nu_{obs.}$) magnitudes and missing percentages.

T (K)	a_1 (%)	τ_1 (ps)	a_2 (%)	τ_2 (ps)	$\langle \tau_s^{C343} \rangle^a$ (ps)	$\Delta\nu_{obs.}^b$ (cm^{-1})	% missed
308	38	242	62	3996	2570	692	66
318	51	272	49	3870	2035	681	67
323	73	209	27	3276	1037	544	73
333	63	198	37	2537	1063	535	75

^aAverage solvation time, $\langle \tau_s \rangle$, can be reproduced within $\pm 10\%$ uncertainty. ^bUncertainty $\pm 100 \text{ cm}^{-1}$

3.4 Conclusion

In summary, the present work reports a new DES based on glucose, urea and water ([Glu:Ure:Wat (6:4:1 weight ratio)]) and presents temperature dependent solute-centered relaxation dynamics through time-resolved fluorescence measurements. This transparent colorless DES is stable at room temperature ($T_f = 299 \pm 2\text{K}$) with a measured $T_g = 236 \text{ K}$. This glucose based non-ionic and biodegradable DES does not reveal any strong signature of spatial heterogeneity upon measurements with a variety of fluorescent probes having lifetimes ~1-5 ns but displays a pronounced temporal heterogeneity via strong fractional viscosity dependence of solute rotation times. Dynamic Stokes shift measurements employing a temporal resolution of ~85 ps reveals bi-exponential solvation response for C343 in this DES while no such solvation response could be recorded for C153. This has been attributed partly to the location of the probes linked to their chemical nature, and partly to the broad temporal resolution employed. Bi-

exponential solvation response with time constants of ~ 200 ps and ~ 4 ns has been argued to originate from structural H-bond relaxations, and restricted reorientations of H-bonded species coupled to collective H-bond relaxations. Dielectric relaxation measurements, and simulation studies of H-bonding dynamics and collective single particle reorientational relaxations are required to understand the molecular mechanisms for the solvent relaxations reflected by the time-resolved fluorescence measurements for this system. The bottleneck for simulations could, however, be the availability of appropriate interaction potentials for the components, leading to formation of DES or DES-like medium upon mixing at the desired temperature as in experiments. This caveat notwithstanding, an attempt in this direction is warranted for a better understanding of molecular relaxations in this exciting and biodegradable solvent.

References:

1. M. Ikeda, *Toxicol. Lett.* **64**, 191 (1992).
2. M. Aksoy, *Environ. Health Perspect.* **82**, 193 (1989).
3. B. W. Lee, K. T. Kelsey, D. M. Hashimoto, B. Yakes and T. Seitz, *J. Occup. Environ. Med.* **39**, 960 (1997).
4. D. Majumdar, C. Dutta and S. Sen, *Transport. Res. D-TR E.*, **13**, 524 (2008).
5. J. E. Lewis, R. Biswas, A. G. Robinson, and M. Maroncelli, *J. Phys. Chem. B* **105**, 3306 (2001).
6. S. V. Dzyuba and R. A. Bartsch, *Angew. Chem. Int. Ed.* **42**, 148 (2003).
7. A. M. Scurto, K. Hutchenson and B. Subramaniam, *ACS Symposium Series*, **1006**, 3 (2009).
8. J. P. Hallett, C. L. Kitchens, R. Hernandez, C. L. Liotta and C. A. Eckert, *Acc. Chem. Res.* **39**, 531 (2006).
9. C. A. Eckert, C. L. Liotta, D. Bush, J. S. Brown and J. P. Hallett, *J. Phys. Chem. B* **108**, 18108 (2004).
10. M. J. Earle and K. R. Seddon, *Pure Appl. Chem.* **72**, 1391 (2000).
11. M. Maroncelli, X. X. Zhang, M. Liang, D. Roy and N. P. Ernsting, *Faraday Discuss.* **154**, 409 (2012).
12. B. L. Bhargava and S. Balasubramanian, *J. Phys. Chem. B* **111**, 4477 (2007).
13. H. K. Kashyap and R. Biswas, *J. Phys. Chem. B* **112**, 12431 (2008).
14. E. L. Smith, A. P. Abbott, K. S. Ryder, *Chem. Rev.* **114**, 11060 (2014).
15. Q. H. Zhang, K. D. O. Vigier, S. Royer, F. Jerome, *Chem. Soc. Rev.* **41**, 7108 (2012).
16. M. Francisco, A. Bruinhorst, and M. C. Kroon, *Angew. Chem. Int. Ed.* **52**, 3074 (2013).
17. B. Guchhait, S. Das, S. Daschakraborty and R. Biswas, *J. Chem. Phys.* **140**, 104514 (2014).
18. A. Das, S. Das and R. Biswas, *Chem. Phys. Lett.* **581**, 47 (2013).
19. K. Mukherjee, S. Das, E. Tarif, A. Barman, and R. Biswas, *J. Chem. Phys.* **149**, 124501 (2018).
20. A. Paiva, R. Craveiro, I. Aroso, M. Martins, R. L. Reis and A. R. C. Duarte, *ACS Sustainable Chem. Eng.* **2**, 1063 (2014).
21. A. P. Abbott, D. Boothby, G. Capper, D. L. Davies, and R. K. Rasheed, *J. Am. Chem. Soc.* **126**, 9142 (2004).
22. D. V. Wagle, H. Zhao and G. A. Baker, *Acc. Chem. Res.* **47**, 2299 (2014).

23. P. D. de María and Z. Maugeri, *Curr. Opin. Chem. Biol.* **15**, 220 (2011).
24. J. H. Clark and S. J. Tavener, *Org. Process Res. Dev.* **11**, 149 (2007).
25. W. M. Nelson, *Green solvents for chemistry, Perspectives and Practice*, New York, NY: Oxford University Press New York, 2003.
26. J. M. DeSimone, *Science* **297**, 799 (2002).
27. A. Das, S. Das, R. Biswas *J. Chem. Phys.* **142**, 034505 (2015).
28. M. Espino, M. Á. Fernández, F. J. V. Gomez and M. F. Silva, *TrAC Trends in Analytical Chemistry* **76**, 126 (2016).
29. K. Mukherjee, E. Tarif, A. Barman, R. Biswas, *Fluid Phase Equilib.* **448**, 22 (2017).
30. M. Francisco, A. van den Bruinhorst, and M.C. Kroon, *Green Chem.* **14**, 2153 (2012).
31. S. Rajkhowa, A. Das, S. Mahiuddin, and R. Biswas, *J. Chem. Eng. Data* **57**, 3467 (2012).
32. Y. Dai, J. van Spronsen, G.-J. Witkamp, R. Verpoorte and Y. H. Choi, *Anal. Chim. Acta* **766**, 61 (2013).
33. S. Gore, S. Baskaran, and B. Koenig, *Green Chem.* **13** 1009 (2011).
34. W-C. Huang, D. Zhao, N. Guo, C. Xue and X. Mao, *J. Agric. Food Chem.* **66**, 11897 (2018).
35. Y. H. Choi, J. van Spronsen, Y. Dai, M. Verberne, F. Hollmann, Isabel W.C.E. Arends, G. J. Witkamp, and R. Verpoorte, *Plant Physiol.* **156**, 1701 (2011).
36. E. Durand, J. Lecomte, B. Baréa, G. Piombo, E. Dubreucq and P. Villeneuve, *Process Biochem.* **47**, 2081 (2012).
37. A. Hayyan, M. A. Hashim, M. Hayyan, F. S. Mjalli and I. M. AlNashef, *J. Clean. Prod.* **65**, 246 (2014).
38. Z-F. Wei, X-Q. Wang, X. Peng, W. Wang, C-J. Zhao, Y-G. Zu, Y-J. Fu, *Ind. Crop. Prod.* **63**, 175 (2015).
39. R. J. Sánchez-Leija, J. A. Pojman, G. Luna-Bárceñas, and J. D. Mota-Morales, *J. Mater. Chem. B* **2**, 7495 (2014).
40. M. H. Zainal-Abidin, M. Hayyan, A. Hayyan and N. S. Jayakumar, *Anal. Chim. Acta* **979**, 1 (2017).
41. M. Faggian, S. Sut, B. Perissutti, V. Baldan, I. Grabnar and S. Dall'Acqua, *Molecules* **21**, 1531 (2016).
42. I. M. Aroso, R. Craveiro, Â. Rocha, M. Dionísio, S. Barreiros, R. L. Reis, A. Paiva and A. R. C. Duarte, *Int. J. Pharm.* **492**, 73 (2015).

43. M. B. Haider, D. Jha, B. M. Sivagnanam and R. Kumar, *J. Chem. Eng. Data* **63**, 2671 (2018).
44. S. Sun, Y. Niu, Q. Xu, Z. Sun, and X. Wei, *Ind. Eng. Chem. Res.* **54**, 8019 (2015).
45. L. Millia, V. Dall'Asta, C. Ferrara, V. Berbenni, E. Quartarone, F. M. Perna, V. Capriati, P. Mustarelli, *Solid State Ionics* **323**, 44 (2018).
46. B. Guchhait, H. A. R. Gazi, H. K. Kashyap and R. Biswas, *J. Phys. Chem. B* **114**, 5066 (2010).
47. H. A. R. Gazi and R. Biswas, *J. Phys. Chem. A* **115**, 2447 (2011).
48. G. Berchiesi, G. Rifaiani, G. Vitali and F. Farhat. *J. Therm. Anal.* **44**, 1313 (1995).
49. K. Mukherjee, A. Das, S. Choudhury, A. Barman and Ranjit Biswas, *Journal of Physical Chemistry B* **119**, 8063 (2015).
50. B. Guchhait, S. Daschakraborty and R. Biswas, *J. Chem. Phys.* **136**, 174503 (2012).
51. G. Markou, I. Angelidaki, D. Georgakakis, *Appl. Microbiol. Biotechnol.* **96**, 631 (2012).
52. K. B. Möllers, D. Cannella, H. Jørgensen, N. U. Frigaard, *Biotechnology for Biofuels*, **7**, 1 (2014)
53. G. Imperato, E. Eibler, J. Niedermaier and B. König, *Chem. Commun.* **9**, 1170 (2005).
54. C. Russ and B. König, *Green Chem.* **14**, 2969 (2012).
55. L. Hua, R. Zhou, D. Thirumalai and B. J. Berne, *Proc. Natl. Acad. Sci. U. S. A.* **105**, 16928 (2008).
56. A. Das and C. Mukhopadhyay, *J. Phys. Chem. B* **113**, 12816 (2009).
57. D. Bandyopadhyay, S. Mohan, S. K. Ghosh and N. Choudhury, *J. Phys. Chem. B* **118**, 11757 (2014).
58. D. Soletto, L. Binaghi, A. Lodi, J. C. M. Carvalho, A. Converti, *Aquaculture* **243**, 217 (2005)
59. L. B. Sagle, Y. Zhang, V. A. Litosh, X. Chen, Y. Cho, and P. S. Cremer, *J. Am. Chem. Soc.* **131**, 9304 (2009).
60. B. J. Bennion and V. Daggett, *Proc. Natl. Acad. Sci. U.S.A.* **100**, 5142 (2003).
61. A. Gertrudes, R. Craveiro, Z. Eltayari, R. L. Reis, A. Paiva, and A. R. C. Duarte, *ACS Sustainable Chem. Eng.* **5**, 9542 (2017).
62. A. Hayyan, F. S. Mjalli, I. M. AlNashef, Y. M. Al-Wahaibi, T. Al-Wahaibi, M. A. Hashim, *J. Mol. Liq.* **178**, 137 (2013).

63. L. P. Silva, L. Fernandez, J. H. F. Conceicao, M. A. R. Martins, A. Sosa, J. Ortega, S. P. Pinho and J. A. P. Coutinho, *ACS Sustainable Chem. Eng.* **6**, 10724 (2018).
64. L. Duan, L-L. Dou, L. Guo, P. Li and E-H. Liu, *ACS Sustainable Chem. Eng.* **4**, 2405 (2016).
65. S. Mouden, P. G. L. Klinkhamer, Y. H. Choi and K. A. Leiss, *Phytochem Rev* **16**, 935 (2017).
66. C. Florindo, M. M. Oliveira, L. C. Branco, I. M. Marrucho, *J. Mol. Liq.* **247**, 441 (2017).
67. V. Fischer & W. Kunz, *Mol. Phys.* **112**, 1241 (2014).
68. M. L. Horng, J. A. Gardecki, A. Papazyan and M. Maroncelli, *J. Phys. Chem.* **99**, 17311 (1995)
69. Š. Vajda, R. Jimenez, S. J. Rosenthal, V. Fidler, G. R. Fleming and E. W. Castner, Jr. *J. Chem. Soc. Faraday Trans.* **91**, 867 (1995).
70. E. Tarif, K. Mukherjee, A. Barman and R. Biswas, *J. Chem. Sci.* **131**, 43 (2019).
71. E. Tarif, B. Saha, K. Mukherjee, P. De and R. Biswas, *J. Phys. Chem. B* (2019): DOI: 10.1021/acs.jpcc.9b00889
72. N.E. Levinger, *Curr. Opin. Colloid Interface Sci.* **5**, 118 (2000).
73. K. Kumbhakar, E. Tarif, K. Mukherjee and R. Biswas, *J. Mol. Liq.* **290**, 111225 (2019).
74. S. S. Hossain and A. Samanta, *Phys. Chem. Chem. Phys.* **20**, 24613 (2018).
75. S. S. Hossain and A. Samanta, *J. Phys. Chem. B* **121**, 10556 (2017).
76. Y. Liu, Y. Zhang, S-N. Chen, J. B. Friesen, D. Nikolić, M. P. Choules, J. B. McAlpine, D. C. Lankin, R. A. Gemeinhart, G. F. Pauli, *Fitoterapia* **127**, 212 (2018).
77. A. Das and R. Biswas, *J. Phys. Chem. B* **119**, 10102 (2015).
78. T. Pradhan and R. Biswas, *J. Phys. Chem. A* **111**, 11514 (2007).
79. B. Guchhait and R. J. Chem. Phys. **138**, 114909 (2013).
80. T. Pradhan, H. A. R. Gazi, B. Guchhait and R. Biswas, *J. Chem. Sci.* **124**, 355 (2012).
81. R. Biswas, A. R. Das, T. Pradhan, D. Touraud, W. Kunz and S. Mahiuddin, *J. Phys. Chem. B* **112**, 6620 (2008).
82. L. Horng, J. A. Gardecki and M. Maroncelli, *J. Phys. Chem. A* **101**, 1030 (1997).
83. K. Dahl, R. Biswas, N. Ito, and M. Maroncelli, *J. Phys. Chem. B* **109**, 1563 (2005).
84. T. Pradhan, P. Ghoshal, R. Biswas, *J. Chem. Sci.* **120**, 275 (2008).
85. S. Koley, H. Kaur and S. Ghosh, *Phys. Chem. Chem. Phys.* **16**, 22352 (2014).

86. N. Sarma, J. M. Borah, H. A. R. Gazi, B. Guchhait, S. Mahiuddin and R. Biswas, *J. Phys. Chem. B* **115**, 9040 (2011).
87. S. Indra, B. Guchhait and R. Biswas, *J. Chem. Phys.* **144**, 124506 (2016).
88. D. M. Cristancho, D. R. Delgado, F. Martínez, M. A. A. Fakhree, A. Jouyban, *Rev. Colomb. Cienc. Quím. Farm.* **40**, 92 (2011).
89. S. Das, R. Biswas, and B. Mukherjee, *J. Phys. Chem. B* **119**, 11157 (2015).
90. F. Perrin, *J. Phys. Radium*, **5**, 497 (1934).
91. H. Jin, G. A. Baker, S. Arzhantsev, J. Dong and M. Maroncelli, *J. Phys. Chem. B* **111**, 7291 (2007).
92. B. Guchhait, H. A. R. Gazi, H. K. Kashyap and R. Biswas, *J. Phys. Chem. B* **114**, 5066 (2010).
93. G. B. Dutt, T. K. Ghanty, *J. Phys. Chem. B* **107**, 3257 (2003).
94. M. F. Shlesinger, G. M. Zaslavsky and J. Klafter, *Nature (London)* **363**, 31 (1993).
95. J. Habasaki and K. L. Ngai, *J. Chem. Phys.* **129**, 194501 (2008).
96. Z. Hu, X. Huang, H. V. R. Annapureddy and C. J. Margulis, *J. Phys. Chem. B* **112**, 7837 (2008).
97. Sandipa Indra and Ranjit Biswas, *J. Phys. Chem. B* **120**, 11214 (2016).
98. R. S. Fee and M. Maroncelli, *Chem. Phys.* **183**, 235 (1994).
99. C-M. Hu and R. Zwanzig, *J. Chem. Phys.* **60**, 4354 (1974)
100. A. Samanta, *J. Phys. Chem. B* **110**, 13704 (2006)
101. X-X. Zhang, M. Liang, J. Hunger, R. Buchner and M. Maroncelli *J. Phys. Chem. B*, **117**, 15356 (2013)
102. X-X. Zhang, M. Liang, N. P. Ernsting and M. Maroncelli, *J. Phys. Chem. B* **117**, 4291 (2013).
103. Y. H. Zhao, M. H. Abraham, A. M. Zissimos, *J. Org. Chem.* **68**, 7368 (2003).

Chapter 4

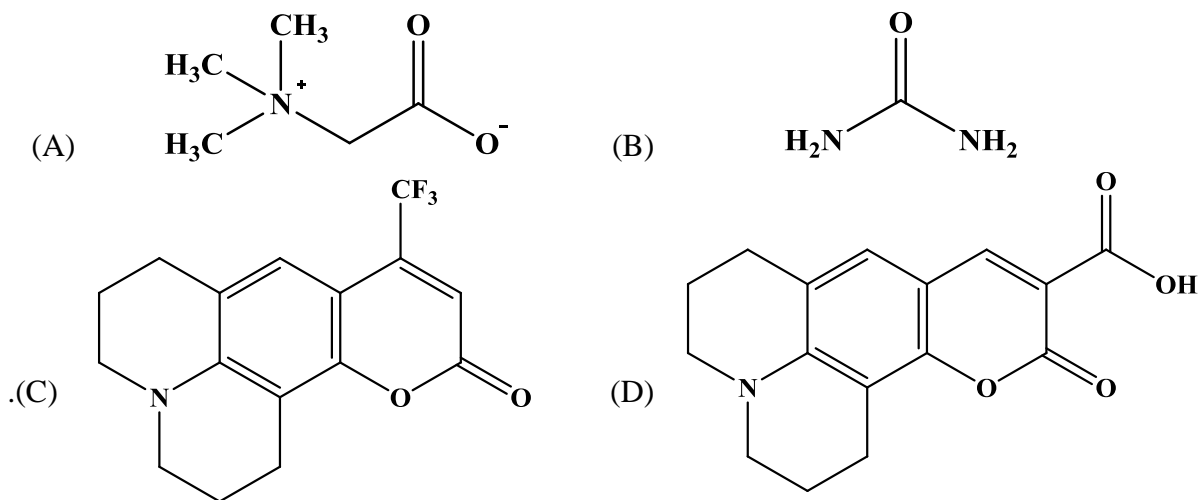
Interaction and Dynamics in Betaine Based Deep Eutectic Solvent: Temperature Dependent Time-Resolved Fluorescence Spectroscopic Measurements

4.1 Introduction

Demand for environment friendly and less toxic solvent leads to the invention of different types of solvents such as room temperature super critical fluids(RTSFs),¹⁻³ gas expanded liquids (GXLs),⁴⁻⁶ room temperature ionic liquids (RTILs)⁷⁻¹⁰ and deep eutectic solvents (DESs)¹¹⁻¹⁶. Deep eutectic solvent (DES) is a new generation potential alternative to the conventional molecular solvents and possess exquisite solvent properties. Plentiful natural and biodegradable chemicals along with huge possible combinations, easy preparation, low cost, favorable transportation, minimal vapor pressure and other physicochemical features have made DESs interesting system for basic science research and its applications as host media in different areas. Extensive hydrogen bond formation among the H-bond donors (HBD) and H-bond acceptors (HBA), and entropy gain for being in the liquid phase contribute to the depression of melting temperature in DESs. Proper selection of eco-friendly and biodegradable components keeps DESs always in the focus of green solvents.^{13,17-25} Selection of a solvent with desirable properties is critical for a selective reaction and/or specific application, for example, extraction, dissolution, separation, purification and so on. Solution properties (thermal stability, viscosity, polarity, toxicity etc.) of the DESs depend upon its components and composition. Therefore, desirable properties of DESs can be achieved by the appropriate selection of its components and composition.²⁶⁻³⁰ Thus, the selection of the component of DES is vital, and one prefers naturally abundant compounds, such as, amino acids, urea, sugars and substances like these to preserve greenness and eco-sustainability of the resultant DESs.^{19,25,31-35} DESs prepared from these natural raw materials are known as naturally abundant deep eutectic solvents (NADESs) and utilized in various interdisciplinary areas.^{23,33,36-46}

In this work we have taken betaine, urea and water as components of deep eutectic solvent (see Scheme 4.1). Betaine is a trimethyl derivative of glycine (amino acid) present in bacteria, invertebrates, plants, various foods and mammals.⁴⁷⁻⁵⁵ Moreover, non-toxic nature encourages to select betaine as one of the components of DES.⁵⁶ Betaine is used as an osmolyte,⁵⁷ a methyl group source for different biochemical reactions,⁵⁸ and in treatment of several diseases.⁵⁹⁻⁶¹ Another component of the DES under investigation is urea, the most common nitrogenous fertilizers used and also have immense impact on protein stability and functionality.⁶²⁻⁶⁷ Interestingly, betaine can be served as an osmolyte in the preservation of protein against the extreme physical conditions,⁶⁸ while urea acts as a protein denaturant. Note that the stability of protein depends on the ratio of osmolytes and urea.^{69,70} Therefore, betaine, urea and water based DES would be interesting system for understanding interspecies interactions and their dynamics. Physical properties of betaine or urea based DESs were studied before and used for various purposes.⁷¹⁻⁷⁷ Betain-urea based deep eutectic solvents have been employed for stabilization of proteins,^{78,79} extraction of bioactive compounds,⁸⁰ biomedical applications,⁸¹ etc. For preservation and stabilization of DNA, one needs to understand how DNA molecules interact with these novel solvent system as this interaction is crucial for the DNA stabilization and functionality.⁸² The study of interaction and dynamics in these DESs is essential for smart applications (for example, protein preservation). Moreover, interaction and dynamics present in DESs may help to understand many biochemical processes that involve poorly water-soluble but fairly lipid-soluble metabolites which are nicely soluble in DESs.^{33,35}

Scheme 4.1: Chemical structures of (A) Betaine, (B) Urea, (C) Coumarin 153 and (D) Coumarin 343



As the properties of the DESs depend on its structure, dynamics and interaction, thus, property-driven application of DESs insist comprehensive understanding of structure, dynamics and interaction present in it. Structure, dynamics and interaction of DESs have been studied using different experimental techniques such as neutron diffraction,^{83,84} pulsed field gradient (PFG) NMR,^{85,86} dielectric relaxation,^{16,30,87} fs-RIKES,⁸⁸ 2D-IR,^{89,90} time-resolved fluorescence,^{15,29,87,91} and also by computer simulation⁹²⁻⁹⁵. Here, we have made an attempt to investigate dynamics and interaction of [Bet+Ure+Wat] DES using steady state and time-resolved fluorescence spectroscopy. For the fluorescence measurements two different types of probe have been chosen: hydrophobic coumarin 153 (C153), and hydrophilic coumarin 343 (C343).

4.2 Experimental Details

4.2.1 Sample Preparation

Betaine ($\geq 99.0\%$, Sigma-Aldrich, $T_m \approx 574$ K) and Urea ($\geq 98\%$, Sigma-Aldrich, $T_m \approx 405-408$ K) were vacuum-dried (~ 300 K) overnight before use, and Millipore water was used for sample preparation. Laser grade coumarin 153 (C153) (Sigma-Aldrich) and coumarin 343 (C343) (Sigma-Aldrich) were used as received. Betaine, urea and water [Bet:Ure:Wat (11.7:12:1; weight ratio)] were taken in a screw-capped glass vial and heated at ~ 343 K with constant stirring at ~ 600 rpm in a hot oil bath for ~ 2 h. A colorless transparent liquid (i.e. the DES) was formed and allowed to cool gradually to the room temperature (~ 298 K). For solubility checking, required amount of three components were taken in a container and kept under constant stirring at 600 rpm at 298 K. This mixture becomes opaque ('B' of Fig. A.b.1) and never formed transparent solution at 298 K. The resultant DES prepared following the 'appropriate' method is a transparent liquid at that temperature ('A' of Fig. A.b.1; $T_f = 279 \pm 2$ K). Above observation suggests that the system under study is not a mere multi-component mixture containing betaine, urea and water in liquid phase but a DES only. Hydrophobic C153 and hydrophilic C343 were employed for all the optical measurements as local reporters. Stock solutions of C153 and C343 were prepared in carrier solvents. For optical measurements few drops of probes solution prepared in carrier solvent taken into the preparation container prior to the DES constituent, and carrier solvent was evaporated off. To overcome the solubility problem of probe in the prepared DES due to high viscosity we have adopted this approach. All the optical measurements are

performed well above the glass transition temperature (T_g) (see Fig. A.b.2) of [Bet+Ure+Wat] DES. Note that composition of betaine, urea and water for DES prepared here are different from the existing one⁹⁶ and thus this DES (under study) can be termed as a new one. Prepared DES was transferred into a preheated quartz cuvette (path length 1 cm). Before measurements, sufficient time was allowed to the cuvette (placed into the sample chamber) for thermal equilibration (with uncertainty ± 1 K). Note that external probe (C153 and C343, for structure see Scheme 4.1) concentration was maintained at $\leq 10^{-5}$ M in all optical measurements.

Refractometer (RUDOLPH, J357), automated density-cum-sound analyzer (Anton Paar, DSA5000) and micro viscometer (AMVn, Anton Paar), were employed respectively for refractive index, density and viscosity measurements.^{14,91} These data are summarized in Table A.b.3 (Appendix). Glass transition temperature (T_g) of the prepared DES was measured by a differential scanning calorimeter (DSC, TA Instrument Q2000) and the calorimetric trace is shown in Fig. A.b.2. Note that all measurements presented here were performed well above (90-130 K) the T_g of the [Bet+Ure+Wat] DES as the measured T_g for this DES is ~ 218 K.

4.2.2 Steady State Measurements

UV-Visible spectrophotometer (UV-2600, Shimadzu) and fluorimeter (Fluorolog, Jobin-Yvon, Horiba) connected with peltier-temperature controller were used for steady state absorption and fluorescence emission collection, respectively. Prior to analysis, solvent blanks were subtracted from the probe spectra and transformed properly to the frequency domain for further analyses and frequency determination.^{24,87}

4.2.3 Time-Resolved Fluorescence Measurements

Time-correlated single photon counting (LifeSpec-ps, Edinburgh Instruments, U. K.) technique along with 409 nm (LED) excitation laser source have been employed for time-resolved fluorescence measurements and the details of this setup discussed elsewhere.^{14,28} The full width at half-maximum (FWHM) of the instrument response function (IRF) using 409 nm excitation laser source and scattering solution was found to be ~ 85 ps. Based on the standard protocol we have performed dynamic Stokes shift and anisotropy measurements.⁹⁷⁻¹⁰¹

Details regarding time-resolved fluorescence spectroscopic measurements have been described in chapter 2.

4.3 Results and Discussion

4.3.1 Steady State Absorption and Emission of Two Different Probes: Hydrophobic C153 and Hydrophilic C343

Temperature ($303 \leq T/K \leq 343$) dependent steady state absorption and emission spectra of C153 and C343, dissolved in [Bet+Ure+Wat] DES are shown in Fig. 4.1. The spectral features of C153 and C343 are similar and nearly insensitive to the temperature, though one expects that C153 and C343, owing respectively to their hydrophobic and hydrophilic nature, would explore different environments and therefore spectral features would not be the same. These results indicate that the solute–solvent interactions remain unaffected within the temperature range $303 \leq T/K \leq 343$, for both the solutes. In DESs this type of insensitivity of steady state spectral behavior of C153 to temperature variation has been observed previously.^{24,87} This insensitivity to temperature is somewhat counter-intuitive because temperature rise is expected to reduce the dielectric constant (and hence polarity) of the medium.¹⁰²⁻¹⁰⁴ Therefore, observed result is probably the outcome of the preferential solvation of probes by the more polar species of the DES components (betaine ($\mu \sim 12$),¹⁰⁵ urea ($\epsilon_0 \sim 4$)¹⁰⁶ water ($\epsilon_0 \sim 80$)¹⁰⁷; for molten urea, $\epsilon_0 \sim 65$,¹⁶ with a liquid phase dipole moment (μ) of ~ 7 D) present in the [Bet+Ure+Wat] DES. Excitation wavelength dependence fluorescence measurements provide information regarding the spatially distributed different environments surrounding the probe molecules within its excited state lifetime. Spatial homogeneity refers to the average uniform density fluctuation around the solute and thus the emission peak frequency (of a dissolved solute) would be insensitive to the excitation wavelength ($\lambda_{exc.}$). Fig. A.b.4 represents the emission peak frequencies ($\nu_{em.}$) of C153 and C343 as a function of excitation wavelength ($\lambda_{exc.}$). $\lambda_{exc.}$ -induced $\Delta\nu_{em.}$ ($= \nu_{em,peak}(\lambda_{blue,exc.}) - \nu_{em,peak}(\lambda_{red,exc.})$) obtained for C153 and C343 is within $100\sim 280$ cm^{-1} which suggests that the present DES is mildly heterogeneous within the lifetime (see Table A.b.5) of these probes. Moreover, to check the fast fluctuation in the medium a short lifetime probe trans-2-[4-(dimethylamino)styryl]benzothiazole (DMASBT) ($\tau_{lif} \approx 750$ ps in

[Bet+Ure+Wat]) has been employed and λ_{exc} dependence of $\nu_{\text{em.}}$ monitored. Results for DMASBT are also shown in the same figure. $\lambda_{\text{exc.}}$ -induced shift of $\nu_{\text{em.}}$ for DMASBT is found to be similar as those for C153 and C343 in this DES, supporting the view of homogeneous solution structure in the timescale of $\sim 1\text{-}5$ ns.

Temperature dependent ($303 \leq T/\text{K} \leq 343$) average lifetimes ($\langle \tau_{\text{life}} \rangle$) for C153 and C343 in this DES are summarized in Table A.b.5. Note that average lifetime of C343 in this DES are insensitive to temperature, whereas a decrease of $\sim 30\%$ is observed for C153. This may reflect different solvation environments surrounding these hydrophilic (C343) and hydrophobic (C153) probes.

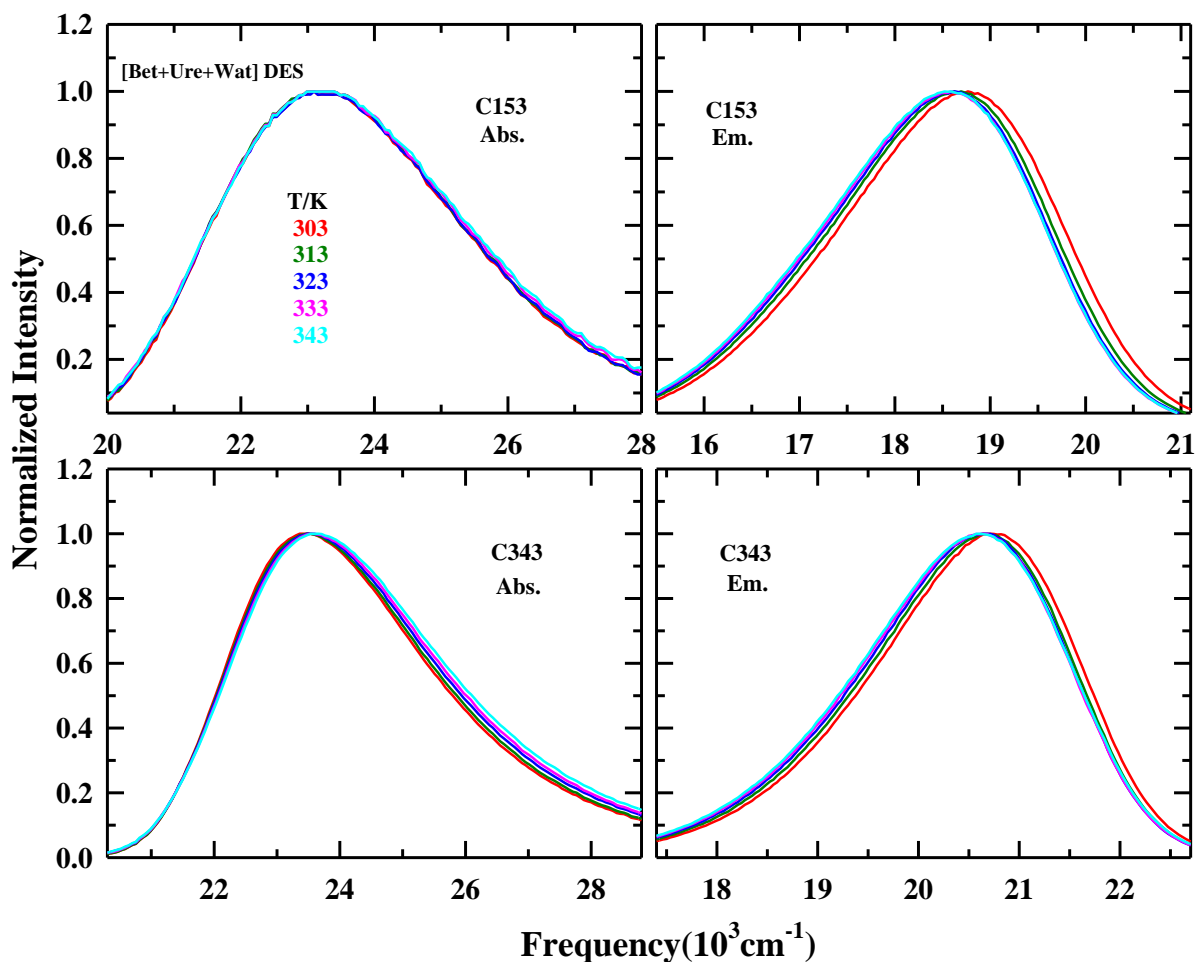


Fig. 4.1: Temperature dependent absorption (left panels) and emission (right panels) spectra of C153 and C343 in [Bet+Ure+Wat] DES. All representations are color coded.

4.3.2 Solute Rotation: Coupling with Medium Viscosity

Time-resolved fluorescence intensity decays, $I_{\text{para}}(t)$ and $I_{\text{perp}}(t)$, of C153 (upper panel) and C343 (lower panel) dissolved in [Bet+Ure+Wat] DES are shown in Fig. A.b.6. Representative rotational anisotropy decays, $r(t)$, of C153 (upper panel) and C343 (lower panel) in [Bet+Ure+Wat] DES at 323 K are displayed in Fig. 4.2. Solid black lines are the bi-exponential fits going through the data points and the corresponding fit parameters are summarized in Table 4.1. This biphasic nature of friction experienced by probe molecules in [Bet+Ure+Wat] DES are characterized by a minor (~20%) component with time constant ~100 ps, followed by a dominating, slower component with a time constant of a few nanoseconds. As increase in temperature leads to decrease in solution viscosity (see Table A.b.3), it is expected that the friction felt by a rotating molecule would also be less. Therefore, $\langle \tau_r \rangle$ follows the same trend as viscosity with temperature (see Table 4.1). Next the coupling between solute rotation and solution viscosity is explored by showing the measured solute rotation times, $\langle \tau_r \rangle$, as a function of temperature-scaled viscosity, η/T in a log-log plot (See Fig. 4.3) for C153 (upper panel) and C343 (lower panel). A fractional viscosity dependence of average rotational time ($\langle \tau_r \rangle$) of the type, $\langle \tau_r \rangle \propto (\eta/T)^p$ with $p \approx 0.5$, suggests the existence of pronounced temporal heterogeneity in the medium. This type of strong fractional viscosity dependence has also been observed in ionic DESs.^{14,108} Interestingly, irrespective of inherent chemical nature, C153 and C343 show similar decoupling from medium viscosity.

In the same figure,(Fig. 4.3), stick and slip hydrodynamic predictions ($\tau_r = \eta V f C / k_B T$)^{28,109,110} for the rotation of C153 and C343 in [Bet+Ure+Wat] are also shown by dashed lines. In these calculations, volume $V^{\text{C153}} = 246 \text{ \AA}^3$ ($V^{\text{C343}} = 243 \text{ \AA}^3$), shape factor $f^{\text{C153}} = 1.71$ ($f^{\text{C343}} = 1.99$), $C_{\text{stick}}^{\text{solute}} = 1$, and $C_{\text{slip}}^{\text{C153}} = 0.24$ ⁹⁷ ($C_{\text{slip}}^{\text{C343}} = 0.18$ ¹¹¹) have been used for these solutes. $\langle \tau_r \rangle$ of C153 and C343 fall between stick and slip predictions at high temperature or at lower η/T values, but become sub-slip at lower temperatures (higher η/T). This deviation from

hydrodynamic predictions for both the solutes at lower temperature is probably arising from non-hydrodynamic angular moves, such as, orientation jumps and persistent inertia-driven motion.

112-114

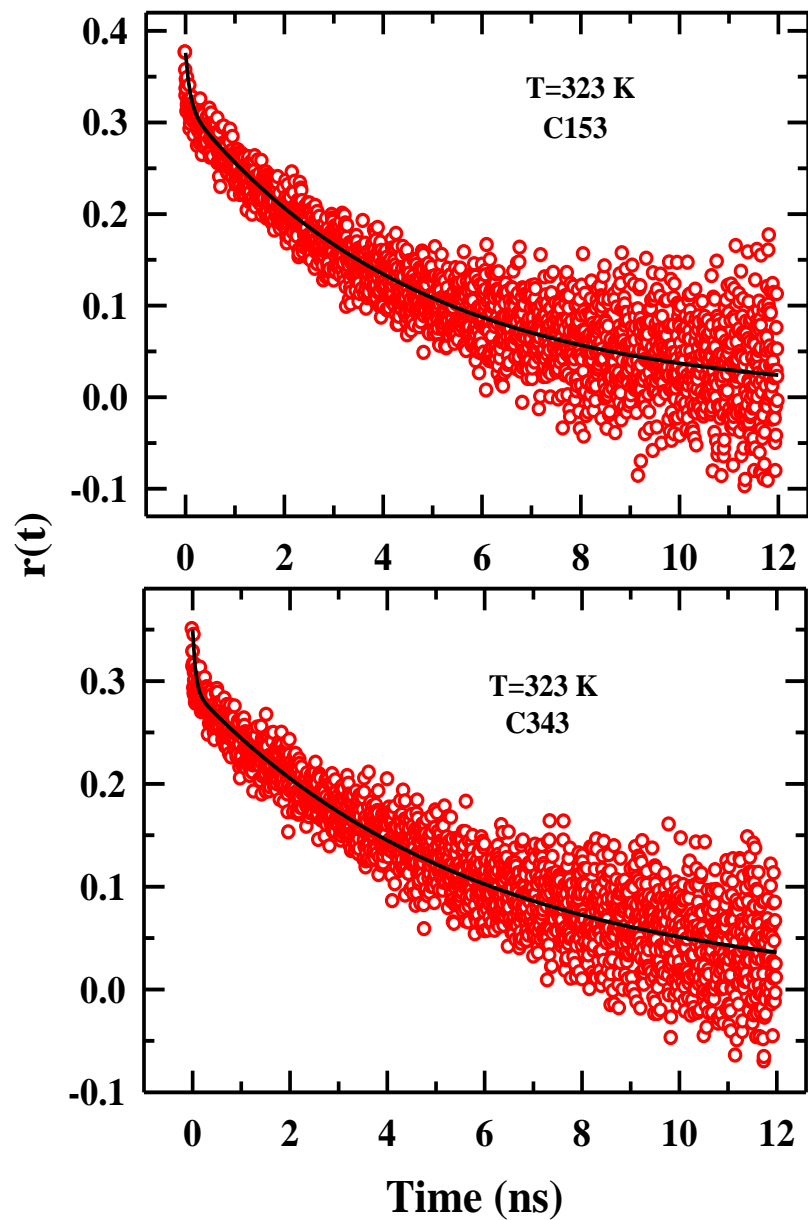


Fig. 4.2: Representative time-resolved fluorescence anisotropy ($r(t)$) decays of C153 (upper panel) and C343 (lower panel) in [Bet+Ure+Wat] DES at 323 K. Lines going through data denote bi-exponential fits.

Table 4.1: Bi-exponential fit parameters for the temperature dependent $r(t)$ of C153 and C343 in [Bet+Ure+Wat] DES.

C153 in [Bet+Ure+Wat] DES					
T/K	a_1 (%)	τ_1 (ps)	a_2 (%)	τ_2 (ps)	$\langle \tau_r \rangle^a$ (ps)
303					
308	20	84	80	6812	5466
313	18	70	82	5731	4712
318	16	89	84	5038	4246
323	15	92	85	4651	3967
328	11	118	89	3742	3343
333	14	98	86	2866	2478
338	12	108	88	2298	2035
343	14	114	86	1707	1484
C343 in [Bet+Ure+Wat] DES					
303					
308	21	62	79	8598	6805
313	20	54	80	7760	6219
318	14	57	86	6464	5567
323	17	62	83	5753	4786
328	9	65	91	4602	4194
333	13	80	87	3837	3349
338	14	72	86	3042	2626
343	10	61	90	2301	2077

^aAverage rotational time, $\langle \tau_{rot} \rangle$, can be reproduced within $\pm 10\%$ uncertainty

Next, estimated activation energies (E_a) associated with solute (C153/C343) rotation and viscosity of the medium are shown in Fig. 4.4. E_a associated with the solute rotation is expected to be similar to that from viscosity if solute rotation is regulated by the bulk solution viscosity. In [Bet+Ure+Wat] DES, temperature dependent measurements of solution viscosity provide an activation energy, $E_a^{\eta} \approx 56.73 \text{ kJ mol}^{-1}$, which is ~ 2 times greater than that obtained from temperature dependent C153/C343 rotation times ($E_a^{C153} \approx 31.39 \text{ kJ mol}^{-1}$ and $E_a^{C343} \approx 29.68 \text{ kJ mol}^{-1}$). This is a direct reflection of the partial decoupling of solute rotation from solution viscosity, shown in Fig. 4.3.

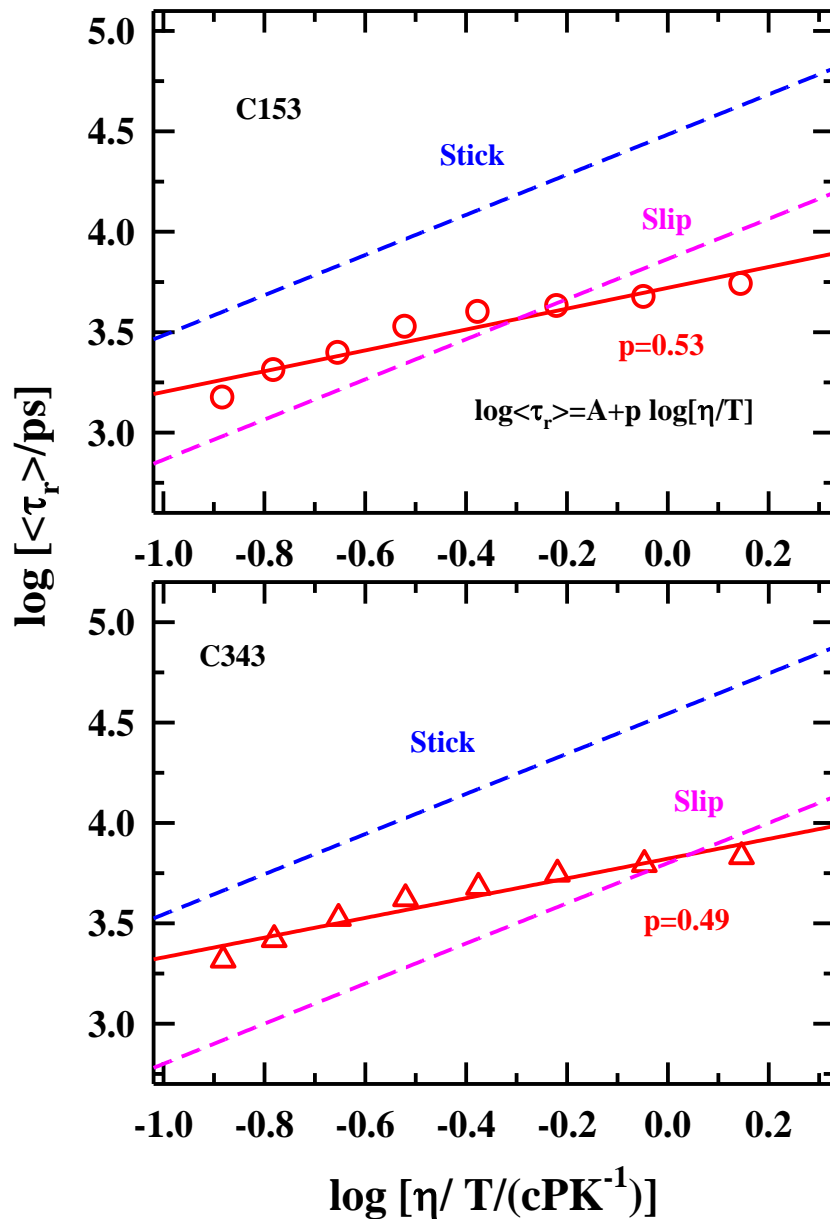


Fig. 4.3: Viscosity coupling of average rotation times ($\langle\tau_r\rangle$) for C153 and C343 in [Bet+Ure+Wat] DES. Temperature-dependent average rotational times are shown as a function of temperature-reduced viscosity (η/T) in a log-log fashion. Lines through the data represent fits to the following expression: $\log \langle\tau_r\rangle = A + p \log[\eta/T]$. Dashed lines represent the hydrodynamic (Stokes-Einstein-Debye) predictions, $\tau^{SED} = (V\eta/k_B T)fC$, where V denotes volume, f shape factor and C solute-solvent coupling parameter, and $k_B T$ Boltzmann constant times the absolute temperature.

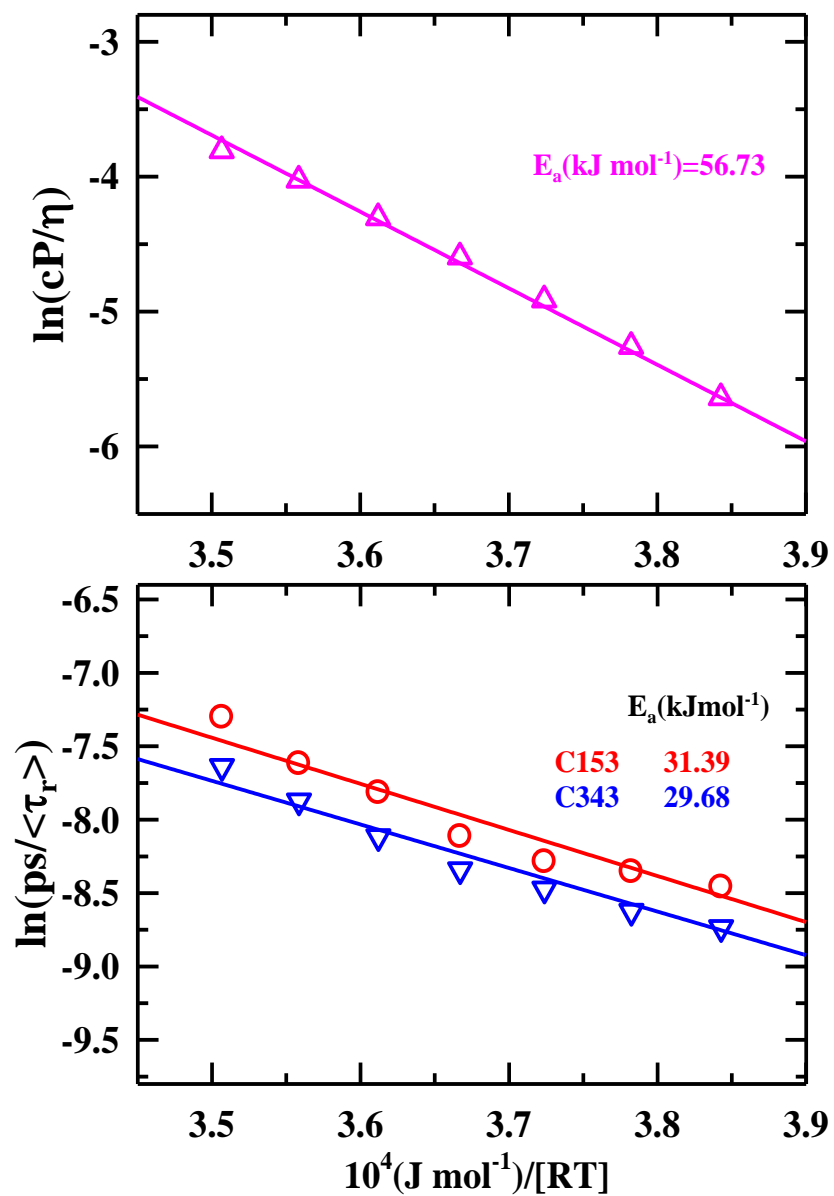


Fig. 4.4: Arrhenius plot for temperature dependent viscosity coefficients (η) for [Bet+Ure+Wat] DES, and average rotation times ($\langle\tau_r\rangle$) of two different solutes dissolved in it. Solid lines represent fits through the respective data sets. Note the activation energies for η and $\langle\tau_r\rangle$. All representations are color coded.

4.3.3 Solvation Dynamics

Fig. A.b.7 presents fluorescence transients of C343 in [Bet+Ure+Wat] DES at the short wavelength (blue: 450 nm) and long wavelengths (red: 590 nm) along with the tri-exponential fits. Parameters of the tri-exponential fits are presented in the inset. Only decay at the lower wavelength (blue), and rise followed by decay at the higher wavelength (red) is a hallmark of Stokes shift dynamics.^{28,115} Fig. A.b.7 displays this feature for C343 in [Bet+Ure+Wat] DES where data were taken at 303 K. Time-resolved emission spectra (TRES) along with steady state spectrum are shown in Fig. 4.5 (upper panel). Blue shift in the steady state spectrum relative to TRES at $t = \infty$ indicates incomplete equilibration of solvent environments surrounding the excited C343 in [Bet+Ure+Wat] DES during the steady state fluorescence emission. Magnitude of dynamic Stokes shift for C343 in [Bet+Ure+Wat] DES is $\sim 800 \text{ cm}^{-1}$ with an estimated missing component of $\sim 70\%$ (calculated using the Fee-Maroncelli method¹¹⁶) of the total dynamics. This means the broad temporal resolution ($\sim 85 \text{ ps}$) employed in the measurements could detect only the slower portion of the dynamics, leaving out completely the sub-picosecond and sub-50 ps relaxations. These relaxation timescales are quite feasible for this DES because it contains small dipolar molecules (urea and water), and all the constituents are capable of participating in H-bonding. Collective low frequency motions of H-bonded species are known to generate sub-picosecond solvation response, while reorientational relaxations of urea and water in this medium are expected to contribute to the sub-50 ps dynamics. Missing percentage increases with increasing temperature (see Table 4.2). Therefore, we refrain from measurements of Stokes shift dynamics at higher temperatures. Representative temperature dependence of solvation response function $S(t)$ is shown in Fig. 4.5 (lower panel). Fit parameters are summarized in Table 4.2. Solvation response obtained is described by a fast $\sim 250 \text{ ps}$ component and a slower one with a few nano-second ($\sim 3 \text{ ns}$) time constant, both with nearly equal amplitudes.

Now we discuss about the probable origin for these solvation timescales for C343 in [Bet+Ure+Wat] DES. In the absence of DR data and simulations we speculate the following. The fast solvation component may arise from structural hydrogen bonding among the constituents of this DES.¹⁶

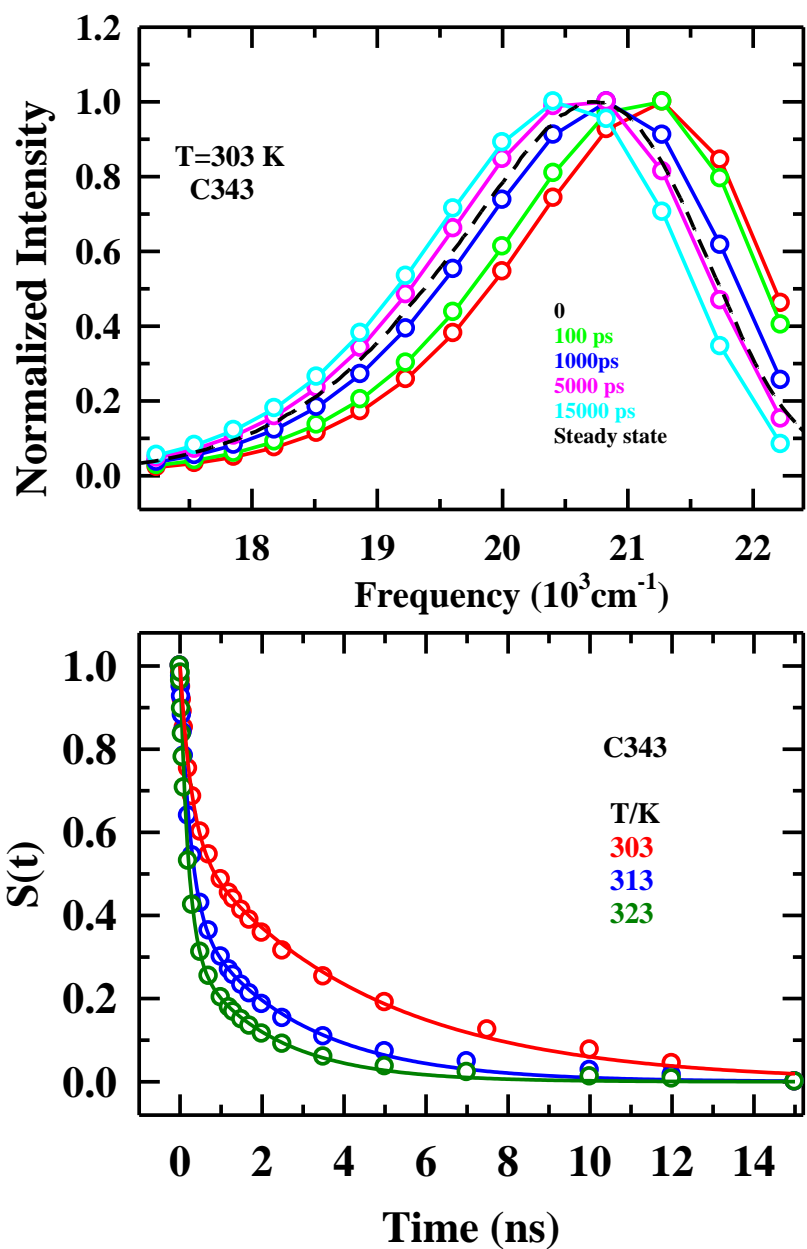


Fig. 4.5: Time-resolved emission spectra (TRES) (upper panel) at different time slices constructed from the measured intensity decays of C343 dissolved in [Bet+Ure+Wat] DES and the corresponding steady state emission spectrum. Temperature dependent solvation response functions, $S(t)$, of C343 in [Bet+Ure+Wat] DES are shown in the lower panel. Solid lines through the data points represent bi-exponential fits to the $S(t)$.

The relaxation of the structural H-bonding involves centre-of-mass diffusion of the participating species, and a timescale of ~200-300 ps can easily arise from translational diffusion of urea and water molecules. The multi nanosecond component probably originates from the restricted rotation coupled to collective H-bond dynamics involving the N-H group of urea acting as H-bond donor and C=O (of urea or/and betaine) as a H-bond acceptor.⁸⁷ Simulations and measurements with sharper temporal resolution are required to fully map and understand the solvation response of this important deep eutectic solvent.

Table 4.2: Bi-exponential fit parameters for temperature dependent solvation response functions, $S(t)$, obtained with C343 in [Bet+Ure+Wat] DES along with observed dynamic Stokes shift ($\Delta\nu_{obs.}$) magnitudes and missing percentages.

T (K)	a_1 (%)	τ_1 (ps)	a_2 (%)	τ_2 (ps)	$\langle \tau_s^{C343} \rangle^a$ (ps)	$\Delta\nu_{obs.}^b$ (cm^{-1})	% missed
303	44	270	56	3894	2299	863	64
313	58	247	52	2689	1542	830	69
323	68	197	42	2033	987	779	72

^aAverage solvation time, $\langle \tau_s \rangle$, can be reproduced within $\pm 10\%$ uncertainty. ^bUncertainty $\pm 150 \text{ cm}^{-1}$

4.4 Conclusion

Here we have reported preparation of a new DES composed of betaine, urea and water ([Bet:Ure:Wat (11.7:12:1 weight ratio)]) and explored temperature dependent solute-centered relaxation dynamics employing time-resolved fluorescence measurements. This DES is stable at a temperature lower than room temperature ($T_f = 297 \pm 2\text{K}$) with a measured $T_g \sim 218 \text{ K}$. Excitation wavelength dependent steady state fluorescence measurements using probes with widely different lifetimes suggest mild-spatial heterogeneity in the medium. Interestingly, time-resolved fluorescence anisotropy measurements depict strong fractional viscosity dependence for solute rotation times, which has been interpreted in terms of pronounced temporal heterogeneity. Dynamic Stokes shift measurements with a temporal resolution of ~85 ps reveal bi-exponential

solvation response for C343 in [Bet+Ure+Wat] at 303 K with an estimated missing component of ~70 % of the full dynamics. Bi-exponential solvation response with time constants of ~250 ps and ~3 ns has been detected. This biphasic response is speculated to arise from structural H-bond relaxations, and restricted reorientations of H-bonded species coupled to collective H-bond relaxations. Ultrafast dynamics measurements employing sharper temporal resolution and simulation studies are required to map the full dynamics and understand the molecular mechanisms related to solvation energy relaxation in this biodegradable medium.

References:

1. C. A. Eckert, B. L. Knutson and P. G. Debenedetti, *Nature* **383**, 313 (1996).
2. J. E. Lewis, R. Biswas, A. G. Robinson, and M. Maroncelli, *J. Phys. Chem. B* **105**, 3306 (2001).
3. S. V. Dzyuba and R. A. Bartsch, *Angew. Chem. Int. Ed.* **42**, 148 (2003).
4. C. A. Eckert, C. L. Liotta, D. Bush, J. S. Brown and J. P. Hallett, *J. Phys. Chem. B* **108**, 18108 (2004).
5. J. P. Hallett, C. L. Kitchens, R. Hernandez, C. L. Liotta and C. A. Eckert, *Acc. Chem. Res.* **39**, 531 (2006).
6. A. M. Scurto, K. Hutchenson and B. Subramaniam, *ACS Symposium Series*, **1006**, 3 (2009).
7. M. J. Earle and K. R. Seddon, *Pure Appl. Chem.* **72**, 1391 (2000).
8. B. L. Bhargava and S. Balasubramanian, *J. Phys. Chem. B* **111**, 4477 (2007).
9. M. Maroncelli, X. X. Zhang, M. Liang, D. Roy and N. P. Ernsting, *Faraday Discuss.* **154**, 409 (2012).
10. H. K. Kashyap and R. Biswas, *J. Phys. Chem. B* **112**, 12431 (2008).
11. E. L. Smith, A. P. Abbott, K. S. Ryder, *Chem. Rev.* **114**, 11060 (2014).
12. H. Zhang, K. D. O. Vigier, S. Royer, F. Jerome, *Chem. Soc. Rev.* **41**, 7108 (2012).
13. M. Francisco, A. Bruinhorst, and M. C. Kroon, *Angew. Chem. Int. Ed.* **52**, 3074 (2013).
14. B. Guchhait, S. Das, S. Daschakraborty and R. Biswas, *J. Chem. Phys.* **140**, 104514 (2014).
15. A. Das, S. Das and R. Biswas, *Chem. Phys. Lett.* **581**, 47 (2013).
16. K. Mukherjee, S. Das, E. Tarif, A. Barman, and R. Biswas, *J. Chem. Phys.* **149**, 124501 (2018).
17. J. M. DeSimone, *Science* **297**, 799 (2002).
18. W. M. Nelson, *Green solvents for chemistry, Perspectives and Practice*, New York, NY: Oxford University Press New York, 2003.
19. A. P. Abbott, D. Boothby, G. Capper, D. L. Davies, and R. K. Rasheed, *J. Am. Chem. Soc.* **126**, 9142 (2004).
20. J. H. Clark and S. J. Tavener, *Org. Process Res. Dev.* **11**, 149 (2007).
21. P. D. de María and Z. Maugeri, *Curr. Opin. Chem. Biol.* **15**, 220 (2011).

22. D. V. Wagle, H. Zhao and G. A. Baker, *Acc. Chem. Res.* **47**, 2299 (2014).
23. A. Paiva, R. Craveiro, I. Aroso, M. Martins, R. L. Reis and A. R. C. Duarte, *ACS Sustainable Chem. Eng.* **2**, 1063 (2014).
24. A. Das, S. Das, R. Biswas *J. Chem. Phys.* **142**, 034505 (2015).
25. M. Espino, M. Á. Fernández, F. J. V. Gomez and M. F. Silva, *TrAC Trends in Analytical Chemistry* **76**, 126 (2016).
26. M. Francisco, A. van den Bruinhorst, and M.C. Kroon, *Green Chem.* **14**, 2153 (2012).
27. S. Rajkhowa, A. Das, S. Mahiuddin, and R. Biswas, *J. Chem. Eng. Data* **57**, 3467 (2012).
28. B. Guchhait, H. A. R. Gazi, H. K. Kashyap and R. Biswas, *J. Phys. Chem. B* **114**, 5066 (2010).
29. B. Guchhait, S. Das, S. Daschakraborty and R. Biswas, *J. Chem. Phys.* **140**, 104514 (2014).
30. K. Mukherjee, A. Das, S. Choudhury, A. Barman and R. Biswas, *J. Phys. Chem. B* **119**, 8063 (2015).
31. A. P. Abbott, D. Boothby, G. Capper, D. L. Davies, and R. K. Rasheed, *J. Am. Chem. Soc.* **126**, 9142 (2004).
32. S. Gore, S. Baskaran and B. Koenig, *Green Chem.* **13** 1009 (2011).
33. Y. Dai, J. van Spronsen, G.-J. Witkamp, R. Verpoorte and Y. H. Choi, *Anal. Chim. Acta* **766**, 61 (2013).
34. W-C. Huang, D. Zhao, N. Guo, C. Xue and X. Mao, *J. Agric. Food Chem.* **66**, 11897 (2018).
35. Y. H. Choi, J. van Spronsen, Y. Dai, M. Verberne, F. Hollmann, Isabel W.C.E. Arends, G. J. Witkamp, and R. Verpoorte, *Plant Physiol.* **156**, 1701 (2011).
36. M. A. Kareem, F. S. Mjalli, M.A. Hashim and I.M. AlNashef, *Fluid Phase Equilib.* **314**, 52 (2012).
37. M. Faggian, S. Sut, B. Perissutti, V. Baldan, I. Grabnar and S. Dall'Acqua, *Molecules* **21**, 1531 (2016).
38. E. Durand, J. Lecomte, B. Baréa, G. Piombo, E. Dubreucq and P. Villeneuve, *Process Biochem.* **47**, 2081 (2012).
39. A. Hayyan, M. A. Hashim, M. Hayyan, F. S. Mjalli and I. M. AlNashef, *J. Clean. Prod.* **65**, 246 (2014).

40. Z-F. Wei, X-Q.Wang, X. Peng, W. Wang, C-J. Zhao, Y-G. Zu, Y-J. Fu, *Ind. Crop. Prod.***63**, 175 (2015).
41. R. J. Sánchez-Leija, J. A. Pojman, G. Luna-Bárceñas, and J. D. Mota-Morales, *J. Mater. Chem. B* **2**, 7495 (2014).
42. M. H. Zainal-Abidin, M. Hayyan, A. Hayyan and N. S. Jayakumar, *Anal. Chim. Acta* **979**, 1 (2017).
43. I. M. Aroso, R. Craveiro, Â. Rocha, M. Dionísio, S. Barreiros, R. L. Reis, A. Paiva and A. R. C. Duarte, *Int. J. Pharm.* **492**,73 (2015).
44. M. B. Haider, D. Jha, B. M. Sivagnanam and R. Kumar, *J. Chem. Eng. Data* **63**, 2671 (2018).
45. S. Sun, Y. Niu, Q. Xu, Z. Sun, and X. Wei, *Ind. Eng. Chem. Res.* **54**, 8019 (2015).
46. L. Millia, V. Dall'Asta, C. Ferrara, V. Berbenni, E. Quartarone, F. M. Perna, V. Capriati, P. Mustarelli, *Solid State Ionics* **323**, 44 (2018).
47. W. Xing and C. B. Rajashekar, *Environ. Exp. Bot.* **46**, 21 (2001).
48. V. V. Kuznetsov and Shevyakova, *Physiol. Plant.* **100**, 320 (1997).
49. S. Konosu and T. Hayashi, *Bull. Jpn. Soc. Sci. Fisheries* **41**,743 (1975).
50. S. E. C. Davies, R. A. Chalmers, E. W. Randall, R. A. Iles, *Clin. Chim. Acta.* **178**, 241 (1988).
51. A. Sakamoto, Y. Nishimura, H. Ono, and N. Sakura, *Pediatr. Int.* **44**:409 (2002).
52. H. Koc, M. H. Mar, A. Ranasinghe, J. A. Swenberg and S. H. Zeisel, *Anal. Chem.* **74**, 4734 (2002).
53. D. H. Waggle, M. A. Lambert, G. D. Miller, E. P. Farrell and C. W. Deyoe, *Cereal Chemistry* **44**, 48 (1967).
54. S. A. S. Craig, *Am. J. Clin. Nutr.* **80**, 539 (2004).
55. S. H. Zeisel, *Clin. Chem. Lab. Med.* **51**, 467 (2013).
56. K. C. Hayes, A. Pronczuk, M. W. Cook, M. C. Robbins, *Food. Chem. Toxicol* **41**, 1685 (2003).
57. S. A. Kempson, K. Vovor-Dassu and C. Day, *Cell Physiol. Biochem.* **32**, 32 (2013).
58. L. Hoffmann, G. Brauers, T. Gehrman, D. Haussinger, E. Mayatepek, F. Schliess and B. C. Schwahn, *Am. J. Physiol. Gastrointest Liver Physiol.* **304**, G835 (2013).

59. M. Zhang, X. Wu, F. Lai, X. Zhang, H. Wu and T. Min, *J. Agric. Food. Chem.* **64**, 4068 (2016).
60. A. Lawson-Yuen and H. L. Levy, *Mol. Genet Metab.* **88**, 201 (2006).
61. E. Kathirvel, K. Morgan, G. Nandgiri, B. C. Sandoval, M. A. Caudill, T. Bottiglieri, S. W. French and T. R. Morgan, *Am. J. Physiol. Gastrointest Liver Physiol.* **299**, G1068 (2010).
62. L. Hua, R. Zhou, D. Thirumalai and B. J. Berne, *Proc. Natl. Acad. Sci. U. S. A.* **105**, 16928 (2008).
63. A. Das and C. Mukhopadhyay, *J. Phys. Chem. B* **113**, 12816 (2009).
64. D. Bandyopadhyay, S. Mohan, S. K. Ghosh and N. Choudhury, *J. Phys. Chem. B* **118**, 11757 (2014).
65. D. Soletto, L. Binaghi, A. Lodi, J. C. M. Carvalho, A. Converti, *Aquaculture* **243**, 217 (2005).
66. L. B. Sagle, Y. Zhang, V. A. Litosh, X. Chen, Y. Cho, and P. S. Cremer, *J. Am. Chem. Soc.* **131**, 9304 (2009).
67. B. J. Bennion and V. Daggett, *Proc. Natl. Acad. Sci. U.S.A.* **100**, 5142 (2003).
68. M.T. Kidd, P.R. Ferket and J.D. Garlich, *World Poult. Sci. J.* **53**, 125 (1997).
69. P.H. Yancey, *J. Exp. Biol.* **208**, 2819 (2005).
70. C-X. Zenga, S-J. Qi, R-P. Xin, B. Yang, Y-H. Wang, *J. Mol. Liq.* **219**, 74 (2016).
71. A. P. Abbott, G. Capper, D. L. Davies, K. J. McKenzie and S. U. Obi, *J. Chem. Eng.* **51**, 1280 (2006).
72. E. L. Smith, A. P. Abbott and K. S. Ryder, *Chem. Rev.* **114**, 11060 (2014).
73. A. P. Abbott, G. Capper, D. L. Davies, R. K. Rasheed and V. Tambyrajah, *Chem. Commun.*, 70 (2003).
74. P. B. Sánchez, B. González, J. Salgado, J. J. Parajó and Á. Domínguez, *J. Chem. Thermodynamics* **131**, 517 (2019).
75. I. M. Aroso, A. Paiva, R. L. Reis and A. R. C. Duarte, *J. Mol. Liq.* **241**, 654 (2017).
76. S. Khodaverdian, B. Dabirmanesh, A. Heydari, E. Dashtban-Moghadam and K. Khajeh F. Ghazi, *Int. J. Biol. Macromol.* **107**, 2574 (2018).
77. K. Wardhani, E. A. Krisanti and G. Andika, *AJChE* **18**, 1 (2018).
78. N. Li, Y. Wang, K. Xu, Y. Huang, Q. Wen, X. Ding, *Talanta*, **152**, 23 (2016).

79. S. Khodaverdian, B. Dabirmanesh, A. Heydarib, E. Dashtban-moghadama , K. Khajeha and F. Ghazi, *Int. J. Biol. Macromol* **107**, 2574 (2018).
80. L. Duan, L-L. Dou, L. Guo, P. Li, and E-H. Liu, *ACS Sustainable Chem. Eng.* **4**, 2405 (2016).
81. B. Olivares, F. Martínez, L. Rivas, C. Calderón, J. M. Munita, and P. R. Campodonico, *Sci. Rep.* **8**, 14900 (2018).
82. H. Zhao, *J. Chem. Technol. Biotechnol* **90**, 19 (2015).
83. O. S. Hammond, D. T. Bowron and K. J. Edler, *Green Chem.***18**, 2736 (2016),
84. A. Faraone, D. V. Wagle, G. A. Baker, E. C. Novak, M. Ohl, D. Reuter, P. Lunkenheimer, A. Loidl, and E. Mamontov, *J. Phys. Chem. B* **122**, 1261 (2018).
85. C. D'Agostino, R. C. Harris, A. P. Abbott, L. F. Gladden and M. D. Mantle, *Phys. Chem. Chem. Phys.* **13**, 21383 (2011).
86. C. D'Agostino, L. F. Gladden, M. D. Mantle, A. P. Abbott, E. I. Ahmed, Azhar Y. M. Al-Murshedi and R. C. Harris, *Phys. Chem. Chem. Phys.*, **17**, 15297 (2015).
87. K. Mukherjee, E. Tarif and A. Barman and R. Biswas, *Fluid. Phase. Equilibria* **448**, 22 (2017).
88. R. Biswas, A. Das, and H. Shirota, *J. Chem. Phys.* **141**, 134506 (2014).
89. Y. Cui and D. G. Kuroda, *J. Phys. Chem. A* **122**, 1185 (2018).
90. Y. Cui, K. D. Fulfer, J. Ma, T. K. Weldeghiorghis and D. G. Kuroda, *Phys. Chem. Chem. Phys.* **18**, 31471 (2016).
91. A. Das and R. Biswas, *J. Phys. Chem. B*, **119**, 10102 (2015).
92. S. Das, R. Biswas and B. Mukherjee, *J. Phys. Chem. B* **119**, 11157 (2015).
93. S. Das, R. Biswas, and B. Mukherjee, *J. Chem. Phys.* **145**, 084504 (2016).
94. S. Das B. Mukherjee and R. Biswas, *J. Chem. Sci.* **129**, 939 (2017).
95. S. Kaur, A. Gupta and H. K. Kashyap, *J. Phys. Chem. B* **120**, 6712 (2016).
96. M. H. Zainal-Abidin, M. Hayyan, A. Hayyan and N. S. Jayakumar, *Anal. Chim. Acta* **979**, 1 (2017)
97. L. Horng, J. A. Gardecki and M. Maroncelli, *J. Phys. Chem. A* **101**, 1030 (1997).
98. K. Dahl, R. Biswas, N. Ito, and M. Maroncelli, *J. Phys. Chem. B* **109**, 1563 (2005).
99. T. Pradhan, P. Ghoshal, R. Biswas, *J. Chem. Sci.* **120**, 275 (2008).

100. M. L. Horng, J. A. Gardecki, A. Papazyan and M. Maroncelli, *J. Phys. Chem.* **99**, 17311 (1995).
101. N. Sarma, J. M. Borah, H. A. R. Gazi, B. Guchhait, S. Mahiuddin and R. Biswas, *J. Phys. Chem. B* **115**, 9040 (2011).
102. C. Ronne, L. Thrane, P-O. Astrand, A. Wallqvist, K. V. Mikkelsen, and S. O. Keiding, *J. Chem. Phys.* **107**, 5319 (1997).
103. M. Petrowosky and R. Frech, *J. Phys. Chem. B* **113**, 16118 (2009).
104. J. Hunger, A. Stoppa, S. Schrodle, G. Hefter, and R. Buchner, *Chem. Phys. Chem.* **10**, 723 (2009).
105. J. Rak, P. Skurski and M. Gutowski, *J. Chem. Phys.* **114**, 10675 (2001).
106. B. Jagannadh and L. Sirdeshmukh, *Bull. Mater. Sci.* **3**, 423 (1981).
107. R. Buchner, J. Barthel, J. Stauber, *Phys. Lett.* **306**, 57 (1999).
108. B. Guchhait, S. Daschakraborty and R. Biswas, *J. Chem. Phys.* **136**, 174503 (2012).
109. F. Perrin, *J. Phys. Radium* **5**, 497 (1934).
110. H. Jin, G. A. Baker, S. Arzhantsev, J. Dong and M. Maroncelli, *J. Phys. Chem. B* **111**, 7291 (2007).
111. G. B. Dutt and T. K. Ghanty, *J. Phys. Chem. B* **107**, 3257 (2003).
112. M. F. Shlesinger, G. M. Zaslavsky and J. Klafter, *Nature (London)* **363**, 31 (1993).
113. J. Habasaki and K. L. Ngai, *J. Chem. Phys.* **129**, 194501 (2008).
114. Z. Hu, X. Huang, H. V. R. Annapureddy and C. J. Margulis, *J. Phys. Chem. B* **112**, 7837 (2008).
115. B. Guchhait and R. J. Chem. Phys. **138**, 114909 (2013).
116. R. S. Fee and M. Maroncelli, *Chem. Phys.* **183**, 235 (1994).

Chapter 5

Are Water-Xylitol Mixtures Heterogeneous? An Investigation Employing Composition and Temperature Dependent Dielectric Relaxation and Time-Resolved Fluorescence Measurements

5.1 Introduction

Biologically important molecules, especially the building blocks of cell walls, nucleic acids, exoskeletons and also the regulators of the human body's functions, constitute an important area of research. A thorough understanding of microscopic interaction and dynamics in aqueous phase is necessary for smarter application of biologically relevant molecules, such as, amino acids, saccharides, polyols etc. Xylitol is a polyhydroxy alcohol which contains five hydroxyl groups attached to five separate carbon atoms and is represented by the chemical formula, $CH_2OH(CHOH)_3CH_2OH$. Xylitol is considered as natural sugar because it is found in many vegetables, fruits, and also produced in the human metabolism process.¹ Pure xylitol is as sweet as sugar and believed to reduce dental plaque, caries, and assists in remineralization of teeth.²⁻⁴ Lower glycemic-index value (GI~7) of xylitol makes it a potential alternative to commonly used sugars (glucose GI~100) for diabetic patients.^{5,6} Xylitol, like many other polyols, is widely used as a food additive because of non-carcinogenicity, low energy content, and other relevant features.^{5,7,8}

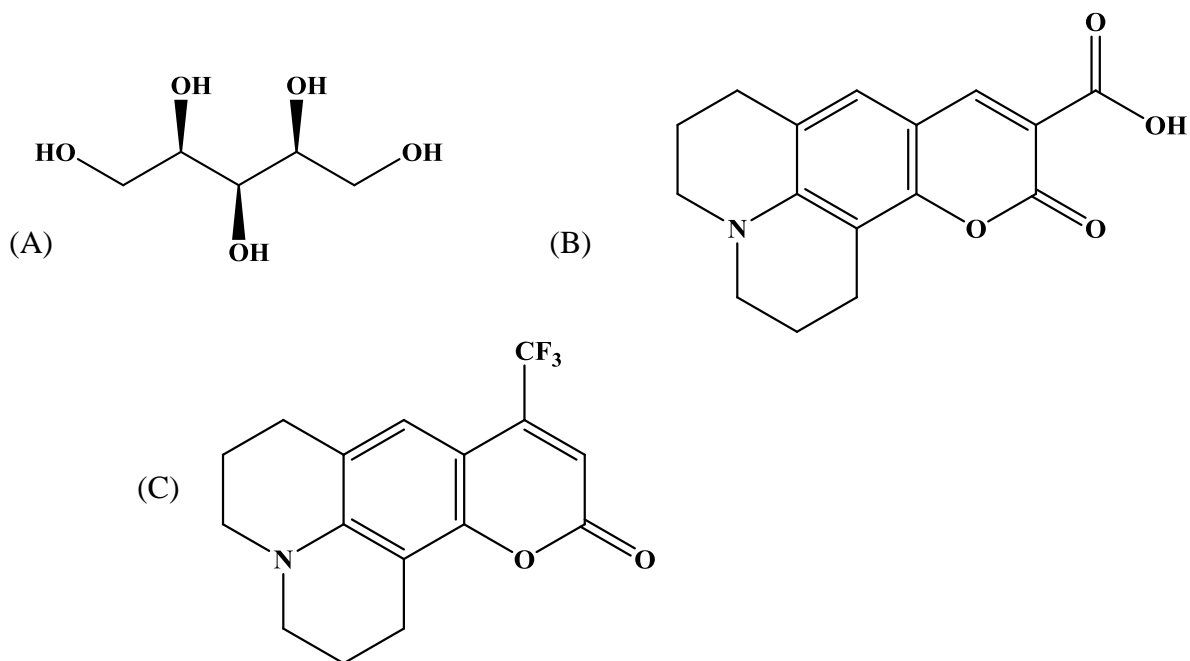
Structure and dynamics of pure water undergo considerable changes in the presence of external solutes and co-solvents (such as sugar, alcohol etc.).⁹⁻¹³ Identification of the origins for such changes in solute-solvent mixtures is an important aspect. Water-sugar and/or water-polyol mixtures are critically relevant to processes that sustain life, and assume importance in food sciences and cryopreservation technology. In water-sugar or water-polyol mixtures, presence of hydrophilic and hydrophobic interactions adds to the complexity in the solution structural and dynamical properties via resolving the interparticle interactions in a new way, and modifying the motional features of the mixture components. Aqueous solutions of sugar or polyol is known to stabilize proteins and other biological substances.¹⁴⁻¹⁶ The stabilization of proteins may occur via

either changing their internal structural characteristics or altering the external medium properties that are in contact with them. It is believed that stabilization (by external stimuli) of protein occurs through processes such as preferential solvation, alteration of water structure etc.¹⁷⁻¹⁹ Sometimes it may be assisted by the solution-phase spatio-temporal heterogeneity.²⁰ Thus, a thorough knowledge of structure and dynamics of aqueous solutions containing sugar or other polyols is critical for understanding the activity of biologically relevant molecules in aqueous environments, and their preservation at cryogenic temperatures.

Relaxation in glass-forming liquids (such as sugar, polyols) has been studied by using various techniques (such as dielectric relaxation, light scattering etc.).²¹⁻²⁴ Notably, those studies explore the impact of water on glass transition temperature as well as relaxation behavior. Interestingly, in many glass forming liquids an ultraslow dynamics was detected in dielectric relaxation (DR),²⁵⁻²⁸ and dynamic light scattering (DLS)^{29,30} measurements. This ultraslow process is different from the viscosity related structural (α) relaxation and was explained by long-range density fluctuations or hydrogen bonded cluster diffusion. A low-frequency Debye peak in the imaginary part of the permittivity is a characteristic representation of an ultraslow process. This Debye peak has been observed in alcohols and their mixtures which represents slower dynamics than the viscosity-related (α) relaxation.^{25,26} Note low frequency Debye peak has been observed in xylitol and supports presence of ultraslow process other than viscosity related structural (α) relaxation.³¹ Although ultraslow relaxation processes in water-xylitol mixtures were detected in dynamic light scattering (DLS) measurements, small-angle neutron scattering (SANS) experiments did not find any significant excess scattering or any structural inhomogeneity in the medium.³² These SANS results therefore raise a debate regarding the interpretation of ultra-slow relaxation detected in DLS measurements in terms of cluster formation. Most of these studies either focused on slow dynamics of xylitol^{21,27,31} or relaxations of water-xylitol mixtures^{22,33} at lower temperatures. Though, there exist a few sporadic studies^{24,32} at higher temperatures (>298 K), a thorough and uniform study of dynamics and interaction in water-xylitol mixtures addressing the solution heterogeneity aspect at temperatures higher than room temperature is still lacking.

We address the solution heterogeneity aspect in this paper via steady state and time-resolved fluorescence measurements, and DR experiments in the temperature range, 295-323 K. Temperatures beyond 323 K have not been considered because (i) we wanted to explore the solution characteristics at a temperature range not too away from the physiological temperature (~310 K) given the fact that xylitol is produced during metabolism, (ii) the DR dynamics becomes faster at higher temperature, particularly those at lower xylitol concentrations, which eventually become undetectable in our frequency window, and (iii) the heterogeneity signature becomes weaker upon increasing temperature. We presume that extensive interaction of water molecules with xylitol may lead to orientational relaxation slower than bulk neat water, and this may be detected in the present DRS measurements. In addition, exploration of the viscosity coupling to solute and solute-centered dynamics would lead to a qualitative information regarding microheterogeneous nature of these solutions. In this work, measurements have been carried out for water-xylitol mixtures in various concentrations (2.31 mol% to 9.62 mol%) of xylitol. DRS technique has already been used to understand the dynamics of pure solvents,³⁴⁻³⁷ water-alcohol mixtures,^{13,38} deep eutectic solvents (DESs)^{39,40} and other media. TRF measurements of non-reactive solution dynamics and DR is intimately related, and a combination of them has been employed to explore dynamics and interaction in many different systems.^{11,41-44} For fluorescence measurements, we have used non-reactive hydrophilic coumarin 343 (C343) and hydrophobic coumarin 153 (C153) as external probes to profile the medium frictional response on a dissolved solute. We have refrained from measuring the solvation dynamics (via dynamic Stokes shift measurements) of these probes in these mixtures as water response is too fast to be detected by the present set-up (see later). Chemical structures of xylitol, coumarin 343 and coumarin 153 are shown in Scheme 5.1.

Scheme 5.1: Chemical structures of (A) Xylitol, (B) Coumarin 343 and (C) Coumarin 153



5.2 Experimental Details

5.2.1 Sample Preparation

Laser grade coumarin 153 (C153) and coumarin 343 (C343) were from Sigma-Aldrich, and used as received. Xylitol was from Sisco Research Laboratories (SRL, India) and used as received. Solutions of six different concentrations of xylitol were prepared by dissolving required amount of xylitol (by weight) in millipore water at room temperature. Stock solutions of C153 and C343 were prepared in carrier solvents, such as, heptane and acetone, respectively. A few μL of these stock solutions were taken into quartz cuvettes (optical path length 1 cm), and the carrier solvent was evaporated off. Approximately 3 mL of sample solution (water+xylitol) was then poured into the cuvette and, complete dissolution of C153/C343 grains in sample solution was ensured. Concentration of C153 (or C343) in each of these sample solutions were maintained at $\sim 10^{-5}$ M.

5.2.2 Viscosity and Refractive Index Measurements

Temperature dependent viscosity coefficient and refractive index of water-xylitol mixtures were measured by using AMVn automated micro-viscometer from Anton Paar (falling ball method) and automated temperature controlled refractometer (RUDOLPH, J357), respectively.^{43,45,46}

5.2.3 Steady State and Time-Resolved Fluorescence Measurements

Steady state absorption and emission spectra were collected using a UV-visible spectrophotometer (UV-2600, Shimadzu) and a fluorimeter (Fluorolog, JobinYvon, Horiba), respectively, and data analysis were carried out following the protocol described elsewhere.^{44,47-49}

Time-resolved fluorescence measurements were performed using a time correlated single photon counting (TCSPC) (LifeSpecps, Edinburgh Instruments, U. K.) setup fitted with a diode laser of 409 nm wavelength (details provided elsewhere).⁵⁰⁻⁵² The instrument response function (IRF) measured using scattering solution was found to be ~ 85 ps. Time resolved fluorescence anisotropy ($r(t)$) measurements were performed following standard protocol described in chapter 2.^{10,53-56}

5.2.4 Dielectric Relaxation Spectroscopy

Dielectric spectra were collected using a PNA-L Network Analyzer (N5230C) combined with a probe kit (85070E) operating in the frequency range $0.2 \leq \nu / GHz \leq 50$. Around 8-10 ml solution of each mixture was used for all the measurements. Details regarding DR measurements have been provided in chapter 2.^{57,58}

Among all measurements presented here, some of the DR spectra fit to 2-D (2-Debye) and rest to 3-D (3-Debye) relaxations. Fits were employed to obtain the best simultaneous descriptions of both the measured $\varepsilon'(\nu)$ and $\varepsilon''(\nu)$. Different combinations of Debye, Cole-Cole and Cole-Davidson processes were attempted but did not obtain any better description than the fits chosen here (shown in Fig. A.c.1).

5.3 Results and Discussion

5.3.1 Dielectric Relaxation Measurements: Concentration and Temperature Dependence

Fig. 5.1 presents the concentration and temperature dependent real (ϵ') and imaginary (ϵ'') components of the measured complex dielectric relaxation (DR) spectra of water-xylitol mixtures along with simultaneous multi-Debye fits. Concentration dependent measurements were done at 295 K and at six different xylitol concentrations (mol%). The highest concentration chosen here is limited by the aqueous solubility of xylitol at 295 K. For a comparison, we have also shown our experimental DR spectra of pure water at 295 K in the same (upper) panel. Fit parameters are summarized in Table 5.1. Two aspects could be immediately realized from these concentration dependent spectra. First observation is the gradual decrease of the estimated static dielectric constant (ϵ_0) upon increase of xylitol concentration in the aqueous solution. Second, the peak position in the imaginary component (ϵ'') shifts to lower frequency with xylitol concentration, producing longer relaxation times at higher concentrations. The concentration dependent slowest DR timescale (τ_1) falls in ~50-80 ps range, the fastest (τ_3) being <10 ps. Another timescale (τ_2) also appears at this temperature which is somewhat slower than the fastest but covers the range ~13-26 ps.

The decrease of ϵ_0 with xylitol concentration is expected because ϵ_0 of xylitol is ~40.⁵⁹ Note DR measurements with appropriate frequency coverage for neat water have revealed two relaxation timescales(~9 ps and ~1 ps) in pure water at ~293 K.⁶⁰ We also have observed the ~9 ps timescale in our DR measurements for pure water at 295 K, although we have missed the fast 1 ps timescale due probably to our limited frequency coverage at the high-frequency wing (up to 50 GHz only). We may therefore associate the <10 ps DR timescale observed for xylitol solutions with the DR of bulk-like water molecules. The other two DR timescales (τ_1 and τ_2) are much slower than the DR timescale of bulk pure water and thus may have connection to xylitol orientation dynamics. The slowest timescale (τ_1 ~48-80 ps) and its amplitude (8-32%) increases with increasing xylitol concentration and therefore supports the connection of xylitol molecules to the slow (compared to neat water) DR dynamics in these aqueous mixtures.

Notably, the second slower component (τ_2) dominates the total relaxation (~68-55%) and also becomes longer with xylitol concentration.

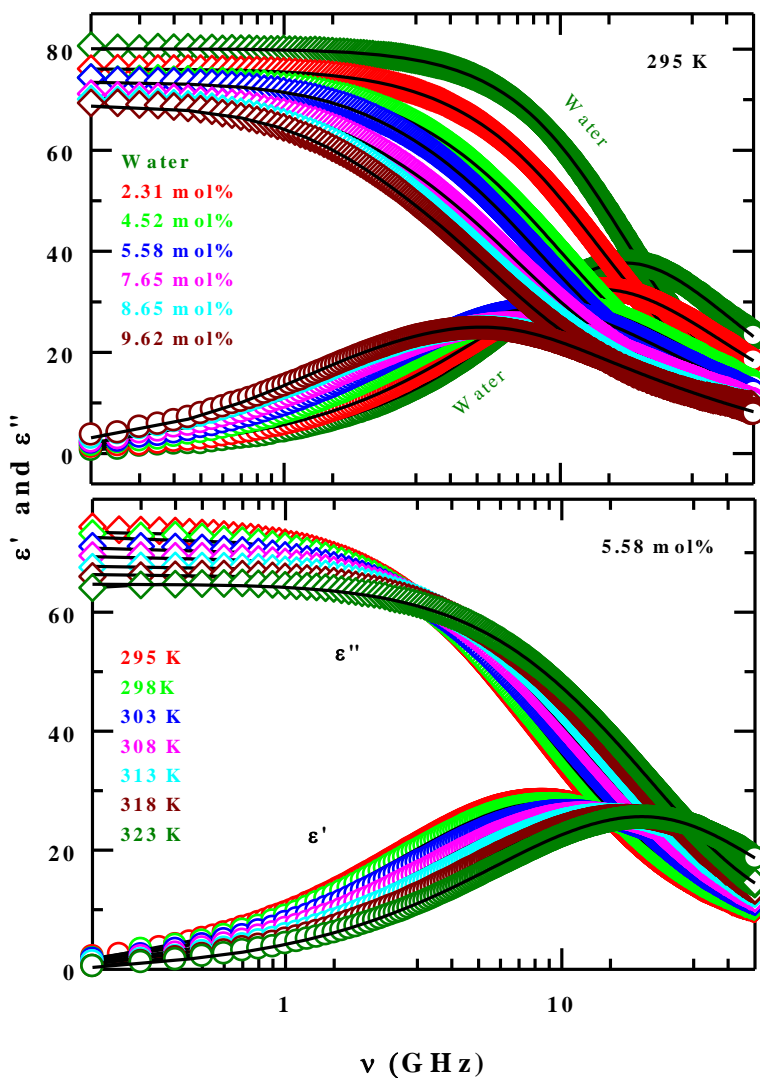


Fig. 5.1: Upper panel: DR spectra of water-xylitol mixtures at 295 K within the frequency regime, $0.2 \leq \nu/\text{GHz} \leq 50$ at various xylitol concentrations. Lower panel: Temperature dependence of the real (ϵ') and imaginary (ϵ'') parts of the measured complex DR spectra of water-xylitol (5.58 mol%). Solid lines through data represent simultaneous fits using multi-Debye relaxation model. Spectra at different xylitol concentrations and different temperatures are color-coded. Green color represents DR response of neat water.

Table 5.1: Parameters obtained from the 3-D/2-D fits of the complex dielectric response functions of water-xylitol mixtures for all the concentrations at 295 K.

Mole % Xylitol	T (K)	ϵ_0	$\Delta\epsilon_1^a$ %	τ_1^b (ps)	$\Delta\epsilon_2$ %	τ_2 (ps)	$\Delta\epsilon_3$ %	τ_3 (ps)	ϵ_∞	n_D^c	$\epsilon_\infty - n_D^2$	$\langle \tau^{DR} \rangle$ (ps)
Water	295	80.1	-	-	100	9.3	-	-	4.7	1.333	2.92	9.3
2.31	295	76.4	7.6	48	67.8	13	24.6	6.6	6.1	1.358	4.26	14
	298	76.1	5.7	46	51.5	15	42.8	7.9	6.6	1.358	4.76	14
	303	73.7	2.7	51	25.3	17	72.6	7.6	5.9	1.359	4.05	11
	308	72.5	2.6	47	21.6	16	75.5	7.2	5.7	1.359	3.85	10
	313	72.3	-	-	15.5	16	84.5	6.7	4.8	1.359	2.95	8
	318	70.2	-	-	14.1	19	85.9	6.5	4.9	1.360	3.05	8
	323	68.9	-	-	13.9	16	86.1	5.8	3.9	1.360	2.05	7
4.52	295	73.9	15.7	49	66.4	16	17.9	6.2	6.8	1.378	4.90	19
5.58	295	73.4	20.7	57	63.5	18	15.8	5.7	6.7	1.386	4.78	24
	298	72.7	18.7	56	62.0	18	19.3	6.4	7.1	1.386	5.18	23
	303	70.8	15.4	55	52.9	19	31.7	6.9	7.0	1.386	5.08	21
	308	69.4	11.9	54	47.8	18	40.3	7.1	6.9	1.386	4.97	18
	313	67.8	9.0	52	41.2	18	49.8	6.9	6.7	1.385	4.78	15
	318	66.4	5.7	58	35.9	18	58.4	6.8	6.5	1.386	4.57	13
	323	64.7	4.8	55	30.7	17	64.5	6.3	6.1	1.386	4.18	12
7.65	295	70.7	25.1	68	60.6	21	14.3	6.0	6.9	1.399	4.94	31
8.65	295	70.1	29.8	77	55.7	24	14.5	6.7	7.0	1.405	5.02	37
9.62	295	68.9	31.7	80	54.8	26	13.6	5.6	7.1	1.410	5.11	40
	298	67.9	28.6	78	53.2	28	18.2	6.6	7.2	1.410	5.21	38
	303	66.2	25.0	76	52.3	25	22.7	6.6	7.2	1.410	5.21	34
	308	65.5	23.6	69	51.3	23	25.1	6.6	7.3	1.410	5.31	30
	313	63.7	18.6	64	49.9	22	31.5	6.6	7.3	1.410	5.31	25
	318	62.4	16.5	58	47.6	20	35.9	6.4	7.1	1.410	5.11	21
	323	61.8	16.1	50	47.4	18	36.5	6.0	7.0	1.410	5.01	19

- a) Indicates dispersion amplitude ($\Delta\epsilon_i$, $i=1-3$) of a given dispersion step in percentage.
- b) τ_i ($i=1-3$) are better within $\pm 5\%$ of the reported values (based on 2-3 independent measurements).
- c) Measured refractive index at 295 K.

Now, what could be the likely origins for these two slower timescales, τ_1 and τ_2 . In water-xylytol mixtures, it is quite natural to expect that the relaxation dynamics would be regulated by both H-bonding fluctuation dynamics and orientation relaxations.⁶¹ Interestingly, the magnitudes of τ_2 (~13-26 ps) corroborates well with the concentration dependent peak times corresponding to the peak frequencies in ϵ'' displayed in the upper panel ($\tau_{peak} = 1/2\pi\nu_{peak}$, with $\nu_{peak}^{2.31mol\%} \sim 15$ GHz producing ~12 ps, and $\nu_{peak}^{9.62mol\%} \sim 5$ GHz producing ~32 ps). Stokes-Einstein-Debye (SED)^{53,62-64} relation with stick boundary condition, $\tau_r = 3\eta V / k_B T$, predicts values of molecular rotation times for xylytol and water at 295 K in these solutions either too large or inconsistent to be favorably compared to the observed τ_1 and τ_2 or to their amplitude-weighted average, $\langle \tau_{DR} \rangle = \sum_{i=1}^2 a_i \tau_i$. Table A.c.2 (Appendix) provides this comparison after connecting τ_r with τ_{DR} as follows, $\tau_r = \frac{\ell(\ell+1)}{2} \times \tau_{DR}$, and for DR, $\ell = 1$. Molecules were treated as spheres in the SED predictions with molecular volumes (V) for water^{65,66} was 10.9 \AA^3 and for xylytol⁶⁷ 107.3 \AA^3 . It is therefore quite clear that molecular rotation times cannot cogently explain these two relaxation times. In light of the recent findings for acetamide containing deep eutectics,⁶¹ these components may derive contributions from H-bond fluctuation dynamics and collective single particle reorientational relaxations. Simulation studies are therefore required to confirm this conjecture.

The temperature dependent (295 K to 323 K) DR spectra shown in the lower panel (Fig. 5.1) are a representative of the DR measurements that we have carried out for three (2.31, 5.58 and 9.62 mol %) of the six different xylytol concentrations considered here. Here also these spectra fit to multi-Debye model, and the fit parameters are summarized in Table 5.1. With temperature, peak of ϵ'' shifts toward higher frequency. This is because of lowering of solution viscosity with the rise in solution temperature leading to faster relaxation. As the slower relaxation becomes faster upon rise in temperature with concomitant loss of amplitude, distinct relaxations may merge together at higher temperatures to produce total relaxations with fewer steps. This is the reason for two-step relaxation at higher temperatures for the lowest xylytol concentration studied here. Note also that the fastest relaxation component (τ_3) remains nearly insensitive to temperature

variation whereas the other two show relatively stronger temperature dependence. This may be due to the limited frequency coverage of the present measurements which is unable to detect temperature-induced shortening of the fastest DR timescale.

Fig. 5.2 shows the viscosity dependence of the average DR relaxation times ($\langle \tau_{\text{DR}} \rangle$) for aqueous xylitol solutions at the lowest (upper panel) and the highest (lower panel) concentrations. SED predictions with stick boundary condition for water and xylitol molecules using the experimental temperature dependent solution viscosity coefficients (η , see Table 5.2) are also shown in these panels for comparison. Clearly, the SED predictions for xylitol are highly over-estimated relative to the average values from measurements at both the concentrations, whereas the calculations for water are strikingly close. Note these average times are the amplitude-weighted average of the DR relaxation times. A fit of these data to the expression, $\langle \tau_{\text{DR}} \rangle = A\eta^p$, provides a value for the power ($p=1.06$) very similar to that for SED prediction ($p=1$) at 2.31 mol% . However, at 9.62 mol%, $p=0.82$, which is smaller than unity. We therefore infer that these xylitol solutions are not strongly heterogeneous in the temperature range studied. In order to confirm this observation we have carried out both steady state and time-resolved fluorescence measurements using hydrophobic (C153) and hydrophilic (C343) probes of comparable molecular volumes,^{53,68} results of which are presented below.

5.3.2 Steady State Measurements

Fig. 5.3 presents the UV-VIS absorption and steady state fluorescence emission spectra for C153 and C343 in these aqueous xylitol solutions at 298 K. For comparison, spectra of these solutes in neat water are also provided in the respective panels. It is quite evident that these spectra exhibit weak xylitol concentration dependence. In addition, C153 spectra in these aqueous solutions are slightly red-shifted than those in neat water, while the reverse (though faint) is seen for C343. This is probably because of their inherent preferences for solvation environments. The solution heterogeneity aspect is subsequently explored by monitoring the excitation wavelength dependence of the emission peak wavelengths for these solutes in these solutions at 298 K. Fig. 5.4 shows these results by showing a xylitol concentration dependence of the total dispersion of the peak emission wavelength ($\lambda_{\text{exc}}^{\text{em,peak}}$) at a given concentration upon changing the excitation

wavelength (λ_{exc}) from blue to red across the corresponding absorption spectrum: $\Delta\lambda(c) = \lambda_{\text{red,exc}}^{\text{em,peak}}(c) - \lambda_{\text{blue,exc}}^{\text{em,peak}}(c)$. Clearly, these solutions are mildly heterogeneous as the total dispersion of the peak emission wavelength ($\Delta\lambda$) is not significant and remains limited only within ~4-6 nanometer for both the solutes.

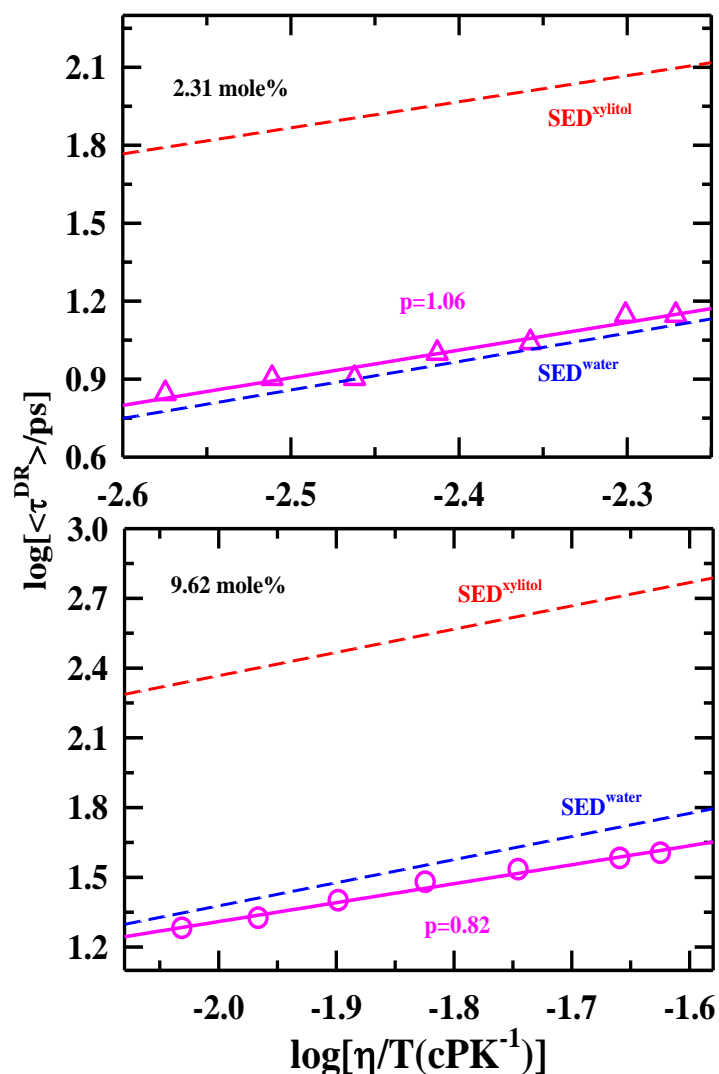


Fig. 5.2: (η/T) dependence of the average DR relaxation times ($\langle\tau_{\text{DR}}\rangle$) for aqueous xylitol solutions at the lowest (upper panel) and the highest (lower panel) concentrations. SED predictions with stick boundary condition for water and xylitol molecules using the experimental temperature dependent solution viscosity coefficients (η , see Table 5.2) are also shown in these panels for comparison.

Table 5.2: Viscosity, density and average rotational time $\langle\tau_r\rangle$ of water-xylitol mixtures at different mole % of xylitol and temperatures

Xylitol mol%	T (K)	η (cP)	$\langle\tau_r\rangle$ (ps)[C153] ^a	$\langle\tau_r\rangle$ (ps)[C343] ^b	Density (g/cm ³)
2.31	298	1.49	143	143	1.0537
	303	1.33	132	127	1.0519
	308	1.19	115	119	1.0498
	313	1.08	95	100	1.0475
	318	0.98	87	91	1.0441
	323	0.86	83	84	1.0407
4.52	298	2.29	201	195	1.0963
	303	2.04	183	174	1.0941
	308	1.87	160	166	1.0918
	313	1.63	130	129	1.0886
	318	1.44	119	115	1.0853
	323	1.30	108	109	1.0813
5.58	298	2.92	222	263	1.1153
	303	2.52	189	215	1.1130
	308	2.26	157	180	1.1105
	313	1.96	148	164	1.1078
	318	1.75	138	150	1.1049
	323	1.60	125	120	1.1019
7.65	298	4.35	335	350	1.1479
	303	3.71	280	304	1.1453
	308	3.19	222	251	1.1427
	313	2.78	207	190	1.1391
	318	2.44	170	168	1.1370
	323	2.16	158	150	1.1339
8.65	298	5.35	354	399	1.1616
	303	4.50	292	357	1.1590
	308	3.87	268	298	1.1561
	313	3.35	243	252	1.1529
	318	2.90	180	205	1.1484
	323	2.55	166	173	1.1449
9.62	298	6.54	458	445	1.1741
	303	5.45	360	357	1.1718
	308	4.62	280	310	1.1686
	313	3.96	245	298	1.1658
	318	3.44	203	256	1.1626
	323	3.01	180	196	1.1580

a,bUncertainty \pm 10%

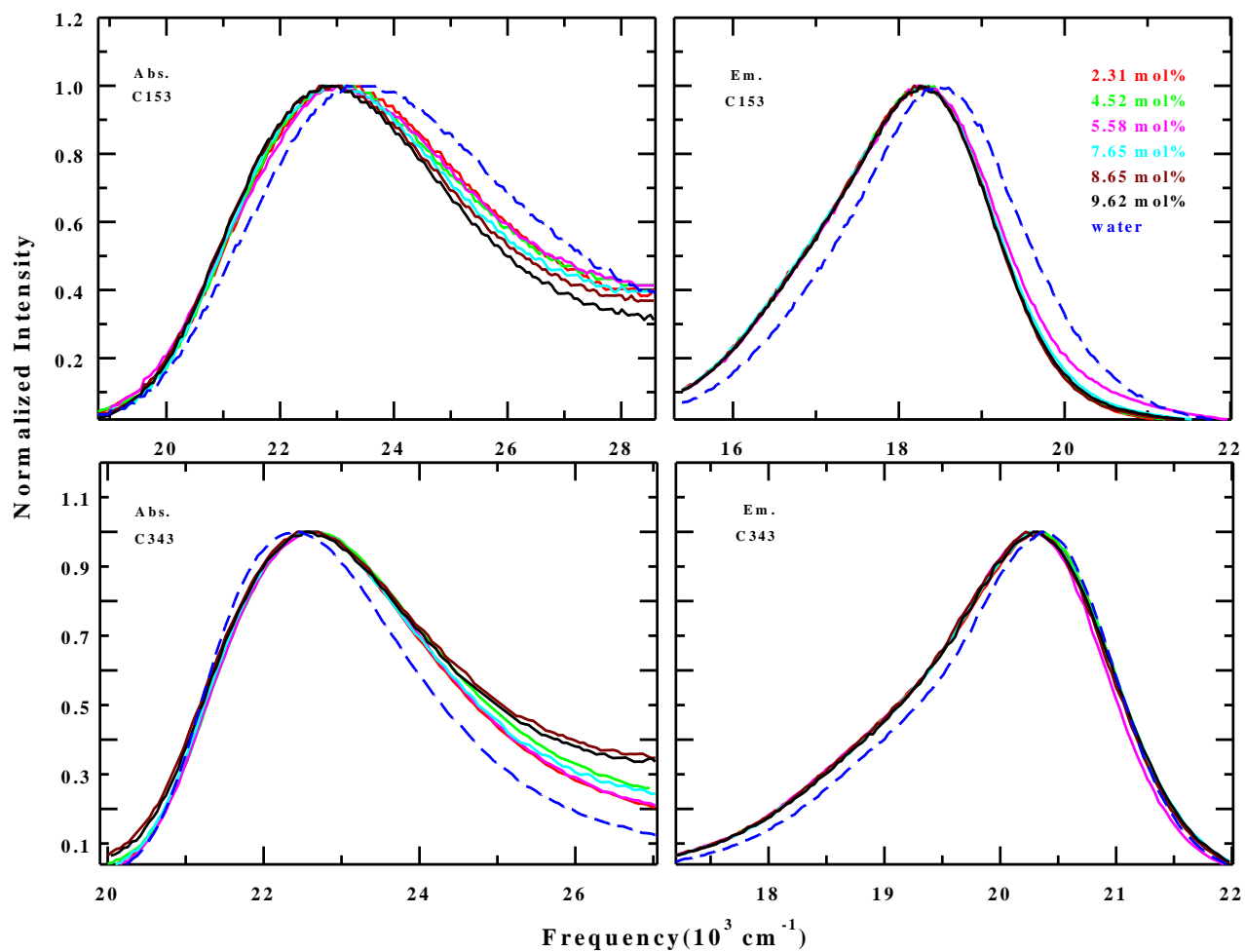


Fig. 5.3: Absorption (left panels) and emission (right panels) spectra of C153 and C343 in water-xylytol mixtures at different concentration (2.31, 4.52, 5.58, 7.65, 8.65, 9.62 mole %) of xylytol at 298 K. Blue broken lines represent the absorption and emission spectra of C153 and C343 in neat water.

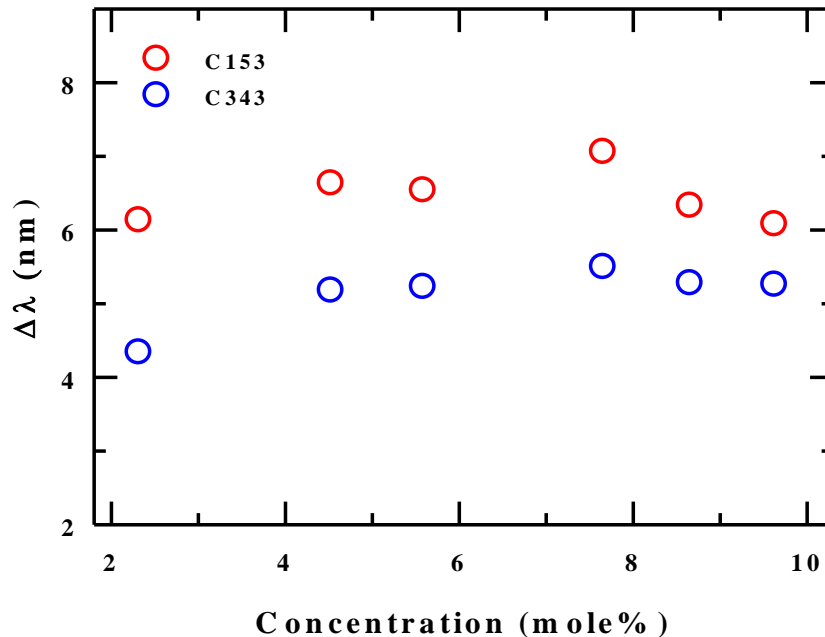


Fig. 5.4: Excitation wavelength ($\lambda_{exc.}$) dependence of fluorescence emission peak wavelength difference (between red and blue end, $\Delta\lambda = \lambda_{red,exc}^{em,peak} - \lambda_{blue,exc}^{em,peak}$) for C153 (red circles) and C343 (blue circles) in water-xylitol mixtures at all xylitol mol% studied. The excitation wavelengths are from 380 nm to 460 nm for C153, and 396 nm to 466 nm for C343 with 10 nm interval, scanning wavelengths that can cover ~60% of the total intensity on both sides of the peak of the respective absorption spectra.

5.3.3 Time-Resolved Fluorescence Measurements

Next we follow the temperature and concentration dependence of dynamic fluorescence anisotropy, $r(t)$, for these solutes in these solutions. Fig. 5.5 depicts the representative dependence where the collected data for the lowest and highest concentrations at room temperature (for concentration dependence), and for the highest concentration at 298 K and 323 K (for temperature dependence) are compared. Both these solutes show dependencies on these two solution parameters. As mentioned earlier, measured $r(t)$ decays for both the solutes fit adequately to single exponentials and quality of fitting are shown in Fig. A.c.3. This might be due to the limited temporal resolution employed (~85 ps) in the present measurements.⁵³

Fits through these data are also shown in these panels, and the corresponding fit parameters summarized in Table 5.2. Average solute rotation times ($\langle\tau_r\rangle$) in this table is the relaxation time constant (τ_r) associated with the underlying single-exponential decay function. This time constant, following the temperature dependence of viscosity, is becoming faster with temperature for all these solutions. The coupling to the viscosity of the solute rotation times in these solutions is then explored in Fig. 5.6 where the measured $\langle\tau_r\rangle$ are shown as a function of temperature-scaled viscosity, η/T , in a double-logarithmic fashion for both C153 (upper panel) and C343 (lower panel). Fit of these data to the viscosity dependence of the type, $\langle\tau_r\rangle \propto \eta^p$, then produces (represented by the solid line through the data) p values (~ 0.8) which are not too away from unity. Such values for the fraction power suggest presence of mild temporal heterogeneity in these solutions. Note also that these p values are quite close to those obtained from DR measurements, and therefore inferences drawn from both these different experiments regarding solution dynamics corroborate well to each other. Combining steady state fluorescence results with these relaxation measurements, one may then conclude that these solutions are not too spatially and temporally inhomogeneous.

If the relaxation times – be it from DR measurements or from dynamic fluorescence anisotropy experiments – follow closely the solution viscosity, then the activation energies extracted from the respective temperature dependent measurements should be agreeing well to each other. This exercise is undertaken next and the results are shown in Fig. 5.7. Arrhenius-type temperature dependence is found for average rotational times for both the solutes in these solutions; so are for the average dielectric relaxation times and viscosity coefficients. Representative data for three different xylitol concentrations are shown for these observables along with the associated activation energies, E_a . Note the one-to-one correspondence between the activation energies at individual concentrations and the agreement among the concentration averaged activation energies, $\langle E_a \rangle_c$, which ranges between $\sim 21 \text{ kJmol}^{-1}$ to $\sim 23 \text{ kJmol}^{-1}$. Such a good agreement among activation energies from different measurements originates from the overwhelming dominance of the frictional response of the system on these solution-phase relaxation processes in the temperature range studied, and the frictional resistance is nearly quantified by the macroscopic solution viscosity. This near-hydrodynamic coupling to solution viscosity (of

relaxation dynamics) suggests mild spatio-temporal heterogeneity in these aqueous xylitol solutions at these temperatures. This is different from our earlier observation for other sugar containing binary mixtures.²⁰

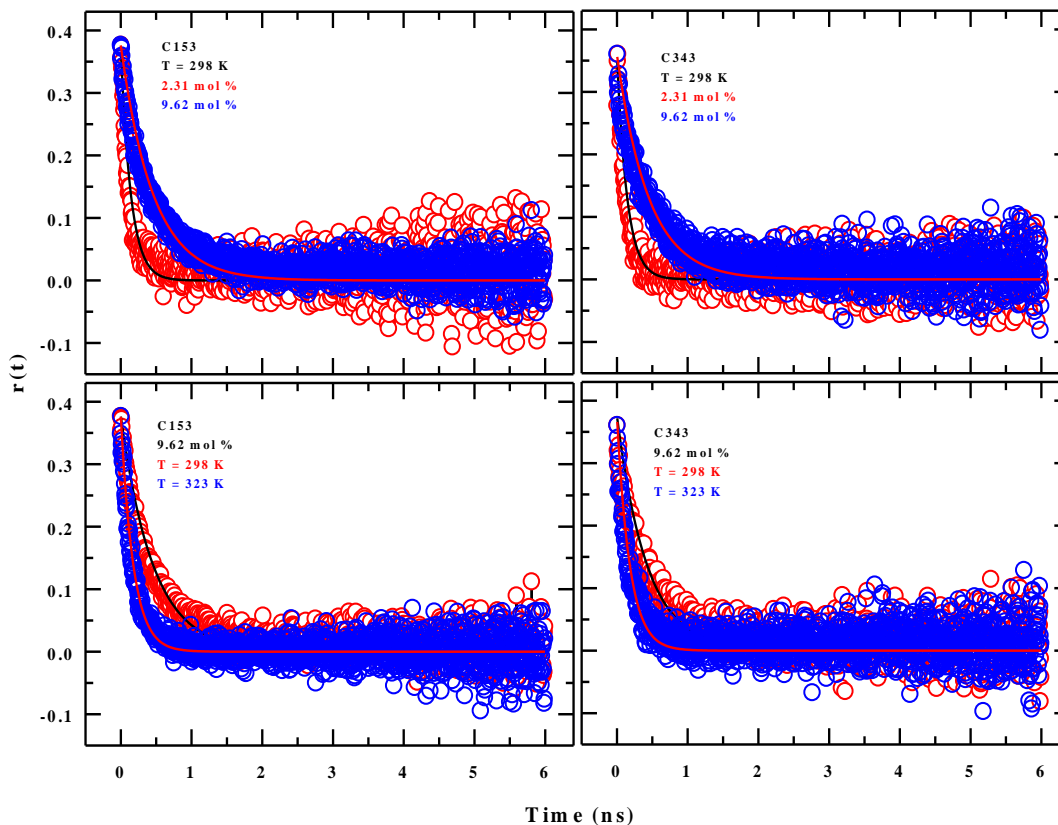


Fig. 5.5: Representative time-resolved fluorescence anisotropy ($r(t)$) decays for C153 (left panels) and C343 (right panels) in water-xylitol mixture with 2.31 and 9.62 mol% of xylitol (upper panel) and also at 298 K and 323 K (lower panel). Lines going through data denote single exponential fits. (Residuals of $r(t)$ decays are shown in Fig. A.c.3, Appendix).

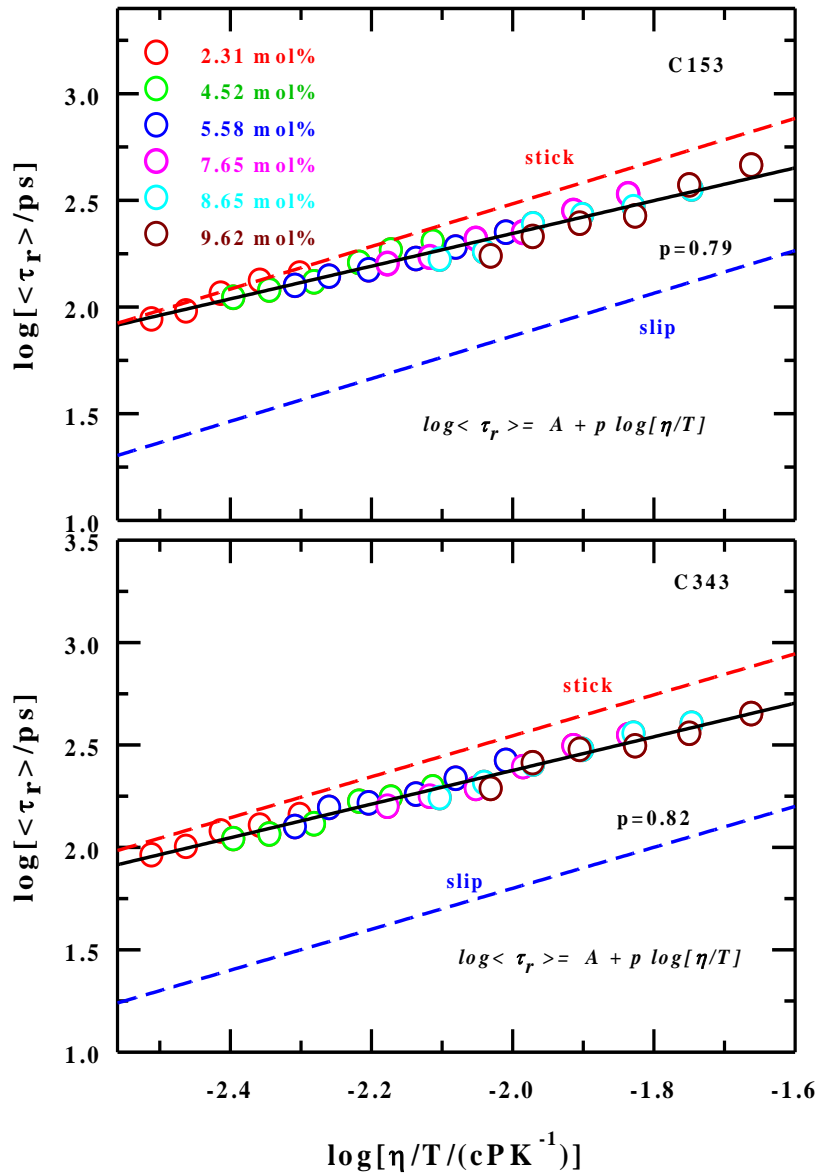


Fig. 5.6: Viscosity coupling of rotation times ($\langle \tau_r \rangle$) for C153 and C343 in water-xylytol mixtures at various xylytol concentrations are plotted. Temperature-dependent measured rotation times are shown as a function of temperature reduced viscosity (η/T) in a log–log fashion. Lines through the data represent fits to the following expression: $\log \langle \tau \rangle = A + p \log[\eta/T]$. Broken lines represent the hydrodynamic (SED) predictions, $\tau_r^{SED} = (V\eta/k_B T)fC$, where V -volume, f -shape factor and C -solute-solvent coupling parameter. All these parameters are taken from Ref. 53 and Ref. 68 for C153 and C343, respectively.

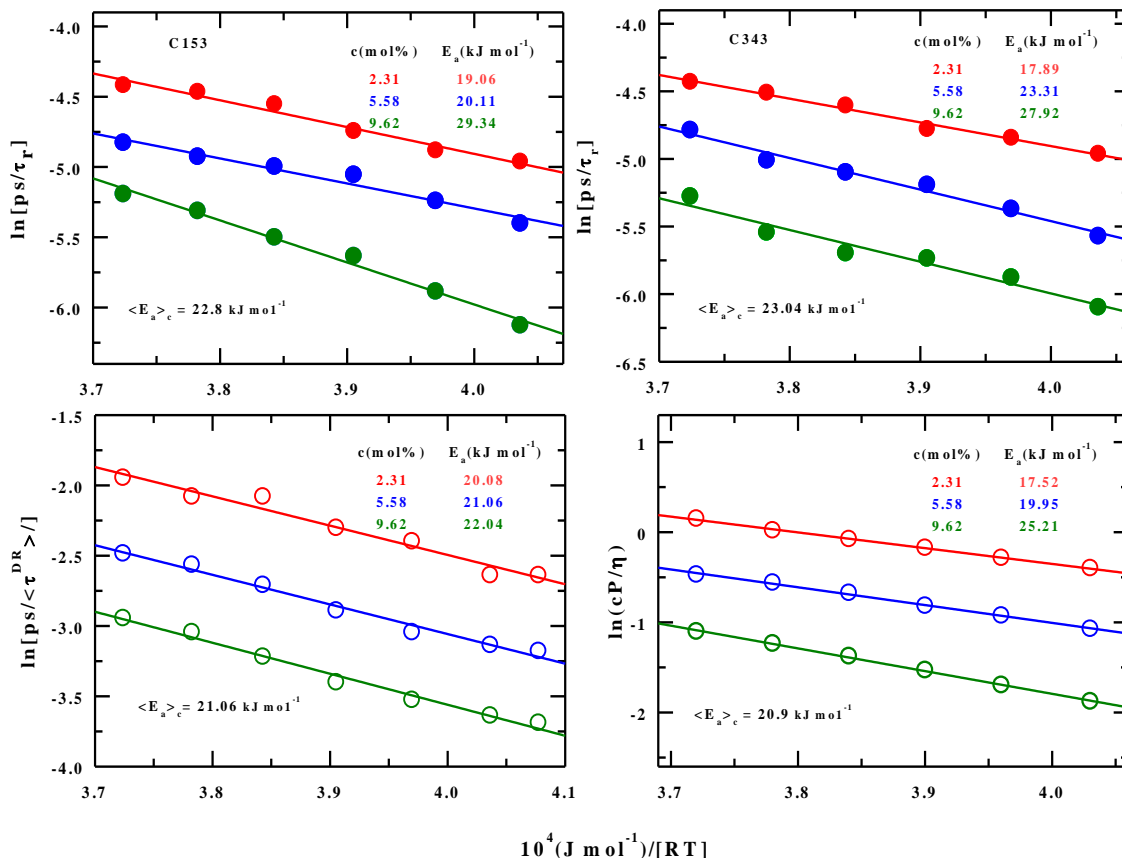


Fig. 5.7: Arrhenius plot of $\ln(1/\langle \tau_r \rangle)$ versus $1/RT$ for C153 (upper left panel) and C343 (upper right panel) rotation times in water-xylitol mixtures (upper panels), and the same for the DR rotation times and viscosity coefficients (lower panels). Solid lines represent fits through the respective data sets.

5.4. Conclusion

In conclusion, the temperature dependent DR and fluorescence measurements suggest near-homogeneous solution structure and dynamics for these aqueous xylitol solutions in the temperature range studied. Multi-probe measurements do not indicate substantial concentration dependent spectral shift, indicating no dramatic change in over-all polarity of the system in presence of this poly-hydroxy alcohol. In addition, we do not find any evidence for cluster formation resulting from extensive H-bond interaction between water and xylitol molecules. In fact, the extent of viscosity coupling of probe rotation times observed in these solutions only

indicates a mild heterogeneity. Measured DR timescales do not match the hydrodynamic predictions for molecular rotation of these species, leaving space for explanation in terms of H-bond fluctuation dynamics and collective single particle reorientation relaxation. Extensive computer simulations are necessary for microscopic understanding of the DR relaxation processes of these solutions, although the challenge here is to construct, at least qualitatively correctly, the inter- and intra-molecular interaction pair potentials. Such an effort is in progress.

References:

1. R. Vasilescu, A. M. Ionescu, A. Mihai, S. Carniciu and C. I. Tîrgoviște, Proc. Rom. Acad., Series B 2, 125 (2011).
2. L. M. Steinberg, F. Odusola and I. D. Mandel Clin Prev Dent. 14, 31(1992).
3. Y. Miake, Y. Saeki, M. Takahashi and T. Yanagisawa, J. Electron Microsc. 52, 471 (2003).
4. K. K. Makinen, Med Princ Pract. 20, 303 (2011).
5. K. Foster-Powell, S. H. A. Holt, and J. C. Brand-Miller, Am J Clin Nutr 76, 5 (2002).
6. H. Förster, S. Boecker and A. Walther, Fortschr Med. 95, 99 (1977).
7. T. Pepper and P. M. Olinger, Food Technol. 42, 98 (1988).
8. D. Birkhead, Acta Odontol Scand. 52, 116 (1994).
9. S. Indra and R. Biswas, J. Chem. Sci. 128, 1943 (2016).
10. T. Pradhan, P. Ghoshal and R. Biswas, J. Chem. Sci. 120, 275 (2008).
11. S. Indra, B. Guchhait and R. Biswas, J Chem Phys. 144, 124506 (2016).
12. H. A. R. Gazi and R. Biswas, J. Phys. Chem. A 115, 2447 (2011).
13. T. Sato and R. Buchner, J. Phys. Chem. A 108, 5007 (2004).
14. N. Gheibi, A. A. Saboury, K. Haghbeen and A. A. Moosavi-Movahedi, J. Biosci. 31, 355 (2006).
15. J. K. Kaushik and R. Bhat, J. Phys. Chem. B 102, 7058 (1998).
16. N. K. Jain and I. Roy, Protein Sci. 18 24 (2009).
17. K. Gekko and T. Morikawa, J. Biochem. 90, 39 (1981).
18. V. V. Mozhaev and K. Martinek, Enzyme Microb. Technol. 6, 50 (1984).
19. G. Dipaola and B. Belleau, Can. J.Chem. 56, 848 (1978).
20. S. Indra and R. Biswas, J. Phys. Chem. B 120, 11214 (2016).
21. M. Nakanishi and R. Nozaki, Phys. Rev. E, 81 041501 (2010).
22. T. Psurek, S. Maslanka, M. Paluch, R. Nozaki and K. L. Ngai, Phys. Rev. E 70, 011503 (2004)
23. D. L. Sidebottom, Phys. Rev. E 76, 011505 (2007).
24. K. Elamin, J. Sjostorm, H. Jansson and J. Swenson, J Chem Phys. 136, 104508 (2012).
25. H. Jansson, R. Bergman and J. Swenson, Phys. Rev. Lett. 104, 017802 (2010).
26. R. Casalini and C. M. Roland, J. Chem. Phys. 135, 094502 (2011).
27. Y. Yomogida, A. Minoguchi and R. Nozaki, Phys. Rev. E 73, 041510 (2006).
28. K. Kaminski, P. Wlodarczyk, L. Hawelek, K. Adrjanowicz, Z. Wojnarowska, M. Paluch, E. Kaminska, Rev. E 83, 061506 (2011).
29. D. L. Sidebottom and T. D. Tran, Phys. Rev. E 82, 051904 (2010).
30. A. Patkowski, H. Gläser, T. Kanaya and E. W. Fischer, Phys. Rev. E 64, 031503 (2001).
31. R. Bergman, H. Jansson and J. Swenson, J. Chem. Phys. 132 044504 (2010).
32. K. Elamin, S. Cazzato, J. Sjostorm, S. M. King and J. Swenson, J. Phys. Chem. B 117, 7363 (2013).
33. D. N. Rander, Y. S. Joshi, K. S. Kanse and A. C. Kumbharkhane, Indian J. Phys. 90, 67 (2016).

34. D. A. Turton, J. Hunger, A. Stoppa, G. Hefter, A. Thoman, M. Walther, R. Buchner and K. Wynne, *J. Am. Chem. Soc.* 131, 11140 (2009).
35. J. Hunger, A. Stoppa, S. Schrödle, G. Hefter and R. Buchner, *Chem. Phys. Chem.* 10, 723 (2009).
36. U. Kaatz and K. Giese, *J. Phys. E: Sci. Instrum.* 13, 133 (1980).
37. J. Barthel, K. Bachhuber, R. Buchner and H. Hetzenauer, *Chem. Phys. Lett.* 165, 369 (1990).
38. S. Mashimo and S. Kuwabara, *J. Chem. Phys.* 90, 3292 (1989).
39. K. Mukherjee, E. Tarif, A. Barman and R. Biswas, *Fluid. Phase. Equilib.* 448, 22 (2017).
40. K. Mukherjee, A. Das, S. Choudhury, A. Barman and R. Biswas, *J. Phys. Chem. B* 119, 8063 (2015).
41. S. Indra and R. Biswas, *J. Chem. Sci.* 128, 753 (2016).
42. S. Indra and R. Biswas, *J. Chem. Phys.* 142, 204501 (2015).
43. A. Das and R. Biswas, *J. Phys. Chem. B* 119, 10102 (2015).
44. B. Guchhait and R. Biswas, *J. Chem. Phys.* 138, 114909 (2013).
45. H. A. R. Gazi, H. K. Kashyap and R. Biswas, *J. Chem. Sci.* 127, 61 (2015).
46. B. Guchhait, S. Das, S. Daschakraborty and R. Biswas, *J. Chem. Phys.* 140, 104514 (2014).
47. T. Pradhan, R. Biswas, *J. Phys. Chem. A* 111, 11514 (2007).
48. H. A. R. Gazi, B. Guchhait, S. Daschakraborty and R. Biswas, *Chem. Phys. Lett.* 501, 358 (2011).
49. B. Guchhait, H. A. R. Gazi, H. Kashyap and R. Biswas, *J. Phys. Chem. B* 114, 5066 (2010).
50. T. Pradhan, H. A. R. Gazi, B. Guchhait and R. Biswas, *J. Chem. Sci.* 124, 355 (2012).
51. R. Biswas, A. R. Das, T. Pradhan, D. Touraud, W. Kunz, S. Mahiuddin, *J. Phys. Chem. B* 112, 6620 (2008).
52. A. Das, S. Das and R. Biswas, *Chem. Phys. Lett.* 581, 47 (2013).
53. M. L. Horng, J. A. Gardecki and M. Maroncelli, *J. Phys. Chem. A* 101, 1030 (1997).
54. A. Das, S. Das and R. Biswas, *J. Chem. Phys.* 142, 034505 (2015).
55. A. J. Cross and G. R. Fleming, *Biophys. J.* 46, 45 (1984).
56. S. Koley, H. Kaur and S. Ghosh, *Phys. Chem. Chem. Phys.* 16, 22352 (2014).
57. C. J. F. Böttcher and P. Bordewijk, *Theory of Electric Polarization*. (Elsevier: Amsterdam, The Netherlands, 1978).
58. P. R. Bevington, *Data Reduction and Error Analysis for the Physical Sciences*; McGraw-Hill: New York 1969.
59. A. A. Maryott and E. R. Smith, *Table of Dielectric Constants of Pure Liquids* National Bureau of Standards Circular 514, United States Department of commerce
60. R. Buchner, J. Barthel and J. Stauber, *Chem. Phys. Lett.* 306, 57 (1999).
61. K. Mukherjee, S. Das, E. Tarif, A. Barman and R. Biswas, *J. Chem. Phys.* 149, 124501 (2018).
62. J. L. Dote, D. Kivelson and R. N. Schwartz, *J. Phys. Chem.* 85, 2169 (1981).
63. A. Das, R. Biswas and J. Chakrabarti, *J. Phys. Chem. A* 115, 973 (2011).
64. A. Das, R. Biswas and J. Chakrabarti, *Chem. Phys. Lett.* 558, 36 (2013).

65. C. J. F. Bottcher, *Rec. Trav. Chim.* 65, 14 (1946).
66. M. Lucas, *J. Phys. Chem.* 80, 359 (1976).
67. F. F. Liu, L. Ji, L. Zhang, X. Y. Dong and Y. Sun, *J. Chem. Phys.* 132, 225103 (2010).
68. G. B. Dutt and T. K. Ghanty, *J. Phys. Chem. B* 107 3257 (2003).

Chapter 6

Exploring Aqueous Solution Dynamics of an Amphiphilic Diblock Copolymer: Dielectric Relaxation and Time-Resolved Fluorescence Measurements

6.1 Introduction

Amphiphilic block copolymers, made of hydrophobic and hydrophilic segments, are well known to form ordered self-assembly such as cylinders, bicontinuous structures, micelles, vesicles, and other complex aggregations.¹ Among these various nanostructures, micelles are the most studied morphologies in an aqueous medium, where micelle formation takes place upon appropriate hydrophobicity/hydrophilicity balance, wherein the impact of micelle hydrophobic block is compensated by the water soluble hydrophilic segment.² Polymeric micelles have widely been considered as convenient nano-carriers for drug³ and gene delivery,⁴ diagnostic imaging,⁵ and so forth. Admirable biocompatibility, lower critical micellar concentration (CMC) value, aqueous solution stability, high solubilization ability of a large number of hydrophobic drugs in their micellar core, etc. made polymeric micelle an excellent carrier in the biomedical field.^{6,7i} Compared to surfactant micelles, polymeric micelles are generally more stable, with a remarkably lowered CMC, and have a slower rate of dissociation, allowing retention of loaded drugs for a longer period of time and, eventually, achieving higher accumulation of a drug at the target site.⁸ Unlike the conventional low-molecular weight surfactants and lipids, block copolymers have the advantage of modifying their shape and functionality depending on both their intrinsic properties (block-block interaction parameter) and extrinsic properties (molecular weight, block composition, solvent composition, concentration of the solution, etc.).

Diverse biologically relevant self-organized aggregates such as micelles,^{9,10} reverse micelles,^{11,12} vesicles,^{13,14} macromolecules and polymer aggregates,^{15,16} have frequently been used to study solvent dynamics using fluorescence spectroscopy. Among the different self-aggregate systems, micelles have been repeatedly used as model systems for confined reaction media.^{17,18} Exploring dynamics in these media is critical because often micellar interface is heterogeneous, and this

heterogeneity can considerably impact the course of a chemical reaction occurring at these interfaces.^{19,20} In addition, micelle may be considered as a model bio-mimetic system for understanding the interaction of a biologically relevant species with the interface and subsequent transportation and release of it at a desired place. Thus, a thorough knowledge of microenvironment structure, dynamics and interaction with guest molecules is essential to control and/or suitably alter to meet the demands of daily care products, pharmaceutical and biomedical necessities.

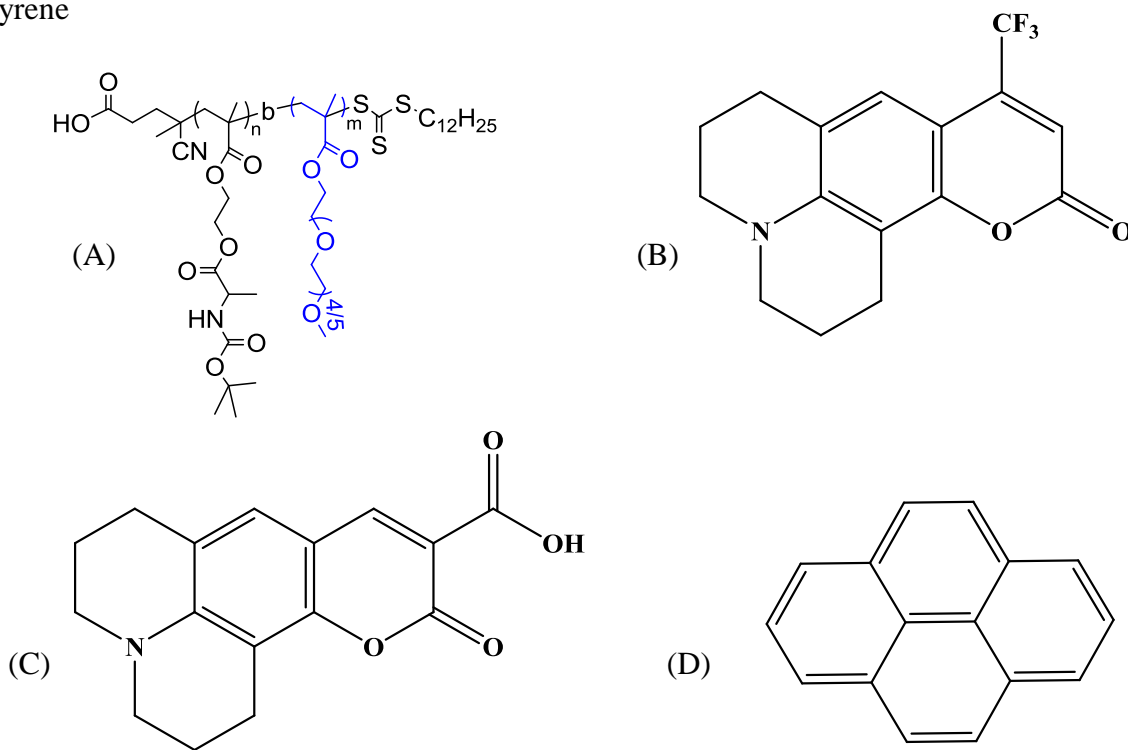
Neutron scattering,²¹ nuclear magnetic resonance (NMR),^{22,23} fluorescence,²⁴ static and dynamic light scattering(DLS)²⁵ measurements have been used earlier to understand block copolymer micelles.^{26,27} Dynamics and interaction in solution phase of several different copolymers have been explored using a variety of ultrafast fluorescence techniques such as fluorescence resonance energy transfer (FRET),²⁸ fluorescence correlation spectroscopy,²⁹ fluorescence Stokes shift, and anisotropy relaxations.^{30,31} Dielectric relaxation spectroscopy (DRS) probes the inherent medium dynamics,^{32,33} and has been utilized to explore polarization relaxations in a variety of systems that include pure solvents,³⁴ ionic liquids,³⁵ deep eutectic solvents (DESs),³⁶ organic electrolytes,³⁷ polymer solution,³⁸ micelles,³⁹ and reverse micelles.⁴⁰ However, a thorough and systematic investigation combining dielectric relaxation and pico-second resolved fluorescence spectroscopic techniques is still lacking for aqueous solutions of diblock copolymers. In order to provide such information of diblock copolymers possessing potential for applications, here we have employed DR and TRF measurements for exploring interaction and dynamics of poly(2-(((*tert*-butoxycarbonyl)alanyl)oxy)ethyl methacrylate)-*b*-poly(polyethylene glycol monomethyl ether methacrylate) (P(Boc-L-Ala-HEMA)-*b*-PPEGMA)) diblock copolymer in its aqueous solutions. These diblock copolymers were synthesized and characterized by Prof. Priyadarsi De's group, IISER, Kolkata, India.⁴¹ In these polymers amino acid segment has been used as a hydrophobic block because of their remarkable advantages, namely, good biocompatibility, non-toxicity and, more importantly, availability of side functional groups. The utility of these side functional groups is targeted for conjugation with molecules of biological relevance after the *tert*-butoxycarbonyl (Boc) deprotection followed by post-polymerization modification reactions.⁴² On the other hand, the oligo(ethylene oxide) side chains are uncharged, water-soluble, non-toxic, biocompatible, and thus advantageous towards smarter applications.⁴³

6.2 Experimental Section

6.2.1 Materials and Sample Preparation

Coumarin 153 (C153) (Sigma Aldrich), coumarin 343 (C343) (Sigma Aldrich) and pyrene (Sigma Aldrich) were used as received. For the preparation of micellar nanoaggregates in aqueous solution, de-ionized (DI) water was added drop-wise to the dried block copolymers and kept under stirring for about 10 min. Four different polymers⁴¹ (2a, 2b, 2c and 2d) with same number of hydrophobic chain length ($n=18$) and different number of hydrophilic chain length (2a ($m=20$); 2b ($m=36$); 2c ($m=61$) and 2d ($m=85$)) were used in this work. Using this similar procedure, a series of micellar solutions of different concentrations (1, 5, 10 mg/mL) were prepared for all measurements at 25 °C. For optical measurements, the concentration of coumarin 153 (C153) and coumarin 343 (C343) were maintained to $\sim 10^{-5}$ M in each sample. The structures of synthesized diblock copolymer, C153, C343, and pyrene are shown in Scheme 6.1.

Scheme 6.1. (A) P(Boc-L-Ala-HEMA)-*b*-PPEGMA), (B) Coumarin 153, (C) Coumarin 343 and (D) Pyrene



6.2.2 Dynamic Light Scattering (DLS)

DLS measurements were conducted at 25 °C in a Malvern Nano Zetasizer instrument. The system was equipped with a He–Ne laser operating at a wavelength of 633 nm and a detection angle of 173°. Polymer solutions were filtered through a 0.45 µm syringe filter prior to measurement.

6.2.3 Density, Viscosity and Refractive Index Measurements

An automated temperature controlled density-cum-sound analyzer (Anton Paar, DSA 5000) was used for density measurements, and viscosity coefficients (η) were measured using a microviscometer (AMVn, Anton Paar).^{44,45} Refractive indices of the micellar solutions were measured using an automated temperature controlled refractometer (RUDOLPH, J357).⁴⁶

6.2.4 Steady State Measurements

Absorption spectra were recorded using UV-visible spectrophotometer (UV-2600, Shimadzu). Steady state emission spectra were obtained from fluorimeter (Fluorolog, Jobin-Yvon, Horiba). Before analysis, solvent blanks were subtracted from the spectra and converted properly to the frequency domain for further analysis and frequency determination.^{47,48}

6.2.5 Time-Resolved Fluorescence Measurements

Time-correlated single photon counting (TCSPC) technique along with 409 nm (LED) excitation source was used for the time-resolved fluorescence measurements and the details of this setup are described elsewhere.^{49,50} The full width at half-maximum (FWHM) of the instrument response function (IRF) obtained using 409 nm excitation sources and a scattering solution was ~80 ps. Established standard protocol has been followed for the anisotropy measurements.⁵¹⁻⁵⁴

Time-resolved fluorescence intensity decays of C153 in different polymeric solutions at magic angle (54.7°) were also collected for average lifetime measurements.⁵⁵

Details regarding time-resolved fluorescence spectroscopic measurements have been described in chapter 2.

6.2.6 Dielectric Relaxation Spectroscopy

The collection of DR data and associated analysis protocol are similar as discussed in chapter 2.⁵⁶⁻⁵⁸ All DR measurements were performed using a PNA-L Network Analyzer (N5230C) combined with a probe kit (85070E) operating in the frequency range $0.2 \leq \text{GHz} \leq 50$. Approximately 8 mL solution of each system was used, keeping all the external parameters fixed. Details regarding DR measurements can be found elsewhere

For all measurements presented here, 2D fits (2Debye processes) were employed to obtain the best simultaneous descriptions of the measured $\epsilon'(\nu)$ and $\epsilon''(\nu)$. Different combinations of Debye, Cole-Cole and Cole-Davidson processes were attempted but no better descriptions were found.

6.3 Results and Discussion

6.3.1 Self-Assembly Behaviour of the Diblock Copolymers

The synthesized diblock copolymers, **2a-2d**, contain hydrophilic (PPEGMA) and hydrophobic (P(Boc-L-Ala-HEMA)) segments, thus expected to undergo self-assembly under proper conditions. All the diblock copolymers are completely soluble in water without any external assistance, because of the significant introduction of the hydrophilic PPEGMA entity into all the copolymer chains. The critical aggregation concentration (CAC) of the copolymers were determined by virtue of fluorescence spectroscopy (Fig. A.d.1) using pyrene as a luminescent probe due to its high sensitivity to the microenvironment polarity change.^{59,60} As illustrated in Fig. A.d.2, the CAC of **2a-2d** were measured from the cross-section of two linear fitting curves of I_{388}/I_{368} vs. $\log(\text{polymer concentration})$ plot. Notice that increase in hydrophilic length leads to a higher CAC value (Table A.d.3). This is expected because increased hydrophilicity induces better dissolution of these amphiphilic polymer molecules by the aqueous environment. For these polymeric micelles, lower CAC value gives an advantage for its application as a carrier as lower CAC may help to resist dissociation on dilution inside the body fluid.⁶¹

In the next step, the size of the self-assembled particles in an aqueous medium from **2a-2d** was investigated by DLS measurement. The number-average hydrodynamic diameters, D_h , were in the range of 14 ± 0.8 nm (polydispersity index, PDI = 0.459) to 20 ± 1.0 nm (PDI = 0.333) in an

aqueous medium at a polymer concentration of 1.0 mg/mL (Fig. A.d.4) and concentration-dependent D_h values are tabulated in Table A.d.3. These D_h values are above the threshold value (~5.5 nm) of excretion limit and avoid renal excretion.⁶² Furthermore, these values are much lower than 100 nm and help to bypass RES (reticuloendothelial systems) uptake.⁶³ Nevertheless, fluorescence and DLS measurements confirmed micelle formation from **2a-2d** in water.

6.3.2 Steady State Absorption and Emission

Fig. 6.1 represents the absorption and emission spectra of coumarin 153 (C153) in aqueous micellar solutions of diblock copolymer (1 mg/mL). Average spectral peak frequencies at different polymer concentrations (1, 5 and 10 mg/mL) are summarized in Table 6.1. For comparison, steady state absorption and emission spectra of C153 in pure water are also shown in the same figure. Clearly, the absorption spectra of C153 in aqueous polymer solutions show a much weaker blue-shift (compared to that in neat water) than that for the corresponding fluorescence spectra. Blue shift of emission spectra in these polymeric micellar solutions (relative to that in water) suggests local environments probed by C153 are less polar than water. This suggests that C153, due to its hydrophobic nature, locates itself at the micelle-water interface. This blue shift in emission spectra relative to water has already been observed for bile salt aggregates,⁶⁴ and micellar mixtures.⁶⁵ Note that the extent of spectral blue-shift does not depend upon the number of hydrophilic chain (as for **2a**, **2b**, **2c** and **2d**) in these aqueous polymeric micellar solutions. This observation provides a support in favour of C153 being located at the micellar interface. A sharp increase of emission intensity over that in bulk water (controlled experiments with same C153 concentration), shown in Fig. A.d.5, further supports this view of C153 location in these polymeric micellar solutions. Excitation wavelength dependence of fluorescence emission of C153 in these micellar solutions (shown in Fig. A.d.6) suggests that, these solutions, within the lifetime of C153, are spatially homogeneous in nature. Here, spatial homogeneity refers to the ‘uniformity’ in microenvironments that surround the probe molecules in different micellar aggregates present in the solution. If microenvironments around probe molecules in different aggregates in solution are similar or the interconversion among dissimilar environments is much faster than the average excited state lifetime of the probe, then the fluorescence emission occurs from the excited probe molecules surrounded by a completely relaxed, fluctuation-averaged ‘single’ environment. This leads to insensitivity of the

fluorescence emission energy to the choice of probe excitation wavelength. This is reflected in our emission spectra (Fig. A.d.6) collected after varying the excitation wavelength. Note the emission peak frequencies corresponding to different excitation wavelengths are nearly similar (within the uncertainty of $\pm 250\text{cm}^{-1}$). An excitation wavelength dependence of fluorescence emission is then interpreted in terms of differing solvation environments (spatial heterogeneity) surrounding the dissolved probe molecules.

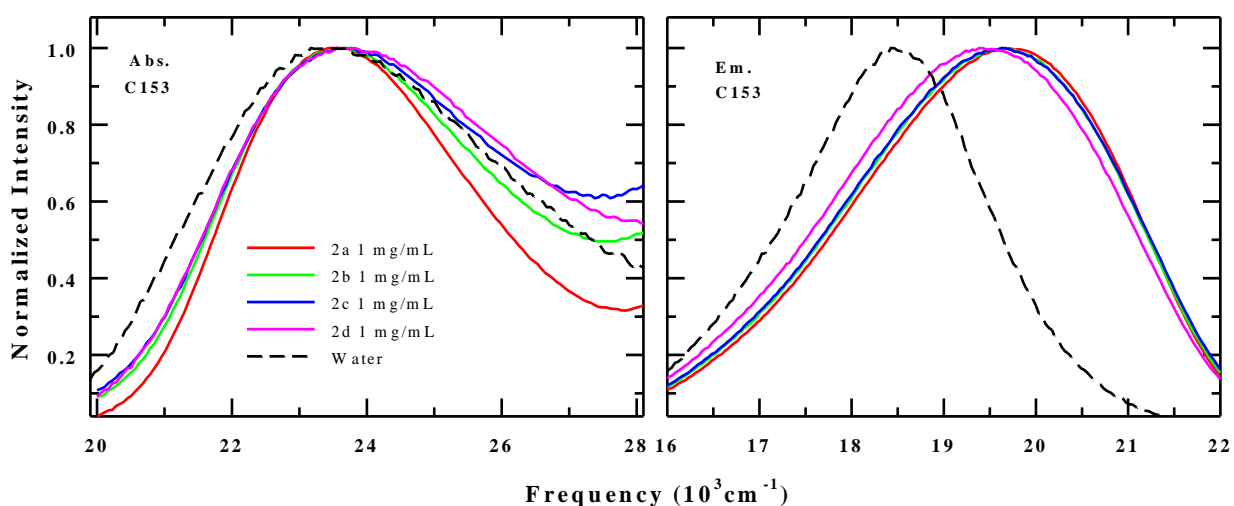


Fig. 6.1: Absorption and emission spectra of C153 in aqueous micellar solutions of diblock copolymers (**2a**, **2b**, **2c**, **2d**) with 1 mg/mL polymer concentration. Spectra of different polymers are color-coded. Black broken lines represent the absorption and emission spectra of C153 in water.

Table 6.1: Absorption and Emission peak frequency of C153 in different polymeric (**2a**, **2b**, **2c**, **2d**) micelle solutions at three different concentrations at ~25 °C.

Polymer	Absorption ^m			Emission ^m		
	Peak frequency (10^3 cm^{-1})			Peak frequency (10^3 cm^{-1})		
	1 mg/mL	5 mg/mL	10 mg/mL	1 mg/mL	5 mg/mL	10 mg/mL
2a	23.57	23.59	23.59	19.69	19.87	20.00
2b	23.63	23.67	23.64	19.64	19.79	19.87
2c	23.68	23.79	23.68	19.64	19.72	19.75
2d	23.72	23.67	23.73	19.45	19.70	19.74

^mThese data are reproduced within the uncertainty of $\pm 250 \text{ cm}^{-1}$ (based on 2-3 independent measurements).

6.3.3 Solute Rotation and Probe Location

Dynamic fluorescence anisotropy measurements provide an estimate of the restriction experienced by a dissolved solute while undergoing rotation in its own environment.⁶⁶ Representative time-resolved fluorescence anisotropy decay ($r(t)$) for C153 in one of these micellar solutions and the corresponding bi-exponential fit is shown in Fig. 6.2. Fig. A.d.7 presents the corresponding intensity decays at the parallel and perpendicular polarizations for this solution. $r(t)$ decays at other polymeric micellar solutions are provided in Fig. A.d.8. Bi-exponential fit parameters for the measured $r(t)$ decays are summarized in Table 6.2. Note these bi-exponential anisotropy decays are characterized by a dominant (~60%) fast relaxation (~60 picoseconds) component and a relatively slower nanosecond component. This behaviour of relaxation represents the bimodal nature of frictional resistance of the local environment to the rotational motion of the solute. It is also clear from Table 6.2 that increase of the number of hydrophilic chain in polymer does not have significant impact on the average rotational time ($\langle \tau_r \rangle$) of the probe (C153). Such an observation indicates that C153 resides near to the hydrophobic surface, supporting the conclusion from steady state spectroscopic results. Furthermore, average rotational time (~ 1 ns) of C153 in this polymeric micelle is approximately 10-15 times greater than that (~50 ps)⁵² for C153 in neat water, although the bulk viscosity of the

aqueous polymeric solution (shown in Table A.d.9) is comparable to that of neat water.⁵² This supports the view that C153 in these polymeric solutions resides at the water-micelle interface.

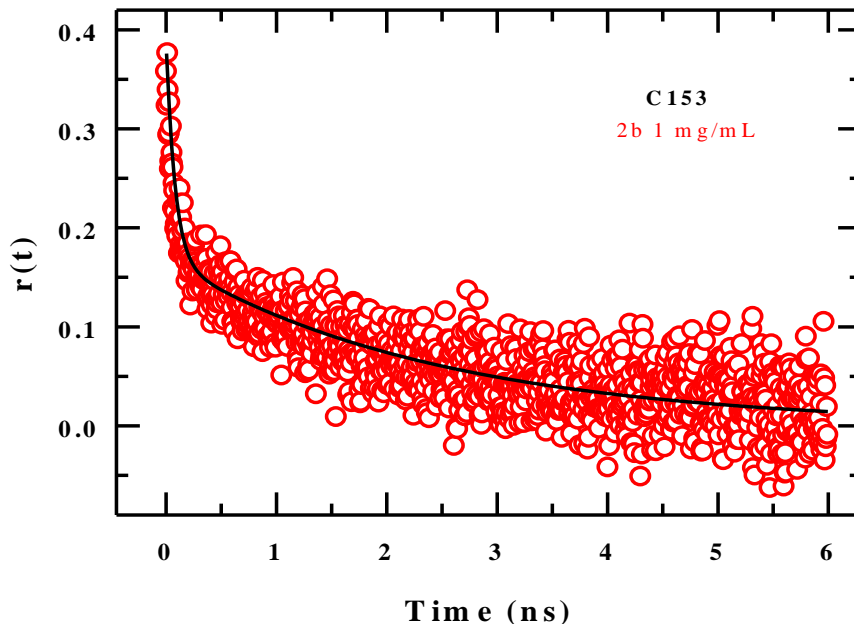


Fig. 6.2: Representative time-resolved fluorescence anisotropy ($r(t)$) decay for C153 in aqueous polymer solution (**2b**). Black line going through the data denotes bi-exponential fit.

Polymer concentration dependent rotational anisotropy decays, shown in Fig. 6.3 and bi-exponential fit parameters in Table 6.2, indicate that increase of polymer concentration slows down the probe rotation. Interestingly, the nanosecond timescale becomes longer with polymer concentration whereas the sub-100 ps timescale shows relatively much weaker concentration dependence. This is due to the increase in the number of micellar aggregates (“crowding”) with polymer concentration which is consistent with the DLS results that indicate near-insensitivity of the micellar size to the polymer concentration but increase in scattering intensity (Table A.d.3). For further confirmation of probe location, dynamic anisotropy measurements using a hydrophilic probe coumarin 343 have been carried out that produced average rotation times in the ~300-800 ps range (shown in Table A.d.10). This much faster average rotation time for a probe (C343) comparable to the size of C153 indicates C343 preferentially locates in the more

labile water-like environments.^{53,67} However, these C343 environments in these aqueous solutions are neither bulk water-like nor like those for C153 which penetrates deeper due to hydrophobicity, but rather away from the deep palisade layer and toward the outer periphery of the micellar interface. Formation of more micellar structures at higher concentrations (“crowding”) is likely to reduce the mobility of the interfacial water molecules, inhibiting further the solute rotation. Concentration-dependent rotational anisotropy decays of C343 are shown in Fig. 6.4. Data summarized in Table A.d.10 reflects that average rotational time for C343 slows down with polymer concentration, which corroborates well with the observation of lengthening of C153 rotation times in these solutions.

Table 6.2: Parameters from bi-exponential fits to concentration-dependent anisotropy decays measured using C153 in different polymeric (**2a**, **2b**, **2c**, **2d**) micellar solutions at ~25 °C.

Sample	Conc. (mg/mL)	a_1 (%)	τ_1 (ns)	a_2 (%)	τ_2 (ns)	$\langle\tau_r$ (ns) \rangle^u	$\langle\tau_{if}$ (ns) \rangle^o
2a	1	60	0.070	40	2.04	0.86	3.34
	5	58	0.055	42	2.36	1.02	3.20
	10	70	0.052	30	4.38	1.35	3.42
2b	1	57	0.079	43	2.41	1.08	3.64
	5	61	0.065	39	3.29	1.32	3.70
	10	64	0.063	36	4.09	1.51	3.81
2c	1	59	0.069	41	2.24	0.96	3.80
	5	65	0.062	35	3.52	1.27	3.93
	10	66	0.059	34	3.80	1.33	3.85
2d	1	61	0.096	39	2.31	0.96	3.96
	5	64	0.069	36	2.78	1.04	3.84
	10	75	0.051	25	4.40	1.14	3.68

^uFit parameters have been obtained after fixing the r_0 values at 0.376⁵³ (C153) and 0.35⁶⁸ (C343). Individual time constants are better than $\pm 8\%$ of the reported values. ^oThese data can be reproduced within the $\pm 5\%$ uncertainty

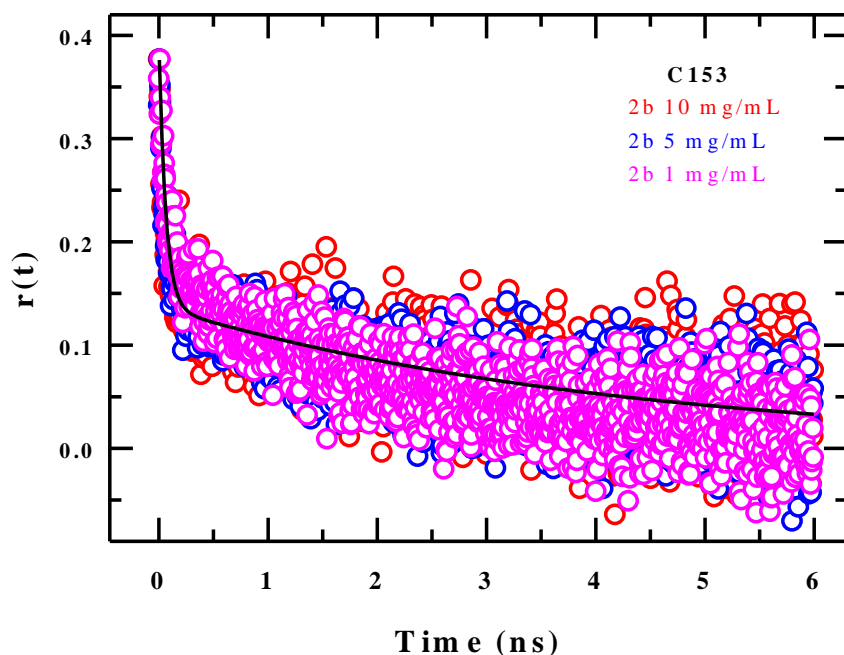


Fig. 6.3: Polymer concentration dependence of rotational anisotropy ($r(t)$) decays for C153 in aqueous polymer solution (**2b**). Decays at different concentrations (mg/mL) are color-coded.

Due to much faster medium relaxation compared to the time resolution available, we were unable to detect the Stokes shift dynamics for the solutions under study. Average fluorescence lifetime decays for C153 in these solutions have been collected. Excited state average lifetimes, $\langle \tau_{lif} \rangle$ obtained from time-integrating the tri-exponential fits to the lifetime decays, are summarized in Table 6.2. Individual tri-exponential fit parameters are provided in Table A.d.11 (Appendix). Note in these tables that not only the average lifetimes are similar in all these polymeric micellar solutions but also the individual amplitudes and time constants remain nearly insensitive to the polymer concentration. This suggests micro-environments surrounding the probe are similar in all these aqueous solutions. This corroborates well with the view that C153 resides at the interface, and polymer concentration cannot alter this preferential location for C153.

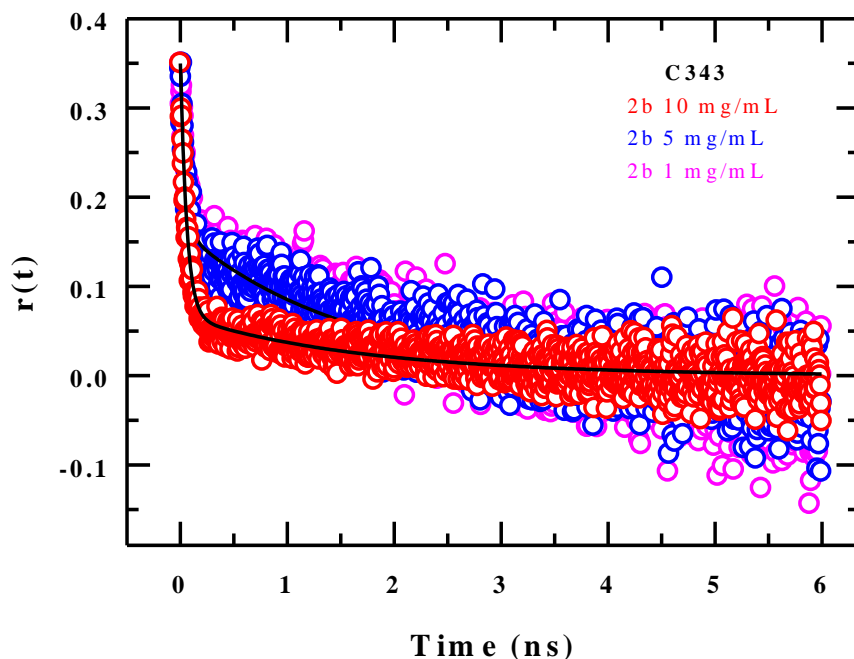


Fig. 6.4: Time-resolved fluorescence anisotropy ($r(t)$) decays for C343 in aqueous polymer solution (**2b**) at different concentrations (1, 5 and 10 mg/mL). Decays at different concentrations are color-coded.

6.3.4 Dielectric Relaxation

Fig. 6.5 represents the real (ϵ') and imaginary (ϵ'') components of the complex dielectric spectra of polymeric micellar solutions (10 mg/mL) along with 2-Debye fits. Fit parameters are shown in Table 6.3. Tabulated data suggest two DR time scales, and they are in ~ 40 ps and ~ 10 ps ranges. This may represent two different relaxation mechanisms (involving the same or different species) in these micellar media. Note this ~ 40 ps component, although changes slightly with the identity of the polymer, is too small to be considered seriously. However, a comparison between the residuals obtained from single and two Debye fits (Fig. A.d.12) suggests that the presence of this slow component might be real. If we allow for this then the relatively faster ~ 10 ps timescale may be attributed to the DR of bulk-like water as separate DR measurements of neat water in this frequency window provide a single Debye relaxation with a DR time ~ 9 ps (see Table 6.3).⁶⁹ The slower ~ 40 ps timescale then may be considered to originate from the relaxation of those water molecules which are residing at the micellar interface. Note such

slower relaxations have been observed earlier in aqueous solutions containing biologically relevant molecules such as lipids, proteins, nucleic acids etc. and confined water systems (micelle, reverse micelle etc).⁷⁰

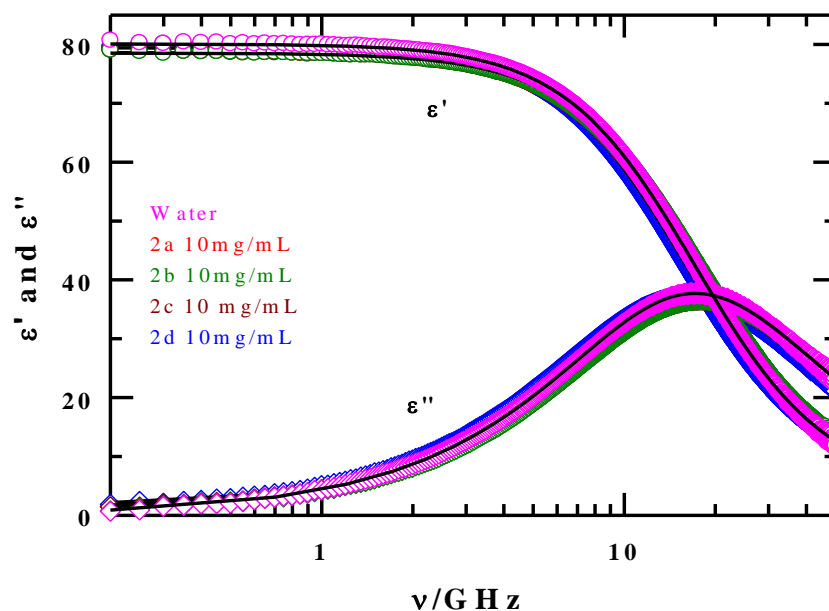


Fig. 6.5: Real (ϵ') and imaginary (ϵ'') components of the measured DR spectra for aqueous micellar solutions of different polymers (**2a**, **2b**, **2c**, **2d**) at 10 mg/mL concentration. Measurements were done in the frequency regime, $0.2 \leq \nu/\text{GHz} \leq 50$ and at $\sim 25^\circ\text{C}$. Solid lines through these data represent simultaneous fits using 2D relaxation model. Note the collected DR spectrum for neat water (pink) is nearly indistinguishable from those for polymer solutions.

The small, less-than-a-percent, amplitude of the slow relaxation observed here may indicate that the population of water molecules residing in the interfacial regions is extremely small. Such a negligible population of interfacial, “slow” water molecules might be the reason for us not being able to detect the Stokes shift dynamics in these polymeric micellar systems. This may be one of the significant differences between the micelles created by these diblock copolymers, and those by the conventional more-studied surfactants.^{20,33} Note also that the measured reorientational dynamics of C153 in these aqueous micellar solutions is faster than that observed with the same

probe in non-ionic aqueous micellar solutions of Triton X 100 (TX100) and n-octyl- β -D-thioglucoside (OTG) of comparable viscosity.⁶⁵ These differences in solute-centred dynamics (solute rotation and solvation) between the classical surfactant solutions and the present diblock copolymeric systems warrant further study.

Table 6.3: Parameters obtained from simultaneous 2D fits to real (ϵ') and imaginary (ϵ'') components of the measured DR spectra for aqueous polymer solutions at 10mg/mL polymer concentration and ~ 25 °C.

System (10 mg/mL)	ϵ_s	$\Delta\epsilon_1$	τ_1^a (ps)	$\Delta\epsilon_2$	τ_2 (ps)	ϵ_∞	n_D	κ_{fit} (S/m)	χ^2
2a	79.4	0.20	47	73.7	9.6	5.5	1.264	0.01	0.013
2b	78.5	0.20	34	73.3	8.9	5.0	1.264	0.01	0.009
2c	78.6	0.40	36	73.1	8.9	5.1	1.265	0.01	0.005
2d	80.0	0.44	37	73.9	9.9	5.7	1.264	0.01	0.005
Water (~ 22 °C)	80.1	-	-	75.4	9.3	4.7	1.263	-	0.062

τ_i^a ($i = 1-2$) are better within $\pm 5\%$ of the reported values.

6.4 Conclusion

In conclusion, megahertz-gigahertz dielectric relaxation and pico-second resolved fluorescence measurements were used to explore and understand the solution dynamics in aqueous milieu containing P(Boc-L-Ala-HEMA)-*b*-PPEGMA diblock copolymers with tunable segment lengths. Two coumarin probes, C153 (hydrophobic) and C343 (hydrophilic), have been employed independently to explore the different environments in these solutions and the corresponding magnitudes of the frictional resistance exerted by the different local environments. An introduction of appropriate amphiphilicity into copolymer permits to investigate their self-assembly behaviour in water. The synthesized diblock copolymers⁴¹ formed well-defined spherical micelles of nanoscopic size. The hydrophobic probe, due to its preferential location at

the micellar interface, experiences greater frictional resistance than the hydrophilic counter-part, although the latter reports stronger polymer concentration dependence of the frictional retardation than the former. Steady state and time-resolved fluorescence spectroscopic results suggest that the hydrophobic probe resides at the water-micelle interface whereas the hydrophilic probe prefers to locate in the water-like environment. In addition, DRS results suggest possible presence of “slowed down” water molecules at the interfacial region although the population of such “slow” water molecules in this region might be very small. Such thin hydration layers around the aggregates possessing relatively smaller hydrodynamic radii may have specific use as a carrier through tortuous path of nanometer dimension.

References:

1. Y. Mai and A. Eisenberg, *Chem. Soc. Rev.* **41**, 5969 (2012).
2. G. Gaucher, M. H. Dufresne, V. P. Sant, N. Kang, D. Maysinger and J. C. Leroux, *J. Controlled Release* **109**, 169 (2005).
3. K. Kataoka, A. Harada and Y. Nagasaki, *Adv. Drug Deliv. Rev.* **47**, 113 (2001).
4. X. B. Xiong, A. Falamarzian, S. M. Garg and A. Lavasanifar, *J. Controlled Release* **155**, 248 (2011).
5. S. Mukherjee, H. Dinda, L. Shashank, I. Chakraborty, R. Bhattacharyya, J. D. Sarma and R. Shunmugam, *Macromolecules* **48**, 6791 (2015).
6. V. P. Torchilin, *Cell Mol. Life Sci.* **61**, 2549 (2004).
7. G. S. Kwon, *Crit. Rev. Ther. Drug. Carr. Syst.* **20**, 357 (2003).
8. S. Movassaghian, O. M. Merkel and V. P. Torchilin, *Wiley Interdiscip. Rev.: Nanomed. Nanobiotechnol.* **7**, 691 (2015).
9. M. Kumbhakar, T. Goel, T. Mukherjee and H. Pal, *J. Phys. Chem. B* **108**, 19246 (2004).
10. H. Shirota, Y. Tamoto and H. Segawa, *J. Phys. Chem. A* **108**, 3244 (2004).
11. J. S. Lundgren, M. P. Heitz and F. V. Bright, *Anal. Chem.* **67**, 3775 (1995).
12. B. Guchhait, P. K. Ghorai and R. Biswas, *J. Phys. Chem. B* **117**, 3345 (2013).
13. S. S. Mojumdar, S. Ghosh, T. Mondal and K. Bhattacharyya, *Langmuir* **28**, 10230 (2012).
14. R. Hutterer, F. W. Schneider, W. T. Hermens, R. Wagenvoort and M. Hof, *Biochem. Biophys. Acta* **1414**, 155 (1998).
15. L. Frauchiger, H. Shirota, K. E. Uhrich and E. W. Castner, Jr. *J. Phys. Chem. B* **106**, 7463 (2002).
16. C. D. Grant, M. R. DeRitter, K. E. Steege, T. A. Fadeeva and E. W. Castner, Jr. *Langmuir* **21**, 1745 (2005).
17. T. Dwars, E. Paetzold and G. Oehme, *Angew. Chem. Int. Ed.* **44**, 7174 (2005).
18. U. Mandal, S. Ghosh, S. Dey, A. Adhikari and K. Bhattacharyya, *J. Chem. Phys.* **128**, 164505 (2008).
19. B. Samiey, C.-H. Cheng and J. Wu, *J. Chem.* **2014**, 908476 (2014).
20. N. Nandi, K. Bhattacharyya and B. Bagchi, *Chem. Rev.* **100**, 2013 (2000).
21. N. J. Jain, V. K. Aswal, P. S. Goyal and P. Bahadur, *J. Phys. Chem. B.* **102**, 8452 (1998).
22. H. Walderhaug and O. Söderman, *Curr. Opin. Colloid Interface Sci.* **14**, 171 (2009).

23. J. Kriz, B. Masar and D. Doskocilova, *Macromolecules* **30**, 4391 (1997).
24. P. Rajdev, D. Basak and S. Ghosh, *Macromolecules* **48**, 3360 (2015).
25. N. J. Jain, V. K. Aswal, P. S. Goyal and P. Bahadur, *J. Phys. Chem. B.* **102**, 8452 (1998).
26. R. Ganguly, V. K. Aswal, P. A. Hassan, I. K. Gopalkrishnan and J. V. Yakhmi *J. Phys. Chem. B* **109**, 5653 (2005).
27. K. Mortensen and W. Brown, *Macromolecules* **26**, 4128 (1993).
28. J. Chen, F. Zeng, S. Wu, J. Zhao, Q. Chen and Z. Tong, *Chem. Commun.* **0**, 5580 (2008).
29. D. K. Sasmal, A. K. Mandal, T. Mondal, K. Bhattacharyya *J. Phys. Chem. B* **115**, 7781 (2011).
30. G. B. Dutt, *J. Phys. Chem. B* **109**, 4923 (2005).
31. P. Sen, S. Ghosh, K. Sahu, S. K. Mondal, D. Roy and K. Bhattacharyya, *J. Chem. Phys.* **124**, 204905 (2006).
32. D. A. Turton, J. Hunger, A. Stoppa, G. Hefter, A. Thoman, M. Walther, R. Buchner and K. Wynne, *J. Am. Chem. Soc.* **131**, 11140 (2009).
33. R. Biswas, N. Rohman, T. Pradhan and R. Buchner, *J. Phys. Chem. B* **112**, 9379 (2008).
34. J. Barthel, K. Bachhuber, R. Buchner and H. Hetzenauer, *Chem. Phys. Lett.* **165**, 369 (1990).
35. C. Daguinet, P. J. Dyson, I. Krossing, A. Oleinikova, J. Slattery, C. Wakai and H. Weingärtner, *J. Phys. Chem. B* **110**, 12682 (2006).
36. K. Mukherjee, E. Tarif, A. Barman and R. Biswas, *Fluid Phase Equilib.* **448**, 22 (2017).
37. J. Barthel, R. Buchner, P.-N. Eberspächer, M. Muünsterer, J. Stauber and B. Wurm, *J. Mol. Liq.* **78**, 83 (1998).
38. M. Rohmann and M. Stockhausen, *J. Chem. Soc. Faraday Trans.* **88**, 1549 (1992).
39. S. Imai and T. Shikata, *Langmuir* **15**, 8388 (1999).
40. M. D'Angelo, D. Fioretto, G. Onori, L. Palmieri and A. Santucci, *Phys. Rev. E* **54**, 993 (1996).
41. E. Tarif, B. Saha, K. Mukherjee, P. De and R. Biswas, *J. Phys. Chem. B* **123**, 5892 (2019).
42. N. Liu, B. Li, C. Gong, Y. Liu, Y. Wang and G. Wu, *Colloids Surf. B* **136**, 562 (2015).
43. H. Otsuka, Y. Nagasaki and K. Kataoka, *Adv. Drug Deliv. Rev.* **64**, 246 (2012).
44. A. Das and R. Biswas, *J. Phys. Chem. B* **119**, 10102 (2015).
45. B. Guchhait, S. Daschakraborty and R. Biswas, *J. Chem. Phys.* **136**, 174503 (2012).
46. B. Guchhait, S. Das, S. Daschakraborty and R. Biswas, *J. Chem. Phys.* **140**, 104514 (2014).

47. T. Pradhan and R. Biswas, *J. Phys. Chem. A* **111**, 11514 (2007).
48. B. Guchhait and R. Biswas, *J. Chem. Phys.* **138**, 114909 (2013).
49. T. Pradhan, H. A. R. Gazi, B. Guchhait and R. Biswas, *J. Chem. Sci.* **124**, 355 (2012).
50. A. Das, S. Das and R. Biswas, *Chem. Phys. Lett.* **581**, 47 (2013).
51. A. J. Cross and G. R. Fleming, *Biophys. J.* **46**, 45 (1984).
52. T. Pradhan, P. Ghoshal and R. Biswas, *J. Chem. Sci.* **120**, 275 (2008).
53. M. L. Horng, J. A. Gardecki and M. Maroncelli, *J. Phys. Chem. A* **101**, 1030 (1997) .
54. S. Indra and R. Biswas, *J. Chem. Phys.* **142**, 204501 (2015).
55. S. Indra, B. Guchhait and R. Biswas, *J. Chem. Phys.* **144**, 124506 (2016).
56. C. J. F. Böttcher and P. Bordewijk, *Theory of electric polarization*, Elsevier, Amsterdam, The Netherlands, 1978.
57. F. Kremer and A. Schönhal, *Broadband Dielectric Spectroscopy*. (Springer, Berlin, Germany,, 2003)
58. P. Bevington, *Data Reduction and Error Analysis for the Physical Sciences*. (McGrawHill: New York, 1969).
59. G. Kwon, M. Naito, M. Yokoyama, T. Okano, Y. Sakurai and K. Kataoka, *Langmuir* **9**, 945 (1993).
60. T. Rager, W. H. Meyer, G. Wegner and M. A. Winnik, *Macromolecules* **30**, 4911 (1997).
61. H. Cabral, K. Miyata, K. Osada and K. Kataoka, *Chem. Rev.* **118**, 6844 (2018).
62. M. E. Fox, F. C. Szoka and J. M. J. Frechet, *Acc. Chem. Res.* **42**, 1141 (2009).
63. M. L. Adams, A. Lavasanifar and G. S. Kwon, *J. Pharm. Sci.* **92**, 1343 (2003).
64. J. Maiti, V. Kalyani, S. Biswas, F. Rodriguez-Prieto, M. Mosquera and R. Das, *J. Photochem. Photobiol. A: Chemistry* **346**, 17 (2017).
65. C. C. Ruiz, *Photochem. Photobiol. Sci.* **11**, 1331 (2012).
66. J. R. Lakowicz, *Principles of fluorescence spectroscopy*, Springer, New York, 3rd edn, 2006.
67. G. B. Dutt and T. K. Ghanty, *J. Phys. Chem. B* **107**, 3257 (2003).
68. S. Koley, H. Kaur and S. Ghosh, *Phys. Chem. Chem. Phys.* **16**, 22352 (2014).
69. R. Buchner, J. Barthel and J. Stauber *Chem. Phys. Lett.* **306**, 57 (1999).
70. K. Mukherjee, A. Barman and R. Biswas, *J. Mol. Liq.* **222**, 495 (2016).

Chapter 7

Dynamics at the Non-Ionic Micelle/Water Interface: Impact of Linkage Substitution

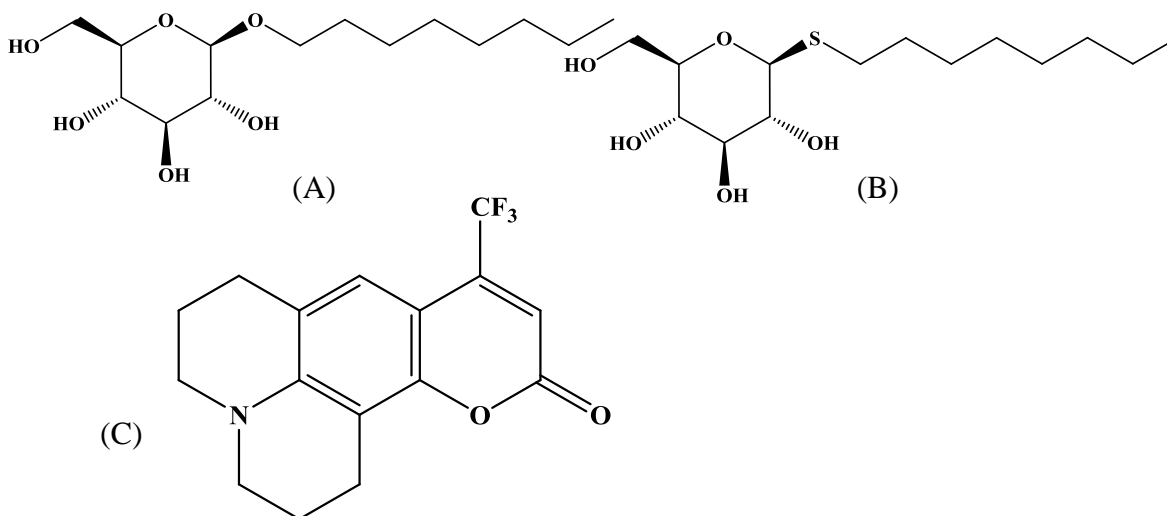
7.1 Introduction

Detergents are frequently used for solubilization and purification of intrinsic membrane proteins because of their amphipathic structure,¹ however, there are detergents such as sodium dodecyl sulfate (SDS)² which facilitate denaturation of proteins. Therefore detergents, depending upon their physical and chemical properties, can act both as a stabiliser and a denaturant for proteins. A thorough understanding about the physicochemical properties of these detergents is then needed for smarter use of them in the field of protein chemistry. Among the detergents currently available, alkyl polyglucosides (APGs) are well known protein solubilising detergents and increasingly being used for solubilization and reconstitution of many membrane proteins.^{3,4} They are also being extensively used as liquid dishwashing agent, in personal care and agrochemical products, and for industrial and institutional cleaning⁵ because of their nontoxic and biodegradable nature. *n*-Octyl- β -D-glucopyranoside (OG) and *n*-octyl- β -D-thioglucopyranoside (OTG) are two examples of such alkyl polyglucosides. In this work we have investigated the effects of replacing connector ‘O’ atom (for *n*-octyl- β -D-glucopyranoside) by a comparatively larger ‘S’ atom (for *n*-octyl- β -D-thioglucopyranoside, see Scheme 7.1) on the water/micelle interfacial dynamics via time-resolved fluorescence measurements (TRF), dielectric relaxation spectroscopic (DRS) studies and differential scanning calorimetry (DSC).

It is well-known that the dynamics of the solvent molecules that are close to the surface of the micelles is different from the dynamics of the solvent molecules that are in the bulk.⁶ It is now established that the dynamics at bio-macromolecule/water interfaces depends on structures⁶⁻¹¹ and charge of the interfaces.^{6,11-13} Subsequently, the structure of the micelle /water interface, depend on alkyl chains,^{10,14-17} nature of counter ions (for ionic surfactants),¹⁸⁻²³ chain length of

the spacer²⁴⁻²⁶ and shape of the monomers^{27,28}. Moreover, sometimes it has been found that the structure of the micelles and the solubility of the non-ionic surfactants depend on the stereochemistry of the head group.²⁹⁻³¹ Incidentally, this is true for *n*-octyl-D-glucosides.³²

Scheme 7.1: Chemical structure of (A) *n*-Octyl- β -D-glucopyranoside, (B) *n*-Octyl- β -D-thioglucopyranoside and (C) Coumarin 153



Instead of having four similar phases in their phase diagrams, *n*-octyl- α -D-glucoside/water and *n*-octyl- β -D-glucoside/water binary mixtures differ distinctly in their phase diagrams.^{33,34} However, in this work, our focus is on interfacial dynamics of the micelles formed by the β -conformers only, where the phase diagrams of *n*-octyl- β -D-glucoside/water and *n*-octyl- β -D-thioglucoside/water systems are quite similar.³⁵ Different experimental techniques, like quasi elastic light scattering (QELS),³⁶ small-angle X-ray scattering (SAXS),³⁷ small-angle neutron scattering (SANS),³⁸ nuclear magnetic resonance(NMR),³⁷ fluorescence spectroscopy³⁹⁻⁴¹ and dynamic light scattering (DLS)^{42,43} have been applied to determine the critical micellization concentration (CMC) values, and estimate shape and size of the micelles, hydration numbers and structure of the hydration layer and the dynamics of the micelles in both *n*-octyl- β -D-glucoside/water and *n*-octyl- β -D-thioglucoside/water solutions. Temperature dependent measurements^{37,43,44} suggest that the dynamics of these non-ionic surfactants are temperature sensitive, though not as much as ethylene oxide (EO)-based non-ionic surfactants, and with increasing temperature the CMC value decreases. Moreover, it has been found that micellization, occurring at the cost of a significant amount of hydration water molecules from each monomer

(undergoing monomer to micelle transition),⁴⁰ of these surfactants strongly depends on the presence of cosolvent,⁴⁵⁻⁴⁷ electrolyte^{48,49} and polymeric substance⁵⁰ in the medium. Although a number of experimental and simulation⁵¹ studies have been carried out so far to explore the dynamics of these two surfactant molecules, the understanding regarding the dynamics of the hydration water molecules at the non-ionic micelle/water interface is still lacking. Herein, we investigate the differences in interfacial dynamics induced by the atom substitution via monitoring the time-resolved fluorescence of a non-reactive solute probe, and explain the observation through auxiliary measurements employing dielectric relaxation and differential scanning calorimetric experiments.

Time-resolved fluorescence measurement has always been a useful technique to probe the environmental dynamics of various media.^{13,52-58} We have employed coumarin 153 (C153), one of the extensively studied fluorescent molecules,⁵⁹⁻⁶⁴ to capture the local dynamics at the interfaces. The main reason behind the selection of C153 as the probe molecule is its hydrophobic character, and previous reports indicate that this fluorescent molecule resides at the palisade water layer surrounding micelles in aqueous solutions.⁶⁵⁻⁶⁷ We have prepared solutions of 15 mM and 30 mM for *n*-octyl- β -D-thioglucopyranoside (CMC ~ 9-10 mM)⁴³ and *n*-octyl- β -D-glucopyranoside (CMC ~ 20-25 mM),⁴⁸ respectively. For confirmation of micelle formation, we have performed fluorescence and DLS measurements. DR dynamics of these two surfactant solutions in the frequency regime, $0.2 \leq \nu(\text{GHz}) \leq 50$, have been followed to understand the aqueous dynamics probed by TRF measurements. Dielectric relaxation spectroscopy has been an excellent technique to investigate medium dynamics of such aqueous macromolecular solutions.⁶⁸⁻⁷³ Note here that a combined DR and TRF study to unravel the impact of atom substitution on dynamics of aqueous micellar interfaces of two similar surfactant molecules is completely new and has not been attempted before.

7.2 Experimental Section

7.2.1 Sample Details

n-Octyl- β -D-glucopyranoside ($\geq 98\%$) and *n*-Octyl- β -D-thioglucopyranoside ($\geq 98\%$) were purchased from Sigma Aldrich and used without further purification. Laser grade C153 was purchased from Sigma Aldrich (99%) and used as received. Millipore water was used for the

preparation of aqueous solution of the surfactants. Aqueous solutions of these surfactants well above the micellar concentrations (OG ~30 mM and OTG ~15 mM) were prepared by dissolving the required amount of OG and OTG in water (Millipore). All measurements were performed at 298±1K. In each sample for optical measurements the concentration of C153 was maintained at ~10⁻⁵ M.

7.2.2 Density and Viscosity Measurements

Density measurements were carried out using an automated-temperature-controlled density-cum-sound analyzer (Anton Paar, model DSA5000). Solution viscosity coefficients (η) were measured via a micro viscometer (AMVn, Anton Paar).^{74,75}

7.2.3 Dynamic Light Scattering (DLS) Measurements

DLS measurements were performed employing a NanoS Malvern instrument equipped with a 4 mW He-Ne laser ($\lambda = 632.8$ nm). All the scattered photons were collected at 173° scattering angle. Detail description can be found elsewhere.⁷⁶

7.2.4 Differential Scanning Calorimetric (DSC) Measurements

DSC (TA Instruments Q2000) technique was applied to investigate the presence of bound water molecules. The samples were taken in a hermetically sealed aluminium pan (40 μ l, Tzero, TA Instruments) to prevent evaporation during the measurements. Description can be found elsewhere.⁷⁷

7.2.5 Steady State Measurements

UV–Visible spectrophotometer (UV-2600, Shimadzu) and fluorimeter (Fluorolog, Jobin-Yvon, Horiba) were used for the collection of steady state absorption and emission spectra, respectively. Spectra were then solvent-blank subtracted and converted properly to the frequency domain before further analyses and frequency determination.⁷⁸⁻⁸⁰

7.2.6 Time-Resolved fluorescence measurements

Time-correlated single-photon counting (TCSPC) coupled with a laser diode ($\lambda_{\text{exc}} = 409$ nm as an excitation light) was used for the time-resolved fluorescence (TRF) measurements, and the setup

description can be found elsewhere.^{58,81} The full width at half-maximum (fwhm) of the instrument response function (IRF) was ~85 ps (using a scattering solution and 409 nm excitation light). Using standard protocol described in chapter 2 we have performed dynamic Stokes shift and anisotropy measurements.^{57,59,82,83}

7.2.7 Dielectric Relaxation Spectroscopy

Dielectric relaxation spectroscopy (DRS) measures the frequency dependent dielectric response of a given medium toward an external electric field, and contains information about the rotational, vibrational and translational motions of the constituents.^{84,85} The DR measurements were performed using a PNA-L Network Analyzer (N5230C) combined with a probe kit (85070E) operating in the frequency range $0.2 \leq \text{GHz} \leq 50$. The collection of DR data and associated analysis protocol are similar as discussed in chapter 2. For all measurements presented here, 1D fits (single Debye processes) were employed to obtain the best simultaneous descriptions of the measured $\epsilon'(\nu)$ and $\epsilon''(\nu)$.

7.3. Results and Discussion

7.3.1 Steady State Measurements

Fig. 7.1 presents the absorption and emission spectra of C153 in 30 mM and 15 mM aqueous solutions of OG and OTG, respectively. Spectral features, provided in Table 7.1, indicate that the steady state environments around the probe molecules in both the solutions are quite similar, although both of the solutions have different surfactant concentrations. Notice here that all the experiments have been performed well above the reported CMC values, which we have checked by performing both controlled fluorescence experiments (see Fig. A.e.1), and dynamic light scattering (see Fig.7.2) measurements.

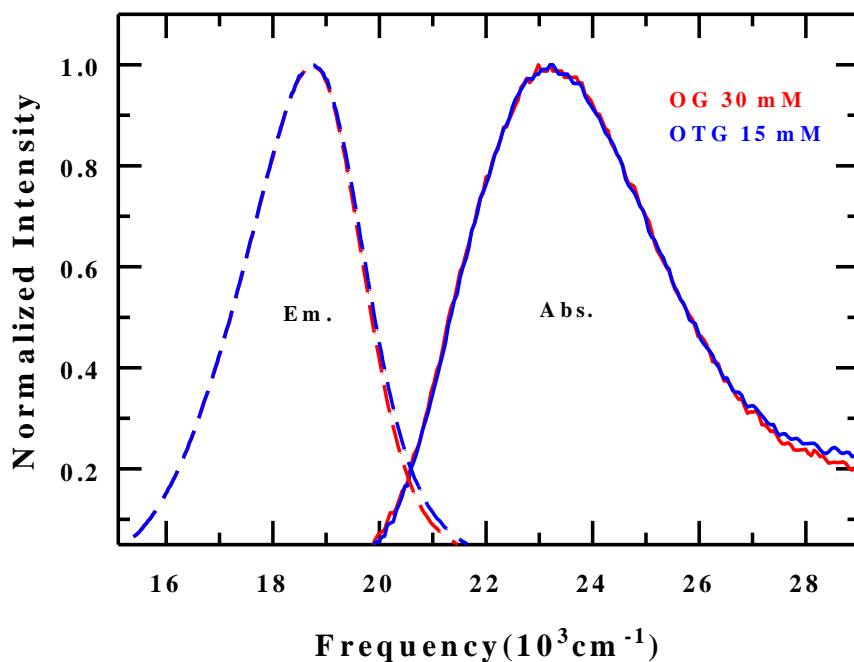


Fig. 7.1: Absorption and emission spectra of C153 in 30 mM and 15 mM aqueous solutions of OG and OTG, respectively. Spectra are color-coded.

Table 7.1. Spectral features of C153 in water, 30 mM and 15 mM aqueous solutions of OG and OTG, respectively.

Medium	$\nu_{abs.} (10^3 \text{cm}^{-1})^a$	$\nu_{em.} (10^3 \text{cm}^{-1})^b$	$\Gamma_{abs.} \text{ (FWHM)}$ (10^3cm^{-1})	$\Gamma_{em.} \text{ (FWHM)}$ (10^3cm^{-1})
OG 30mM	23.17	18.73	4.57	2.64
OTG 15mM	23.18	18.74	4.46	2.70
Water	23.20	18.28	5.14	2.56

^{a,b}These data are reproduced within the uncertainty of $\pm 200 \text{cm}^{-1}$

On the other hand, comparison of the steady state spectral features, especially emission spectra, of C153 in pure water (presented in the same table) with the same in aqueous OG and OTG solutions suggests that, like in other micellar solutions,^{89,90} here also the probe molecules are located at the micelle/water interfaces. Furthermore, the associated narrowing in absorption and broadening in emission spectra (see Table 7.1) of C153 in OG and OTG surfactant solutions

relative to those in neat water indicate location of the probe at less polar region in the surfactant solutions than water.⁶² Analyses of excitation wavelength dependent emission spectra (see Fig. A.e.2) suggest that the environment surrounding the probe solute is nearly homogeneous within the excited state lifetime (~ 4 ns) of the probe. This was also observed for diblock copolymer micelles in aqueous media.⁹¹

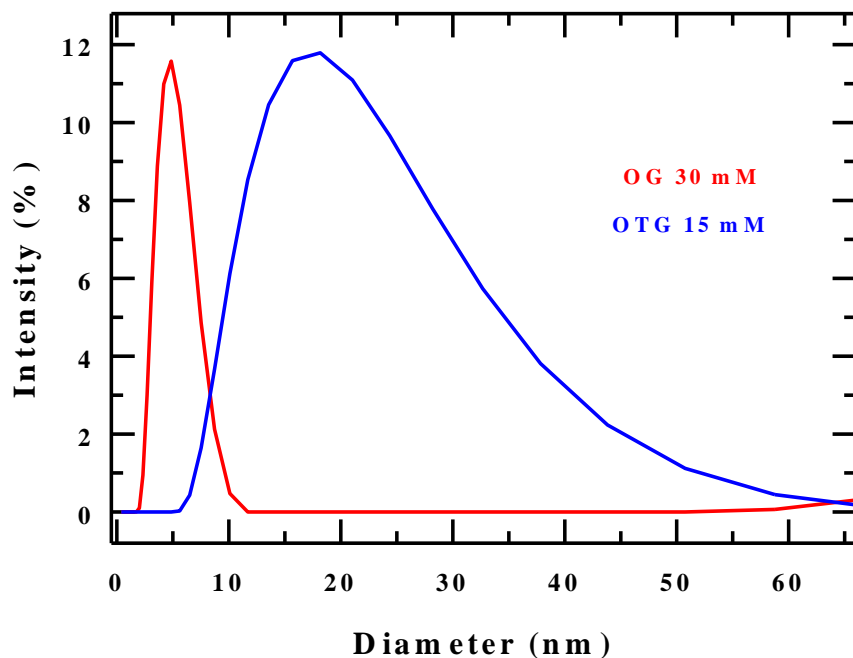


Fig. 7.2: A comparison of the size of aggregates of 30 mM and 15 mM aqueous solutions of OG and OTG, respectively. Representations are color-coded.

7.3.2 Time-Resolved Fluorescence Measurements

7.3.2.1 Rotational Anisotropy Decay, $r(t)$, Analysis: Slower Probe Rotation in OTG

Fig. A.e.3 represents the collected vertically ($I_{para}(t)$) and horizontally ($I_{perp}(t)$) polarized emission decays. Furthermore, Fig. 7.3 and Table 7.2 display the $r(t)$ decays of C153 in the surfactant solutions and the fitting parameters, respectively. Solid lines going through the experimental data points represent the bi-exponential fits and the quality of the fits is shown in Fig. A.e.4.

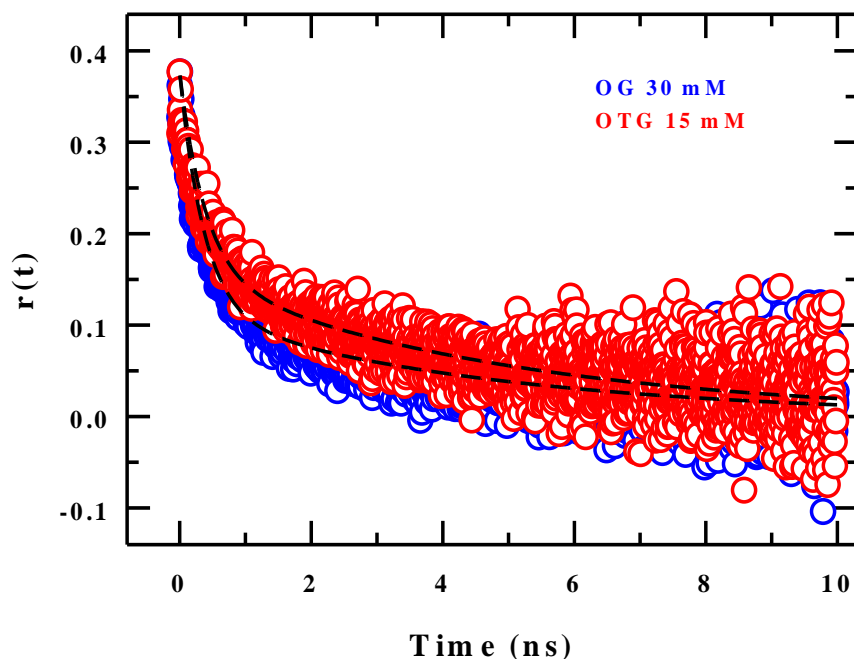


Fig. 7.3: Representative $r(t)$ decays of C153 in 30 mM and 15 mM aqueous solutions of OG and OTG, respectively. Solid lines going through the data points represent bi-exponential fits. Presentations are color-coded.

In both the solutions, $r(t)$ are characterized by a fast component of sub nanosecond timescale, having contribution ~ 60 to 70% , followed by a slower component with a few nanosecond time constant. This relaxation behaviour represents the bimodal nature of the underlying frictional resistance of the local environment to the reorientational dynamics of the solute. Estimated $\langle \tau_r \rangle$ are in good agreement with previous report for OTG solution.⁶⁵ We have fixed r_0 at 0.376 ⁵⁹. The average rotational times, $\langle \tau_r \rangle$, of C153 in OG and OTG solutions are 15-20 times slower than that in neat water (~ 100 ps⁵⁷), although the viscosity coefficients for these aqueous surfactant solutions are comparable to that of neat water (see Table 7.2). This relatively slow rotation of C153 in OG and OTG solutions (compared to that in neat water) indicates the interfacial location of the dissolved probe solute.

Table 7.2: Fit parameters required for $r(t)$ decays of C153 in water, 30 mM and 15 mM aqueous solutions of OG and OTG, respectively.

Medium	a_1 (%)	τ_1 (ps)	a_2 (%)	τ_2 (ps)	$\langle \tau_r \rangle^c$ (ps)	τ_{lif}^d (ns)	η (cP)	Diameter(nm)
OG 30 mM	70	377	30	4547	1628	3.5	0.999	5 ± 1
OTG 15 mM	58	405	42	4828	2263	3.7	1.022	19 ± 2
water	-	-	-	-	~ 100 ps ^a ; ~ 50 ps ^b		0.893	

a) Our measurement; b) Ref. 57, and ^{c,d}uncertainty $\pm 10\%$.

Interestingly, $\langle \tau_r \rangle$ of C153 in OTG solution is slower than that in OG solution (Table 7.2), although in both of the surfactant solutions the micelle/water interfaces are constituted by the same head group (pyranose ring). Moreover, similar steady state spectral features of C153 in both the surfactant solutions indicate similar environment around the probe. Now the simple question: why the friction exerted on the rotating solute (C153) differs from each other in these micelle/water interfaces? Since the only difference between OG and OTG is the presence of different connector atoms (oxygen and sulphur respectively), the extra slowing down of rotational in OTG solution may arise from the specific interaction involving electropositive carbon atom ($-CF_3$: charge on carbon atom calculated using G03,⁹² see Table A.e.5) of C153 and sulphur atom of OTG. Larger size ($S^{radius} = 100$ pm; $O^{radius} = 60$ pm) and lower electronegativity ($S^{EN} = 2.58$; $O^{EN} = 3.44$) than oxygen have made sulphur (better Lewis base) better lone pair donor (ligand) toward the electropositive atom,⁹³ allowing to interact more prominently with the electropositive carbon atom ($-CF_3$). If we consider the specific interaction of $-CF_3$ with S atom of OTG then it should have been reflected in the steady state measurements. However, a strong solute-environment interaction as in the present cases may completely swamp the impact of the specific interaction between $-CF_3$ and S, making the steady state spectral features appear completely free from such solute-solvent specific interactions. Therefore, the similar steady state spectral features for C153 in OG and OTG is

plausible, although slower rotation for C153 in OTG than in OG containing solution provides evidence of solute-surfactant specific interaction.

7.3.2.2 Solvation Dynamics Study: Slower Solvation in OTG

Fig. 7.4 depicts the comparison of the Stokes shift dynamics of C153 in OG and OTG solutions. Moreover, a representative figure for the corresponding fluorescent transients at the red (640 nm) and blue (490 nm) wavelengths along with the tri-exponential fits going through the data are presented in Fig. A.e.6 and Fig. A.e.7 (Appendix). Time-resolved emission spectra (TRES) of C153 in OG and OTG solutions are shown in Fig. A.e.8 along with steady state emission spectrum (dashed lines). Note the steady state emission spectrum is blue shifted compared to emission spectrum at $t = \infty$. This indicates steady state emission takes place from incompletely solvent-relaxed configuration of the laser-excited solute.

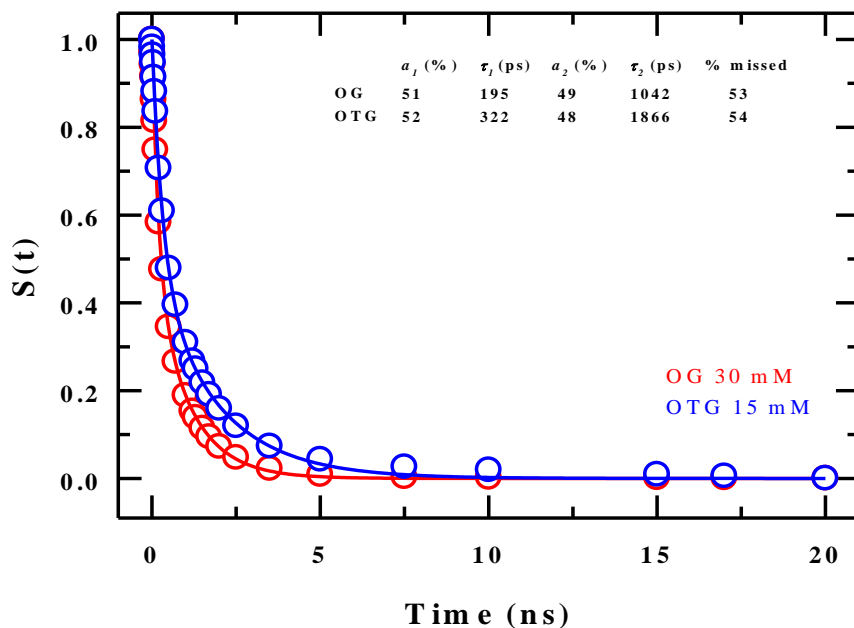


Fig. 7.4: $S(t)$ decays for C153 in 30 mM and 15 mM aqueous solutions of OG and OTG, respectively. Solid lines going through the data points represent the bi-exponential fits. Fit parameters are presented in the inset. Spectra are color-coded.

Dynamical solvent response ($S(t)$) for both of these solutions can be well described by bi-exponential decay functions. Fit parameters along with the missing percentages are presented in the inset. From the figure it is clear that the solvation of the probe molecule is significantly faster (~ 2 times) in OG solution than in OTG solution. We have missed $\sim 30\%$ of the total dynamics for both the solutions due to broad temporal resolution (~ 85 ps) in these measurements. To understand the reason behind this relative slowness of the solvation response in OTG solution, we discuss the following factors.

There exist several reports regarding the slow (sub-nanosecond to multi-nanosecond time scales) solvation dynamics of polar dye molecules in restricted environments like micelles, reverse micelles, cyclodextrins and many other bio-macromolecules.⁹⁴⁻⁹⁷ Most of them indicate that this slow solvation of the probe molecules is mainly due to sluggish dynamics of the interfacial solvent molecules. Furthermore, it has been observed that the dynamic solvent response of dissolved dye molecules gets affected when the interactions (mainly H-bonding) between the micellar surface and water molecules around it are tuned, either physically⁹⁸ or chemically.^{8,99,100} But the question still remains: why the dynamic solvent responses in OTG is approximately twice slower than that in OG, although the micelle/water interfaces in both the surfactant solutions are constituted by same head group. The amplitudes of the relaxation components (see Fig. 7.4), are similar for both the surfactant solutions, although OTG micelles are ~ 4 times larger in size than OG micelles. Interestingly, the slower solvation time constant (τ_2) is ~ 2 times longer without any significant change in the respective amplitudes. This suggests that either the dynamic equilibrium between the bound and bulk water, which is typically assigned for slower $S(t)$ decays in restricted environments,^{97,101,102} has altered upon atom substitution, or the origin of τ_2 is completely new and different. Interestingly, we do not find any signature of bound water in both DSC (see Fig. A.e.9) and DRS (discussed in section 7.3.4) measurements for these surfactant solutions. This observation indicates a secondary role for bound water molecules even if they exist via forming a very thin layer at the interface. The main contributor to this nanosecond solvation component could be the time-dependence in solute-solvent interaction energy due to fluctuations in solute's location via its own rotational and translational motions. Restricted dynamics of the pyranose ring of the surfactant molecule, as previously observed for the ion solvation near the micellar surface,¹⁰³ could also be a possible origin although the

corresponding DR data do not show any additional relaxation timescale over the detected ~ 10 ps time constant. We would, however, like to mention that restricted low amplitude motion of the pyranose moiety may participate in the solvation process contributing to both sub-nanosecond and nanosecond solvation components without being reflected in the measured DR data because of their presence at very low concentrations (milli-molar level) in these aqueous solutions. Similarly, an extremely thin layer of bound water, as reported recently for aqueous solutions of amphiphilic diblock copolymer at higher concentration,⁹¹ might contribute to the sub-nanosecond solvation component without getting detected in the present DR measurements because of extremely low population. Let us discuss further about this contribution arising from solute diffusion (rotation and translation).

Fig. A.e.10 shows the time dependent changes of the width ($\Gamma(t)$) of the time-resolved emission spectra in OG and OTG solutions, where $\Gamma(t)$ first increases and then decreases. However, this change in $\Gamma(t)$ is limited within $\sim 200-400 \text{ cm}^{-1}$, and is much smaller than what was observed in ionic liquids and deep eutectic solvent ($\sim 1000 - 1500 \text{ cm}^{-1}$). This suggests that the environments probed by the solute during its lifetime are nearly similar and thus homogeneous. Table A.e.11 summarizes the hydrodynamic rotational and translational diffusion timescales for C153 employing the measured solution viscosities (water-like, $\eta \sim 1\text{cP}$). Interestingly, calculated translational diffusion timescale (Table A.e.11) is ~ 1 ns which is the timescale of the slow solvation component here. However, the average rotation times for the solute were found to be $\sim 15-20$ times longer than that for the same solute in neat water ($\eta \sim 1\text{cP}$). If this lengthening of solute rotation timescales (over that in water) are attributed to the proportionate local viscous resistance then the modified hydrodynamic solute rotational diffusion times become $\sim 1-1.5$ ns, translational diffusion times become $\sim 15-20$ ns. Considering the magnitude of the variation in the $\Gamma(t)$ discussed above, solute's rotational diffusion is the likely candidate for producing the slow nanosecond solvation components in these aqueous micellar solutions. Note in spatially heterogeneous viscous media (for example, ionic liquids and deep eutectics), $\Gamma(t)$ fluctuates over a wider range (and corroborates well with the corresponding excitation energy dependence of steady state fluorescence emission). This possibly signals participation of solute translation on its own rate of solvation in these heterogeneous media. Relatively smaller fluctuation of $\Gamma(t)$ for

C153 in OG and OTG solutions may therefore be interpreted as a support for solute rotation as a probable origin for the nanosecond solvation component in these aqueous surfactant solutions.

Now we concentrate on the faster, sub-nanosecond, solvation time constant (τ_1) which is also slightly faster for OG solutions. Similar solvation time constant has also been reported for aqueous solutions of other non-ionic surfactants, like triton-X-100,^{8,99} triton-X-165,⁸ and Brij-35,¹⁰⁰ and explained by the collective dynamics of interfacial water molecules. Likewise, we attribute this sub-nanosecond time component to the collective H-bond dynamics of the water molecules at the palisade layer. This faster component does not show appreciable atom-substitution dependence because the chemical nature of the head group remains mostly the same for both the surfactants. Further and careful studies regarding the dynamics of the hydration layer of these two closely similar surfactant molecules are still required to generate a clear understanding of the substitution effects explored here.

7.3.3 DRS Data Analysis

Fig. 7.5 and Fig. A.e.12 show the recorded DRS spectra for the two surfactant solutions at room temperature along with the fit parameters and residuals, respectively. Unlike other aqueous micellar solutions,^{70,71} here we have not found any signature of “slow” water^{97,104-106} molecules; the whole spectrum (within the experimental frequency regime) can be adequately described by a single Debye relaxation step for both the surfactants. However, in earlier study for bile salt solutions⁷⁸ and in other study^{70,71,107} involving different surfactant solutions of comparable concentrations, DR measurements have detected the presence of water molecules slower than those in neat bulk water. Here in these micellar solutions the absence of such slower relaxation may suggest that the hydration layer does exist but is too thin to be detected by the present DRS measurements. This view is in good agreement with the results from DSC measurements discussed earlier, and provides further support to the solute motion as a likely origin for the nanosecond solvation component observed for the present cases.

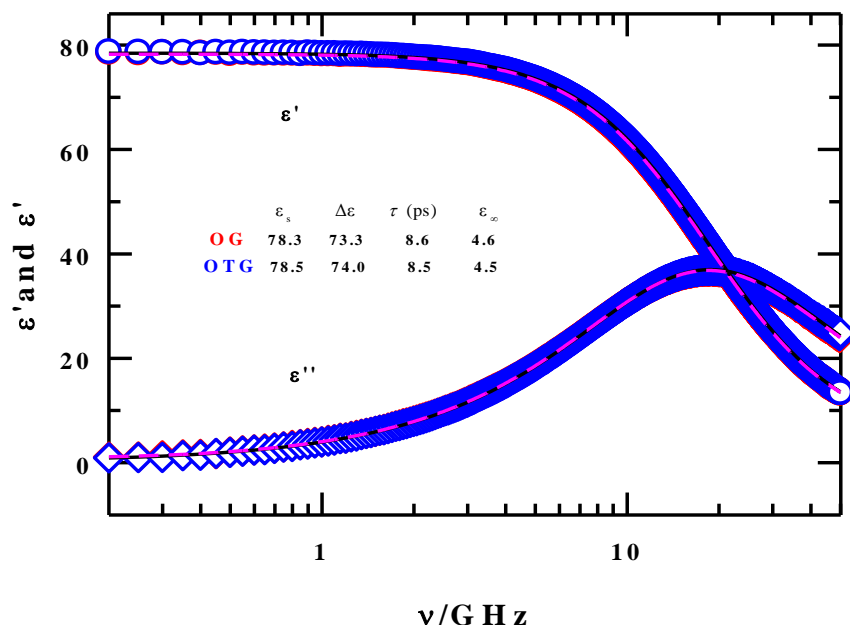


Fig. 7.5: The real (ϵ') and imaginary (ϵ'') components of the measured DR spectra of 30 mM and 15 mM aqueous solutions of OG and OTG, respectively, within the frequency regime, $0.2 \leq \nu/\text{GHz} \leq 50$. Solid lines through these data points represent simultaneous fits using 1D relaxation model. Spectra are color-coded.

7.4 Conclusion

In conclusion, the present work reveals a considerable impact of atom substitution in the surfactant molecules on the interfacial aqueous dynamics. Presence of “slow” water has not been detected by DRS measurements for aqueous solutions of both the surfactants, and corresponding DSC measurements support this observation. Polar probe solute locates at the micelle/water interface for both the surfactants but reports nearly homogeneous solvation environment through steady state spectral features. This interfacial location for the solute is further evidenced in the considerably slowed down rotational dynamics (of the solute) over that in neat water which is nearly as viscous as these aqueous surfactant solutions. Slow nanosecond solvation timescale, typical of that for a variety of other surfactant solutions, has also been found for the aqueous solutions of these surfactants. Solute’s rotational diffusion and solute-solvent specific interaction have been identified as possible contributors to the nanosecond solvation

component and a difference of factor two between them in these surfactant solutions measured using C153.

References:

1. R. M. Garavito and S. F. Miller, *J. Biol. Chem.* **276**, 32403 (2001).
2. A. M. Seddon, P. Curnow and P. J. Booth, *Biochim. Biophys. Acta* **1666**, 105 (2004).
3. M. le Maire, P. Champeil and J. V. Molle, *Biochim. Biophys. Acta* **1508**, 86 (2000).
4. H. Tani, T. Saitoh, T. Kamidate, T. Kamataki and H. Watanabe, *Anal. Sci.* **13**, 747 (1997).
5. K. Hill and O. Rhode, *Fett/Lipid* **101**, 25 (1999).
6. B. Bagchi, *Chem. Rev.* **105**, 3197 (2005).
7. S. N. Jamadagni, R. Godawat and S. Garde, *Annu. Rev. Chem. Biomol. Eng.* **2**, 147 (2011).
8. V. R. Hande and S. Chakrabarty, *J. Phys. Chem. B* **119**, 11346 (2015).
9. M. Kumbhakar, S. Nath, T. Mukherjee and H. Pal, *J. Chem. Phys.* **121**, 6026 (2004).
10. H. Wennerström and B. Lindman, *Phys. Rep.* **52**, 1 (1979).
11. S. Nihonyanagi, J. A. Mondal, S. Yamaguchi and T. Tahara, *Annu. Rev. Phys. Chem.* **64**, 579 (2013).
12. J. A. Mondal, S. Nihonyanagi, S. Yamaguchi and T. Tahara, *J. Am. Chem. Soc.* **132**, 10656 (2010).
13. N. Sarkar, A. Datta, S. Das and K. Bhattacharyya, *J. Phys. Chem.* **100**, 15483 (1996).
14. R. C. Oliver, J. Lipfert, D. A. Fox, R. H. Lo, S. Doniach and L. Columbus, *PLOS ONE* **8**, e62488 (2013).
15. J. A. Mondal, V. Namboodiri, P. Mathi and A. K. Singh, *J. Phys. Chem. Lett.* **8**, 1637 (2017).
16. J. A. Long, B. M. Rankin and D. B. Amotz, *J. Am. Chem. Soc.* **137**, 10809 (2015).
17. R. Nagarajan, *Langmuir* **18**, 31 (2002).
18. A. R. Rakitin and G. R. Pack, *J. Phys. Chem. B* **108**, 2712 (2004).
19. D. P. Bossev, M. Matsumoto and M. Nakahara, *J. Phys. Chem. B* **103**, 8251 (1999).
20. F. S. Lima, I. M. Cuccovia, D. Horinek, L. Q. Amaral, K. A. Riske, S. Schreier, R. K. Salinas, E. L. Bastos, P. A. R. Pires, J. C. Bozelli, Jr., D. C. Favaro, A. C. B. Rodrigues, L. G. Dias, O. A. El. Seoud and H. Chaimovich, *Langmuir* **29**, 4193 (2013).
21. M. Benraou, B. L. Bales and R. Zana, *J. Phys. Chem. B*, **107**, 13432 (2003).
22. Y. Geng, L. S. Romsted, S. Froehner, D. Zanette, L. J. Magid, I. M. Cuccovia and H. Chaimovich, *Langmuir* **21**, 562 (2005).
23. S. Berr, R. R. M. Jones and J. S. Johnson, Jr., *J. Phys. Chem.* **96**, 5611 (1992).
24. R. Zana, M. Benraou and R. Rueff, *Langmuir* **7**, 1072 (1991).

25. S. De, V. K. Aswal, P. S. Goyal and S. Bhattacharya, *J. Phys. Chem.* **100** 11664 (1996).
26. H. Hirata, N. Hattori, M. Ishida, H. Okabayashi, M. Frusaka, R. Zana, *J. Phys. Chem.* **99**, 17778 (1995).
27. J. J. H. Nusselder and J. B. F. N. Engberts, *Langmuir* **7**, 2089 (1991).
28. A. Roda, A. F. Hofmann and K. J. Mysels, *J. Biol. Chem.* **258**, 6362 (1983).
29. S. Abel, F. Y. Dupradeau, E. P. Raman, A. D. MacKerell, Jr. and M. Marchi, *J. Phys. Chem. B* **115**, 487 (2011).
30. T. T. Chong, R. Hashim and R. A. Bryce, *J. Phys. Chem. B* **110**, 4978 (2006).
31. P. Sakya and J. M. Seddon, *Liq. Cryst.* **23**, 409 (1997).
32. B. Focher, G. Savelli, G. Torri, G. Vecchio, D.C. McKenzie, D.F. Nicoli and C.A. Bunton, *Chem. Phys. Lett.* **158**, 491 (1989).
33. V. Kocherbitov and O. Soderman, *Phys. Chem. Chem. Phys.* **5**, 5262 (2003).
34. V. Kocherbitov, O. Soderman and L. Wadso, *J. Phys. Chem. B* **106**, 2910 (2002).
35. S. Ogawa, K. Asakura and S. Osanai, *Carbohydr. Res.* **345**, 2534 (2010).
36. A. D. Aprano, R. Giordano, M. P. Jannelli, S. Magazu, G. Maisano and B. Sesta, *J. Mol. Struct.* **383**, 177 (1996).
37. F. Nilsson, O. Söderman and I. Johansson, *Langmuir* **12**, 902 (1996).
38. P. Thiagarajan, D. M. Tiede, *J. Phys. Chem.* **98**, 10343 (1994).
39. R. M. M. Brito and W. L. C. Vaz, *Anal. Biochem.* **152**, 250 (1986).
40. O. Pastor, E. Junquera and E. Aicart, *Langmuir* **14**, 2950 (1998).
41. S. Saito and T. Tsuchiya, *Chem. Pharm. Bull.* **33**, 503 (1985).
42. R. R. Hantgan, J. V. Braaten and M. Rocco, *Biochemistry* **32**, 3935 (1993).
43. J. A. M. Bolívar, J. Aguiar, J. M. P. García and C. C. Ruiz, *J. Phys. Chem. B* **108**, 12813 (2004).
44. K. Kameyama and T. Takagi, *J. Colloid Interface Sci.* **137**, 1 (1990).
45. B. Hoffmann and G. Platz, *Curr. Opin. Colloid Interface Sci.* **6**, 171 (2001).
46. A. Möller, P. Lang, G. H. Findenegg and U. Keiderling, *J. Phys. Chem. B* **102**, 8958 (1998).
47. C. C. Ruiz, J. A. M. Bolívar, J. M. Hierrezuelo and E. Liger, *Int. J. Mol. Sci.* **14**, 3228 (2013).
48. K. Shinoda, T. Yamaguchi and R. Hori, *Bull. Chem. Soc. Jpn.* **34**, 237 (1961).
49. J. A. M. Bolívar, J. M. Hierrezuelo and C. C. Ruiz, *J. Phys. Chem. B* **110**, 12089 (2006).

50. M. Aoudia and R. Zana, *J. Colloid Interface Sci.* **206**, 158 (1998).
51. P. Konidala, L. He and B. Niemeyer, *J. Mol. Graph. Model.* **25**, 77 (2006).
52. B. Guchhait, R. Biswas and P. K. Ghorai, *J. Phys. Chem. B* **117**, 3345 (2013).
53. P. F. Barbara and W. Jarzeba, *Adv. Photochem.* **15**, 1 (1990).
54. H. Shirota and K. Horie, *J. Phys. Chem. B* **103**, 1437 (1999).
55. N. E. Levinger, *Curr. Opin. Colloid Interface Sci.* **5**, 118 (2000).
56. Š. Vajda, R. Jimenez, S. J. Rosenthal, V. Fidler, G. R. Fleming and E. W. Castner, Jr., *J. Chem. Soc. Faraday Trans.* **91**, 867 (1995).
57. T. Pradhan, P. Ghoshal and R. Biswas, *J. Chem. Sci.* **120**, 275 (2008).
58. T. Pradhan, H. A. R. Gazi, B. Guchhait and R. Biswas, *J. Chem. Sci.* **124**, 355 (2012).
59. M. L. Horng, J. A. Gardecki and M. Maroncelli, *J. Phys. Chem. A* **101**, 1030 (1997).
60. B. D. Wagner, *Molecules* **14**, 210 (2009).
61. R. Baumann, C. Ferrante, E. Kneuper, F. W. Deeg and C. Bräuchle, *J. Phys. Chem. A* **107**, 2422 (2003).
62. M. Maroncelli and G. R. Fleming, *J. Chem. Phys.* **86**, 6221 (1987).
63. L. Reynolds, J. A. Gardecki, S. J. V. Frankland, M. L. Horng and M. Maroncelli, *J. Phys. Chem.* **100**, 10337 (1996).
64. R. Karmakar and A. Samanta, *J. Phys. Chem. A* **106**, 4447 (2002).
65. C. C. Ruiz, *Photochem. Photobiol. Sci.* **11**, 1331 (2012).
66. M. Kumbhakar, *J. Phys. Chem. B* **111**, 12154 (2007).
67. M. Kumbhakar, T. Mukerjee and H. Pal, *Photochem. Photobiol.* **81**, 588 (2005).
68. C. Cametti, S. Marchetti, C. M. C. Gambi and G. Onori, *J. Phys. Chem. B* **115**, 7144 (2011).
69. R. Buchner, C. Baar, P. Fernandez, S. Schrfdle and W. Kunz, *J. Mol. Liq.* **118**, 179 (2005).
70. C. Baar, R. Buchner and W. Kunz, *J. Phys. Chem. B* **105**, 2906 (2001).
71. C. Baar, R. Buchner and W. Kunz, *J. Phys. Chem. B* **105**, 2914 (2001).
72. R. Biswas, N. Rohman, T. Pradhan and R. Buchner, *J. Phys. Chem. B* **112**, 9379 (2008).
73. Y. Feldman, *Dielectric Relaxation in Biological Systems: Physical Principles, Methods and Applications*, Oxford University Press, USA, 2015.
74. H. A. R. Gazi, H. K. Kashyap and R. Biswas, *J. Chem. Sci.* **127**, 61 (2015).
75. A. Das and R. Biswas, *J. Phys. Chem. B* **119**, 10102 (2015).

76. R. K. Mitra, S. S. Sinha and S. K. Pal, *Langmuir* **24**, 49 (2008).
77. K. Mukherjee, A. Barman and R. Biswas, *J. Mol. Liq.* **222**, 495 (2016).
78. T. Pradhan and R. Biswas, *J. Phys. Chem. A* **111**, 11514 (2007).
79. H. A. R. Gazi, B. Guchhait, S. Daschakraborty and R. Biswas, *Chem. Phys. Lett.* **501**, 358 (2011).
80. B. Guchhait and R. Biswas, *J. Chem. Phys.* **138**, 114909 (2013).
81. R. Biswas, A. R. Das, T. Pradhan, D. Touraud, W. Kunz and S. Mahiuddin, *J. Phys. Chem. B* **112**, 6620 (2008).
82. N. Sarma, J. M. Borah, H. A. R. Gazi, B. Guchhait, S. Mahiuddin and R. Biswas, *J. Phys. Chem. B* **115**, 9040 (2011).
83. M. L. Horng, J. A. Gardecki, A. Papazyán and M. Maroncelli, *J. Phys. Chem.* **99**, 17311 (1995).
84. R. Buchner, *Pure Appl. Chem.* **80**, 1239 (2008).
85. U. Kaatzé and K. Giese, *J. Phys. E* **13**, 133 (1980).
86. C.J.F. Böttcher and P. Bordewijk, *Theory of Electric Polarization*, Elsevier, Amsterdam, The Netherlands, 1978.
87. K. Mukherjee, A. Das, S. Choudhury, A. Barman and R. Biswas, *J. Phys. Chem. B* **119**, 8063 (2015).
88. R. Buchner and J. Barthel, *Annu. Rep. Prog. Chem., Sect. C: Phys. Chem.* **91**, 71 (1994).
89. Sonu, S. Kumari and S. K. Saha, *J. Phys. Chem. B* **119**, 9751 (2015).
90. H. Shirota, Y. Tamoto and H. Segawa, *J. Phys. Chem. A* **108**, 3244 (2004).
91. E. Tarif, B. Saha, K. Mukherjee, P. De and R. Biswas, *J. Phys. Chem. B* **123**, 5892 (2019).
92. M. J. Frisch, et al, *Gaussian 03*, revision C.02; Gaussian, Inc.: Pittsburgh, PA, 2003
93. S. S. C. Ammal, N.P. Ananthavel, J. Chandrasekhar, P. Venuvanalingam and M.S. Hegde, *Chemical Physics Letters* **248**, 153 (1996).
94. K. Bhattacharyya, *Chem. Commun.*, **0**, 2848 (2008).
95. S. K. Pal, J. Peon and A. H. Zewail, *Proc Natl Acad Sci U S A.* **99**, 1763 (2002).
96. B. Bagchi, *Water in Biological and Chemical Processes: From Structure and Dynamics to Function*, Cambridge University Press, Cambridge, 2013.
97. N. Nandi and B. Bagchi, *J. Phys. Chem. B* **101**, 10954 (1997).
98. K. Hara, H. Kuwabara and O. Kajimoto, *J. Phys. Chem. A* **105**, 7174 (2001).

99. M. Kumbhakar, T. Goel, T. Mukherjee and H. Pal, *J. Phys. Chem. B* **109**, 14168 (2005).
100. M. Kumbhakar, T. Goel, T. Mukherjee and H. Pal, *J. Phys. Chem. B* **108**, 19246 (2004).
101. S. Sen, D. Sukul, P. Dutta and K. Bhattacharyya, *J. Phys. Chem. B* **106**, 3763 (2002).
102. S. K. Pal, J. Peon, B. Bagchi and A. H. Zewail, *J. Phys. Chem. B* **106**, 12376 (2002).
103. S. Balasubramanian and B. Bagchi. *J. Phys. Chem. B* **105**, 12529 (2001).
104. S. Mashimo, S. Kuwabara, S. Yagihara and K. Higasi, *J. Phys. Chem.* **91**, 6337 (1987).
105. R. Buchner, G. T. Hefter and P. M. May, *J. Phys. Chem. A* **103**, 1 (1999).
106. K.J.Tielrooij, D.Paparo, L.Piatkowski, H.J.Bakker and M. Bonn, *Biophys. J.* **97**, 2484 (2009).
107. P. Fernandez, S. Schrodle, R. Buchner and W. Kunz, *ChemPhysChem* **4** 1065 (2003).
108. Y. H. Zhao, M. H. Abraham and A. M. Zissimos, *J. Org. Chem.* **68**, 7368 (2003).

Chapter 8

Concluding Remarks and Future Problems

We do not dedicate a full chapter for drawing conclusions of the research study reported in this Thesis because each of the chapters includes individual conclusion section. Here we just briefly remind the general finding, and then enlist some exciting problems that may be studied in the near future.

As a general and over-all conclusion, we may state that the prepared highly viscous NADESs show mild spatial heterogeneity but strong fractional viscosity dependence. This strong viscosity dependence is appearing in a temperature range much away from the measured glass transition temperature and has been considered as a signature of pronounced temporal heterogeneity. DRS and TRF measurements show that water-xylitol mixtures are mildly heterogeneous. Structure, dynamics and interaction in bio-mimetic micelles made of diblock copolymers have been explored. Clear impact of the connector atom of surfactants head and tail part is observed on both size of the micelle as well as in the dynamics at their interfaces. Again, these systems were found to be mildly heterogeneous. In a way, one can say that the unifying thread that runs through the chapters in this Thesis is medium heterogeneity.

Now let us enlist a few problems that could be studied in the near future, and briefly discuss.

8.1 Temperature Dependent Dielectric Relaxation (DR) Study of Naturally Abundant Deep Eutectic Solvents (NADESs)

Polarity of the solvent is an essential property for any reaction occurring in that solvent and is provided by the magnitude of the static dielectric constant.¹⁻³ Dielectric relaxation (DR) measurements provide information regarding reorientational relaxation and cooperative dynamics of dipolar species. Therefore it is very exciting to perform DR measurements for solvents to reveal their inherent dynamics and polarity. These informations are critical for solvent selection as reaction media. In chapter 3 and 4 time-resolved fluorescence (TRF) measurements explored solute-centre dynamics of NADESs using external dipolar probes and that showed fractional viscosity dependence of solute rotation. Dynamic fluorescence anisotropy measurements probe the medium friction on a dissolved dipolar solute while DR probes the

medium friction on its own constituent dipolar species. Therefore, temperature dependent DR measurements for these NADESs would be very informative.

8.2 Heterogeneity Aspects in Non-Ionic DESs: Temperature Dependent Time-Resolved Fluorescence and Dielectric Relaxation Measurements

Deep eutectic solvents prepared from the natural components such as carbohydrates, polyhydroxyl alcohols have great impact due to their less toxic and eco-friendly nature. Meta-stable multi-component molten mixtures (i.e. DESs) show fractional viscosity dependence of transport motion in the systems which is usually observed in glass forming liquids near glass transition temperature. Many ionic DESs show this sort of fractional viscosity dependence.⁴⁻⁶ However, TRF measurements of non-ionic (acetamide+urea) DES did not show any temporal heterogeneity signature.⁷ Interestingly, non-ionic (acetamide +urea +polyethylene glycol (PEG)) DES is mildly heterogeneous. Therefore, heterogeneity in the medium is not exclusively associated with ionic DESs and that can be further supported by the result we found in chapter 3 and 4. Several attempts have been made to explore dynamics and interaction of ionic deep eutectic solvents while very few could be found for the non ionic deep eutectic solvents. Investigation of dynamics and interaction of (sorbitol+urea+water) and (sorbitol+urea+PEG) DESs through DR and TRF measurements could be exciting and useful.

8.3 Interaction and Dynamics of Amino Acid Based Deep Eutectic Solvents: Temperature Dependent TRF and DRS Measurements

High vapor pressure, toxicity, many health and environmental issues are associated with conventional organic solvents.⁸⁻¹¹ Therefore, DESs made of protein and amino acids would be an efficient green alternative to the conventional solvents. Moreover, it is believed that NADESs can support in organisms' biological processes through dissolution of metabolites which are sparingly soluble in water and lipids.^{12,13} Therefore, interspecies interaction among the constituents of DESs, would be helpful for the smart applications of these DESs in the biomedical field. In this scenario, investigation of dynamics and interaction of [proline+tartaric acid], [arginine+malic acid], [proline+glucose] DESs using both TRF and DRS would be useful and informative.

8.4 Impact of the Spacer (-CH₂-) on the Dynamics and Physical Properties of Amino Acid Based DESs

Amino acid based DESs would be preferable as green solvents. Dynamics and physical properties of the DESs depend on the constituents and their compositions.^{4,5,14,15} Here in this work we would like to explore the impact of the spacer (-CH₂-) of carboxylic acid (oxalic acid, malonic acid and glutaric acid) on the interaction and dynamics of (proline+carboxylic acid) DESs via temperature dependent TRF and DRS measurements.¹⁶

8.5 High Viscous NADES Based on Glucose, Tartaric Acid and Water

As a demand for eco-friendly alternatives to the conventional organic solvents increases day by day, it is necessary to explore every possible way for the preparation of DESs, especially NADESs. This is because of their less negative impact on the living beings and environment. Here we want to prepare DES based on glucose, tartaric acid and water and explore the medium dynamics and interaction.

8.6 Acid-Induced Fluorescence of Polyethylenimine (PEI) Aggregates: A Spectroscopic Study

Polyethylenimine (PEI) is a polymer with repeating unit composed of the amine group and two carbon aliphatic-CH₂CH₂-spacer.¹⁷ There are three types of PEI molecules –i) Linear PEI (mostly secondary amines) ii) Branched PEI (Primary, Secondary and Tertiary amines) and iii) Dendrimeric PEI (Mostly Primary and Tertiary amines). Polyethylenimines are used in cell culture of weakly anchoring cells to increase attachment.¹⁸ Photoluminescence arises in amino-containing polymers in presence of CO₂.¹⁹ Here we want to study the luminescence behaviour of PEI-water solutions and also the impact (trace amount) of acid (formic acid, acetic acid, isobutyric acid) on that. If those aqueous solutions show intrinsic fluorescence then we will try to find out the probable species with the help of NMR and IR (and others, if needed) spectroscopy. Apart from the basic scientific view it would be very helpful for acid reorganization inside the biologically important moiety as PEI can be used in in-vivo processes.²⁰

References:

1. B. Bagchi, *Molecular Relaxation in Liquids*. (Oxford University Press, New York, 2012).
2. C. Reichardt and T. Welton, *Solvents and Solvent Effects in Organic Chemistry*. (John Wiley & Sons, 2011).
3. E. M. Kosower, *J. Am. Chem. Soc.* **80**, 3253 (1958).
4. B. Guchhait, S. Das, S. Daschakraborty and R. Biswas, *J. Chem. Phys.* **140**, 104514 (2014).
5. A. Das, S. Das and R. Biswas, *Chem. Phys. Lett.* **581**, 47 (2013).
6. B. Guchhait, H. A. R. Gazi, H. K. Kashyap and R. Biswas, *J. Phys. Chem. B* **114**, 5066 (2010).
7. A. Das, S. Das, R. Biswas *J. Chem. Phys.* **142**, 034505 (2015).
8. M. Ikeda, *Toxicol. Lett.* **64**, 191 (1992).
9. M. Aksoy, *Environ. Health Perspect.* **82**, 193 (1989).
10. B. W. Lee, K. T. Kelsey, D. M. Hashimoto, B. Yakes and T. Seitz, *J. Occup. Environ. Med.* **39**, 960 (1997).
11. D. Majumdar, C. Dutta and S. Sen, *Transport. Res. D-TR E.*, **13**, 524 (2008).
12. Y. Dai, J. van Spronsen, G.-J. Witkamp, R. Verpoorte and Y. H. Choi, *Anal. Chim. Acta* **766**, 61 (2013).
13. Y. H. Choi, J. van Spronsen, Y. Dai, M. Verberne, F. Hollmann, Isabel W.C.E. Arends, G. J. Witkamp, and R. Verpoorte, *Plant Physiol.* **156**, 1701 (2011).
14. M. Francisco, A. van den Bruinhorst, and M.C. Kroon, *Green Chem.* **14**, 2153 (2012).
15. S. Rajkhowa, A. Das, S. Mahiuddin, and R. Biswas, *J. Chem. Eng. Data* **57**, 3467 (2012).
16. L. Hao, M. Wang, W. Shan, C. Deng, W. Ren, Z. Shi, H. Lu,
doi.org/10.1016/j.jhazmat.2017.06.050
17. O. Yemul and T. Imae, *Colloid Polym Sci.* **286**, 747 (2008).
18. Y. Sun, W. Cao, S. Li, S. Jin, K. Hu, L. Hu, Y. Huang, X. Gao, Y. Wu and X. J. Liang, *Sci. Rep.* **3**, 3036 (2013).
19. X. Pan, G. Wang, C. L. Lay, B. H. Tan, C. He and Y. Liu, *Sci. Rep.* **3**, 2763 (2013).
20. G. Peluso, O. Petillo, L. Ambrosio, L. Nicolais *J Mater Sci: Mater Med* **5**, 738 (1994).

Appendix A.a

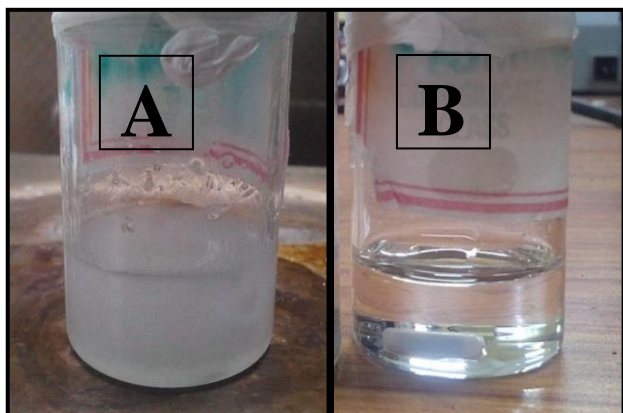


Fig. A.a.1: **A** and **B** are the two [Glu+Ure+Wat (6:4:1; weight ratio)] mixtures. ‘**A**’ was prepared by heating the mixture at 303 K. ‘**B**’ was prepared by mixing all the constituents and heating at ~345 K , and then allowed hot liquid solution to gradually cool down to room temperature (as describe in section 3.2.1). Notice mixture **A** is opaque and semi-solid at room temperature, whereas the DES **B** appears as a transparent solution.

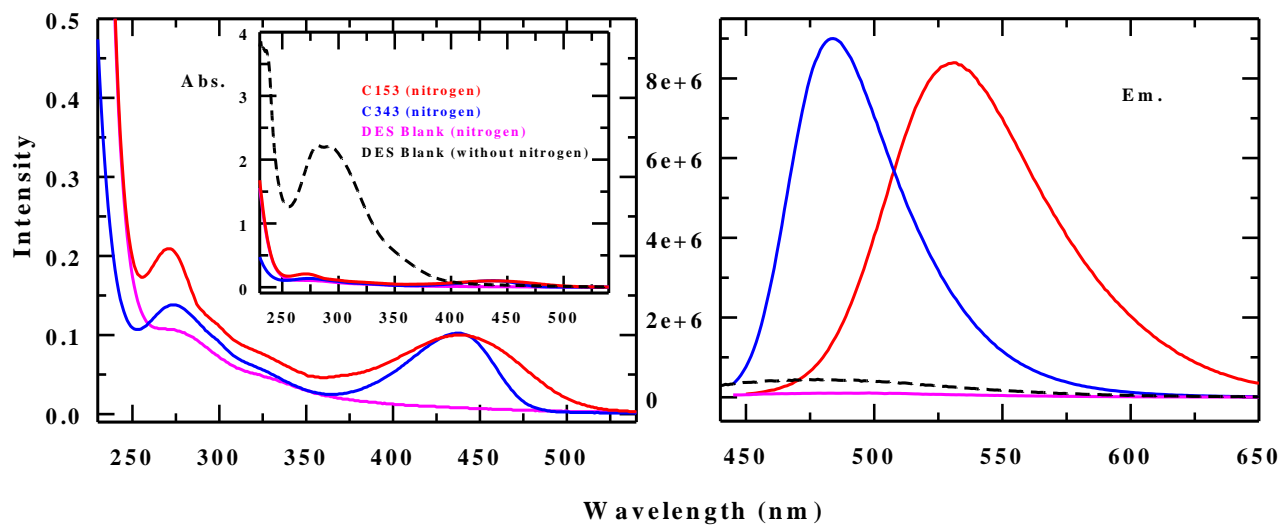


Fig. A.a.2: Absorption (left panel) and emission (right panel) spectral features of C153 and C343 in [Glu+Ure+Wat] DES. Intrinsic absorption (left panel) and emission (right panel) of DES prepared in the presence and in the absence of nitrogen atmosphere are shown in solid pink and black dashed-lines, respectively. Inset of absorption spectrum (left panel) clearly depicts the importance of nitrogen atmosphere in the preparation of DES.

Table A.a.3: Temperature dependence of density, viscosity coefficient, and refractive index of [Glu+Ure+Wat] DES.

T (K)	Viscosity ^b (cP)	Refractive ^a index	Density ^a (g/cm ³)
308		1.51105	1.37693
313		1.51085	1.37374
318	570	1.51044	1.37052
323	376	1.51006	1.36725
328	255	1.50979	1.36393
333	179	1.50950	1.36058
338	129	1.50905	1.35729
343	96	1.50896	1.35396

a) Uncertainty $\pm 5\%$; b) $\pm 10\%$

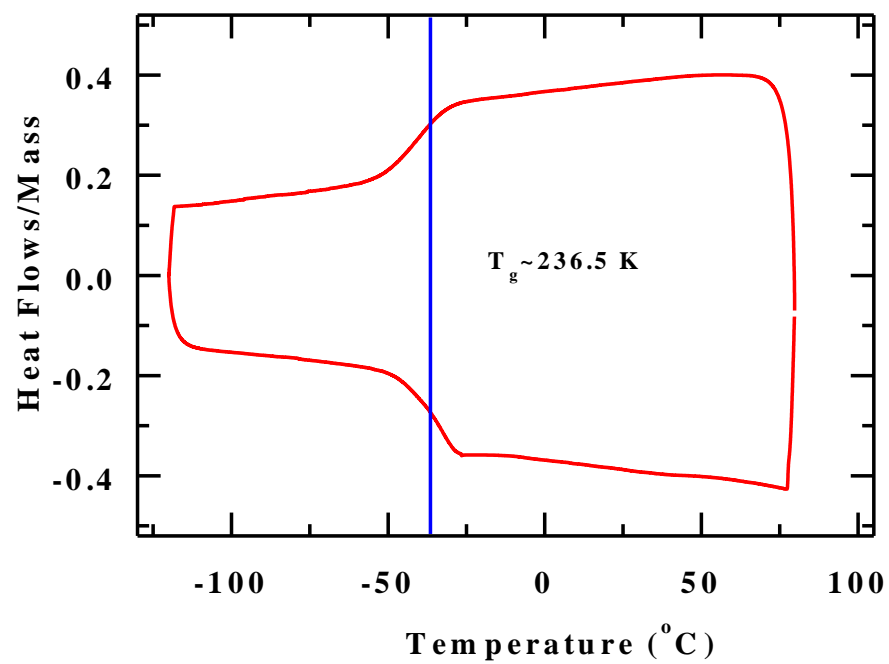


Fig. A.a.4: Differential scanning calorimetric (DSC) trace for [Glu+Ure+Wat] DES. The glass transition temperature (T_g) is indicated.

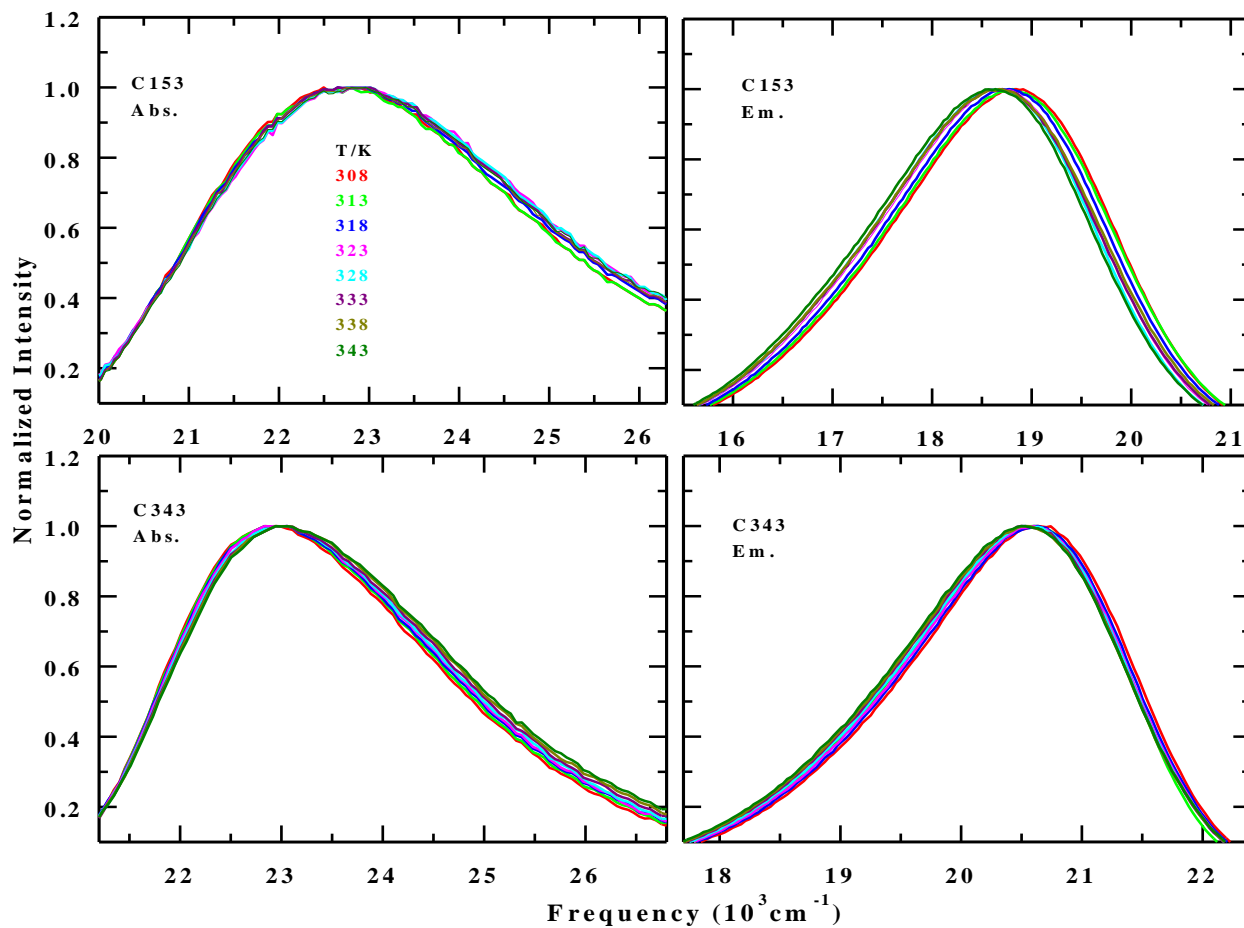


Fig. A.a.5: Temperature dependent ($308 \leq T/K \leq 343$) absorption (left panels) and emission (right panels) spectra of C153 (upper panels) and C343 (lower panels) in [Glu+Ure+Wat] DES. Spectra at different temperatures are colour-coded.

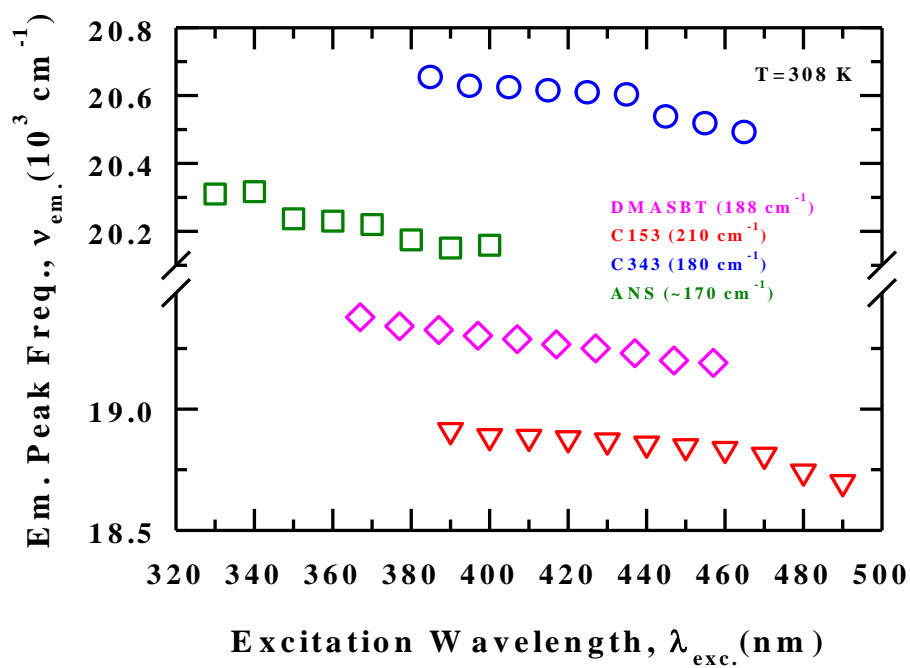


Fig. A.a.6: Excitation wavelength ($\lambda_{exc.}$) dependence of fluorescence emission peak frequencies ($\nu_{em.}$) for C153, C343, DMASBT and ANS in [Glu+Ure+Wat] DES at 308 K.

Table A.a.7: Temperature dependent average fluorescence lifetimes of C153 and C343 in [Glu+Ure+Wat] DES.

T (K)	$\langle \tau_{if}^{C153} \rangle^a$ (ns)	$\langle \tau_{if}^{C343} \rangle^b$ (ns)
308	2.75	3.43
313	2.58	3.41
318	2.43	3.40
323	2.31	3.33
328	2.23	3.45
333	2.15	3.46
338	2.03	3.48
343	1.98	3.47

^{a,b} Uncertainty $\pm 10\%$

Table A.a.8: Average fluorescence lifetimes of C153 and C343 in several common (representative) solvents at 298 K.

Solvent	$\langle \tau_{lif}^{C153} \rangle^c$ (ns)	$\langle \tau_{lif}^{C343} \rangle^d$ (ns)
Acetonitrile	5.74	3.68
Methanol	4.08	3.85
Ethanol	4.72	3.67
Propanol	4.97	3.69
Ethylene glycol	3.43	3.91

^{c,d} Uncertainty $\pm 10\%$

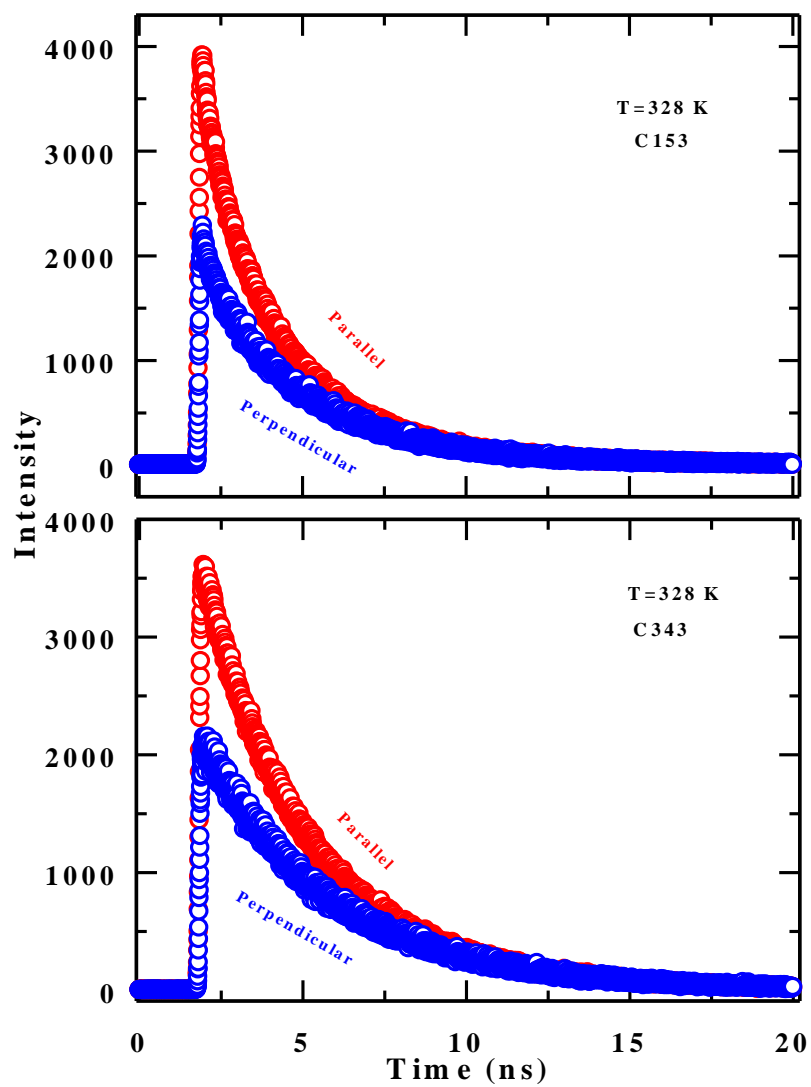


Fig. A.a.9: Representative fluorescence intensity decays of C153 (upper panel) and C343 (lower panel) in [Glu+Ure+Wat] DES at 328 K, collected with different emission polarizations.

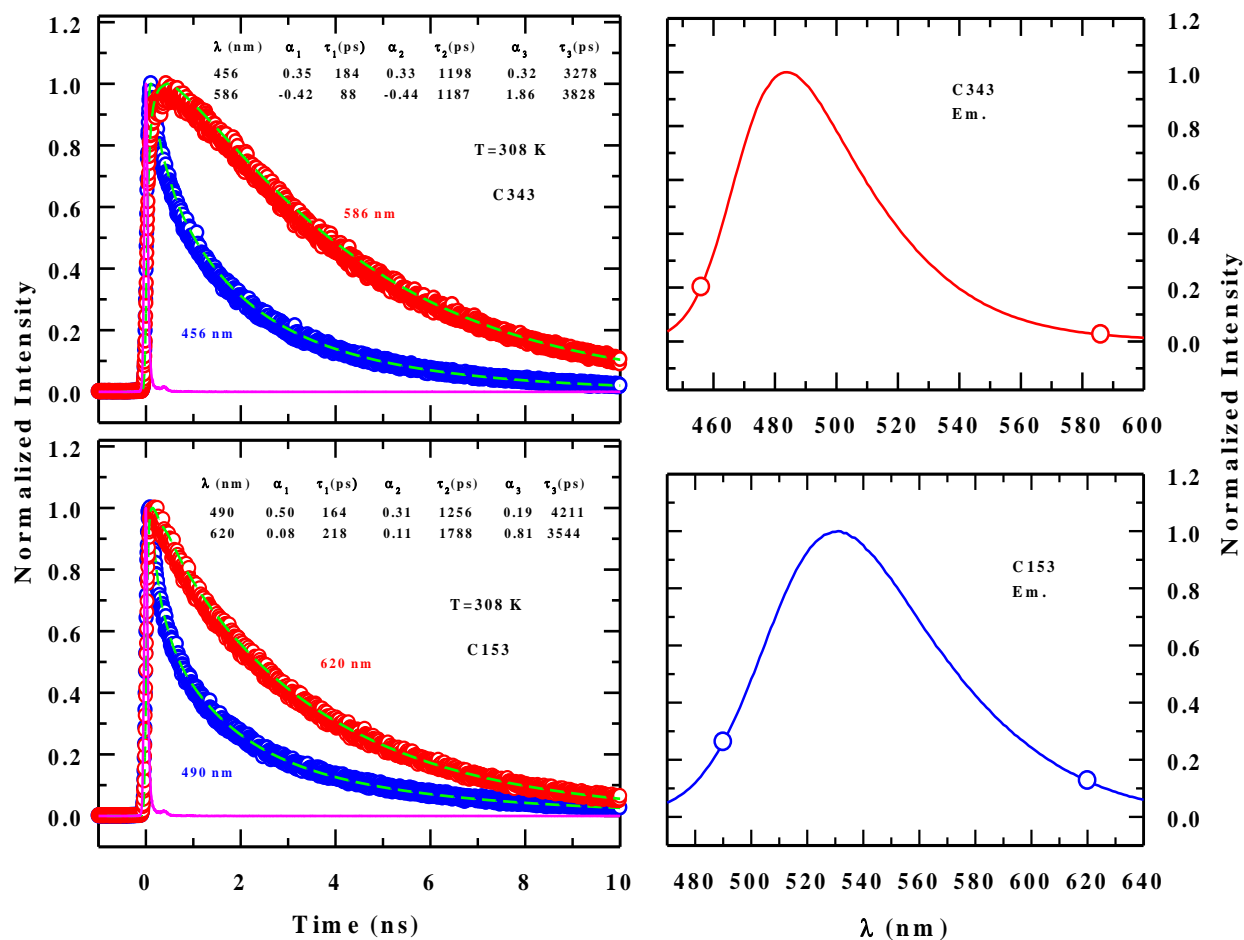


Fig. A.a.10: Representative intensity decay profiles of C153 (upper left panel) and C343 (lower left panel) dissolved in [Glu+Ure+Wat] DES collected at the red and the blue end (wavelength) of the steady state emission spectra (right panels). Pink lines depict the IRF. Circles on the steady state spectra (right panels) represent emission wavelengths at which intensity decays were collected (shown in left panels). Dashed lines (green) through the data represent tri-exponential fits. Fit parameters are given in the inset. All representations are colour-coded.

Table A.a.11: Hydrodynamic molecular rotation times for water, urea and glucose at 308 K calculated using the SED relation with stick boundary condition, $\tau_r = 3\eta V / k_B T$. van der Waals volume of water, urea and glucose used here are calculated from the Ref. 103 indicated below. Note the viscosity at 308 K for ([Glu+Ure+Wat]) DES was obtained from the extrapolation of the high temperature data.

η (cP) (T=308 K)	Water ($V = 17\text{\AA}^3$) τ_r (ns)	Urea ($V = 54\text{\AA}^3$) τ_r (ns)	Glucose ($V = 162\text{\AA}^3$) τ_r (ns)
676	8.11	25.76	77.29

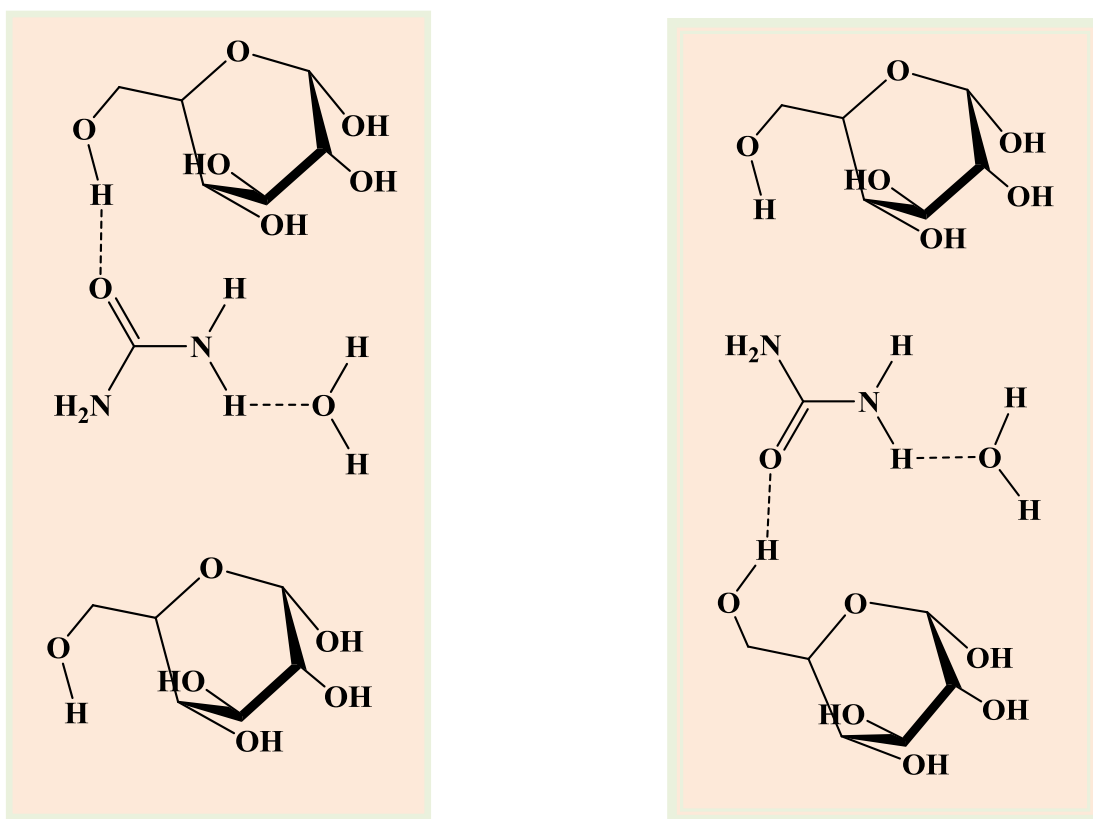


Fig. A.a.12: H-bond dynamics involving the hydrogen atom of the glucose hydroxyl group (-OH as donor site), sp^2 - hybridized oxygen atom of the carbonyl group (-C=O as acceptor) of urea, and the amide hydrogens of the same urea molecule to water oxygens. The restricted rotations of these multiple H-bonded species with simultaneous H-bond breakage may produce timescales in the nanoseconds.

Appendix A.b



Fig. A.b.1: **A** and **B** are the two [Bet+Ure+Wat (11.7:12:1; weight ratio)] mixtures. ‘**A**’ was prepared by mixing all the constituents and heating at ~ 344 K as described in section 4.2.1 (Sample Preparation). ‘**B**’ was prepared by heating the mixture at 298 K for solution preparation and solubility checking. Both the systems were kept at room temperature (~ 298 K). Mixture, **B**, was opaque and semi-solid whereas **A** formed a transparent colourless liquid, DES.

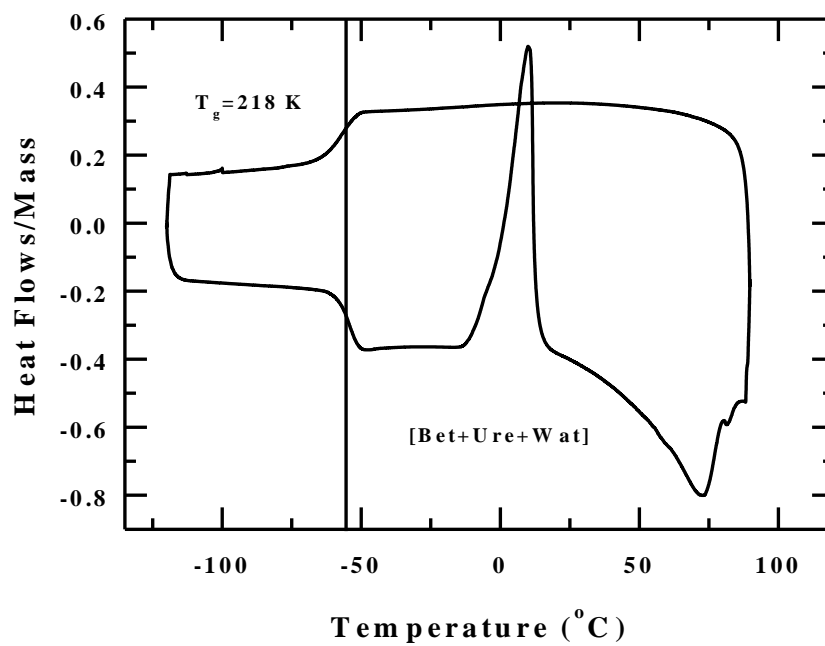


Fig. A.b.2: Differential scanning calorimetric (DSC) trace for [Bet+Ure+Wat] DES. The glass transition temperature (T_g) is indicated

Table A.b.3: Temperature dependence of density, viscosity coefficient, and refractive index of [Bet+Ure+Wat] DES.

T (K)	Viscosity ^a (cP)	Refractive ^b index	Density ^b (g/cm ³)
303		1.49656	1.219047
308	431	1.49672	1.216162
313	281	1.49689	1.213264
318	192	1.49691	1.210346
323	136	1.49696	1.207398
328	99	1.49702	1.204443
333	74	1.49721	1.201593
338	56	1.49745	1.198734
343	45	1.49757	1.195861

a) Uncertainty $\pm 10\%$; b) $\pm 5\%$

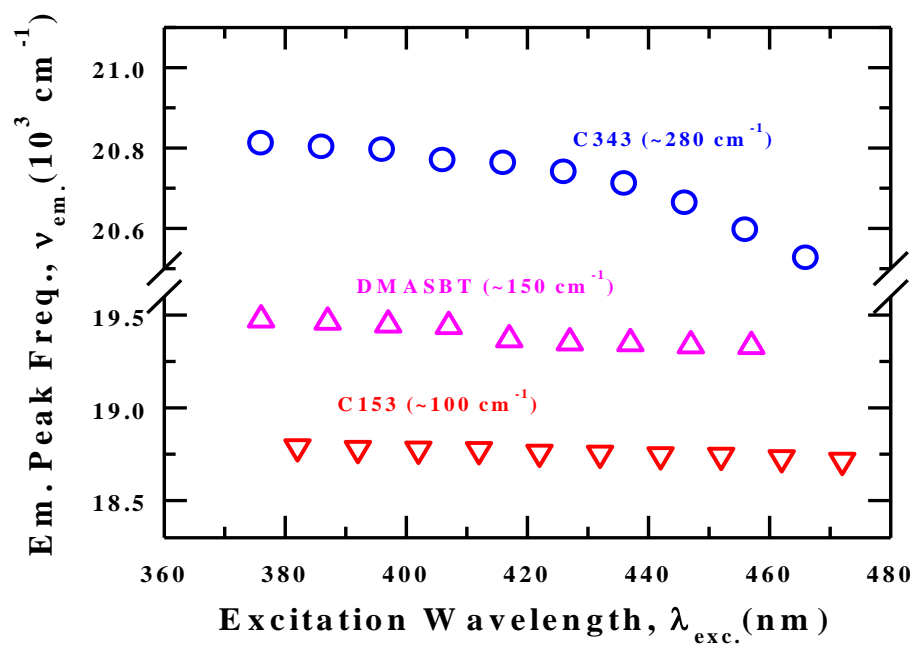


Fig. A.b.4: Excitation wavelength (λ_{exc}) dependence of fluorescence emission peak frequencies (ν_{em}) for C153, C343, DMASBT in [Bet+Ure+Wat] DES at 303 K.

Table A.b.5: Temperature dependent average fluorescence lifetimes of C153 and C343 in [Bet+Ure+Wat] DES.

T (K)	$\langle \tau_{lif}^{C153} \rangle^a$ (ps)	$\langle \tau_{lif}^{C343} \rangle^b$ (ps)
303	3157	3528
308	2906	3595
313	2745	3551
318	2591	3557
323	2549	3549
328	2462	3606
333	2420	3598
338	2346	3537
343	2289	3562

^{a,b}Uncertainty $\pm 10\%$

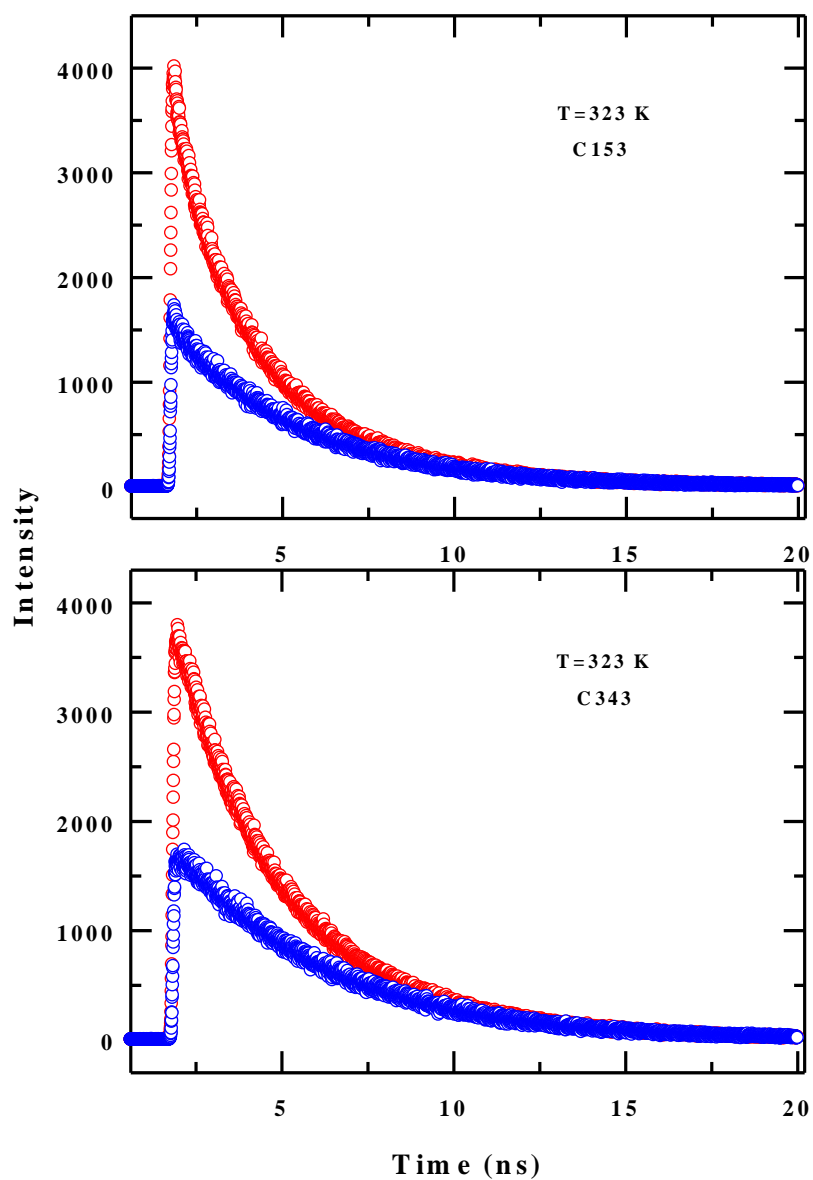


Fig. A.b.6: Representative fluorescence intensity decays of C153 (upper panel) and C343 (lower panel) in [Bet+Ure+Wat] DES at 323 K, collected with different emission polarizations. While the red circles denote intensity decays with parallel polarization, the blue ones with perpendicular polarization.

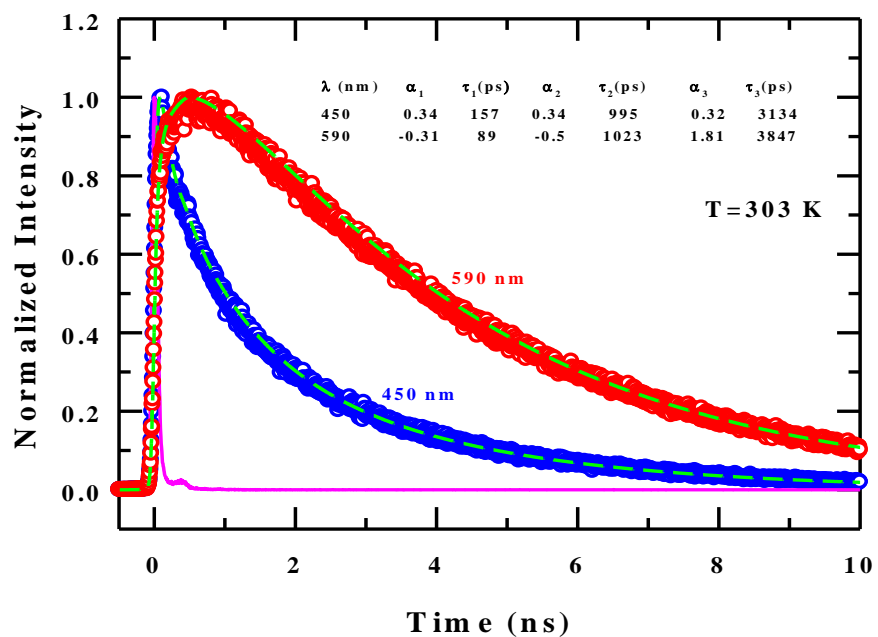


Fig. A.b.7: Representative intensity decay profiles of C343 dissolved in [Bet+Ure+Wat] DES collected at the red and the blue end (wavelength) at 303 K. Pink line represents the instrument response function (IRF).

Appendix A.c

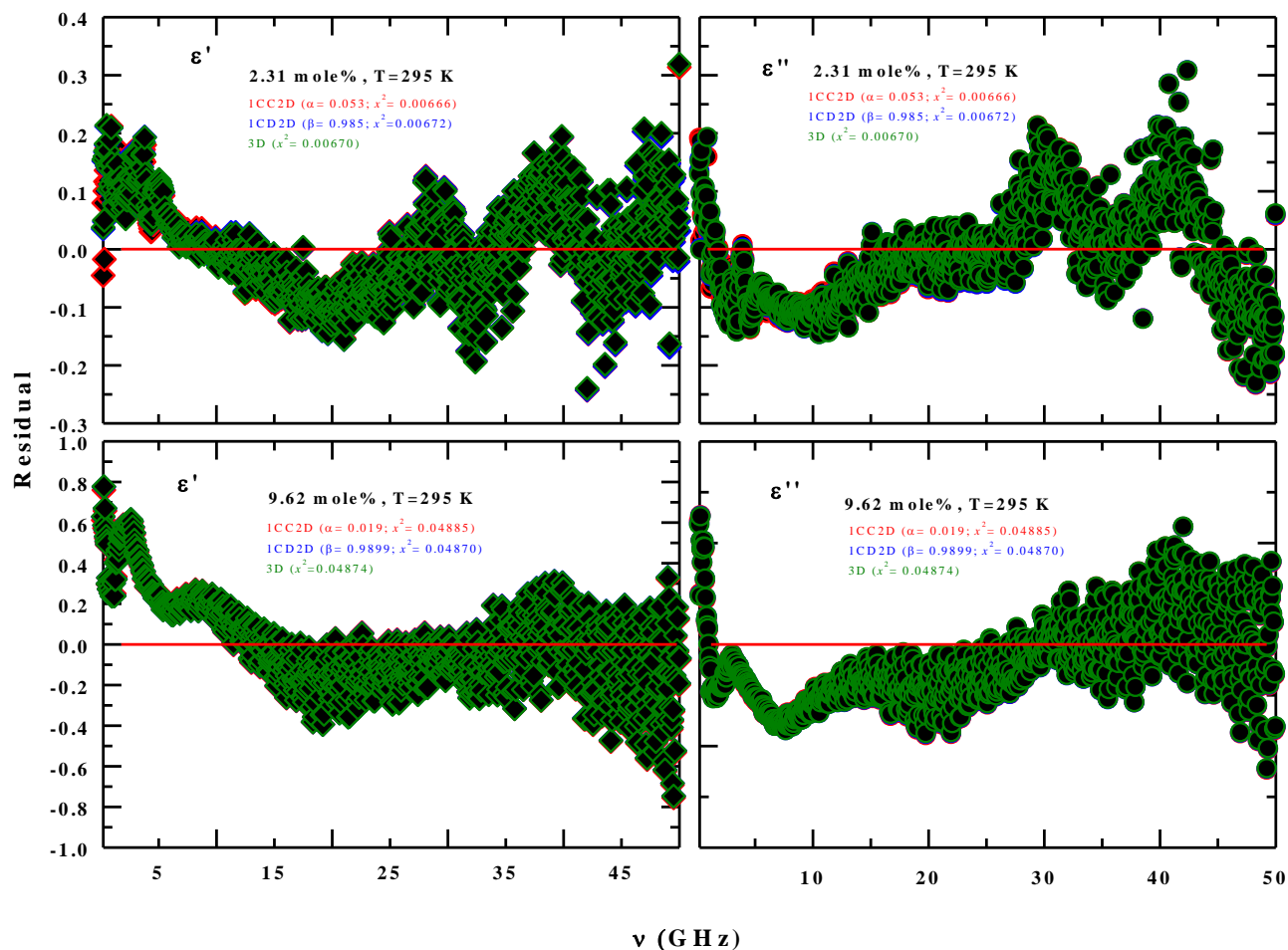


Fig. A.c.1: A representative comparison between the three fit models. Diamonds and circles represent the real ($\epsilon'(\nu)$) and imaginary ($\epsilon''(\nu)$) part of the DR data for the water-xylitol mixtures, respectively. Presentations are color coded.

Table A.c.2: Molecular rotational times from SED relation for water and xylitol molecules in water-xylitol mixtures (using experimental viscosity) at 295 K. From SED using stick boundary condition, $\tau_r = 3\eta V / k_B T$.

Xylitol Mole %	η (cP)	Water ($V = 10.9\text{\AA}^3$) (ps)	Xylitol ($V = 107.3\text{\AA}^3$) (ps)	$\tau_{DR}^{Slowest} = \tau_1$ (ps)	$\langle \tau_{DR}^{i=2} \rangle = \alpha_1 \tau_1 + \alpha_2 \tau_2$ (ps)
2.31	1.58	13	125	48	17
4.52	2.46	20	194	49	22
5.58	3.11	25	246	57	28
7.65	4.67	37	369	68	35
8.65	5.75	46	454	77	43
9.62	7.01	56	554	80	46

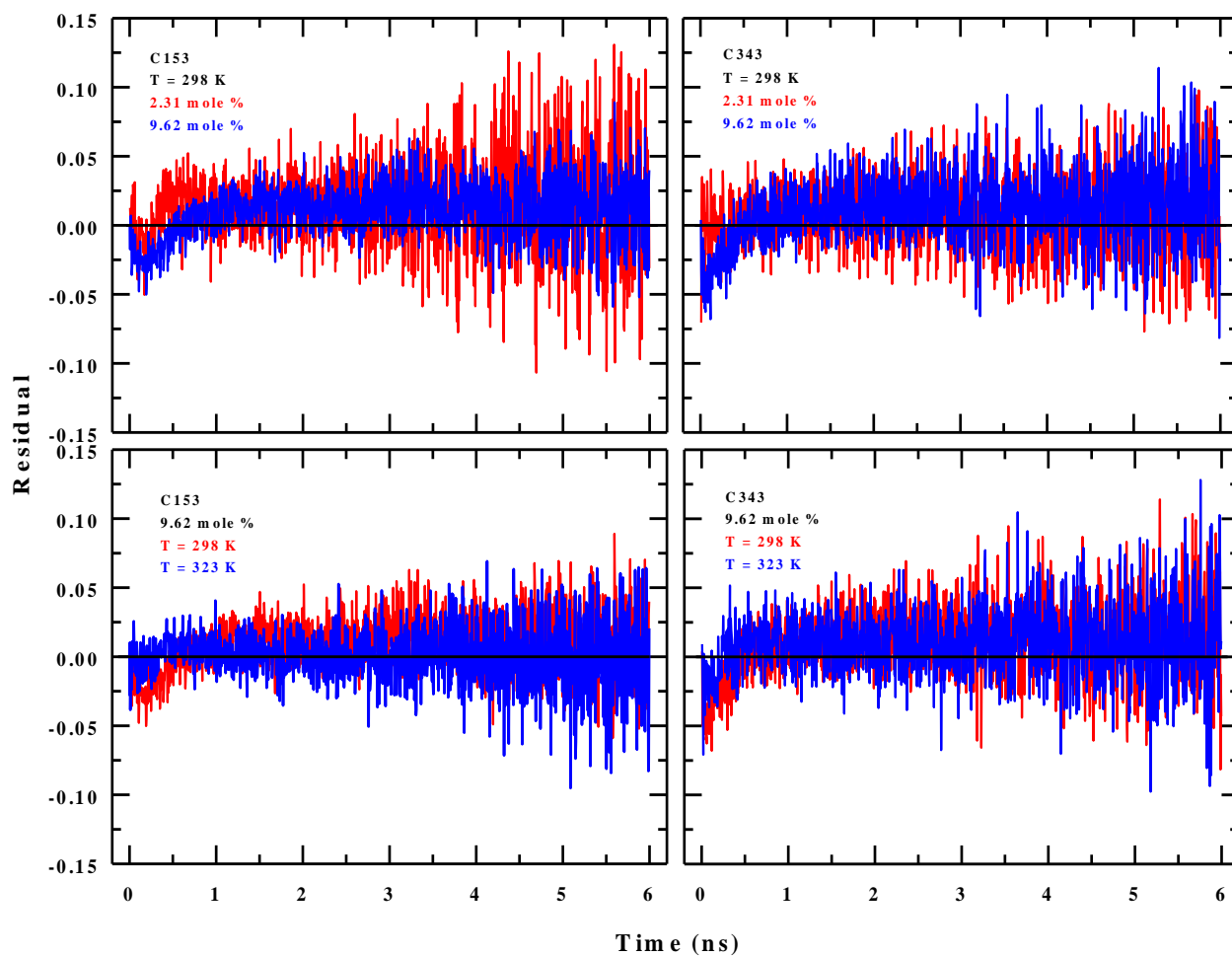


Fig. A.c.3: Residuals of $r(t)$ decays are plotted here to show the validity of fits.

Appendix A.d

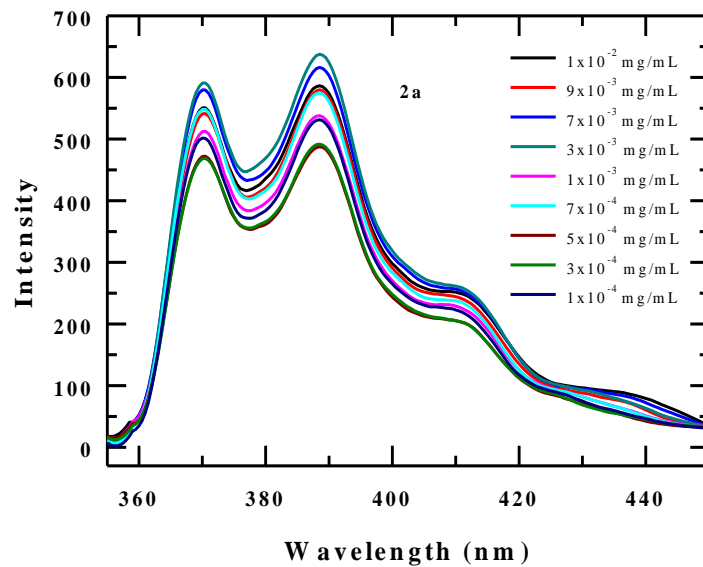


Fig. A.d.1: Variation of fluorescence emission spectra of encapsulated pyrene dye into the polymeric micelles ($\lambda_{\text{exc.}} = 330 \text{ nm}$).

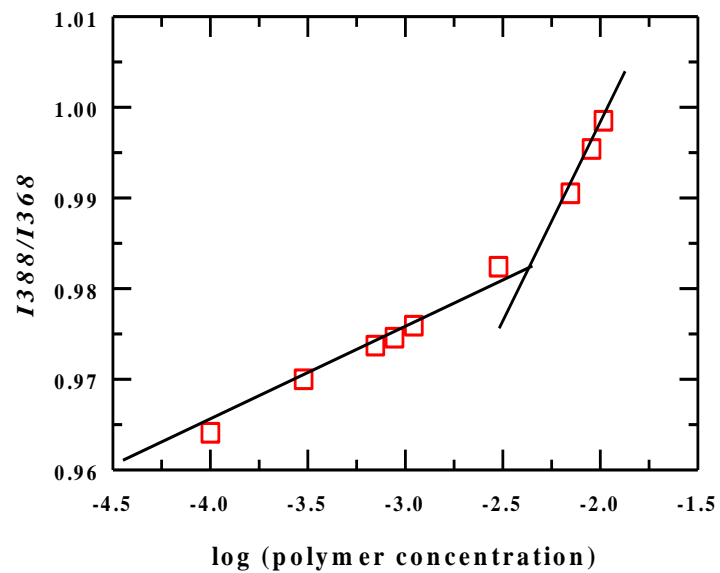


Fig. A.d.2: Determination of CAC of amphiphilic diblock copolymer, P(Boc-L-Ala-HEMA)-*b*-PPEGMA (**2a**).

Table A.d.3: The CAC and size distribution data of the diblock copolymers at varying concentrations in aqueous media.

Polymer	CAC (mg/L)	Hydrodynamic diameter, D_h (nm)		
		1 mg/mL	5 mg/mL	10 mg/mL
2a	4.42	15±0.7	15±0.5	14±2.0
2d	8.06	18±0.5	17±0.7	17±1.0

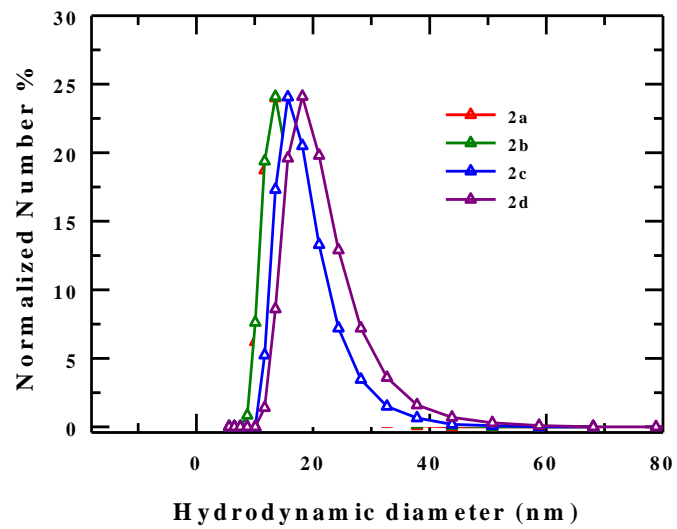


Fig. A.d.4: Particle size distribution of the diblock copolymers, (**2a-2d**) at a concentration of 1 mg/mL in water.

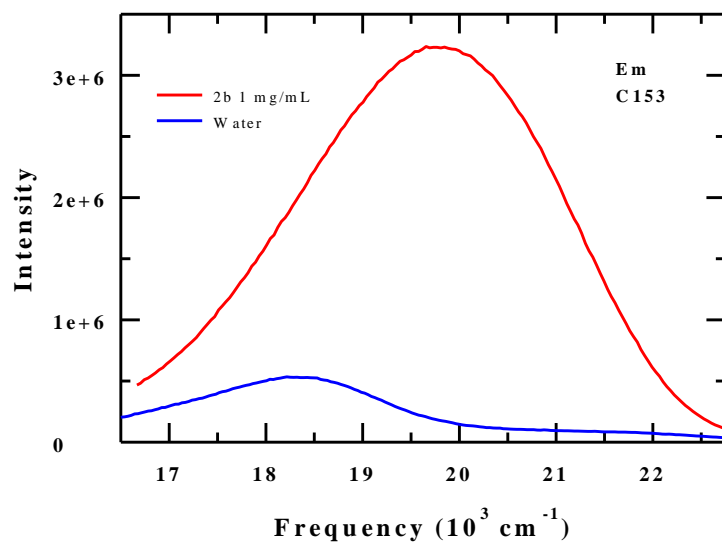


Fig. A.d.5:The steady state emission spectra of C153in pure water and also in micellar media with 1.0 mg/mL polymer concentration (above CMC).

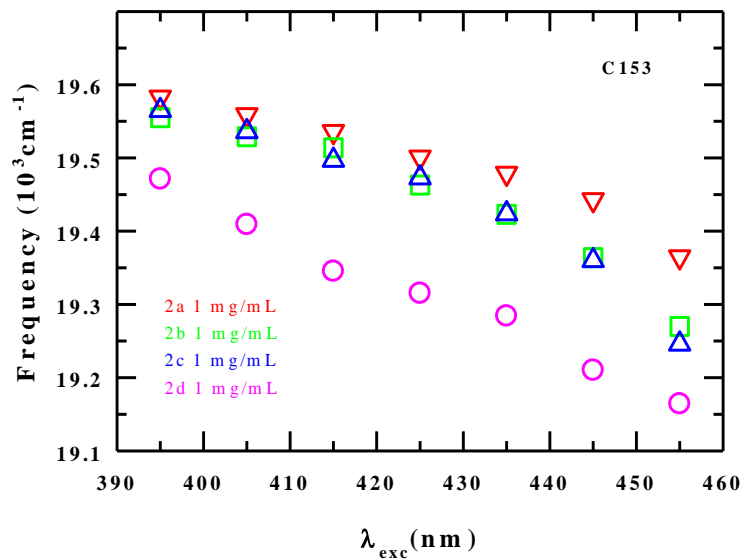


Fig. A.d.6: Excitation wavelength ($\lambda_{exc.}$) dependence of emission spectral peak frequency of C153 in **2a**, **2b**, **2c**, and **2d** solutions at 25 °C. Representations are color-coded.

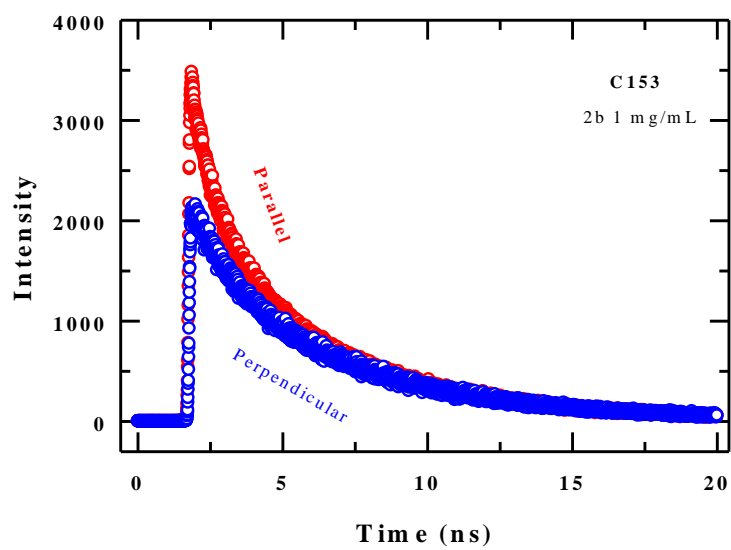


Fig. A.d.7: Representative fluorescence intensity decay profiles for C153 in aqueous polymer solution at different polarizations

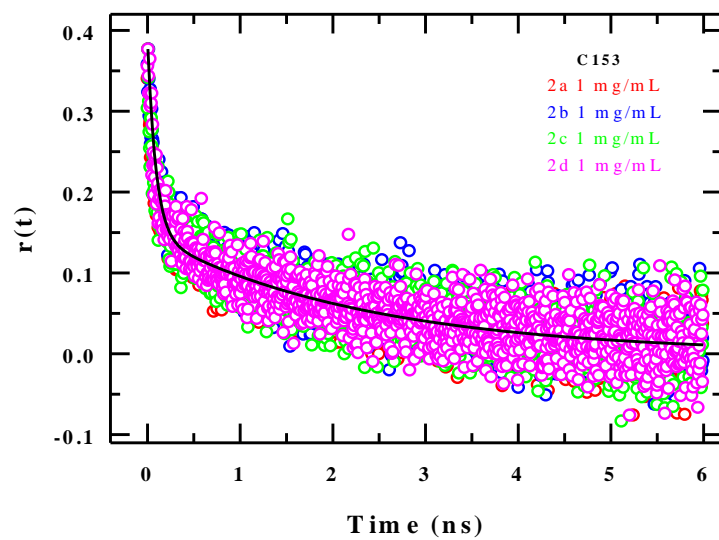


Fig. A.d.8: Rotational anisotropy decays, ($r(t)$), of coumarin 153 in aqueous solutions of different polymers (**2a**, **2b**, **2c**, **2d**).

Table A.d.9: Density, viscosity and refractive index for **2a**, **2b**, **2c**, **2d** polymer solutions as a function of polymer concentration at 25 °C.

Polymer	Concentration (mg/mL)	Refractive Index ^p	Density ^q (g/cm ³)	Viscosity ^r (cP)
2a	0.002	1.26328	0.997053	0.9214
	1	1.26341	0.997223	0.9354
	5	1.26348	0.997429	0.9379
	10	1.26379	0.997770	0.9395
2b	0.002	1.26334	0.997033	0.9254
	1	1.26355	0.997216	0.9435
	5	1.26387	0.997826	0.9455
	10	1.26451	0.998550	0.9773
2c	0.002	1.26339	0.997072	0.9249
	1	1.26343	0.997236	0.9308
	5	1.26388	0.997887	0.9717
	10	1.26464	0.998731	1.0066
2d	0.002	1.26338	0.997077	0.9244
	1	1.26351	0.997250	0.9445
	5	1.26385	0.997867	0.9743
	10	1.26448	0.998660	1.0300

^{p,q}These data can be reproduced within the $\pm 2\%$ uncertainty ; ^rThese data can be reproduced within the $\pm 3\%$ uncertainty (based on 2-3 independent measurements).

Table A.d.10: Bi-exponential fit parameters for the measured anisotropy decay, $r(t)$, and average rotational time $\langle\tau_r\rangle$ for C343 in **2a**, **2b**, **2c**, **2d** at 1 mg/mL concentration and average rotational time $\langle\tau_r\rangle$ for the probe in **2b** and **2d** at 1, 5 and 10 mg/mL concentrations.

Sample	Conc. (mg/mL)	$\alpha_1(\%)$	$\tau_1(ns)$	$\alpha_2(\%)$	$\tau_2(ns)$	$\langle\tau_r(ns)\rangle^a$
2a	1	85	0.072	15	1.77	0.327
2b	1	82	0.073	18	1.71	0.368
	5	56	0.061	44	1.62	0.747
	10	49	0.042	51	1.53	0.800
2c	1	79	0.081	21	1.58	0.396
2d	1	83	0.058	17	1.70	0.337
	5	61	0.051	39	1.57	0.643
	10	58	0.045	42	1.52	0.664

^aUncertainty $\pm 10\%$

Table A.d.11: Average lifetime $\langle \tau_{lif} \rangle$ of C153 in aqueous solutions of **2a**, **2b**, **2c**, **2d** at 1, 5, and 10 mg/mL concentration and 25 °C

Sample	Conc. (mg/mL)	α_1 (%)	τ_1 (ns)	α_2 (%)	τ_2 (ns)	α_3 (%)	τ_3 (ns)	$\langle \tau_{lif} \rangle$ (ns)
2a	1	21	0.11	26	1.68	53	5.47	3.34
	5	24	0.10	25	1.51	51	5.50	3.20
	10	24	0.13	22	1.57	54	5.63	3.42
2b	1	18	0.10	26	1.64	56	5.70	3.64
	5	20	0.12	23	1.58	57	5.81	3.70
	10	22	0.15	20	1.67	58	5.93	3.81
2c	1	18	0.10	23	1.66	59	5.77	3.80
	5	20	0.16	21	1.68	59	6.01	3.93
	10	22	0.14	18	1.54	60	5.90	3.85
2d	1	19	0.12	22	1.70	59	6.04	3.96
	5	18	0.12	24	1.74	58	5.87	3.84
	10	22	0.16	21	1.58	57	5.82	3.68

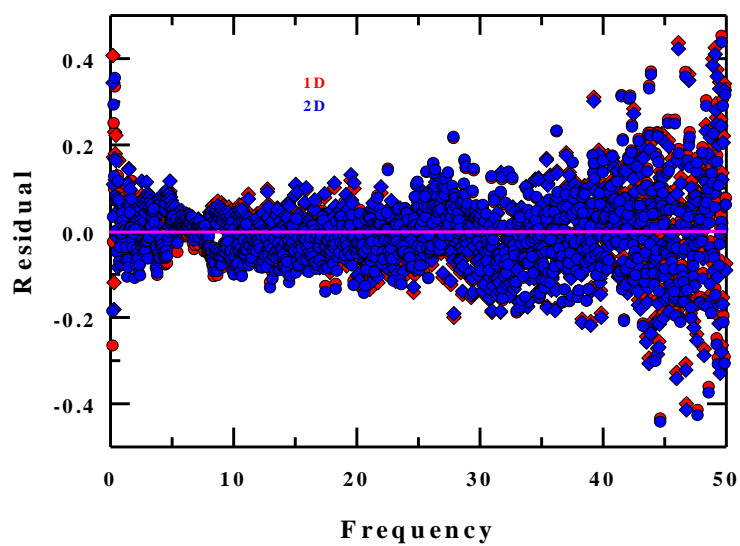


Fig. A.d.12. A representative comparison between the two fitting models. Diamond and circles represent the real and imaginary part of the DR data for the aqueous micellar solution of **2b** polymer (10 mg/mL).

Appendix A.e

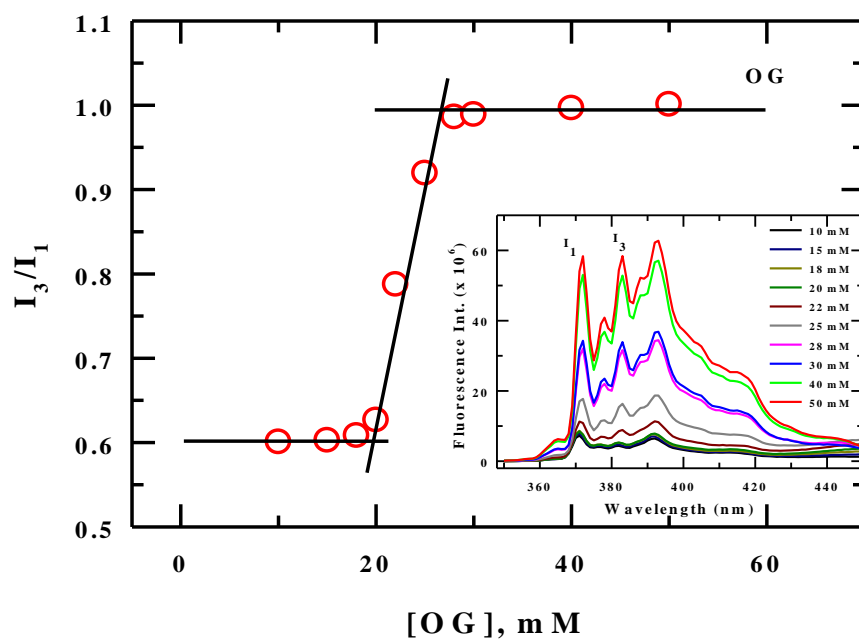


Fig. A.e.1: Change in the fluorescence characteristics (I_3/I_1) of pyrene as a function of OG concentration. The inset shows fluorescence intensity change as a function of OG concentration. Representations are color-coded.

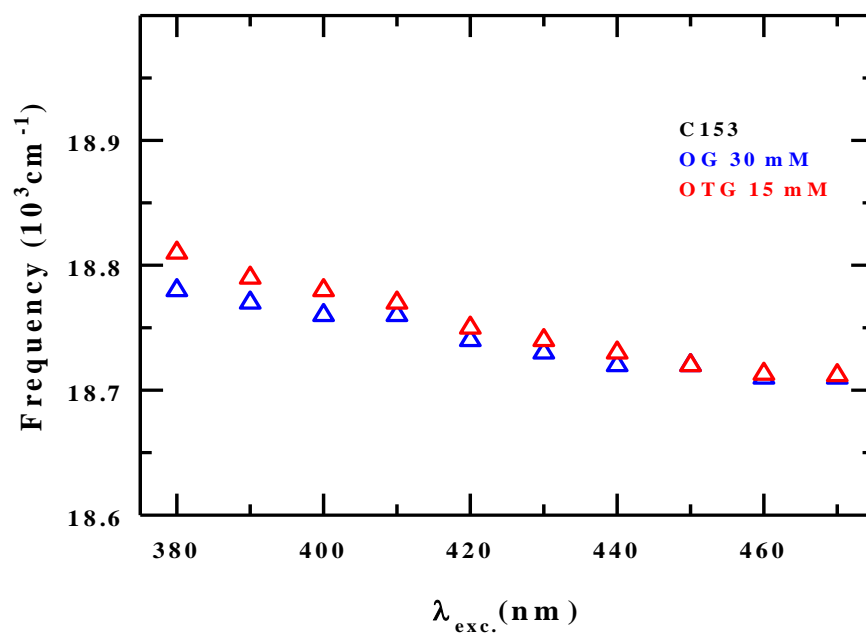


Fig. A.e.2: Excitation wavelength ($\lambda_{\text{exc.}}$) dependence of emission spectral peak frequency of C153 in 30 mM and 15 mM aqueous solutions of OG and OTG, respectively. Representations are color-coded.

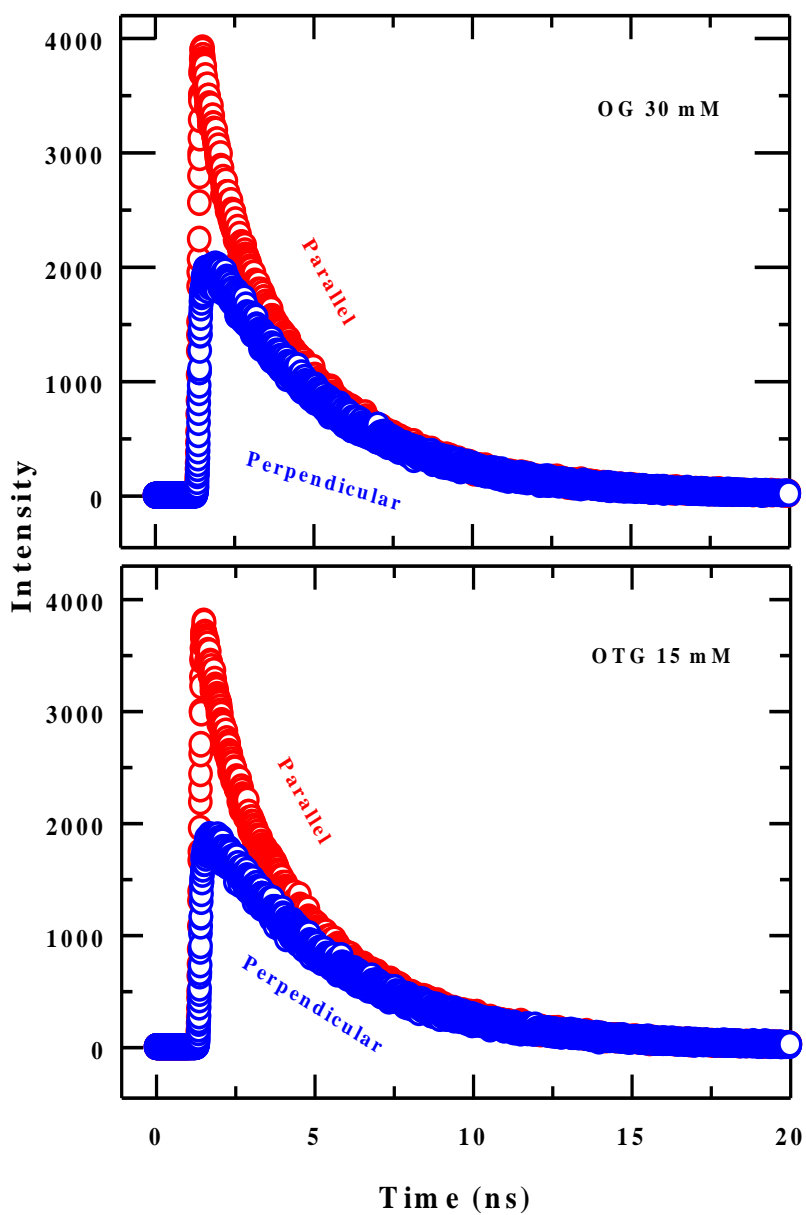


Fig. A.e.3: Representative fluorescence intensity decay profiles of C153 in 30 mM and 15 mM aqueous solutions of OG and OTG, respectively, collected with different polarizations. Representations are color-coded.

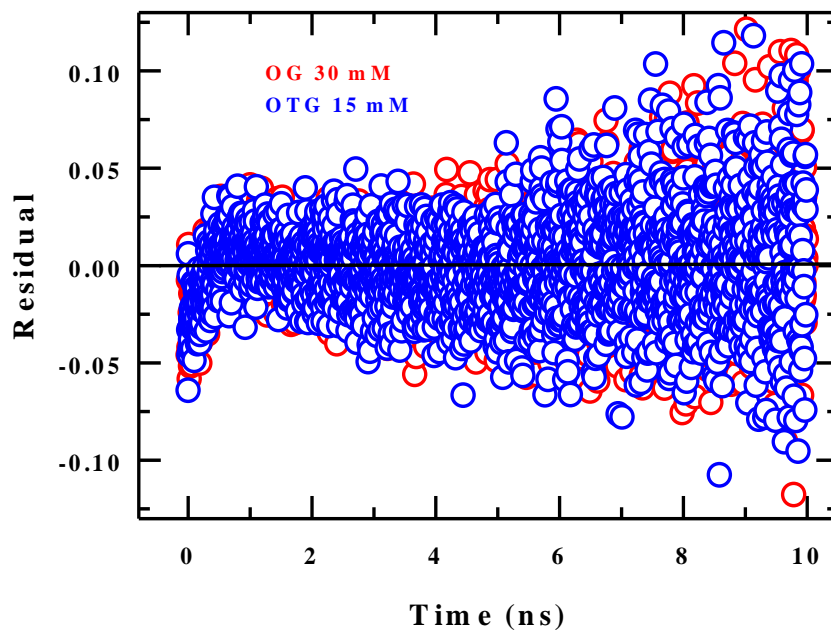


Fig. A.e.4: Residuals for $r(t)$ decay fits of C153 in 30 mM and 15 mM aqueous solutions of OG and OTG, respectively. Representations are color-coded.

Table A.e.5: Charge calculation on $-CF_3$ carbon atom of C153 in water ($\epsilon_0 \sim 80$) using Gaussian03 package

Probe	μ_g HF/3-21G	μ_e CIS/3-21G	$\Delta\mu_e$	$-C^*F_3$ (CIS/3-21G) (Mulliken Charge) a.u.
C153 in water ($\epsilon_0 \sim 80$)	9.11	15.68	6.57	1.213

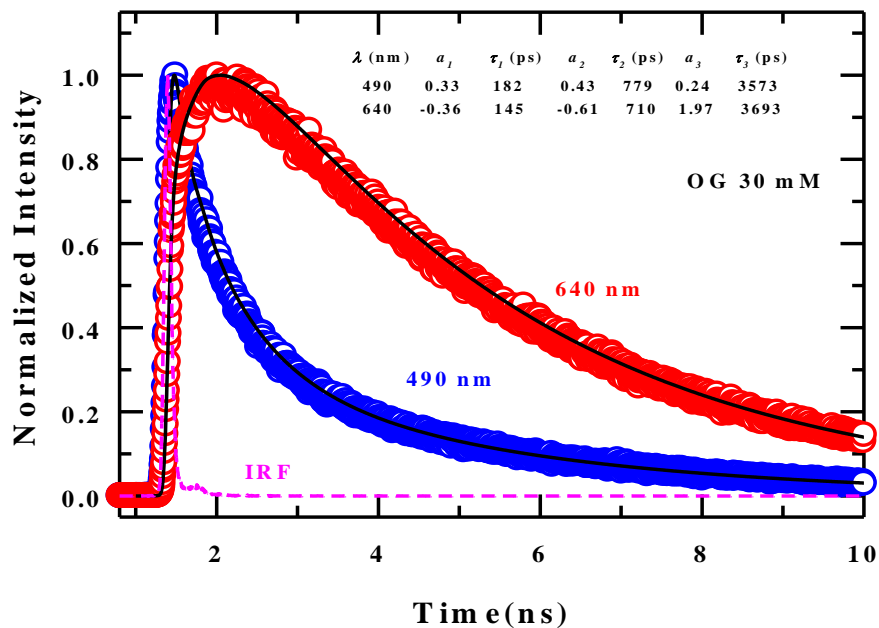


Fig. A.e.6: Representative intensity decay profiles collected at blue (490 nm) and red (640 nm) wavelengths with respect to the steady state emission peak wavelength of C153 in 30 mM aqueous solution of OG. Lines going through the data sets depict the tri-exponential fits through them. Pink dashed lines depict the IRF. Fit parameters are given in the inset. Representations are color-coded.

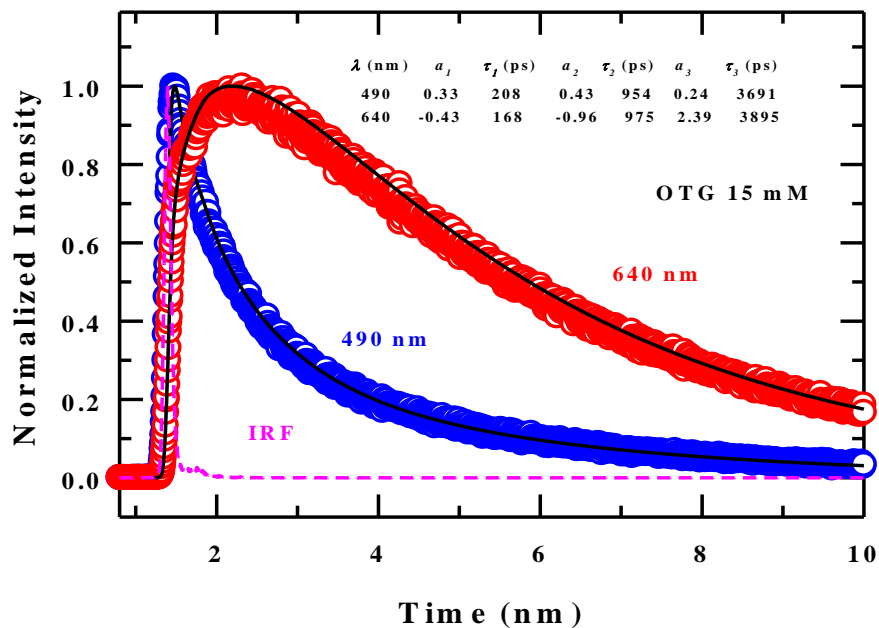


Fig. A.e.7: Representative intensity decay profiles collected at blue (490 nm) and red (640 nm) wavelengths with respect to the steady state emission peak wavelength of C153 in 15 mM aqueous solution of OTG. Lines going through the data sets depict the tri-exponential fits through them. Pink dashed lines depict the IRF. Fit parameters are given in the inset. Representations are color-coded.

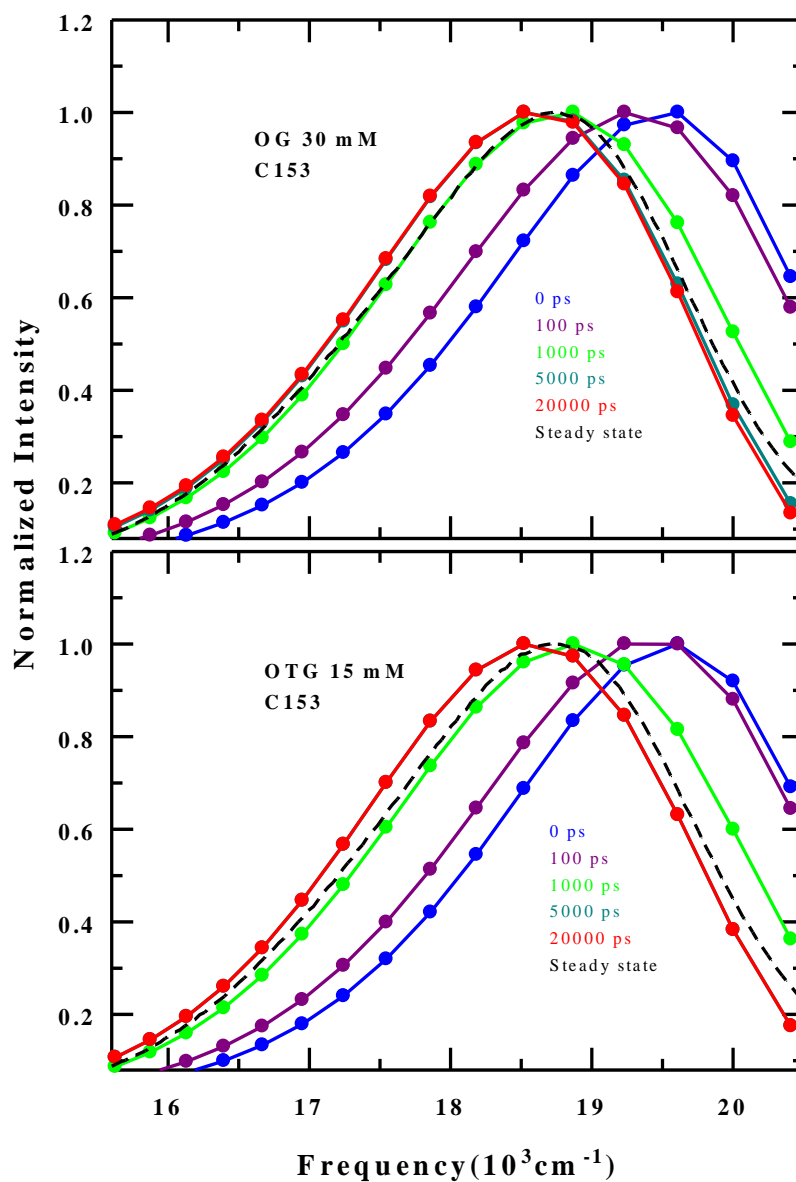


Fig. A.e.8: Representative time-resolved emission spectra (TRES) at different time slices from the experimentally obtained decay profiles of C153 in 30 mM and 15 mM aqueous solutions of OG and OTG, respectively. Dashed lines represent corresponding steady state emission spectra. Representations are color-coded.

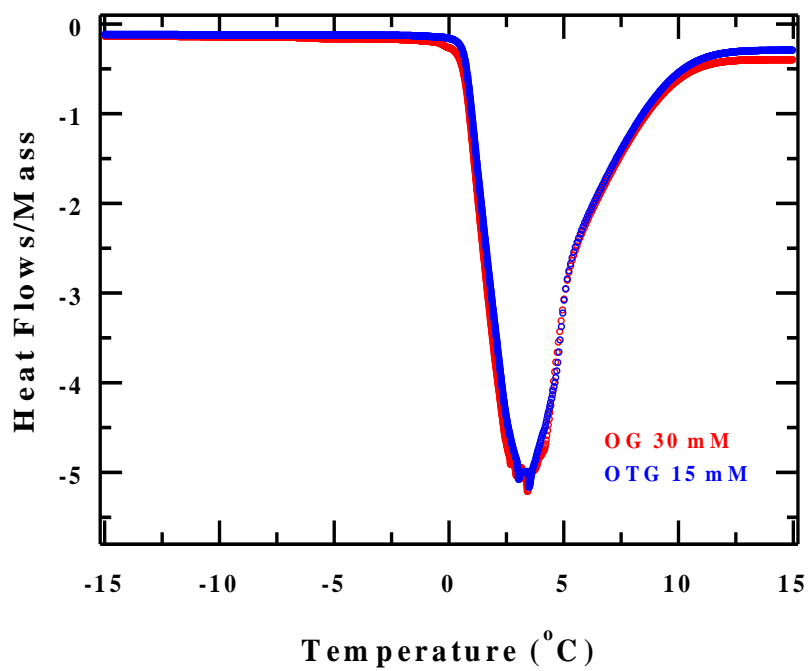


Fig. A.e.9: : DSC traces of 30 mM and 15 mM aqueous solutions of OG and OTG, respectively. Representations are color-coded.

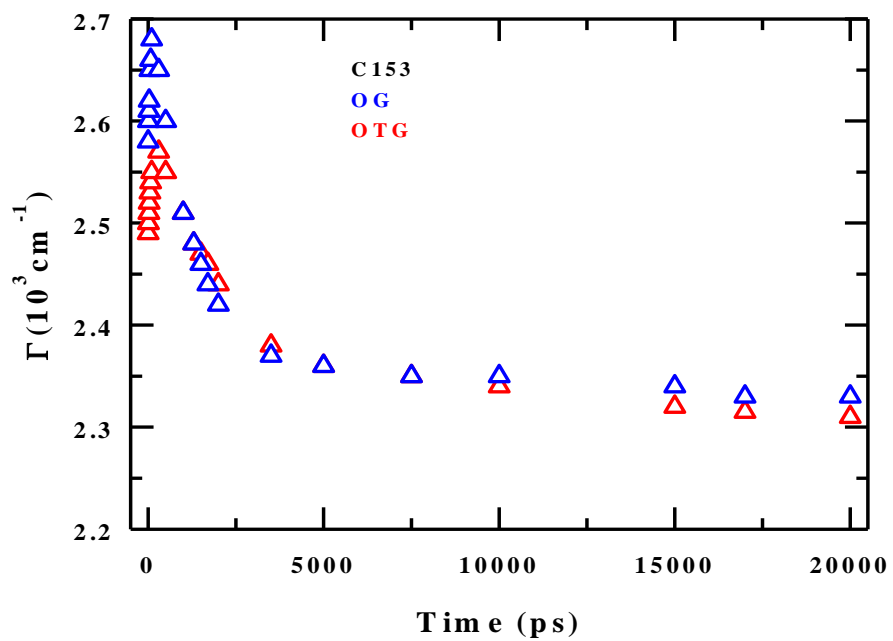


Fig. A.e.10: Time dependence of the full width at half maxima ($\Gamma(t)$) of the time-resolved emission spectra of C153 in 30 mM and 15 mM aqueous solutions of OG and OTG, respectively. Representations are color-coded.

Table A.e.11: Molecular rotational and translational diffusion times from Stokes-Einstein-Debye (SED) and Stokes Einstein (SE) relation respectively, for C153. From SED using stick boundary condition, $\tau_r = \eta V / k_B T$. Where τ_r is reorientational time, V represent the van der Waals volume of the solute consider (calculated using Ref. 108) η is the viscosity of the medium at temperature T and k_B is the Boltzmann constant.

Translational diffusion time, τ_{trans} , of a spherical solute with a diameter σ in a medium of viscosity η at temperature T obtained from SE relation (stick boundary) as $\tau_{trans} = \frac{\sigma^2}{D}$;

$$D = \frac{k_B T}{3\pi\eta\sigma}. \text{ For our systems } \eta = 1cP.$$

Solute	Volume (\AA^3) ^{Cal}	$\tau_r = \eta V / k_B T$ (ps)	$\tau_{trans} = \frac{\sigma^2}{D}$ (ns)
C153	248 (246 ^a)	60	1.085

a) Ref. 59

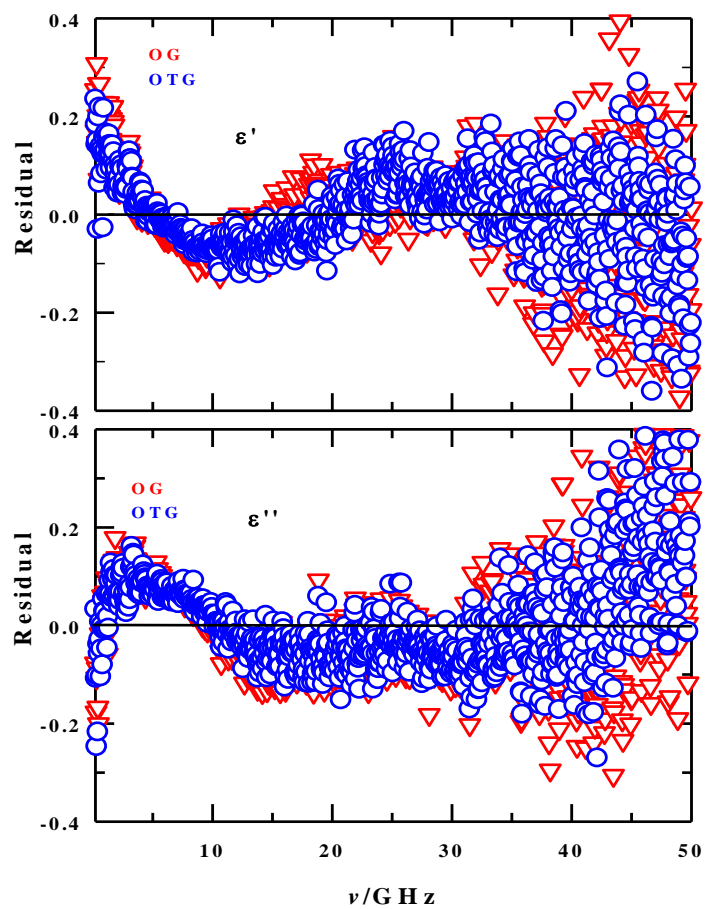


Fig. A.e.12: Residuals from 1-Debye simultaneous fits of the real (upper panel) and imaginary (lower panel) components of the measured DR in 30 mM and 15 mM aqueous solutions of OG and OTG, respectively. Representations are color-coded.